

Cranfield University

School of Engineering

Nanomaterials group

PhD thesis 2002



Dan Portus

**Langmuir-Blodgett films of porphyrins and
phthalocyanines**

Supervisor: Prof. G. J. Ashwell

i. Abstract

Phthalocyanines and porphyrins have been studied for many years as bulk, thick and thin films. Their use in Langmuir and Langmuir-Blodgett films is governed by their peripheral substituents. These can enhance or reduce their ability to form “quality” ultra-thin films.

There are a number of potential and current applications for thin films of porphyrins and phthalocyanines, which include CD-R discs and gas-sensors. It is the latter that this PhD has focussed on.

Ultra-thin films of phthalocyanines, porphyrins and a porphyrin/phthalocyanine hybrid dye were deposited onto glass microscope slides, gold-coated glass microscope slides and quartz crystals. These assemblies were then characterised using Ultraviolet-Visible spectroscopy, pressure-area isotherms, surface plasmon resonance and a quartz crystal microbalance to try and determine the nature of the molecules on the surface of the substrate. The thin films were exposed to chlorine gas and the change in their absorption spectrum and (in some cases) their surface plasmon resonance curve was monitored.

A short series of phthalocyanines showed that the central metal atom can play an important role in the orientation of the macrocycles – with copper adopting an edge-on configuration, zinc, face-down and metal-free, random. This in turn affected the sensitivity of the gas-sensor with the facedown orientation offering a significantly greater response than the other two.

A series of substituted tetraphenylporphyrins also illustrated that the gas-sensitivity of the dye molecules is dependent on the orientation and spacing of the molecules in the film. Generally the response to the chlorine was quite low, but one porphyrin (stearamido) demonstrated a 2nd order decay in the absorbance due to the oxidation of the macrocycle, the time constants being 31 and 425 seconds for the surface and bulk diffusion responses respectively.

The use of differentiation on the Pressure-Area Isotherms of the deposited Langmuir-Blodgett films is a new concept developed in this thesis. It proved a useful tool for looking at the effect of the quality of the film on the gas sensitivity.

ii. Table of Contents

i. Abstract.....	1
ii. Table of Contents.....	2
iii. Table of Figures.....	4
iv. Table of Tables	7
CHAPTER ONE Porphyrins and phthalocyanines.....	8
1. Molecular Electronics	9
1.1 Ordered thin films.....	10
1.1.1 Langmuir-Blodgett deposition.....	10
1.1.2 Characterisation of Langmuir and Langmuir-Blodgett films	13
2. Tetrapyrrole pigments.....	14
2.1 Porphyrins.....	16
2.2 Phthalocyanines (tetraazatetrabenzoporphyrins)	18
2.3 Aromaticity	19
2.4 Modifications for Langmuir-Blodgett deposition.....	21
3. Applications of porphyrins and phthalocyanines in molecular electronics	22
3.1 Dyes for CD discs.....	22
3.2 Photodynamic Therapy	23
3.3 Donor-Acceptor systems with C ₆₀	24
3.4 Third-order nonlinear optics (NLO)	24
3.5 Detection of molecules in the gaseous phase.....	25
3.5.1 Gas detection techniques	28
3.5.2 A survey of gas sensing by thin films of tetrapyrrole pigments	33
4. The aim of this thesis.....	38
CHAPTER TWO Experimental Procedures.....	40
1. Synthesis of Materials.....	41
2. Preparation of Solutions.....	41
3. Pressure-Area Isotherms	42
4. Cleaning of Substrates	44
4.1 Glass slides	44
4.2 Quartz Crystals	45
4.3 Gold-Coated Glass Slides	46
5. Langmuir-Blodgett Deposition.....	46
6. Ultraviolet-Visible Spectroscopy.....	49
6.1 Solution.....	49
6.2 Monolayer.....	49
7. Quartz Crystal Microbalance (QCM) Measurements.....	50
8. Deposition of Gold Layer	52
9. Surface Plasmon Resonance (SPR) Characterisation	54
10. Molecular Modelling	56
11. Chlorine Gas Sensing.....	56
11.1 Surface Plasmon Resonance	56
11.2 Ultraviolet-Visible Spectroscopy.....	58
CHAPTER THREE Results and discussion.....	60

1. Phthalocyanines	61
2. Porphyrins	78
2.1 Tetra-substituted porphyrins	80
2.2 Porphyrins with more than 4 substituents.....	88
3. Bis-phthalocyanine / porphyrin triple-decker sandwich.....	95
4. Chlorine sensitivity	99
4.1 SPR gas sensing	99
4.2 UV-VIS gas sensing.....	102
4.2.1 Phthalocyanines	102
4.2.2 Porphyrins.....	109
4.2.3 Bis-phthalocyanine / porphyrin triple-decker sandwich.....	121
CHAPTER FOUR Conclusions and suggestions for further work.....	122
1. Conclusions.....	123
2. Suggestions for further work	125
2.1 Alterations to deposition conditions	125
2.2 Investigation of chain lengths in ether substituents.....	129
2.3 Potential commercial investigations	129
Appendix.....	130
Explanation of 2 nd differential graphs.....	130
Acknowledgements.....	132
References.....	133

iii. Table of Figures

Figure 1 – H-aggregation on the water surface..... 13

Figure 2 – Chlorophyll a (green plant pigment) 15

Figure 3 – Haem (oxygen transporting molecule in blood)..... 15

Figure 4 – The porphyrin structure and Fischer’s nomenclature..... 16

Figure 5 – IUPAC system for porphyrin nomenclature..... 17

Figure 6 – 29-*H*, 31-*H*-phthalocyanine..... 18

Figure 7 – Outer (red) and inner (blue) protons in a porphyrin macrocycle 19

Figure 8 – Cross-section of the porphyrin macrocycle demonstrating the applied (H) and induced (h) magnetic fields..... 20

Figure 9 – Diagram showing porphyrins and phthalocyanines are Hückel aromatic..... 21

Figure 10 – Cross-section of a CD-R disc 22

Figure 11 – Principles and two mechanisms of PDT of cancer..... 23

Figure 12 – Chlorine accidents around the world..... 27

Figure 13 – Breakdown of type of chlorine accidents by year 28

Figure 14 - Schematic of simple SPR apparatus..... 30

Figure 15 – Typical SPR scan from 38° to 50° 30

Figure 16 – Isotherm trough housed in a cleanroom environment on a vibration isolation table..... 42

Figure 17 – Series 2000 Nima Technology single compartment round trough..... 47

Figure 18 – Alternate layer trough, Nima Technology 622 double compartment..... 48

Figure 19 – Edwards 306A Coating System with water pumps and thickness monitor. 52

Figure 20 – SPR apparatus diagram 54

Figure 21 – First differential of the SPR curve can show the steepest section of the curve..... 57

Figure 22 – SPR gas rig apparatus..... 57

Figure 23 – Phthalocyanine dyes used (supplied by Prof. C. L. Honeybourne)..... 61

Figure 24 – UV-VIS absorption spectrum of dye I in trichloromethane 62

Figure 25 – Demonstration of solid-state packing effects in dye I; dye in trichloromethane (—) and monolayer (—) forms..... 63

Figure 26 – Demonstration of the lack of solid-state packing effects in dye II; dye in trichloromethane (—) and monolayer (—) forms..... 64

Figure 27 – Comparison of the UV-VIS absorbance of III in both trichloromethane (—) and monolayer (—) forms..... 65

Figure 28 – Langmuir pressure-area isotherms of the three phthalocyanines (— dye I, — dye II, — dye III)..... 66

Figure 29 – Isotherm (—) and 2nd differential (—) of dye I..... 68

Figure 30 – Isotherm (—) and 2nd differential (—) of II 70

Figure 31 – Isotherm (—) and 2nd differential (—) of III..... 71

Figure 32 – Area-time graphs of dye I (—) and dye III (—) when held at 10 mN m⁻¹ (arrows indicate where target pressure is attained)..... 72

Figure 33 – Explanation of how phthalocyanine dimension measurements are taken using Chem3D (macrocycle only) 74

Figure 34 – Explanation of how Chem3D interprets the change in the shape of the macrocycle with the insertion of a metal atom (right) when compared with the metal free (left)	75
Figure 35 – Molecular structure of porphyrin dyes used (supplied by Dr. T. Richardson)	78
Figure 36 – UV-VIS absorption spectrum of dye IV in trichloromethane showing the main absorption and satellite bands characteristic to porphyrin dyes	80
Figure 37 – Comparison of a trichloromethane solution of IV (—) and a trichloromethane solution of IV with a few drops of HCl added (—).....	82
Figure 38 – Langmuir pressure-area isotherms of three porphyrins (— dye IV, — dye V, — dye VI)	83
Figure 39 – Isotherm (—) and 2 nd differential (—) of IV	84
Figure 40 – Isotherm (—) and 2 nd differential (—) of V	85
Figure 41 – Isotherm (—) and 2 nd differential (—) of VI.....	86
Figure 42 – Comparison of pressure-area isotherms of dyes VII (—), VIII (—) and IX (—).....	89
Figure 43 – Isotherm (—) and 2 nd differential (—) of VII	90
Figure 44 – Isotherm (—) and 2 nd differential (—) of VIII	91
Figure 45 – Isotherm (—) and 2 nd differential (—) of IX.....	92
Figure 46 – diagram illustrating different representations of areas	92
Figure 47 – Molecular structure of X (supplied by Dr. T. Richardson)	95
Figure 48 – Physical representation of layout of molecules in X.....	95
Figure 49 – Comparison of UV-VIS spectra of X in trichloromethane (—) and monolayer (—) forms	96
Figure 50 – Isotherm (—) and 2 nd differential (—) of X.....	97
Figure 51 – SPR scan of a gold layer (—), dye (I) (—) and dye exposed to 10 ppm chlorine (—) symbols = data, lines = theoretical plot	100
Figure 52 – SPR dose-response curve for I	101
Figure 53 – UV-VIS spectra of a monolayer of I (—) after exposure to 50 ppm chlorine for 30 mins (—) and its subsequent recovery after 24 hours in air (—).....	102
Figure 54 – UV-VIS spectra of a multilayer of I (—) after exposure to 50 ppm chlorine for 30 mins (—) and its subsequent recovery after 24 hours in air (—).....	104
Figure 55 – UV-VIS spectra of I in trichloromethane (—) and after bubbling through 50 ppm for 30 minutes (—)	105
Figure 56 – UV-VIS Spectra of monolayer of II (—) after exposure to 50 ppm chlorine for 30 mins (—) and its subsequent recovery after 24 hours in air (—).....	106
Figure 57 - UV-VIS spectra of a multilayer of II (—) after exposure to 50 ppm chlorine for 30 mins (—) and its subsequent recovery after 24 hours in air (—).....	107
Figure 58 – An example of poor sensitivity to 50 ppm chlorine; LB film of IV (—) and after 30 mins exposure to the gas (—).....	109
Figure 59 – Monolayer of VII (—) after exposure to <10 ppm chlorine for 30 mins (—)	111
Figure 60 – Monolayer of VII (—) after exposure to 10 ppm chlorine for 30 mins (—)	112
Figure 61 – Monolayer of VII deposited at a higher surface pressure (—) after exposure to 10 ppm for 30 mins (—)	113

Figure 62 – Monolayer of VII deposited at a higher pressure (—) after exposure to 50 ppm chlorine for 30 mins (—)	114
Figure 63 – Multilayer of VII (—), after exposure to 10 ppm chlorine for 60 mins (—), after exposure to 50 ppm for 30 mins (—)	116
Figure 64 – UV-VIS spectra of V during exposure to 50 ppm chlorine (arrows indicate direction of peak growth/decay as time progresses).....	117
Figure 65 – Absorbance decrease at 428 nm (■) during exposure to 50 ppm chlorine and the fitted theoretical 2 nd order decay curve (—)	118
Figure 66 – The decay of the normalised absorbance whilst exposed to 50 ppm chlorine (■) and the corresponding results for previous work at low (—) and high (—) deposition pressures.....	119
Figure 67 – Dye X (—), after 24 hours in the dark (—) or 24 hours under normal laboratory lighting (—).....	121
Figure 68 – Mixture of VIII and stearic acid (1:10) in trichloromethane.....	125
Figure 69 – Monolayer of VIII (—) after exposure to 50 ppm chlorine for 30 mins (—)	126
Figure 70 – Monolayer of VIII and S. A.(1:10) (—) after exposure to 50 ppm for 30 mins (—).....	127
Figure 71 – Multilayer (5 passes) of mixed floating film of VIII and S. A. (1:10) (—) after exposure to 50 ppm chlorine for 30 mins (—)	127
Figure 72 – Multilayer of VIII and S. A. mixed film (1:10, 5 passes) with 4 x S. A. spacer layers (—) after exposure to 50 ppm chlorine for 30 mins (—).....	128
Figure 73 – Monolayer of VIII deposited at high pressure (—) and exposed to 50 ppm chlorine for 30 mins (—)	128

iv. Table of Tables

Table 1 – The effect on the nature of the molecules when different head groups, R, are attached to a C ₁₆ H ₃₃ chain (only amphiphilic and weakly amphiphilic molecules are likely to form Langmuir films)	11
Table 2 - $\chi^{<3>}$ values for various phthalocyanines (DFWM = degenerate four-wave mixing).....	25
Table 3 – Advantages and disadvantages of optical sensors compared with other types	28
Table 4 – Summary of research into gas sensing with porphyrins and phthalocyanines	33
Table 5 – Sauerbrey’s calculation symbols	51
Table 6 – Comparison of λ_{max} of monolayers of phthalocyanines	65
Table 7 – Types of special point and the method of determination.....	67
Table 8 – Molecular area as measured by isotherm and QCM.....	73
Table 9 – Measurements taken from Chem3D	73
Table 10 – Angle of bonding of central atom in the phthalocyanine series	75
Table 11 – calculated thickness and optical properties of the phthalocyanine dyes.....	76
Table 12 – Density (g cm ⁻³) calculations for the phthalocyanines.....	77
Table 13 – Substituents attached to porphyrinoid macrocycle	79
Table 14 – UV-VIS characteristics of the monolayers and solutions (trichloromethane) of the three dyes.....	81
Table 15 - Comparison of isotherm and QCM data for dyes IV to VI.....	87
Table 16 – Calculated SPR data for IV, V and VI.....	87
Table 17 – Density (g cm ⁻³) of IV, V and VI in both Langmuir and LB form	87
Table 18 – Comparison of UV-VIS spectra of porphyrin dyes IV-IX (N_{subs} = number of substituents)	88
Table 19 – Theoretical measurements and calculated areas of IX	93
Table 20 - Comparison of isotherm and QCM data for dyes VII to IX.....	93
Table 21 – Calculated SPR data for VII, VIII and IX	94
Table 22 – Density (g cm ⁻³) of VII, VIII, and IX in both Langmuir and LB form.....	94
Table 23 – Comparison of isotherm and QCM data.....	97
Table 24 – Calculated SPR data for X.....	98
Table 25 – Density (g cm ⁻³) of VII, VIII, and IX in both Langmuir and LB form.....	98
Table 26 – Comparison of the response (%) of three dyes in monolayer and multilayer form.....	108
Table 27 – Comparison of poor response of dyes to chlorine	109
Table 28 – Possible sources of water vapour and the effect of increasing Cl ₂ concentration.....	115
Table 29 – Comparison of the quality of the Langmuir-Blodgett film with Chlorine sensitivity	120

CHAPTER ONE

Porphyrins and phthalocyanines

1. Molecular Electronics

Molecular electronics, a field that has burgeoned in the last 2 decades, can be divided into two disciplines: molecular materials for electronics and molecular scale electronics.

The field of molecular materials for electronics (MME) is the search for molecules with an overall set of properties that are either unique, or superior to those of other materials. The device, the application or the actual manufacturing process, may require these properties and there is often a compromise between ease of production and its performance ⁽¹⁾.

If MME is the research into single molecules and their properties, molecular scale electronics (MSE) is the study of groups (or aggregates) of molecules on the nanometer scale. The two fields are inextricably linked; the development of the materials and their enhanced properties leads to a greater understanding of the potential molecular scale electronic devices. A particularly good example of this is the current research being performed by the Nanomaterials group at Cranfield University on molecular rectification both at the nanometer ⁽²⁾ and molecular level. This work could eventually lead to devices with high component density and hence greater computer processor speeds.

Perhaps the most successful application to emerge from research into these areas is the liquid crystal display (LCD). Friedric Reinitzer first discovered liquid crystals in 1888 but it was 80 years before the first LCD was produced (by RCA in 1968). Soon the first calculators (Sharp, 1970) and watches (Seiko, 1973) incorporating liquid crystal displays were on sale. More recently, the development of colour sub-pixels has lead to the production of ultra-thin TVs and computer monitors.

1.1 Ordered thin films

Computer processing chips are constantly being refined to improve their computational speed and efficiency. A key factor in the search for faster processors is the increase in the component density of the devices. To achieve this their construction must be precisely controlled, particularly the deposition of the materials onto the substrate either to form the circuits directly or prior to photolithography.

Langmuir-Blodgett (LB) deposition has been the method of choice for monomolecular level engineering for many years now and the ability to build precise supramolecular structures ⁽³⁾ also provides some hope for MSE applications, including organic conduction of zinc phthalocyanine ^(4, 5). The technique, which is limited to materials capable of forming floating layers on water, provides the opportunity of engineering a film layer-by-layer. Other thin film techniques, such as molecular beam epitaxy, ultra-high vacuum evaporation and spin-coating are still some way from producing the high quality monolayers of LB deposition.

1.1.1 Langmuir-Blodgett deposition

The key feature of molecules used in this technique is their ability to be trapped at the air-water interface. Often they will be amphiphilic in nature; part water-attracting, part water-repelling. This not only prevents them from being pulled into the water subphase, but also allows control over the orientations of the molecules in this floating monolayer (and therefore the subsequently deposited layers).

Traditionally, long chain alcohols and fatty acids have been the material of choice for LB work; the hydrocarbon part ($-\text{CH}_2-$) being hydrophobic and the polar head group ($-\text{COOH}$ or $-\text{OH}$), hydrophilic. The attachment of different functional groups to these hydrocarbon chains can alter the amphiphilic nature of the molecule and hence, the Langmuir films (Table 1) ⁽⁶⁾.

Table 1 – The effect on the nature of the molecules when different head groups, R, are attached to a C₁₆H₃₃ chain (only amphiphilic and weakly amphiphilic molecules are likely to form Langmuir films)

Non amphiphilic molecules	Weakly amphiphilic molecules	Amphiphilic molecules	Alkyl Anions or Cations
<i>Suitable R groups</i>	<i>Suitable R groups</i>	<i>Suitable R groups</i>	<i>Suitable R groups</i>
Hydrocarbon	-C ₆ H ₄ OCH ₃	-CH ₂ OH	-SO ₃ ⁻
-CH ₂ I	-COOCH ₃	-COOH	-OSO ₃ ⁻
-CH ₂ Br		-CN	-C ₆ H ₄ SO ₄ ⁻
-CH ₂ Cl		-CONH ₂	-NR ₃ ⁺
-NO ₂		-CH=NOH	
		-C ₆ H ₄ OH	
		-NHCONH ₂	
		-NHCOCH ₃	

Whilst some Langmuir-film forming materials spread spontaneously on a water surface, most must be deposited onto the water subphase after dissolving in a suitable solvent. This volatile liquid must be chemically inert with respect to the molecule under study and as pure as possible. At the molecular level, even a small degree of contamination can alter the film's properties, so to confirm the purity of the solvent, it is spread without any material dissolved onto the water surface and the area of the trough reduced (compressed). An increase in the surface pressure will be due to contamination either from the solvent or the water subphase. Typically, solvents are also chosen with a relatively short evaporation time, though highly volatile liquids are avoided to ensure accurate determination of the concentration of the solution. Organic solvents, which are water-miscible or water-soluble, tend to be avoided as they pull the molecule into the subphase during spreading.

Whilst the usual composition of the subphase is ultra-pure water, other high surface-tension liquids (such as ethylene glycol or glycerol) may be used. With water, the reduction of contaminants is usually attained through a double cleaning procedure. First it is distilled to remove any inorganic moieties and this pure water is then filtered and exposed to UV light to destroy and remove any organic contaminants. The purity of the water is usually monitored through its resistivity (only accepting that at $18.2 \text{ M}\Omega \text{ cm}^{-1}$ – which is the preset value of ultra-pure water). Finally, a plastic Pasteur pipette attached to a water aspirator is used to remove any extraneous particulates, which may have settled onto the water surface whilst the Wilhelmy plate equilibrated.

The Wilhelmy plate is a short thin strip of chromatography paper attached to a microbalance and partially immersed in the subphase. When the plate has reached equilibrium (i.e. when no more water can be absorbed), it is very sensitive to any changes in the surface tension. A simple set of equations demonstrate how the microbalance can monitor these changes, also known as the surface pressure:

If a plate has dimensions $l \times w \times t$, a density ρ and is immersed in water to a depth h , then the net force acting on the microbalance is:

$$F = \rho g l w t - \rho' g h w t + 2\gamma(t + w) \cos \theta \quad \text{Equation 1}$$

(Force = weight - upthrust + surface tension)

Where γ is the surface tension of the liquid, θ the contact angle of the plate, g the acceleration due to gravity and ρ' is the density of the subphase.

As the microbalance is zeroed before measurements are taken, the weight and upthrust are eliminated from Equation 1.

$$\Delta F = 2(\gamma' - \gamma)(t + w) \quad \text{Equation 2}$$

The difference in force (between immersion in pure water and surfactant-covered water) is now directly proportional to the change in surface tension (where γ' is the surface tension of pure clean water). This is usually defined as the surface pressure (π).

Once the material has been characterised in the Langmuir film, it can be deposited onto a substrate as a Langmuir-Blodgett film. This involves passing a clean (often) glass slide through a compressed floating monolayer. The surface of the substrate can be treated to ensure that it is hydrophilic or –phobic through the use of different chemicals. For example, to produce a hydrophobic glass slide after initial cleaning, the substrate is exposed to dichlorodimethylsilane for several hours.

1.1.2 Characterisation of Langmuir and Langmuir-Blodgett films

Several techniques can be used for analysing a thin film deposited by the Langmuir-Blodgett technique. It is important to discover as much as possible about the orientation of the molecules both pre- and post-deposition. The material can then be tailored to improve their sensitivity to the analyte gas, designed for improved stability at the air-water interface or altered to enhance other important features of the film.

Studying the UV-VIS spectra of these dyes, both in solution and monolayer form, provides clues to the nature of the molecules deposited in the films. A typical example of this is the blue-shifting of a main absorption peak, which is characteristic of H-aggregation. This aggregation, also known as card stacking, is the 2-D arrangement of the molecules on the surface of the water or substrate with the molecules face-to-face but lying on one edge (Figure 1).

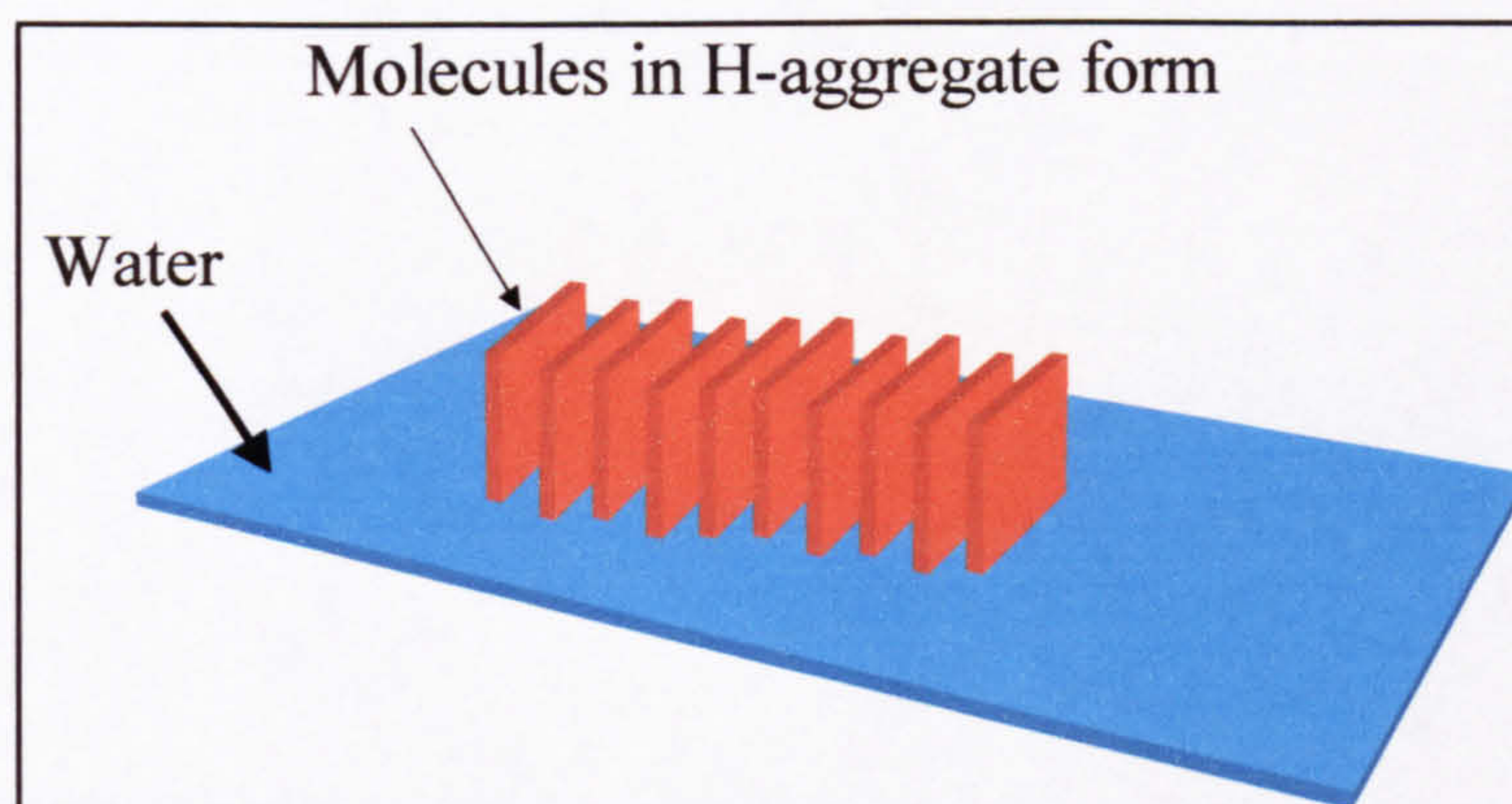


Figure 1 – H-aggregation on the water surface

Further evidence of the specific orientations of the molecules in the solid phase (i.e. the deposited film) can be found with the analysis of the Langmuir pressure-area

isotherm which calculates the area available to each molecule on the water surface. Comparison with the theoretical measurements calculated in Chem3D (CambridgeSoft Ltd.), can indicate whether the molecules are face-down or lying on an edge. Similarly, the use of quartz crystal microbalance (QCM) measurements also calculates the area available to the molecules (this time in the solid phase, i.e. post-deposition) and can give clues to the film orientation. Molecules with long aliphatic chains sometimes show large differences between the molecular areas of the isotherm and QCM due to the chains stretching when being deposited and moving from the high pressure environment of the compressed Langmuir film to the relatively low pressure substrate.

The thickness of the deposited layer can be found through surface plasmon resonance SPR scans, usually with the Kretschmann geometry. By comparing the experimental results with the theoretical curves, the values for thickness and refractive index can be calculated for each layer (i.e. glass substrate, the required thin metal film and the organic LB layer under study).

2. Tetrapyrrole pigments

The materials studied in this PhD fall into the category of tetrapyrrole pigments. In nature these types of dye include chlorophyll (Figure 2) and the oxygen transporting Haem in blood (Figure 3), which are derivatives of the parent tetrapyrrole pigment porphin (or porphyrin) (Figure 4).

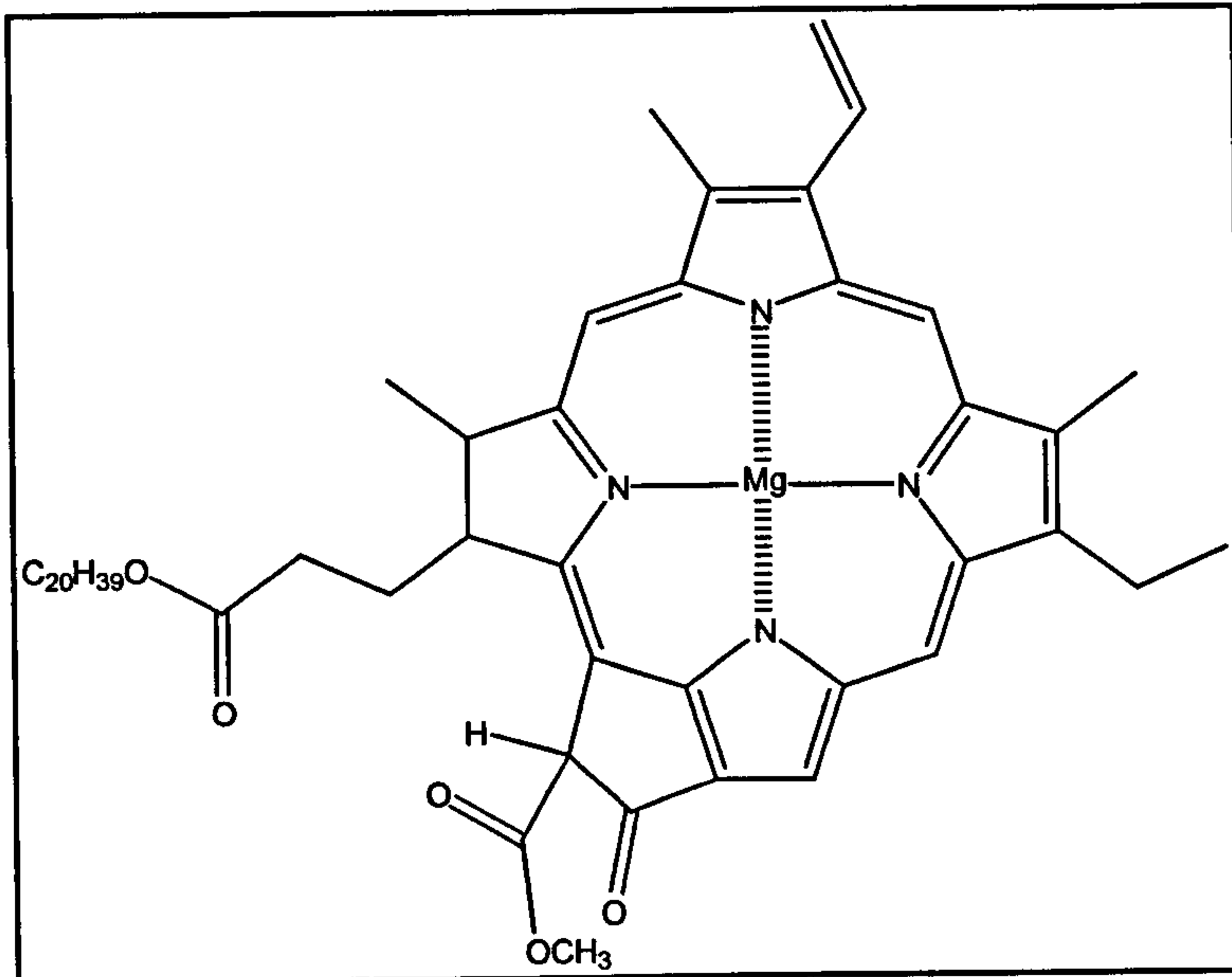


Figure 2 – Chlorophyll a (green plant pigment)

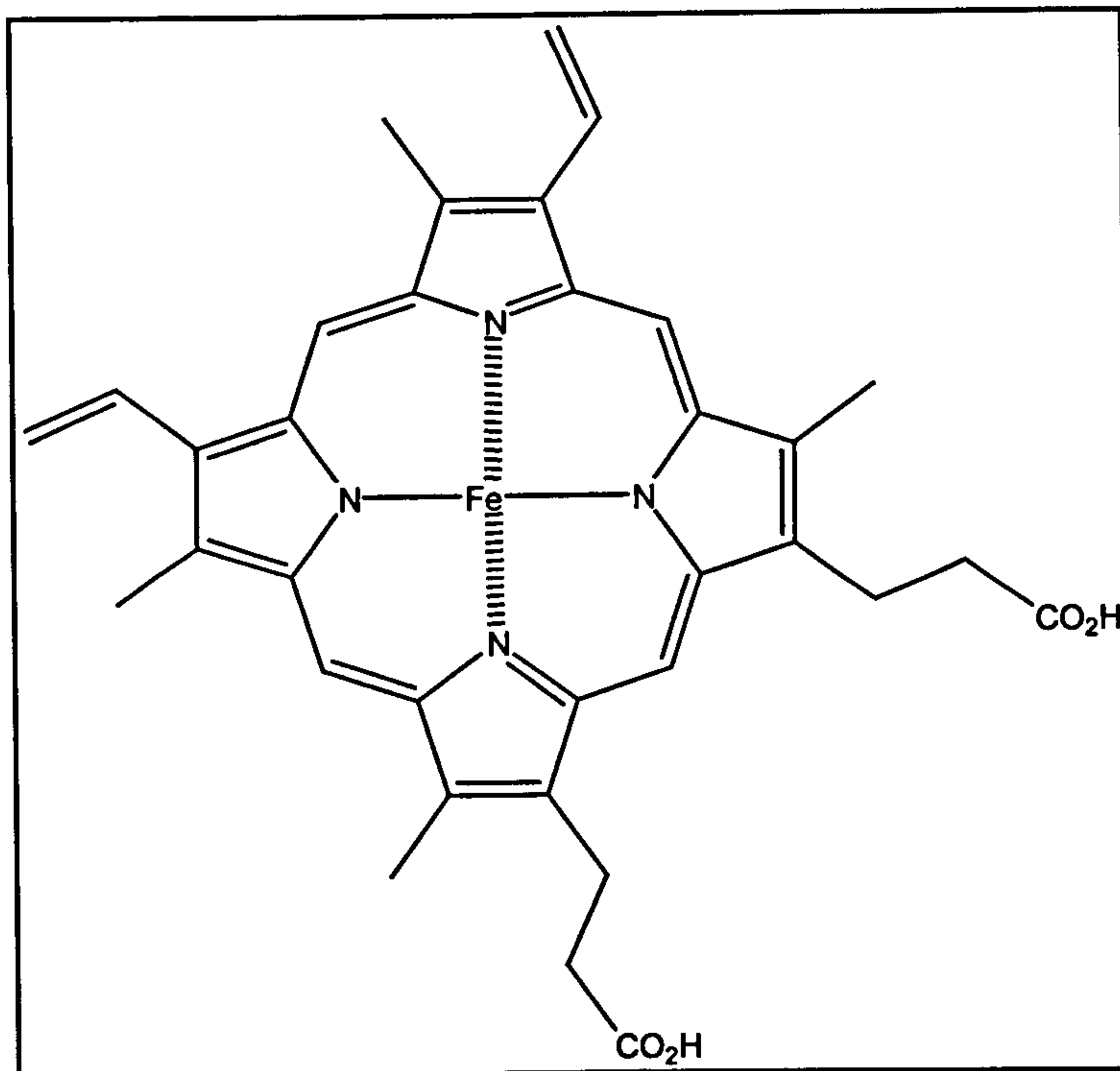


Figure 3 – Haem (oxygen transporting molecule in blood)

2.1 Porphyrins

Although Hans Fischer is widely accepted as the father of modern porphyrin chemistry, the macrocyclic structure of this class of molecules was first proposed by Küster in 1912 ⁽⁷⁾, but considered to be an inherently unstable structure due to the large size of the macrocyclic ring. Only much later when Fischer and his students were able to synthesise Haem in 1929 ⁽⁸⁾, did the proposed macrocyclic structure of these molecules become accepted (Figure 4). Fischer's nomenclature for these molecules can essentially be broken down into 3 parts. Firstly, there are 2 positions on each of the pyrrole rings available for substitution, these were called β -carbons and numbered 1-8. Secondly, the positions next to the Nitrogen in the pyrrole rings were named α -carbons – but left un-numbered. Finally the bridging atoms in the methine groups were labelled meso-carbons and distinguished by the Greek letters α – δ .

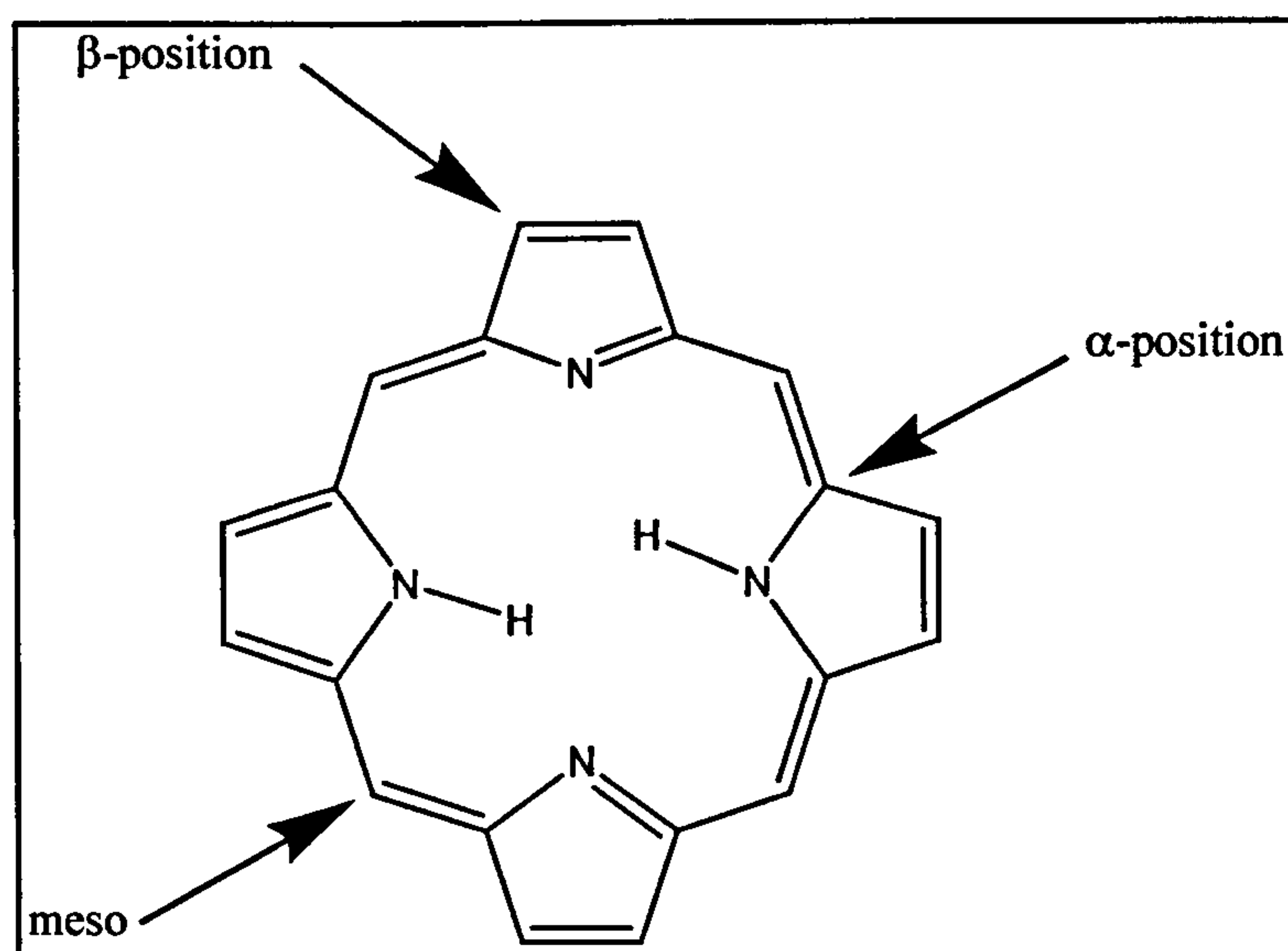


Figure 4 – The porphyrin structure and Fischer's nomenclature

By 1979 IUPAC (International Union of Pure and Applied Chemistry) had determined that this system was too complicated for heavily substituted porphyrins and their own system was finalised in 1987 ⁽⁹⁾. The main difference was that all the atoms were numbered, including the nitrogens. For any chains substituted onto the

macrocycle, the positions of each of those atoms were also mapped. For example, if chloro-butyl was substituted onto the porphyrin at position number 13 the position of the chlorine atom was designated with a superscript and the molecule named 13³-chloro-13-butyl-porphyrin (Figure 5).

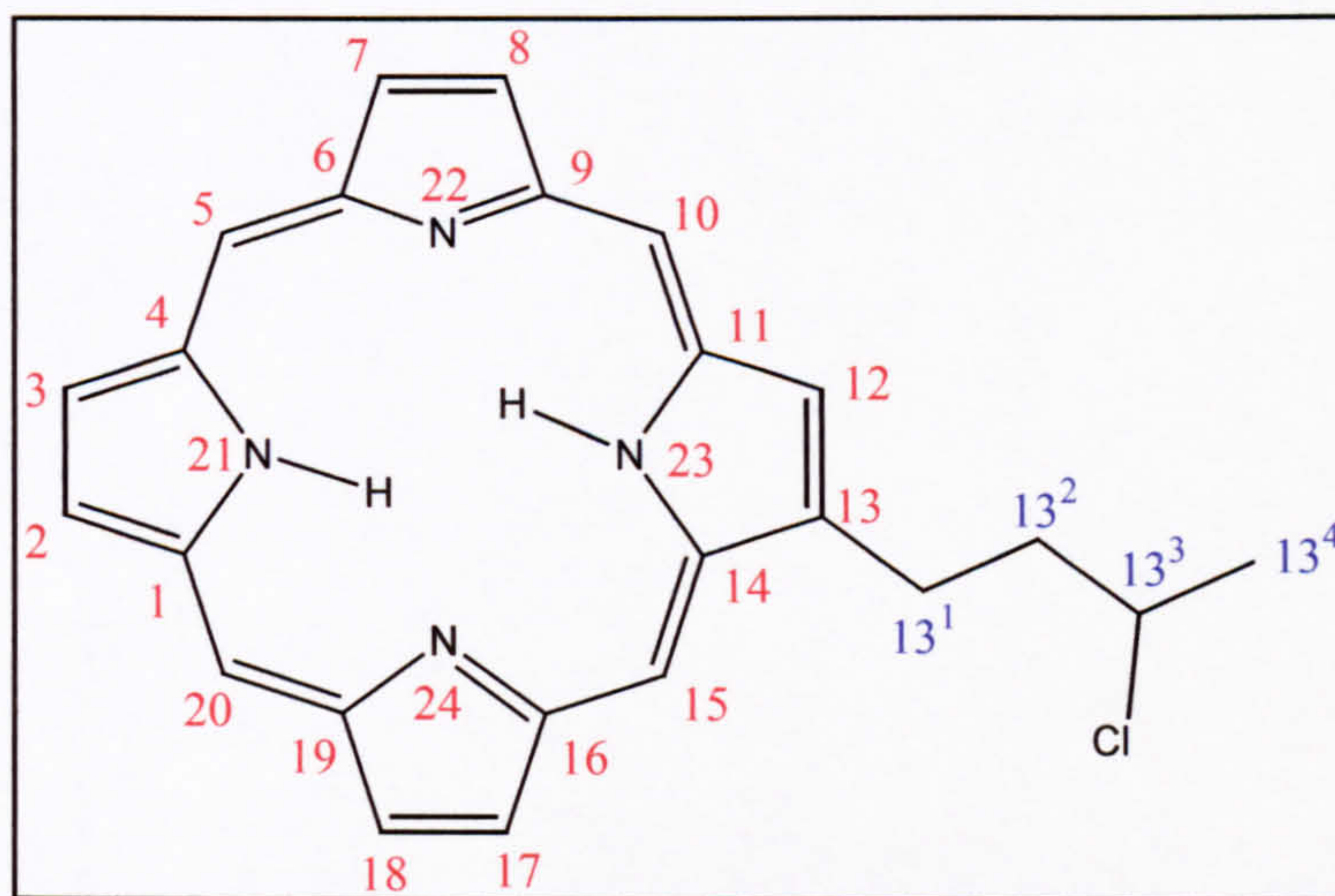


Figure 5 – IUPAC system for porphyrin nomenclature

The co-ordination hole (i.e. the region at the centre of the macrocycle where the Nitrogen atoms can bond with inserted atoms) can complex most metals in the Periodic Table; in some cases, especially for metals with unusually large or small radii (e.g. nickel), the macrocycle must contort to maximise the binding. Other reasons for non-planarity include the oxidation of the porphyrin (producing a non-aromatic macrocycle), substitution of groups onto the central N atoms and the protonation of the nitrogens coupled with bulky substituents on the meso-carbons.

Porphyrins are mainly used in nature to bind metal atoms, becoming vital parts of many biological processes. For example Haem (Figure 3) contains an iron-complexed porphyrin, which in haemoglobin and myoglobin reversibly binds to oxygen. This allows the oxygen to be carried around the body and stored in the muscles. In plant-life, a series of molecules called chlorophylls are vital components of the carbohydrate production needed for the metabolism of both the plant and the animals that consume it. The energy from the sunlight is converted into excited electrons, which are transported by a series of proteins to the actual site of the carbohydrate formation. With the electrons removed, water bound to the magnesium

centre of the chlorophyll molecules is oxidised to replenish the photosynthetic system. The chlorophyll molecules (Figure 2), actually a derivative of 2,3-dihydroporphyrin (also known as chlorin), are grouped together to increase the efficiency of the energy conversion process and ensure that the by-product is oxygen and not harmful intermediates (such as peroxide).

2.2 Phthalocyanines (tetraazatetrabenzoporphyrins)

Phthalocyanines are structurally related to porphyrins. They are not found in nature however, and were discovered by accident in 1907 as a by-product during the synthesis of o-cyanobenzamide ⁽¹⁰⁾. Linstead first used the term phthalocyanine in 1933 to describe a new class of organic compounds (Figure 6) ⁽¹¹⁾. The name itself originates from the Greek words naptha and cyanine meaning blue rock oil.

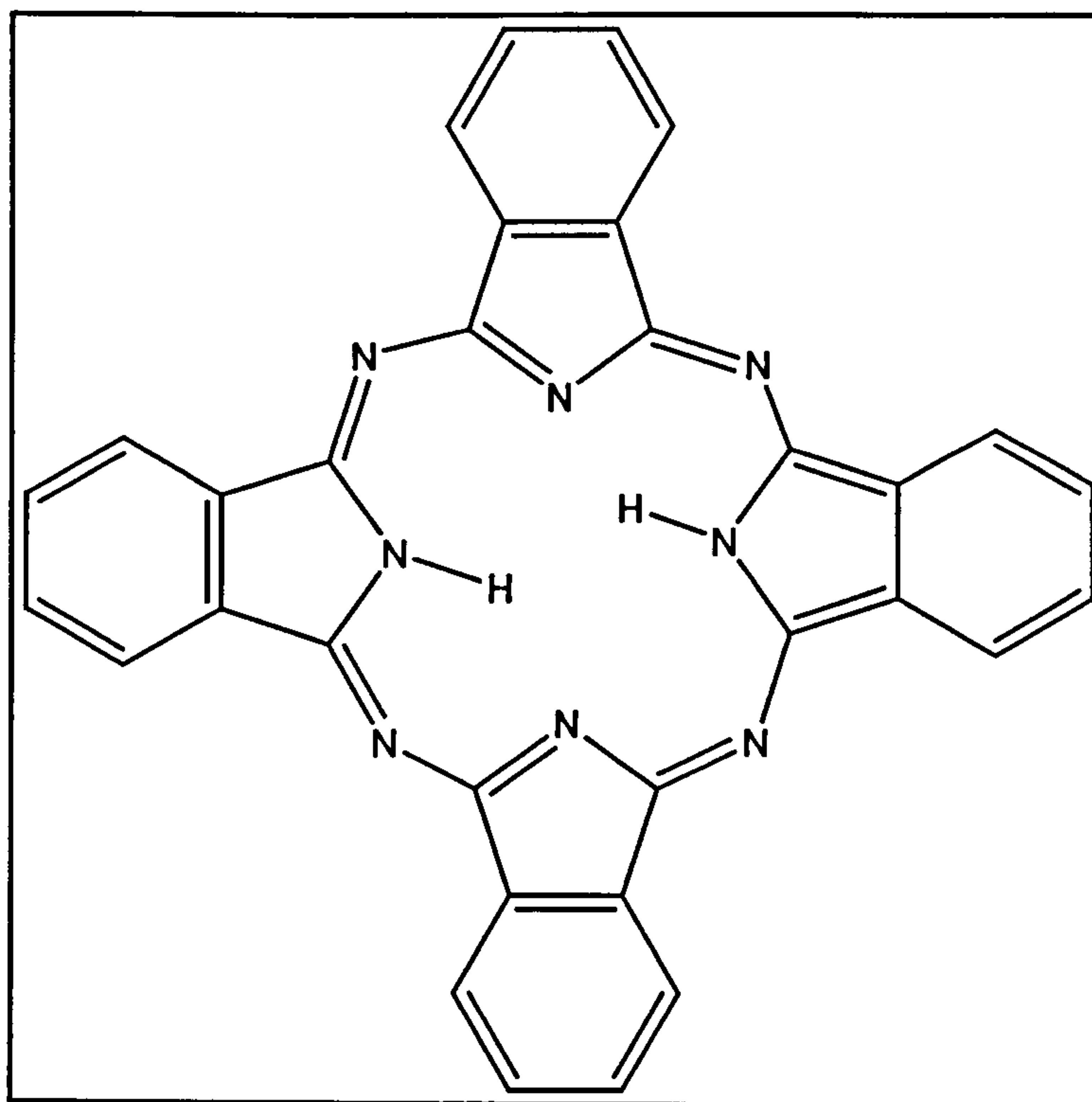


Figure 6 – 29-*H*, 31-*H*-phthalocyanine

2.3 Aromaticity

Both the porphyrin and phthalocyanine molecules are aromatic. This is particularly evident with the H-NMR spectra of the metal-free porphyrins, where the outer protons are $\sim 5\tau$ downfield of TMS but the inner protons are $\sim 4\tau$ **upfield**. This is due to the effect of the induced magnetic field (Figure 7 and Figure 8).

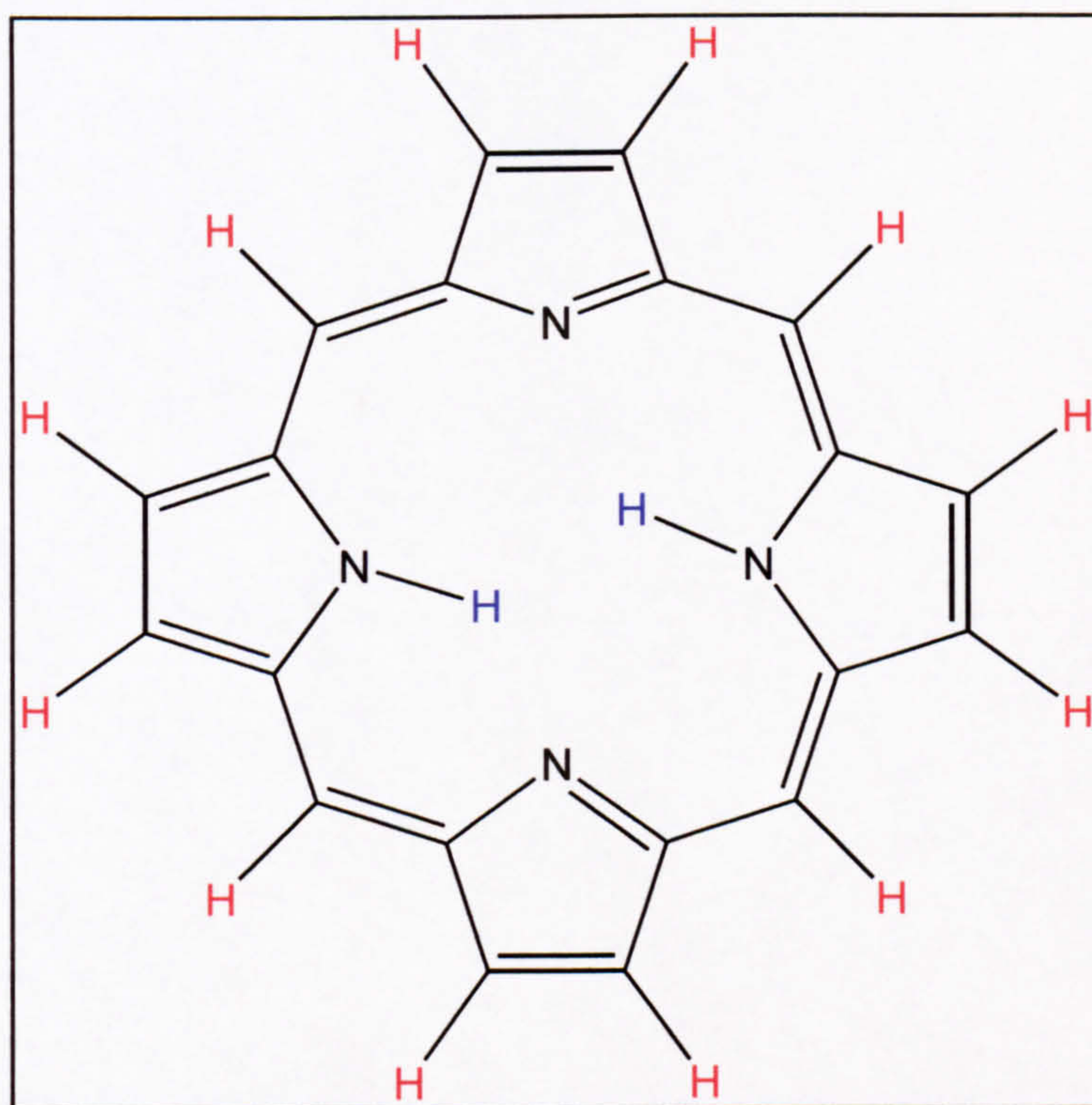


Figure 7 – Outer (red) and inner (blue) protons in a porphyrin macrocycle

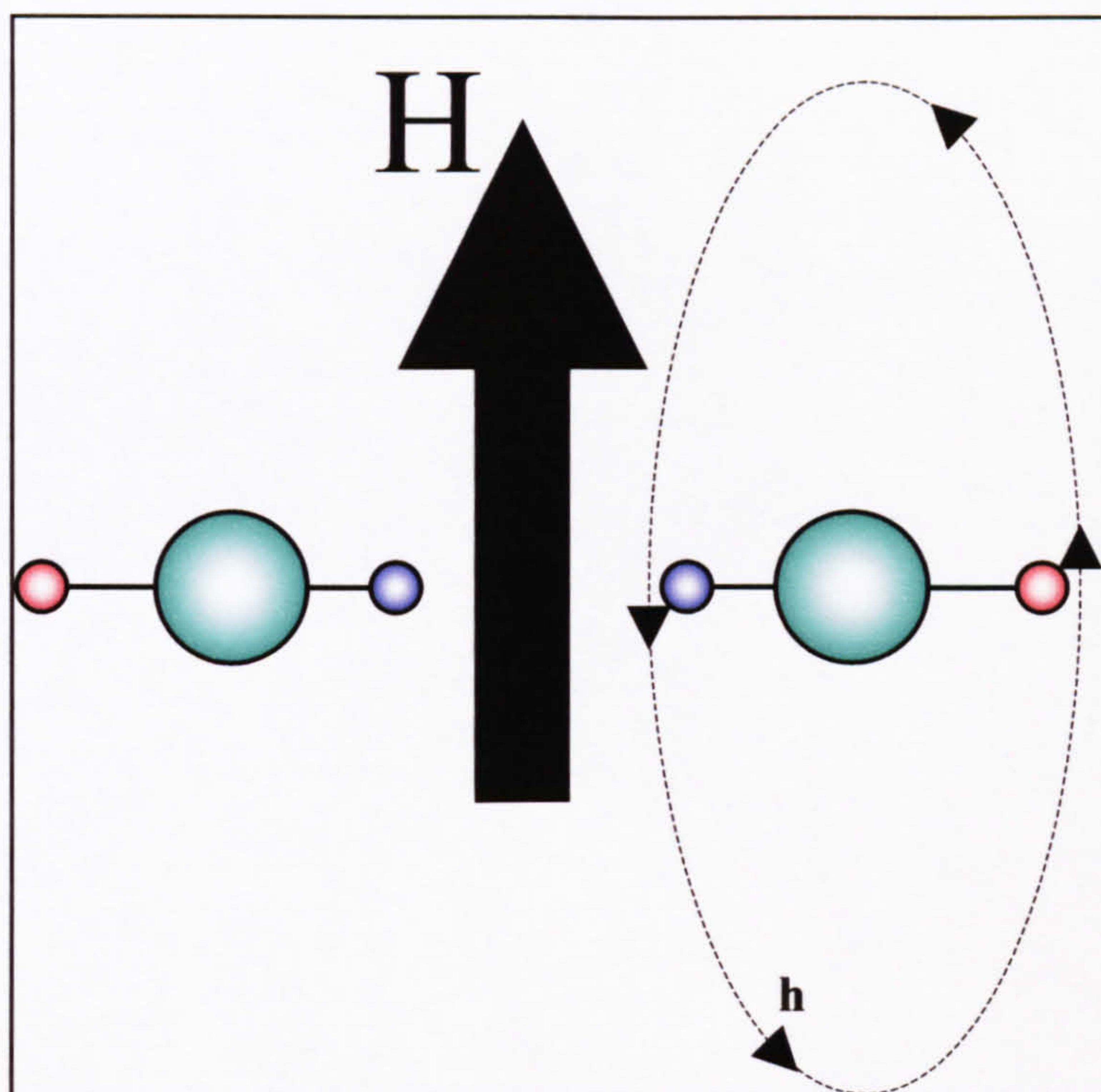


Figure 8 – Cross-section of the porphyrin macrocycle demonstrating the applied (H) and induced (h) magnetic fields

By examining Hückel's law of aromaticity, we can find further evidence of the nature of the bonding in these compounds. Hückel's law states that in order for the system to be aromatic, there must be $4n+2$ pi electrons (where n is an integer) (Figure 9) ⁽¹²⁾.

The atoms involved in the π -electron system are sp^2 hybridised, hence, the aromatic heterocycles tend to be planar ¹³.

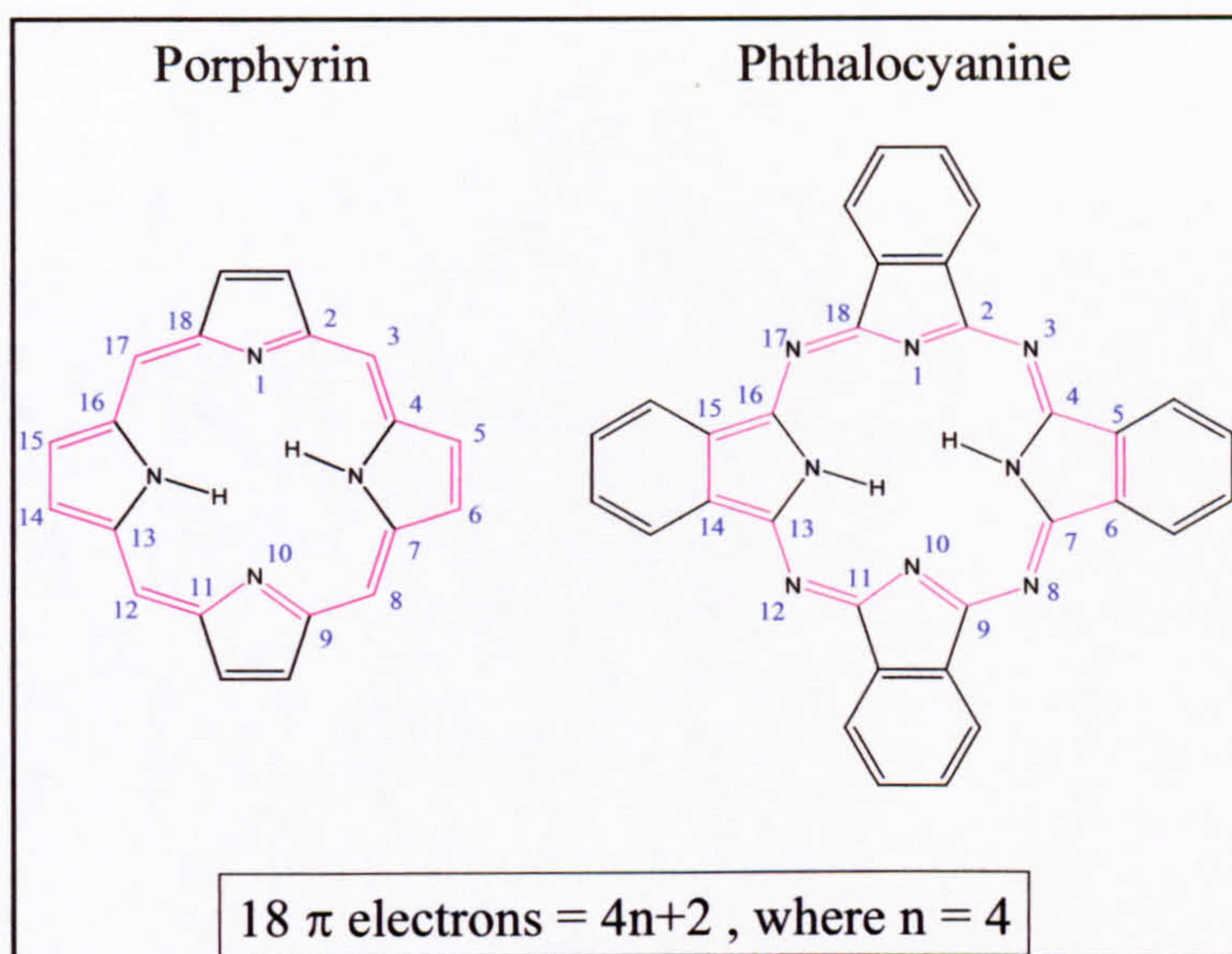


Figure 9 – Diagram showing porphyrins and phthalocyanines are Hückel aromatic

2.4 Modifications for Langmuir-Blodgett deposition

The unsubstituted metal-free porphyrins and phthalocyanines are not particularly suitable for deposition by the LB technique. The central ring system is hydrophilic and it requires substitution of hydrophobic groups such as an alkyl chain to form the amphiphilic molecule required. However it is a balancing act. The aliphatic chain is not usually involved in any of the processes the film may be used for (e.g. gas sensing, organic conduction) and it is there merely to enhance the LB film. Therefore the component density is reduced (particularly with multilayer films) and the response may be weakened. This group (Nanomaterials, Cranfield) are now starting to move away from the traditional long chain LB forming materials and dreaming up shorter chain moieties to improve the component density whilst still forming good Langmuir films.

3. Applications of porphyrins and phthalocyanines in molecular electronics

3.1 Dyes for CD discs

Phthalocyanines are well-known commercial blue-green pigments. In fact, the Bank of England uses a copper-containing metallo-phthalocyanine blue dye in £5 notes⁽¹⁴⁾. Probably the most common use for these macrocycles however, is their role in CD-R discs. The recordable CD consists of several layers (Figure 10)⁽¹⁵⁾. When the reflective layer is silver, the “bottom” of the CD will appear blue with azo as the dye and light green with phthalocyanine. When gold is the metal used, either a green tinge (cyanine) or just a golden colour (phthalocyanine) is seen. The principle behind these CDs involves a recording laser (the same wavelength as the reading laser – 780 nm but 10 times stronger), being focussed on the dye, causing it to absorb the light and convert it to heat (up to 300 °C). The resulting deformation in the polycarbonate layer and decomposition of the dye (altering the refractive index) leaves an optical mark⁽¹⁶⁾. The so-called 1’s and 0’s required for digital storage are derived from changes in the surface detected by the reading laser; the 1 corresponding to a pit wall and the 0 to any flat section.

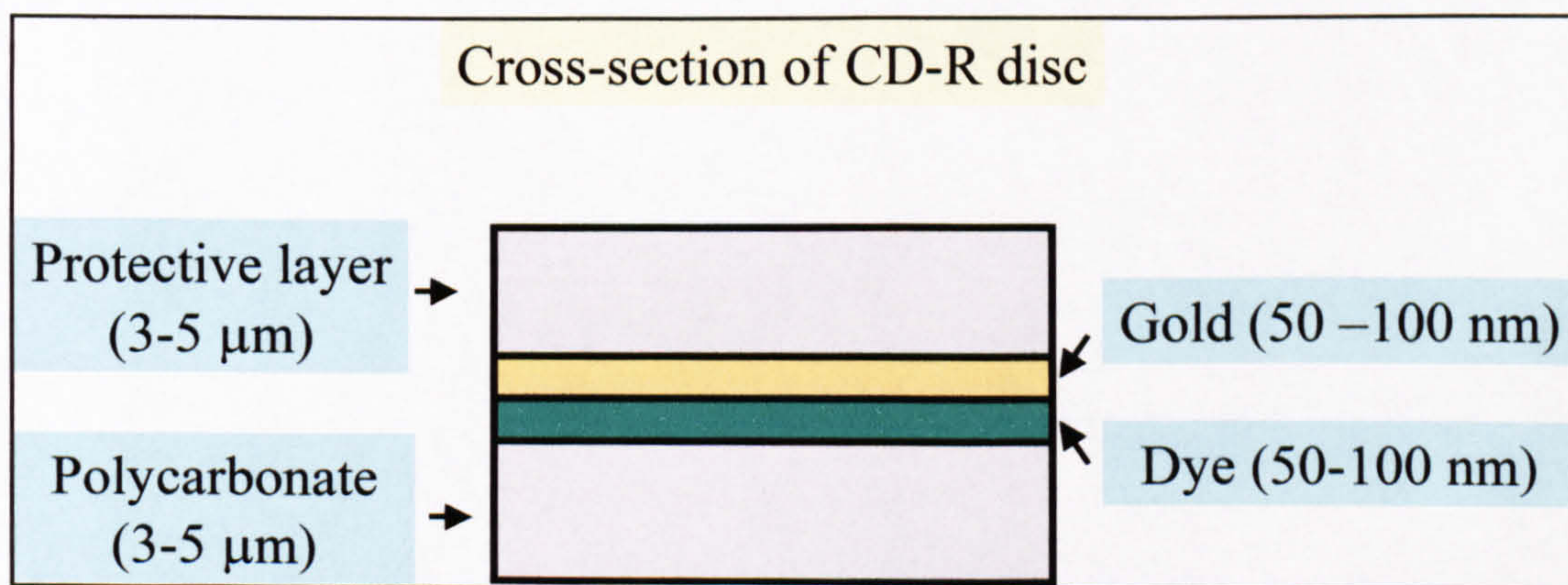


Figure 10 – Cross-section of a CD-R disc

The different types of dyes offer different lifetimes for the stability of the data recorded. For example, the green-tinged cyanine-based CD-Rs are only expected to last around 10 years. Alternatively, the golden or light-green phthalocyanine discs promise stability of up to 100 years. The recent additions of the azo (blue coloured discs) and hybrid (silver) cyanine-phthalocyanine dyes have produced claims that they are as stable as the more expensive derivatives ⁽¹⁷⁾.

3.2 Photodynamic Therapy

The use of phthalocyanines in photodynamic therapy (PDT) has also shown some early promise. The macrocycle is selectively absorbed into the cancerous cell and when irradiated, promotes the generation of singlet oxygen, which destroys the tumour ⁽¹⁸⁾. There are a number of mechanisms being investigated (Figure 11) and clinical trials are currently underway ⁽¹⁹⁾.

It is the treatment of anaerobic tumours however, that is proving the greatest challenge in PDT. Radical photogeneration may offer some hope using irradiation of several phthalocyanines (particularly titanyl moieties) in aqueous suspension to form OH radicals ⁽²⁰⁾.

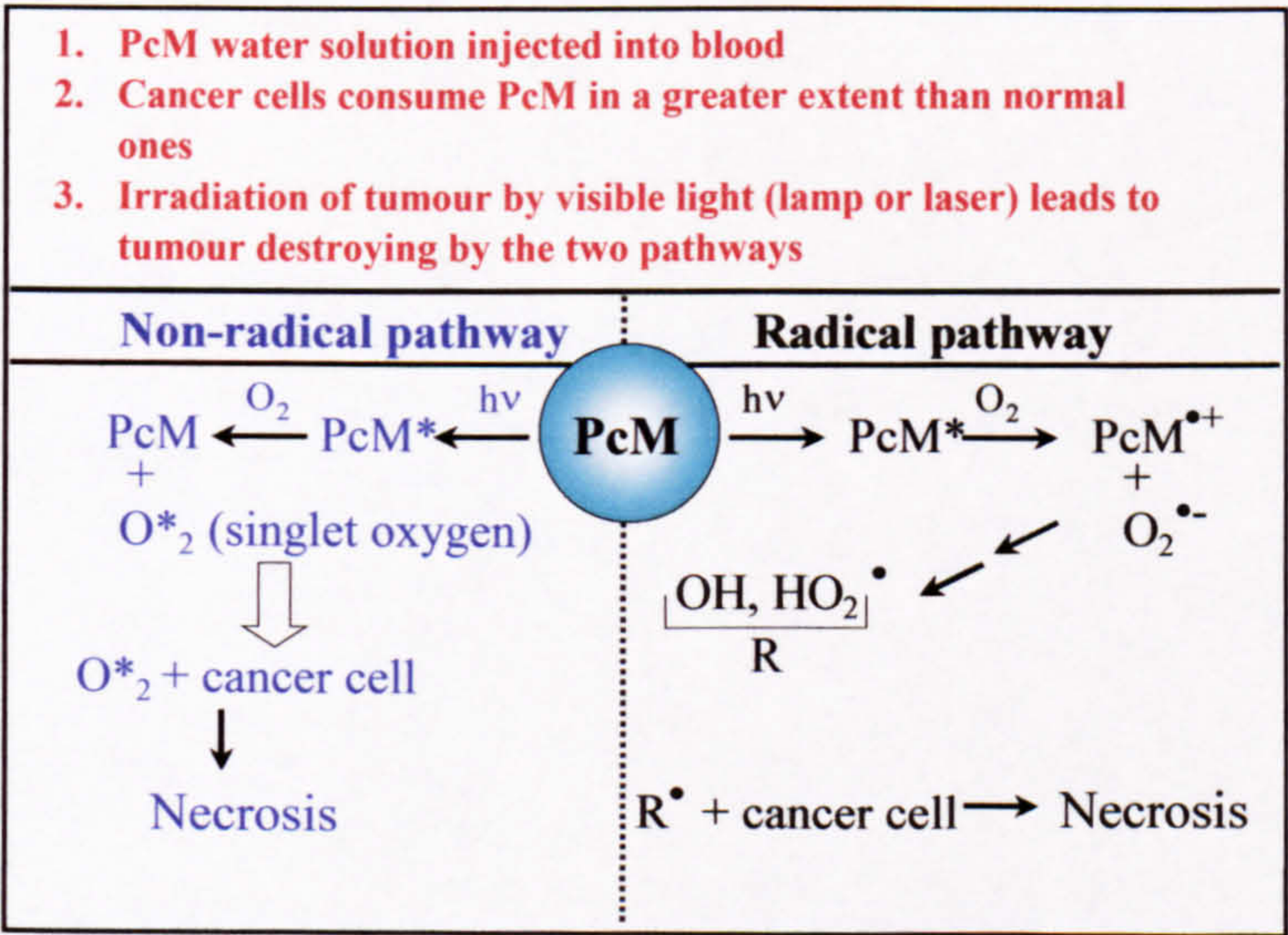


Figure 11 – Principles and two mechanisms of PDT of cancer

3.3 Donor-Acceptor systems with C₆₀

The use of phthalocyanines as a semiconducting material in solar cells or other photoelectric devices has gained a large interest. Indeed some species such as H₂Pc or TiO-Pc are already being used as photoreceptors in laser printers and photocopiers ⁽²¹⁾.

Fullerene (C₆₀) is a well-known electron-acceptor and when combined with phthalocyanines (good electron donors), the potential to form a *p-n* junction and increase the photoconductivity is often found ^(22, 23, 24).

The work on these C₆₀-macrocycle systems is not just restricted to the phthalocyanines. The search for an artificial version of the highly efficient plant photosynthetic light conversion has led researchers to the porphyrin series of compounds ^(25, 26). The porphyrin-fullerene donor-acceptor systems are now being investigated for their use in building devices in the “bottom up” style of molecular engineering that has been grabbing all the headlines ^(27, 28, 29, 30, 31).

3.4 Third-order nonlinear optics (NLO)

In the last few years, phthalocyanines have been studied as targets for second harmonic generation (SHG) ⁽³²⁾. This is the conversion of intense monochromatic light into radiation with twice the frequency (or half the wavelength). In a time when blue lasers were expensive, this application was seen as a method of converting the output from a cheaper 900 nm laser into the more sought after wavelength of 450 nm. Of course, recent laser engineering progress has now made blue lasers much cheaper, but SHG still remains an excellent method of characterising thin films (particularly LB deposited ones).

In order to be SHG-active, the molecules must be non-centrosymmetric; therefore the unsubstituted macrocycles are unsuitable in this application. However, this restriction does not apply to third-order nonlinear optical effects ^(33, 34, 35). The impetus for the increased research activity into nonlinear optical properties of phthalocyanines has been a search for a greater understanding of the structure-property relationship and the strong technical interest in all-optical signal processing ⁽³⁶⁾.

Phthalocyanines and porphyrins are suitable for third-order nonlinear applications as they possess a delocalised π -system and they can contain low-lying energy states (due to metal-to-ligand and ligand-to-metal charge transfer) ⁽³⁷⁾.

Typical values for $\chi^{(3)}$ are shown in Table 2.

Table 2 - $\chi^{(3)}$ values for various phthalocyanines (DFWM = degenerate four-wave mixing)

Molecule	Fundamental Wavelength (nm)	$\chi^{(3)}$ (in units of esu)	Reference
fluoroaluminium phthalocyanine	1060	5×10^{-11}	38
chlorogallium phthalocyanine	1060	2.5×10^{-11}	38
H ₂ -tetrakis (cumylphenoxy) phthalocyanine	605 (DFWM)	1×10^{-9}	39
Pt-tetrakis (cumylphenoxy) phthalocyanine	1064 (DFWM)	2×10^{-10}	37
Pb-tetrakis (cumylphenoxy) phthalocyanine	1064 (DFWM)	2×10^{-11}	37
H ₂ -tetrakis (cumylphenoxy) phthalocyanine	1064 (DFWM)	4×10^{-12}	37

3.5 Detection of molecules in the gaseous phase

In this application there are three characteristics that can describe the ability of the molecules to detect the analyte gas: response time, degree of response and selectivity. The response time is often dependent on the thickness of the sensing material, as the gas must permeate through the sensor head for maximum response. Gas sensing performance can also be optimised where there is a high surface area to volume ratio. Therefore thin films are particularly desirable and LB, spin-coating and thermal evaporation are often the techniques employed. The degree of response may be determined by not only the concentration of sensing molecules but also the number of

sites available for the gas to attack. For example, if the molecules are clustered together it may take more time for the gas to reach all the available reaction sites. The Langmuir-Blodgett deposition technique provides the desired control over both molecular orientation and density in each layer. The third factor is often overlooked when examining a material for its sensitivity to gas. If the sensor is to have commercial potential, it is important to determine whether the sensor is exclusive, selective or comprehensive in the presence of a range of gases. The non-exclusive nature of some sensors can be compensated for however, with the use of a series of different techniques and/or materials which when coupled together in an array (or neural net), forms a “fingerprint” response for a particular gas. In other words, the different responses of each sensor node are used together to determine which gas is present. This is sometimes referred to as an artificial nose ⁽⁴⁰⁾.

The highly conjugated π -system of the porphyrin and phthalocyanines provides rich ultraviolet-visible absorption spectra. The phthalocyanines in particular are readily oxidised and easily form the radical cation, which is a non-aromatic macrocycle and hence, its colour differs greatly ⁽⁴¹⁾. This can be monitored as the sensor is exposed to the analyte gas. The conductivity of the heterocycles provides another opportunity to monitor changes due to interaction with gaseous species. Porphyrins and phthalocyanines can also act as a host material for the adsorption of gases, which can be monitored through the quartz crystal microbalance and surface acoustic wave techniques ^(42, 43, 44).

Organic vapours are mainly concerned with the by-products and reagents of food and plastic processes. The number of gases that could be associated with this group is large. Typical examples are methylbenzene, trichloromethane, propanone and alcohols ⁽⁴⁵⁾.

Another industrially based application is gases that could be considered acid or base precursors. The monitoring of these gases is not only required for leak detection, but also for *in situ* control of reactions ⁽⁴⁶⁾. The gases are those that, when combined with water, form an acidic or basic solution. The most prominent examples are HCl and NH₃.

With possibly the greatest number of applications, oxidising gases are also the most studied of the three groups (see Table 4). Suitable examples of detection of these

gases can be found in such diverse areas as swimming pools (Cl₂), environmental monitoring (O₃), industrial processes (various halides), bomb detection (NO₂) and battery monitors on submarines (Cl₂).

It is the toxic gases that have attracted the most attention and this PhD thesis focuses on the common industrial reagent, chlorine.

Using Lexis®-Nexis® (a news archive database) ⁽⁴⁷⁾, chlorine-related incidents were downloaded from 1992 to 2000 inclusively, then categorised and analysed. Combined with the data published by Greenpeace in 1991 ⁽⁴⁸⁾, this information represents most of the chlorine-related accidents around the world between 1980 and 2000 (Figure 12).

Chlorine accidents can be broken down into a number of scenarios: at the swimming baths (municipal), at a production plant (production), during its use in another process (industrial) or even during transfer between locations (transport) (Figure 13).

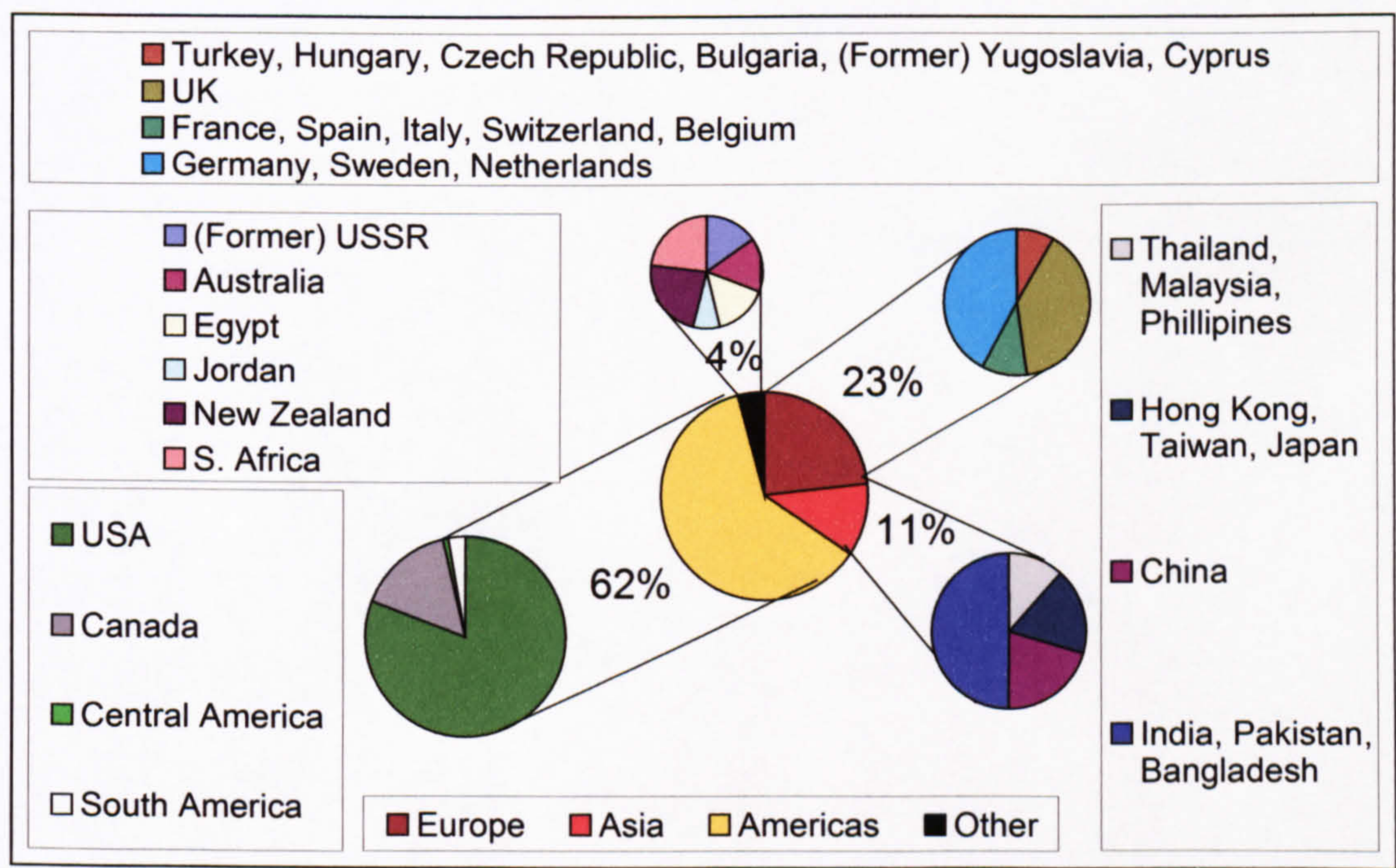


Figure 12 – Chlorine accidents around the world

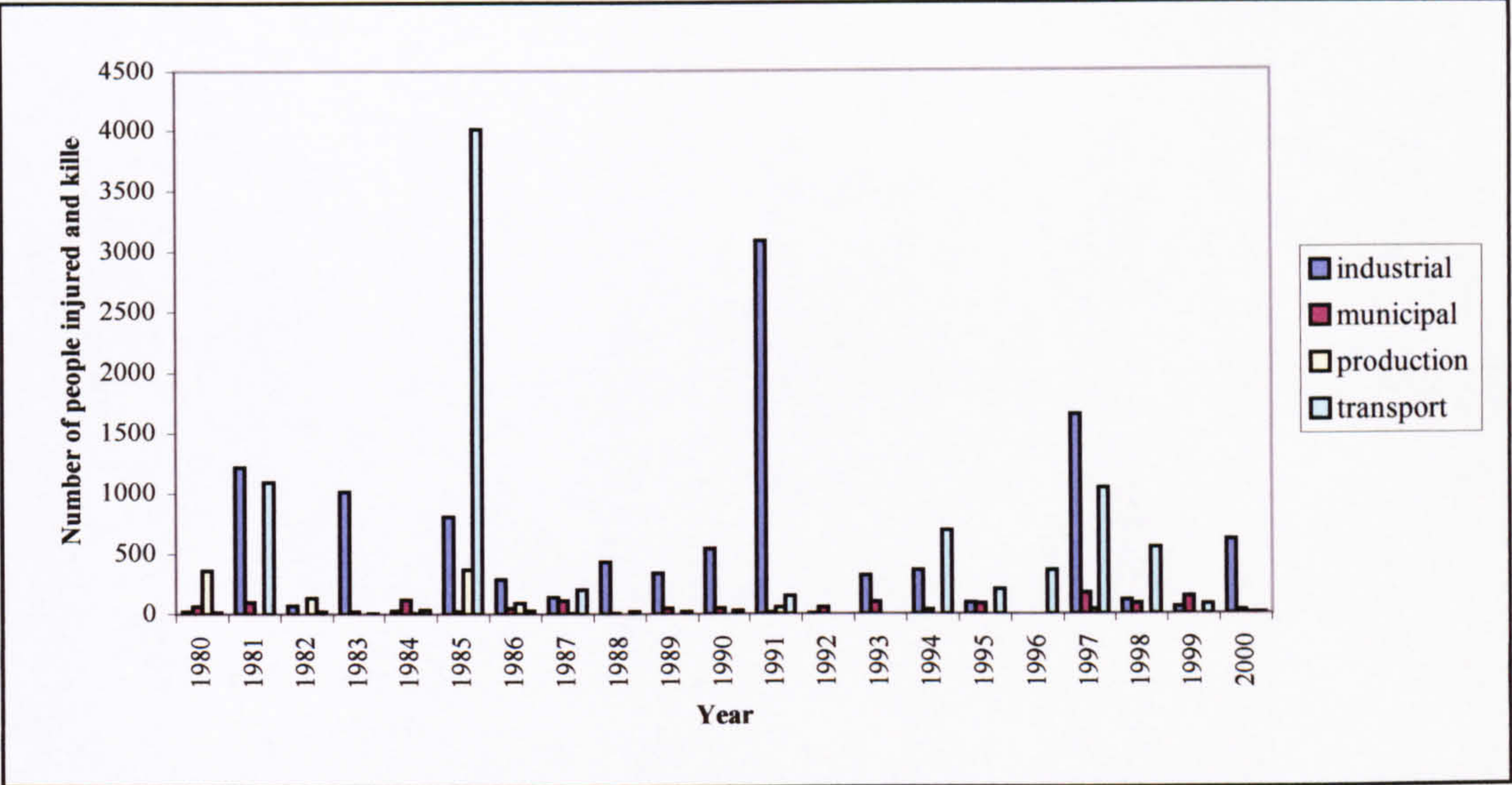


Figure 13 – Breakdown of type of chlorine accidents by year

3.5.1 Gas detection techniques

3.5.1.1 Optical Sensors

There have been many studies on the effect of gases on the optical properties of thin films (*see* Table 4). UV-VIS absorption, in particular has frequently been used to follow the changes in a sensor as it is exposed to the analyte.

The main advantages and disadvantages of optical sensors are shown in Table 3.

Table 3 – Advantages and disadvantages of optical sensors compared with other types

Advantages	Disadvantages
Frequently no requirement for a reference cell	Ambient light can interfere
Often a simple design	Often the sensors have a low selectivity
Easy to miniaturise	There are few long-lifetime, stable, inexpensive light sources

Compounds used in this technique may be tailored to absorb (before or after exposure to the gas) in the 460 and 700 nm regions, which is the wavelength of cheap commercially available LEDs and laser diodes. The signal from a photodiode is then measured and the response of the sensor determined via any change in the absorption at the particular wavelength of the light source. Whilst no reference cell is required, the light intensity may be monitored through a beamsplitter and photodiode to prevent any fluctuations in the output from affecting the response of the sensor.

Other types of “optical” sensor include diffuse reflectance and fluorescence, which produce comparative results to the absorption sensors but are more expensive to produce^(49, 50, 51).

3.5.1.2 Quartz Crystal Microbalance (QCM) sensors

Originally designed to monitor the progress of metal deposition in vacuum evaporators, QCM devices are showing some potential as sensors. Two metal plates separated by a piezoelectric crystal are used to generate a standing wave propagating through the bulk of the material. Any adsorption of vapours onto the surface of these plates results in a change in the resonant frequency of the system and hence, detection by mass. The selectivity of these sensors can be altered with different coatings, though the sensitivity may also depend upon the temperature and humidity of the carrier gas⁽⁵²⁾.

3.5.1.3 Surface Acoustic Wave (SAW) sensors

Similar to QCM based sensors, these also rely upon generating an acoustic wave, though the propagation is primarily along the surface rather than through the bulk of the crystal. This means that the SAW sensor is much more sensitive to changes on the surface than the QCM system. The sensor also operates at much higher frequencies (typically between 25-500 MHz *cf.* 5-30 MHz for QCM crystals) and has a reference line to prevent changes in room temperature or humidity from affecting the detection.

Again, coatings can help to improve selectivity of these devices and the production is relatively straightforward ⁽⁵³⁾.

3.5.1.4 Surface Plasmon Resonance (SPR) sensors

The technique is based upon the changes in a reactive film deposited on a thin gold layer. A laser (typically at 632.8 nm) is fired at the reverse side of the organic-coated gold layer, coupled into the surface plasmon mode with a prism, and the reflected light measured with a detector ⁽⁵⁴⁾ (Figure 14). As the prism is rotated, the measured reflectance follows a characteristic curve (Figure 15).

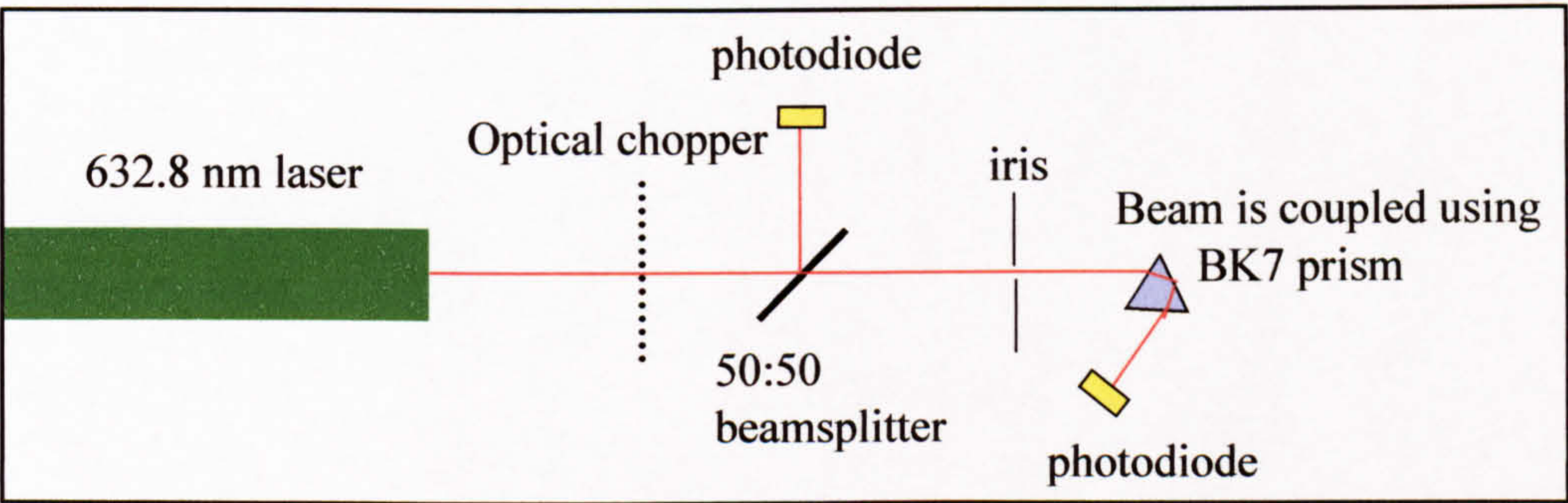


Figure 14 - Schematic of simple SPR apparatus

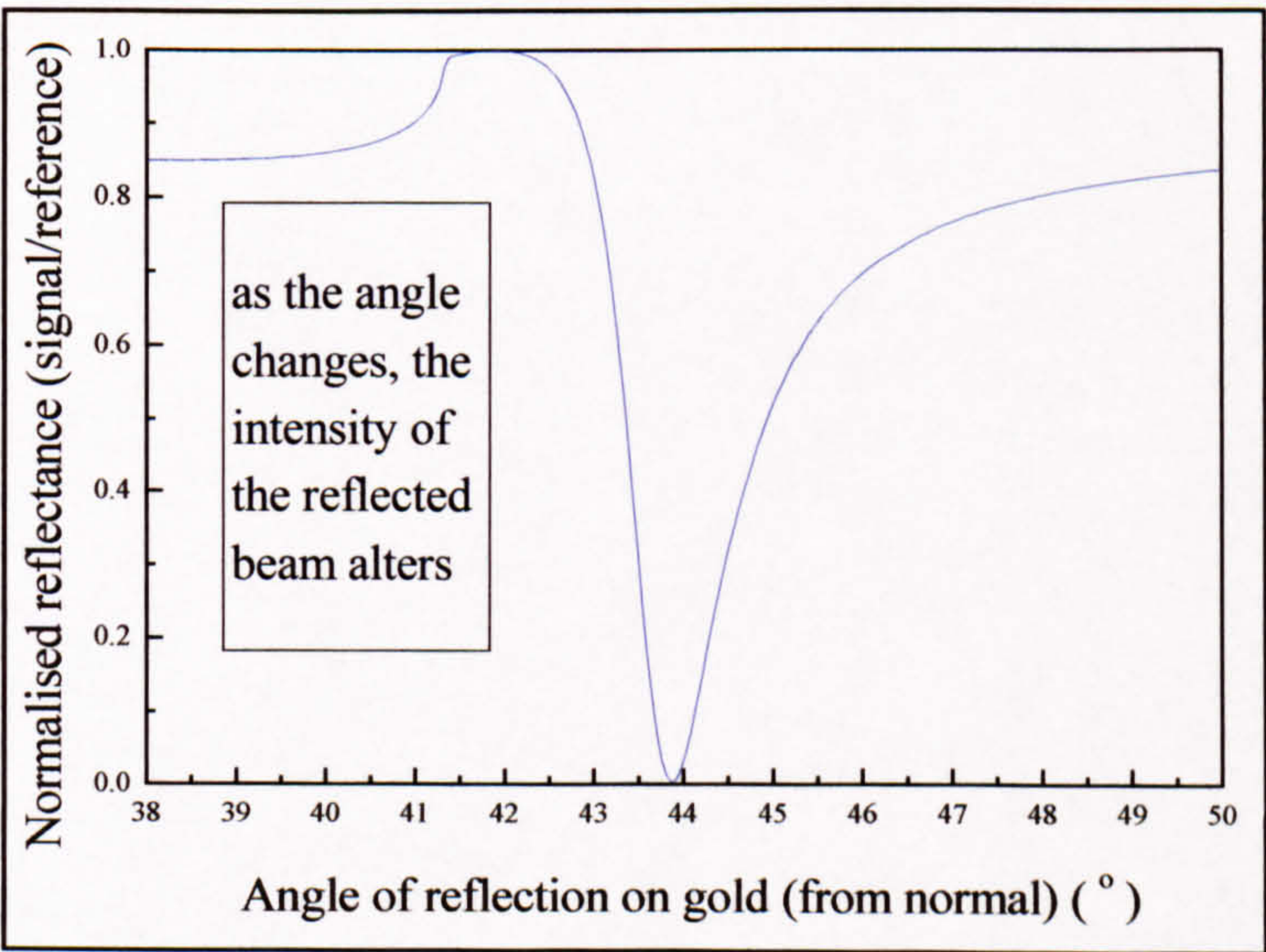


Figure 15 – Typical SPR scan from 38° to 50°

Whilst surface plasmon resonance is a localized effect, the plasmon wave generated does extend up to 200 nm into an overlying dielectric. This makes it a useful technique for monitoring changes close to the gold layer. A change in a deposited LB layer, for example when exposed to a gas, can be monitored through one or more of the following changes:

1. The angle of the minimum reflectance increases or decreases.
2. The depth of the minimum reflectance increases or decreases.
3. The minimum reflectance “dip” broadens or sharpens.

Typically, the fixed angle surface plasmon resonance sensors are preferred as they offer greater commercial potential (particularly the possibility of miniaturisation) ^(55, 56). The important feature of this technique is that before a measured response can be taken, the direction and magnitude of the change in reflected signal must be known. This is to ensure maximum sensitivity to changes in the SPR curve ⁽⁵⁷⁾.

By scanning across a range of angles, the three changes listed above may be detected individually. This might produce more selective sensors but with more equipment required, the potential for miniaturisation would be much lower.

The other alternative for scanning a range of angles is to use a charge coupled diode (CCD) array to capture a range of angles whilst in a fixed position ⁽⁵⁸⁾.

3.5.1.5 Electrochemical sensors

Electrochemical sensors encompass many different technologies: conductivity, semiconductor, capacitance, solid-state ionic and field effect transistor sensors. Of these, the conductive and semiconductive sensors are the most common (see Table 4).

The conductive sensor measures the change in the electrical conductance of a material with exposure to the analyte gas. Often, these sensors produce the best results

(in terms of sensitivity, selectivity or reversibility) when operated at elevated temperature (*see 3.5.2 A survey of gas sensing by thin films of tetrapyrrole pigments*).

Semiconductor sensors have the same disadvantages as the conductive sensors (best operated at elevated temperatures, poor reversibility) but they have improved sensitivity (*see 3.5.2 A survey of gas sensing by thin films of tetrapyrrole pigments*).

3.5.2 A survey of gas sensing by thin films of tetrapyrrole pigments

A summary of the research into phthalocyanine and porphyrin thin films exposed to different types of gases can be found below (Table 4).

Table 4 – Summary of research into gas sensing with porphyrins and phthalocyanines

Type of gas detected	Examples	Sensors used for detection				
		Optical	QCM	SAW	SPR	Electrochemical
Organic	benzene, trichloromethane, propanone	49, 59	44, 60, 61, 62, 63, 64	65	59, 66	67
Acid and Base Precursors	HCl, NH ₃ , SO ₂	68, 69, 70, 71	92	92		72, 73, 74, 75, 76, 77
Oxidising	X ₂ , NO ₂ , O ₃	68, 78, 79, 80, 81, 82, 83, 84, 85, 86, 87, 88	89, 90, 91	92, 93, 94, 95, 96, 97, 98	58, 85, 86, 94, 99, 100, 101, 102, 103	75, 104, 105, 106, 107, 108, 109, 110, 111, 112, 113, 114, 115, 116, 117, 118, 119, 120, 121, 122, 123, 124,

3.5.2.1 Phthalocyanines and oxidising gases

The UV-VIS spectrum of a Langmuir-Blodgett film of a 4-substituted phthalocyanine polysiloxane changes in a number of ways due to the presence of a halogen (I₂). A red-shift in the main absorption peak attributed to the adsorbed I₂ interacting with the π -electrons is accompanied by broadening of the absorption band, which according to quantum mechanics, is the result of a reduction in symmetry (due to LB film damage) and the states π and π^* being split by the adsorbed oxidising gas molecules ⁽⁶⁸⁾. The use of an amphiphilic 8-substituted copper phthalocyanine in a Langmuir-Blodgett film to detect an electron acceptor gas shows that the classic Davydov splitting observed for these structures is not observed after the introduction of an oxidising vapour, indicating that the initial herring-bone formation on the substrate is distorted by the NO₂ molecules. This effect is not seen in metal-free amphiphilic

phthalocyanines, leading to the conclusion that the central metal atom plays an important role in the interaction with electrophilic molecules like NO₂⁽⁸⁴⁾.

A vacuum-sublimed copper phthalocyanine film is an excellent NO₂ sensing material for use with QCM apparatus. When compared with GC-MS, the accuracy is comparable and the expense is much lower although the analysis time is much greater. This QCM method offers a real alternative to the expensive GC-MS⁽⁸⁹⁾. The comparison of different metal centres in a series of 8-substituted ethylhexyloxy phthalocyanines reveals that the central atom affects the response time and the sensitivity of a QCM. These sensors are not reversible even under elevated temperatures, optical absorbance spectra indicating that there is an increase in the number of sites unable to form a charge-transfer complex with NO₂ in the LB film^(90, 91).

The use of a SAW sensor coated in a 4-substituted sulfonated copper phthalocyanine provides an inexpensive, small and sensitive NO₂ sensor. The sensor has a linear response to the electron acceptor gas up to 12 ppm (with a mean sensitivity of 128 Hz/ppm) and an upper limit of 25 ppm. At this saturation point the response time is 10 minutes and the recovery time is 40 minutes; at greater concentrations the film becomes irreversibly damaged⁽⁹³⁾. However the use of lead phthalocyanine shows an even greater sensitivity and reversibility when the substrate is heated. In fact, the sensitivity increases so much for NO₂ that the upper detection limit of the sensor must be lowered to prevent the SAW sensor “jumping” to other frequency modes (when exposed to 0.64 ppm at a substrate temperature of 70 °C the resulting change in frequency is ~3 kHz). When the film thickness is reduced (15 nm) the evaporated lead phthalocyanine has a response time of a few minutes and a sensitivity of 800 Hz/ppm, the detection limit for this sensor at 120 °C is only 5 ppb⁽⁹⁵⁾. Thermal evaporation is expected to produce films that are compact and not easily accessible to the analyte gas. This is not seen with the lead phthalocyanine, clusters are likely to form during deposition initially forming a porous film (sensitivity increases with film thickness up to 10 nm)⁽⁹⁸⁾. The use of simple short chain silicon phthalocyanines (e.g. t-butyl) deposited onto a SAW sensor also shows good sensitivity to oxidising gases and produced a linear response (up to 170 ppm) and a lower detection limit of 40 ppb⁽⁹²⁾. Further investigations into the effect of the central metal atom on the sensitivity and

response time of SAW sensors shows that copper phthalocyanine has a faster response time but lower sensitivity (than iron phthalocyanine) to NO₂ ⁽⁹⁷⁾. When comparing a series of phthalocyanines using SAW and SPR sensors it is notable that thin films are preferred; the response times are much faster for both techniques and the sensitivity of the SPR method is much higher with thin films ⁽⁹⁴⁾.

The Langmuir-Blodgett film of a silicon t-butyl phthalocyanine may be a useful NO₂ sensor because the main absorption peak is at 633 nm (i.e. that of a HeNe laser). The film's absorption spectrum bleaches with exposure to an oxidising gas and partially recovers over a period of days at room temperature. The SPR gas sensing was performed on a silver-coated substrate with 10 layers of ω -tricosenoic acid deposited to protect the metal interface from the corrosive NO₂. The effect of the electron acceptor gas on the SPR curve of the sensor was to induce a small reduction in its halfwidth. There is no observed change in the minimum reflectance or the angle at which this occurs until significantly higher concentrations of the gas are used to attack the film. At this point it is likely that the angular shift observed is the result of the ω -tricosenoic acid protective layer failing to protect the silver film and the formation of an absorbing surface layer on the metal interface ⁽⁸⁶⁾. One interesting departure from the traditional use of silicon photodetectors in SPR experiments is the use of a CCD array to capture the whole SPR curve without the need for rotation stages. The use of a zinc butoxy carbonyl phthalocyanine deposited onto a silver layer to detect of 20 ppm NO₂ is shown to result in a reduction in halfwidth of the SPR curve and a shift to lower angles. This process was irreversible due to the formation of an absorbing layer on the silver ⁽⁸⁶⁾. Some reversibility can be found with the use of a gold layer (instead of silver), as it is more resistant to corrosive gases such as NO₂. The other advantage of using gold is that self-assembled monolayers can be deposited with ease, providing a simple and quick method of coating the film ⁽¹⁰⁰⁾. Thin films of crown-ether- and 8-substituted phthalocyanines which have been spin coated onto gold-coated substrates are capable of detecting NO₂ concentrations of circa 1 ppm. The reversibility is lower than electrochemical equivalent sensors but their dependence on humidity is significantly less ⁽¹⁰¹⁾. The SPR characterisation of a crown-ether phthalocyanine shows that when exposed to an electron-acceptor gas there is a significant reduction in ϵ_i (the imaginary

part of the dielectric permittivity) at wavelengths close to the main absorption band of the dye, and good reversibility^(102, 103).

The comparison of an asymmetric phthalocyanine (with one crown ether ring attached) deposited by two methods (LB and spin coating) shows markedly different semiconducting gas-sensing properties. It is likely that the densely packed and highly ordered Langmuir-Blodgett films hinders the diffusion of the gaseous molecules thereby reducing the exposure of the bulk of the film to the gas which therefore reduces the sensitivity of the film and increases the response and recovery times. The randomly orientated and more porous spin coated films that have a higher sensitivity and lower response time demonstrate that the physical structure and molecular packing of the molecules affect the gas sensor ability⁽⁷⁵⁾.

The effect of NO₂ gases on the conductivity of thin phthalocyanine films can be monitored as a gas sensor⁽¹²⁴⁾. The combination of oxidising gas acting as a π -electron acceptor and the weak interaction between the positive charge (delocalised over the phthalocyanine ring) and the negative charge localised on the NO₂ produces an increase in the conductivity of the film^(104, 105, 108, 115). Whilst the response times are relatively fast, the recovery period is insufficient for practical uses. Therefore the substrate is heated to promote desorption of the gaseous molecules^(106, 109, 110, 114). It can also be shown that for some phthalocyanines, the use of a heated substrate increases the sensitivity of the sensor^(111, 112, 116, 122, 123). Whilst some structurally disordered films can offer more potential sites for the electron-accepting gases^(113, 120), other more ordered films also have high sensitivity and low response and recovery times^(117, 118, 121). A comparison of three different phthalocyanine films, one pure, one cooled to 77 K and one doped (post-deposition) with NO₂ shows that they all follow a linear response to the increase in gas concentration, although the NO₂-doped phthalocyanine sensor has a response 20 times the magnitude of the other two films⁽¹¹⁹⁾.

3.5.2.2 Porphyrins and oxidising gases

A comparison of zinc and metal free sulfonamido porphyrin LB films shows that the former responds poorly to chlorine gas, only resulting in a small decrease in the

Soret absorption band, but that the latter however, forms a dication through the addition of 2 protons to the central ring system. This is characterised by a reduction in the main absorption peak at 420 nm, a decrease in the Q band between 500 and 650 nm and the formation of new bands at 445 and 650 nm. It is thought that the metal atom effectively quenches any protonation of the central ring and a π -radical cation is formed through interaction with the electron acceptor gas. The metal free porphyrin however, forms a dication upon exposure to an oxidising gas (protonation of the central ring is likely to occur due to an interaction between the chlorine and atmospheric water). The orientation of the porphyrin in the Langmuir-Blodgett film is shown to have an effect on its gas sensing properties. The sensitivity is increased when the central ring is parallel to the substrate, thereby making it more accessible to the gas and indicating that it is this π -electron system which is the gas-sensitive region. For this particular porphyrin, the saturation point occurs at 2 ppm and repeated dosing experiments show that the sensitivity is reduced after exposure to concentrations exceeding this. It is also seen that a small increase in temperature of the film increases the sensitivity and reversibility of the gas sensor ^(78, 79, 80).

The use of ultra fast LB deposition with an ethylhexyloxy (EHO) free base porphyrin indicates (by AFM) that clusters of molecules are deposited onto the surface of the substrate and the significant separation between these $\sim 1 \mu\text{m}$ domains allows an easier route for the gas to diffuse through the film. These porphyrin assemblies are much thicker than expected and these island-like formations may be explained by one of two theories. Either the clusters were pre-formed on the water surface or small droplets of water (with the monolayer on) are formed during the transfer process. These droplets evaporate, leaving the porphyrin monolayer in a patchy form and subsequent depositions involve preferential film growth onto these porphyrin assemblies. The macrocycle forms the dication upon reaction with chlorine and as only dry gases were used, the source of the water required to react with the oxidising gas in order to protonate the central ring must be the LB film itself. A comparison of the gas sensing properties of porphyrins trapped in sol gel matrices and their LB equivalents using EHO and ethylbutoxy (EBO) porphyrins demonstrates a greater sensitivity for an electron acceptor gas was found with the dye-doped sol gel films. These sensors are simpler to manufacture although there was evidence of strong moisture dependence, unlike the LB

films. Further studies on the LB films of these porphyrins show that the sensitivity to the gas is reduced when the substrate temperature is increased because desorption is preferred to adsorption ^(80, 81, 82, 87).

A 4-substituted long chain (stearamido) porphyrin reacts rapidly with chlorine gas (5ppm in Nitrogen) in a similar fashion to the ethylhexyloxy and sulfonamido porphyrins mentioned previously. It is more noticeable that the interaction is a two-stage process with a quasi-static decay of the main absorption band (due to oxidation by the gas) coupled with a quasi-exponential growth at 460 and 700 nm (due to dication formation) ⁽⁸³⁾. The use of a silicone rubber matrix to encapsulate a porphyrin free base has the advantage of simpler deposition whilst maintaining a high permeability for the gas to attack the dye. The use of fluorescence as the method of sensing has further indicated the presence of a dication on reaction with an oxidising gas such as Cl₂ and control of film temperature has improved reversibility ⁽⁸⁸⁾.

The use of an SPR sensor with an EHO porphyrin coated onto a silver layer shows some sensitivity for NO₂ at 488 nm but poor detection at 633 nm. It is likely that the optical properties (i.e. thickness and dielectric permittivities of the film) measured at 488 nm are related to the dispersion properties due to the absorption band of the dye. Therefore the true structural properties were estimated from measurements taken at 633 nm ⁽⁹⁹⁾.

4. The aim of this thesis

Some of the dyes studied in this thesis have never been characterised in Langmuir-Blodgett films before. Others (particularly the copper *tert*-butyl phthalocyanine) have been the subjects of numerous research projects on thin film gas sensors and their results are well known. The inclusion of these established films offers the chance to compare and contrast known results with those obtained in this thesis and attempt to identify the role of the chemical structures of these materials in gas sensing.

The accuracy of the analysis of Pressure-Area Isotherms (a key experiment in any Langmuir-Blodgett-based studies) has always been subject to the experience of the experimenter. A technique that relies upon pure fact and not interpretation and

guesswork would provide a more reliable method of analysing the floating Langmuir films and hence offer greater insights into the characterisation of the deposited dyes.

The use of surface plasmon resonance and ultraviolet-visible spectroscopy for gas sensing has long been established. These methods provide the ability to monitor changes in a deposited thin film where there is some change in the electronic properties of the film. For example, for ultraviolet-visible gas sensing to be successful, there must be a change in the absorption spectra after exposure to the analyte gas. In the case of the macrocycles, this may be achieved through the interruption of the delocalised π -electrons flow around the unsaturated ring system.

It is the aim of this thesis to characterise some porphyrins and phthalocyanines, determine an accurate method of analysing the Pressure-Area isotherms and determine whether any of the materials are sensitive to chlorine gas using surface plasmon resonance and ultraviolet-visible spectroscopy.

CHAPTER TWO

Experimental procedures

1. Synthesis of Materials

A short series of phthalocyanines (dyes I to III, p 60) were synthesised by Prof. C. L. Honeybourne (UWE, Bristol) and several free-base porphyrins (IV to IX, p 77) and a triple-layer porphyrin-phthalocyanine complex (X, p 94) were provided by Dr. T. H. Richardson (Sheffield University).

2. Preparation of Solutions

All the materials studied were first dissolved in trichloromethane (UL grade, Ultrafine Ltd.) at a relatively low concentration (circa. 0.01 mg ml^{-1}). Initial analysis showed that even at 0.1 mg ml^{-1} , particulate matter was still present in the solution. The use of this solvent, as opposed to another more suitable solution was due to the heavy emphasis on Langmuir-Blodgett experiments (for which trichloromethane has ideal properties). The material was weighed in a small (12 mm x 4 mm x 4 mm) aluminium boat on an electronic balance (Ohaus 200D, 0.01 mg sensitivity). The boat and the material were transferred into a volumetric flask that had been cleaned in an ultrasonic bath with a series of solvents (isopropanol, trichloromethane and ultra-pure water). The vessel was filled with trichloromethane to the mark on the neck of the flask (the volume of the aluminium boat was considered negligible). The solutions were carefully mixed using wrist rotation to prevent any fracturing of crystals due to more vigorous methods (e.g. sonication, violent vertical shaking etc.). The volumetric flasks were covered with aluminium foil to prevent any light degradation.

3. Pressure-Area Isotherms

The characterisation of the Langmuir films of each dye was performed on a Nima Technology 601 isotherm trough (Figure 16). The PTFE lining was cleaned prior to use with a 1:1 mixture of isopropanol and trichloromethane and lint-free tissues (from Countdown Cleanroom Systems). On a regular basis, the trough was also cleaned with a warm potassium octanoate solution and rinsed with ultra-pure water. Before isotherms could be measured, three calibrations were required. Firstly, the area was measured and compared against the displayed data; the settings were adjusted as required.



Figure 16 – Isotherm trough housed in a cleanroom environment on a vibration isolation table

Secondly, the barrier speed was calibrated using the in-built software. Finally the pressure sensor's microbalance was calibrated for a weight range of 100 mg. Once

these had been performed, the trough was filled with fresh ultra-pure water (obtained from the Millipore (Milli-Q 185 Plus) ultra-pure system (which, in turn, was supplied with water from a Fiestreem Cyclon distillation unit) ensuring that the meniscus of the subphase was sufficiently positive to allow for cleaning. The barrier was closed and, using a plastic Pasteur pipette attached to a water aspirator (Capex 2LC), any dust or particulate matter was removed from the water surface. The water level was adjusted so that the meniscus was only just visible above the level of the PTFE lined side (i.e. a positive meniscus).

A piece of chromatography paper (Whatman chromatography paper, 10 mm x 0.1 mm x ~20 mm) was attached to the pressure sensor, then after lowering into the water, it was lifted out until just before collapse of the meniscus around it. This ensured maximum sensitivity to any changes in the surface tension of the water. The system was then left to allow the paper to equilibrate with absorption of the water (usually this was when the pressure sensor had reached -73 mN m^{-1}). During this time, the water surface was protected from any further contamination with a plastic cover. During the experiments, this cover was removed to prevent water or solvent vapour being trapped at the water-air interface, which might have affected the pressure sensor or floating film. Once the pressure sensor had stabilised the reading was zeroed and the barrier opened. The material being studied was deposited onto the water surface using microsyringes (Hamilton 500 μl or 100 μl), which had been previously washed with trichloromethane and the relevant solution. The dye was spread over the water surface (avoiding the area around the pressure sensor to prevent direct absorption onto the Wilhelmy plate) and allowed to evaporate for around 10 minutes. For very dilute solutions where a large volume of dye was needed to fully appreciate the isotherm graph, no more than 1000 μl was deposited without a break to allow solvent evaporation. In these circumstances, particular care was taken to look for telltale signs of bilayer formation. This can manifest itself in a number of ways. Sometimes lensing can occur where new drops of dye solution is added to a section of subphase with a solid monolayer and forms what looks like a bubble on the surface. More often, film-breaks are visible as thin dark coloured lines around the edges of the surface water area.

The barrier was closed at a uniform rate of $30 \text{ cm}^2 \text{ min}^{-1}$, which is generally considered slow enough for molecular re-orientation on the subphase, slow enough to

mask any dynamic effects but quick enough to prevent the dye collecting at the edges of the trough and distorting the isotherm graph. Once the data has been collected, the material was removed from the water surface using the Pasteur pipette and water aspirator. The trough was again cleaned with the 1:1 solvent mix and lint-free tissues ensuring that all areas were completely free of dye.

4. Cleaning of Substrates

The substrates mainly used in this work were glass microscope slides (BDH super premium microscope slides, 0.8-1.0 mm thickness 25 x 75 mm²), gold-coated glass microscope slides and quartz crystals (International Crystal Manufacturing Co., 10MHz Quartz oscillators).

4.1 Glass slides

The glass slides were rigorously cleaned with the following procedure:

1. Two sets of 19 slides were cleaned in one session, they were only chosen from brand new un-opened packs (each packet containing 50 slides).
2. They were checked for blemishes and scratches (on average 9 or 10 were discarded from each new pack due to flaws), ensuring that the substrates were isolated from finger grease by using powder-free gloves.
3. The slides were mounted in dye racks, immersed in isopropanol and sonicated in a water bath (making sure that the water level of the water was above that of the slides) for 15 minutes.
4. Using plastic tweezers, each slide was removed from the isopropanol, gripped between a gloved forefinger and thumb and wiped in one direction first in an area of lint-tissue previously doused with a little propanone, then in a clean (dry)

area in the same direction. This removed the polish applied to the slides at manufacture without smearing.

5. After wiping, the slides were immediately placed in another staining rack already immersed in trichloromethane.
6. The slides were sonicated in the following solvents for 15 minutes each:
 - a. Trichloromethane
 - b. Isopropanol
 - c. Ultra-pure water
 - d. Isopropanol
 - e. Trichloromethane
 - f. Isopropanol
 - g. Ultra-pure water.
7. Finally the slides were immersed in isopropanol and refrigerated until required.

When the slides were to be used, they were removed from the solvent using plastic tweezers and immediately dried in a fast stream of air. The solvent was “pushed” by the air towards the tweezers to remove any lingering contaminants from the surface of the substrates. The solvent was not allowed to just dry on the slides as this often caused streaks and smears to appear. On warmer days when the solvent was evaporating too quickly for this method, they were removed from the isopropanol and then washed in a stream of ultra-pure water and dried as above.

4.2 Quartz Crystals

These substrates were not only much smaller than the microscope slides but also used more than once. The cleaning was a much simpler process (as no polish was present on the crystals): washing the crystals with trichloromethane, isopropanol and ultra-pure water. Any droplets of water left on the substrate were removed with a lint-free tissue using a dabbing technique to prevent smears, streaking and more importantly, avoiding breaking the crystal’s delicate thin metal arms (which attach the gold electrodes on the surface of the crystal to the power supply and measuring device).

At the conclusion of the experiment, the same procedure was followed to ensure that they were stored in a clean condition.

4.3 Gold-Coated Glass Slides

The microscope slides used for deposition of gold were cleaned as described in the *Cleaning of Substrates – Glass slides* section. After the coating of the gold layer and removal from the vacuum chamber, the slides were washed in the same procedure as the quartz crystals. This time however, any water droplets were either driven from the surface with a stream of air, or allowed to remain (if the substrate was about to be used for deposition). Any use of lint-free tissues to remove the extraneous liquid would have resulted in partial or even full removal of the very thin gold layer.

5. Langmuir-Blodgett Deposition

Once the Langmuir film had been examined using the isotherm technique, a Langmuir-Blodgett film was deposited onto a substrate. For quartz crystals, a Nima Technology series 2000 trough (Figure 17) was used with a vertical dipper modified to hold the circuit box attached to the crystal.



Figure 17 – Series 2000 Nima Technology single compartment round trough

For all other depositions, a Nima technology 622 alternate layer trough with a rotating dipper mechanism was utilized (Figure 18). The procedure employed with both pieces of equipment was essentially the same.

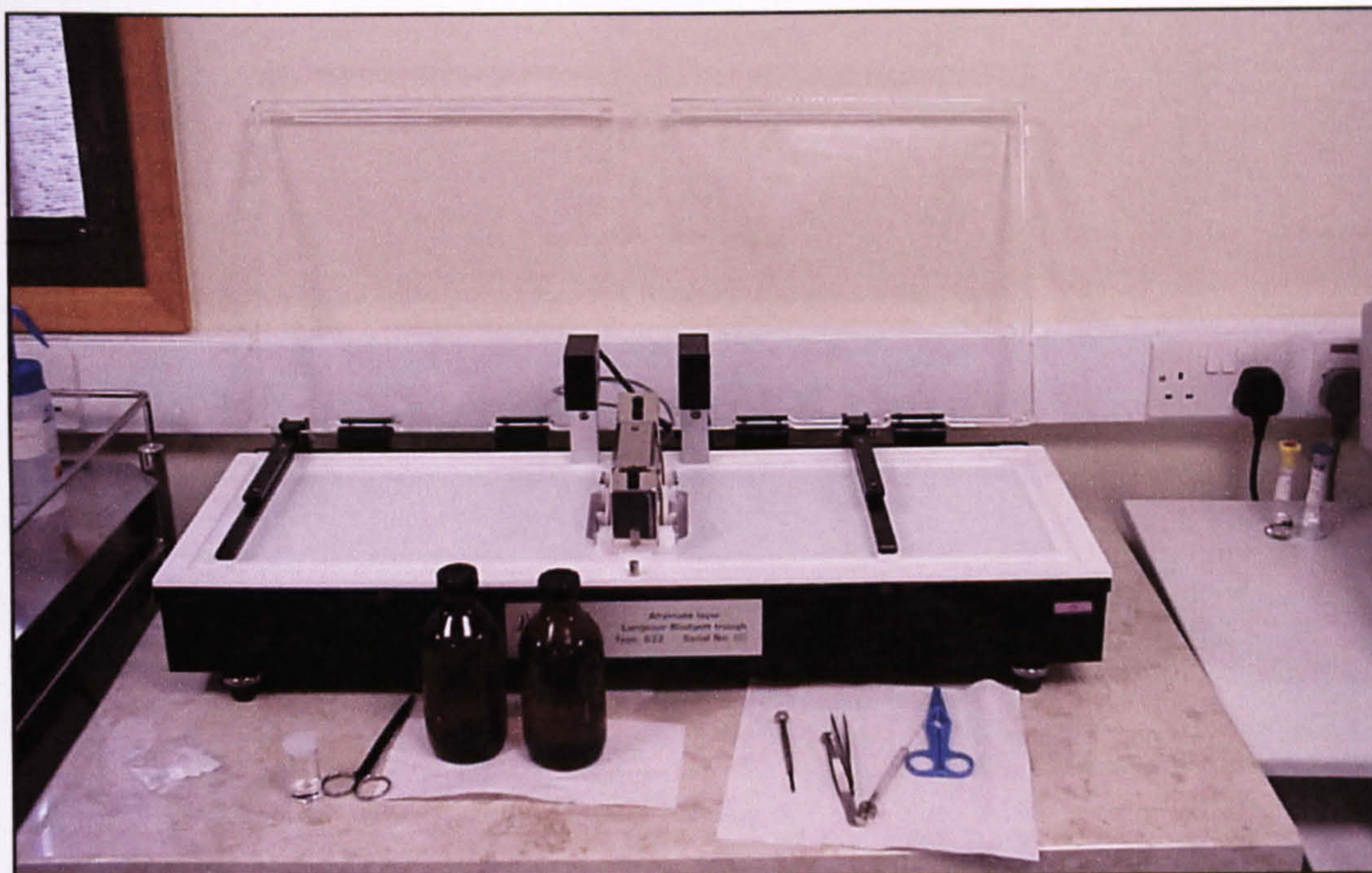


Figure 18 – Alternate layer trough, Nima Technology 622 double compartment

The PTFE lining was cleaned with the same method described in the *Pressure-Area Isotherms* section of this chapter and the pressure sensor's microbalance was calibrated for a weight range of 100 mg. Once the water had been added and the Wilhelmy plate given time to reach its equilibrium (then zeroed), the dye was spread over the water surface (in the case of the alternate layer trough, the side where the slide would penetrate the air-water interface on the down-stroke was kept clean). After allowing the solvent to evaporate, the area available to the molecules on the water surface was reduced to a pre-determined figure and, using a feedback from the surface pressure measurements, the barriers automatically adjusted to maintain this value. For the alternate layer troughs, the deposition of the Langmuir-Blodgett films then proceeded at 7 mm min^{-1} during the breaching of the air-dye-water interfaces and 100 mm min^{-1} elsewhere. For multilayers, the speed was reduced to 50 mm min^{-1} in the region where the newly deposited layer was exposed to the air, to allow it to dry and help reduce the loss of the film on the down-stroke into the clean (water) side of the trough. For the series 2000 troughs, the crystal was lowered into the water **before** any dye was spread. Once the required surface pressure was achieved, the deposition commenced at 7 mm min^{-1} .

In both cases, when the deposition was complete any water droplets were allowed to evaporate in the air for fear of damaging the fragile thin films with a lint-free tissue or a stream of air.

The troughs were cleaned in exactly the same way as described in the *Pressure-Area Isotherms* section of this chapter.

The equipment used for depositing these materials was not area-calibrated. This meant that the transfer ratio (a way of measuring the approximate level of coverage of the substrate) could not be calculated accurately. However, comparisons of the up-stroke and down-stroke ratios of multilayers indicated whether the films were being removed when re-entering the water.

6. Ultraviolet-Visible Spectroscopy

The ultraviolet-visible spectra (UV-VIS spectra) of the dyes both in solution (trichloromethane) and after deposition were recorded using a Perkin Elmer Lambda 7 spectrophotometer.

6.1 Solution

Using a pair of matched quartz cells, a background scan of trichloromethane (in both the sample and reference line) was taken. The cell in the sample line was emptied and refilled with the dye solution (see *D.2 Preparation of Solutions*) and a spectrum between 200 nm and 900 nm obtained. Occasionally, further dilution of the dye was required to prevent saturation at certain wavelengths.

6.2 Monolayer

A background scan of clean dry slides from the same cleaning batch was run before replacing the sample line with the newly deposited substrate. UV-VIS spectra

were obtained between 300 nm and 800 nm, though often the absorption of the glass at 330 nm meant analysis could only take place above 350 nm.

7. Quartz Crystal Microbalance (QCM) Measurements

After cleaning the series 2000 trough (see *Pressure-Area Isotherms*) and the quartz crystal (*Cleaning the substrates – Quartz Crystals*), the Wilhelmy plate was allowed to equilibrate in the freshly cleaned water (a plastic Pasteur pipette and aspirator were used to remove any dust and floating matter from the subphase). In the meantime, the quartz crystal was being driven by a 9.01 V power supply (Thandar TS15) and its frequency recorded. To prevent any external effects such as static, air movement, dust etc. during this period the crystal was housed in a cell lined with aluminium foil and earthed. When the frequency change over 10 minutes was less than 1 Hz the power was cut and the crystal lowered under the water surface. The deposition of the monolayer then commenced (see *Langmuir-Blodgett Deposition*).

Again the crystal was placed in the earthed isolation chamber and the power supply reconnected. The frequency was recorded and noted every 45 minutes. Once the frequency change was less than 1 Hz, the value was compared to that obtained from the clean substrate and using the following calculations, the area per molecule on the substrate calculated (Equations 3-7).

The experiment was repeated for the same dye with fresh films deposited at the same surface pressure. At least 5 measurements were taken for each material and the average molecular area considered. The range of results for each molecule was also examined to determine the degree of order present in the deposited film; an ordered film generally has a lower range of results compared to randomly orientated films.

Sauerbrey’s equations ⁽¹²⁵⁾:

$$\Delta F = \frac{-2F_o^2}{A\sqrt{\rho_q\mu_q}}\Delta m$$

Equation 3

or

$$\Delta m = \frac{-\Delta FA\sqrt{\rho_q\mu_q}}{2F_o^2}$$

Equation 4

Table 5 – Sauerbrey’s calculation symbols

Symbol	Meaning	Unit / Value
Δm	Change in mass	g
ΔF	Change in frequency	Hz
A	Electrode area	2.059 x 10 ⁻⁵ m ²
ρ _q	Density of quartz	2.648 x 10 ⁶ g m ³
μ _q	Shear modulus of quartz	2.947 x 10 ¹³ g m ⁻¹ s ⁻²
F _o	Fundamental frequency of QCM	10 x 10 ⁶ Hz
A _{mol}	Area per molecule	nm ²
MW	Molecular Weight	g mol ⁻¹
N _A	Avogadro’s constant	6.022 x 10 ²³ molecules mol ⁻¹

Therefore

$$\Delta m = -(9.09 \pm 0.01) \times 10^{-10} \Delta F$$

Equation 5

Using ω-tricosenoic acid to calibrate:

$$\Delta m = -(9.44 \pm 0.01) \times 10^{-10} \Delta F$$

Equation 6

Using Equation 4, the change in mass (i.e. the amount deposited) is calculated and the area per molecule was determined by:

$$A_{mol} = \frac{2A(MW) \times 10^{18}}{N_A \Delta m}$$

Equation 7

8. Deposition of Gold Layer

The gold layer was deposited onto glass microscope slides using an Edwards 306A thermal evaporation unit (Figure 19).



Figure 19 – Edwards 306A Coating System with water pumps and thickness monitor

The deposition chamber in the Edwards coater was stored under a slight vacuum. Once this was removed by allowing air into the bell jar, all the areas likely to be exposed to the vacuum and evaporated gold were cleaned with lint-free tissues and isopropanol. The masks used to imprint the desired pattern of gold on the substrates were also cleaned and placed in the workholder ring. The crystal used to monitor the thickness (Intellemetrics SN66HG) was checked for cracks and defects, ensuring no build up of gold around the aperture of the water-cooled crystal-holder. The cleaned glass microscope slides (see *Cleaning of Substrates – Glass Slides*), were dried thoroughly in a vigorous stream of air and placed between the masks. Once the slides

were in position and the crystal tested (using the in-built software), 80 mg of gold (Aldrich, 99.9999% pure) was weighed and placed into a molybdenum boat situated between two low-tension terminals. The boat had previously been cleaned by heating under vacuum and then stored with the gold in an evacuated dessicator. Once the gold was in position, the bell jar was sealed again and ensuring the implosion guard was in place, the air driven from the vacuum chamber with the rotary pump.

When the pressure was close to 6×10^{-2} mbar, the backing chamber (i.e. the region below the deposition area) was exposed to the diffusion pump and then the bell jar itself, by raising the baffle plate. At this point liquid nitrogen was introduced to help speed up the removal of the gases from the system. After a couple of hours of pumping down, the pressure was low enough to have firstly removed any water (below 10^{-4} mbar) and secondly, was suitable for the high quality gold film coating required (no greater than 5×10^{-6}).

The thickness monitor was switched on, allowing the deposition rate to be observed. The voltage applied to the molybdenum boat was slowly increased to a level where the gold was just beginning to pool. At this time, using a pair of polarized glasses, a swirling effect on the surface of the molten gold was observed. The shutter was opened and the voltage again adjusted to allow slow but steady coating of the glass slides (between 0.5 and 1.5 nm min^{-1}).

Once the desired thickness was obtained the shutter was closed and any unused gold in the molybdenum boat burned off. The substrates were then left in the system under vacuum for around 30 minutes to allow the gold to anneal the glass surface.

The diffusion pump was then isolated from the bell jar and the deposition chamber exposed to air. The slides were carefully removed and either cleaned (see *Cleaning of Substrates – Gold Coated Slides*) prior to immediate use or stored in a vacuum dessicator.

All areas exposed to the gold were cleaned thoroughly with lint-free tissues and isopropanol and the chamber stored under a vacuum circa 10^{-2} mbar.

9. Surface Plasmon Resonance (SPR) Characterisation

Directly after coating the glass slides with gold, cleaning and drying them, the slides were used for surface plasmon resonance characterisation (Figure 14 and Figure 20).

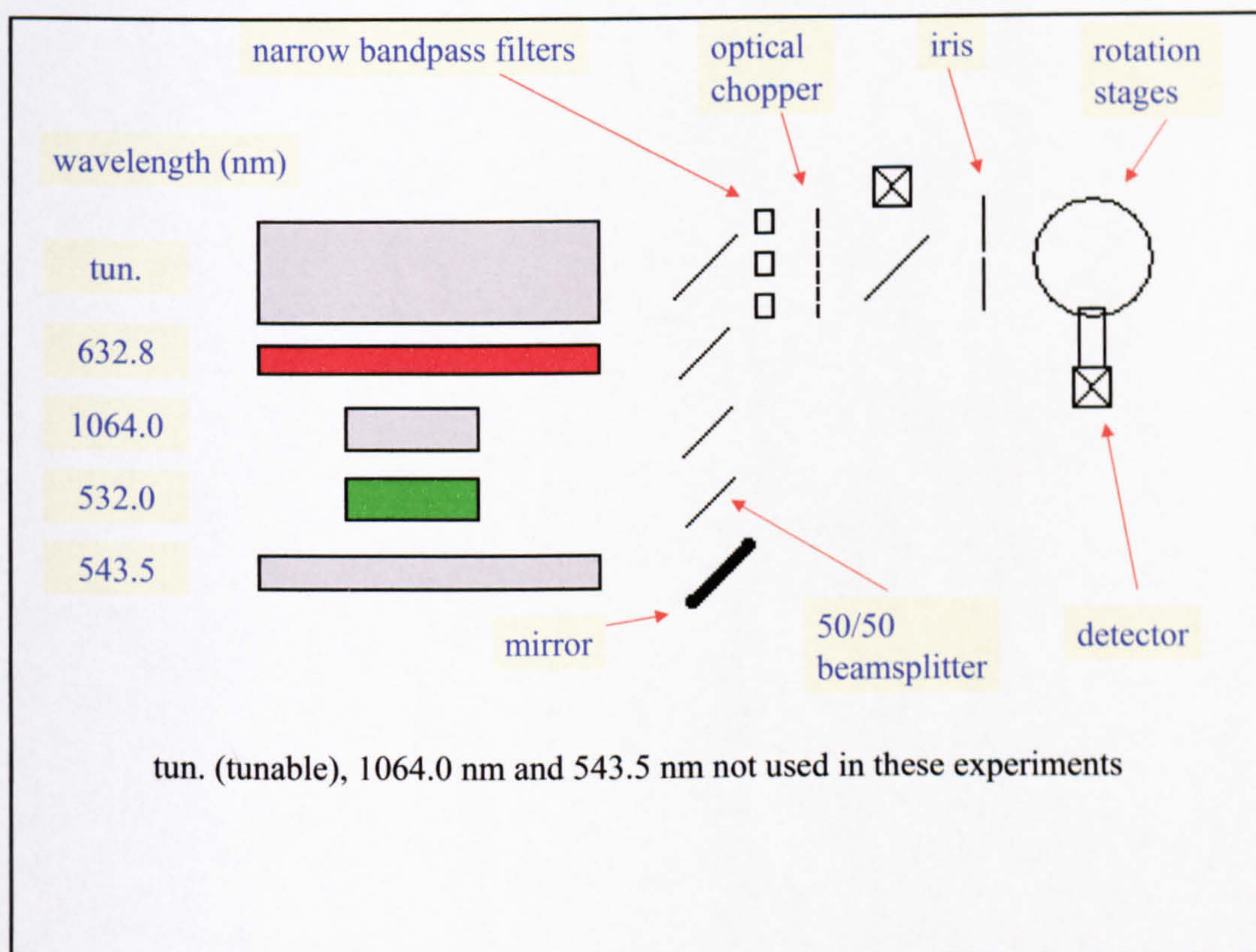


Figure 20 – SPR apparatus diagram

Using gloved hands (sterile non-powdered gloves), the non-coated side of the substrate was wiped with propanone then dried with a lint-free tissue (taking care to only wipe in one direction). A small drop of the matching solution (methyl benzoate, Aldrich 97% pure) was placed in the middle of the gold-free side (this is used to prevent an interface forming between the prism and the glass slide). Holding the slide at an angle, one edge of the BK7 prism was introduced to the base of the slope thereby preventing loss of the

fluid. The top edge of the prism was now pivoted on this base, slowly, to allow capillary action between the two glass components as they came together to drive the matching liquid “up” the interface. By using this technique (as opposed to introducing the prism face-to-face with the slide), the formation of air bubbles was discouraged. Once the two glass components were matched, they were placed on a lint-free tissue to allow any extra liquid to be absorbed by the material and then moved to the rotation stages.

The prism was placed directly against the far walls of the sample stage and one of the ends of the slide made flush with an end of the metal holder. This was to ensure that scans took place at the same location. The bottom rotation stage’s locking screw was released and the prism manually rotated until the beam was reflected off the front face straight back down the beam line (which equated to an internal reflected angle of 60°). The top stage was also adjusted to align the sample detector to the beam. Both locking screws were tightened and a scan from 60° to 50° performed. The position of the front-face-reflected beam was noted at 50° and the stages’ micrometers reset to 0. Again the locking screws were undone and this time the stages set to reflect the beam to the position now marked as 50° . A scan of 241 points between 50° and 38° was then performed ensuring that the pre-amplifiers and the lock-in amplifiers were set to maximise the signal without saturation ⁽⁵⁴⁾.

The data were automatically normalised and the results were compared with theoretical calculations. A series of error-reducing programs (including a simplex least squares analysis, Monte Carlo simulation and hybrid Monte-plex analysis) were used to find the set of values required to produce the obtained experimental data. This was often a black art and many attempts were required to produce least square errors which were low enough to be considered viable (generally below 1.5×10^{-3}). Each scan was “fitted” to theoretical data at least 4 times and the average (including the variation) considered.

To make comparisons simple, results are reported only for 632.8 nm, although some scans were performed at 532.0 nm as a method of checking the veracity of some results (mainly the thickness as other results vary with wavelength).

10. Molecular Modelling

Chemdraw and Chem3D (CambridgeSoft Ltd) were used to draw the structure of each molecule, which could then be converted into a 3-Dimensional representation. A simple minimisation procedure built into the 3D package was used to reduce the internal steric hindrance of the molecule (caused by the positions of the atoms) by adjustment of bond lengths and angles. The results gave approximate values of the dimensions of the molecules. This allowed the orientation of the molecules to be estimated from SPR, QCM and Isotherm results.

11. Chlorine Gas Sensing

SPR and UV-VIS Spectroscopy assessed the sensitivity of the response of an LB film to chlorine (in the ppm range, balanced by nitrogen).

11.1 Surface Plasmon Resonance

The first experiment performed was to check that the reflected intensity did not change when just gold was exposed to the chlorine gas (i.e. that the gold didn't react to the gas). In total, 4 dyes were studied with this technique, though only 2 provided enough sensitivity to detect a change.

After the sample had been deposited onto a fresh gold slide, the material was characterised by surface plasmon resonance. From the SPR result obtained, the first differential of the curve indicated the steepest section (Figure 21) and hence the position of the prism required for maximum sensitivity during the fixed angle experiments on the gas rig (Figure 22).

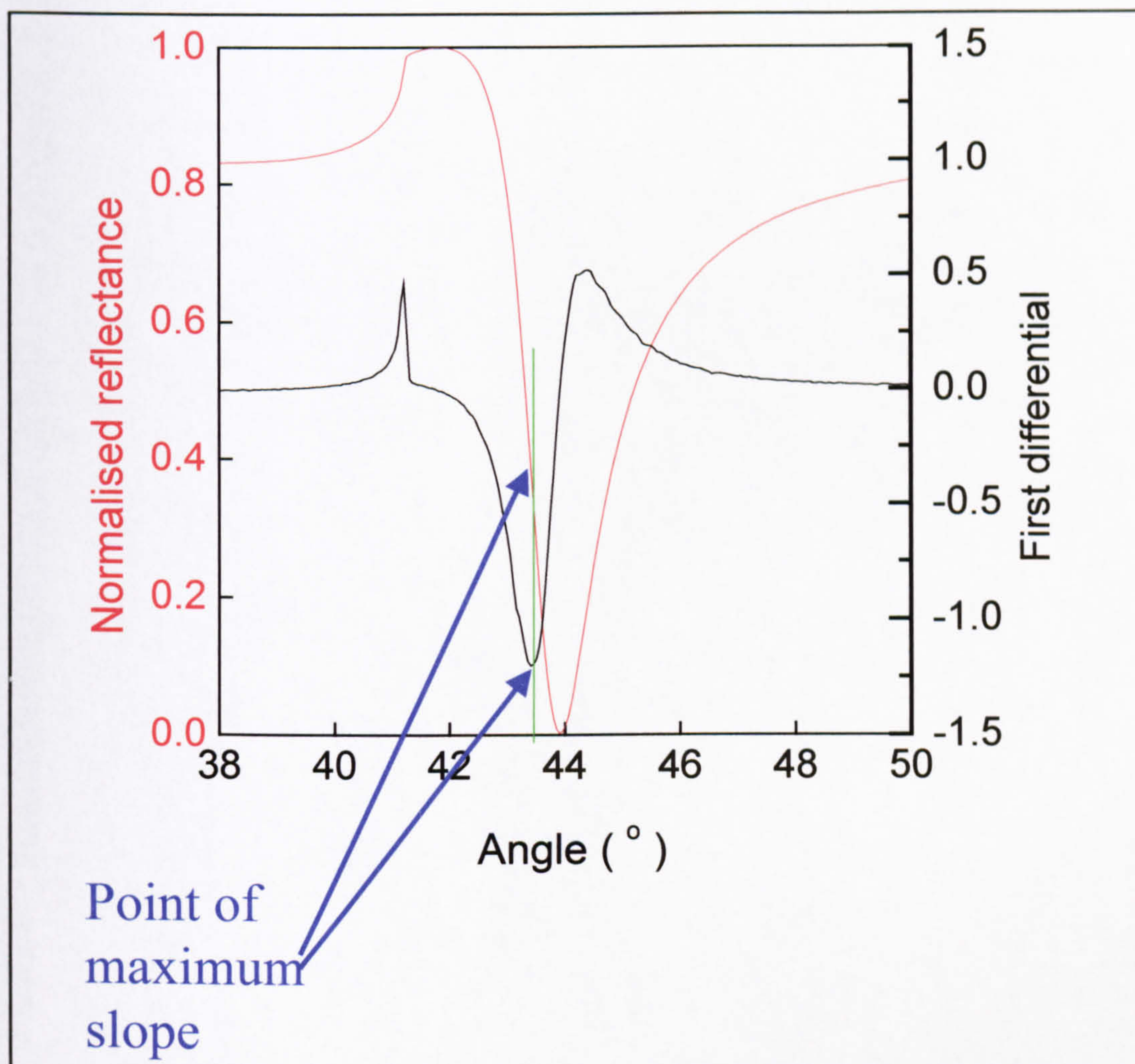


Figure 21 – First differential of the SPR curve can show the steepest section of the curve

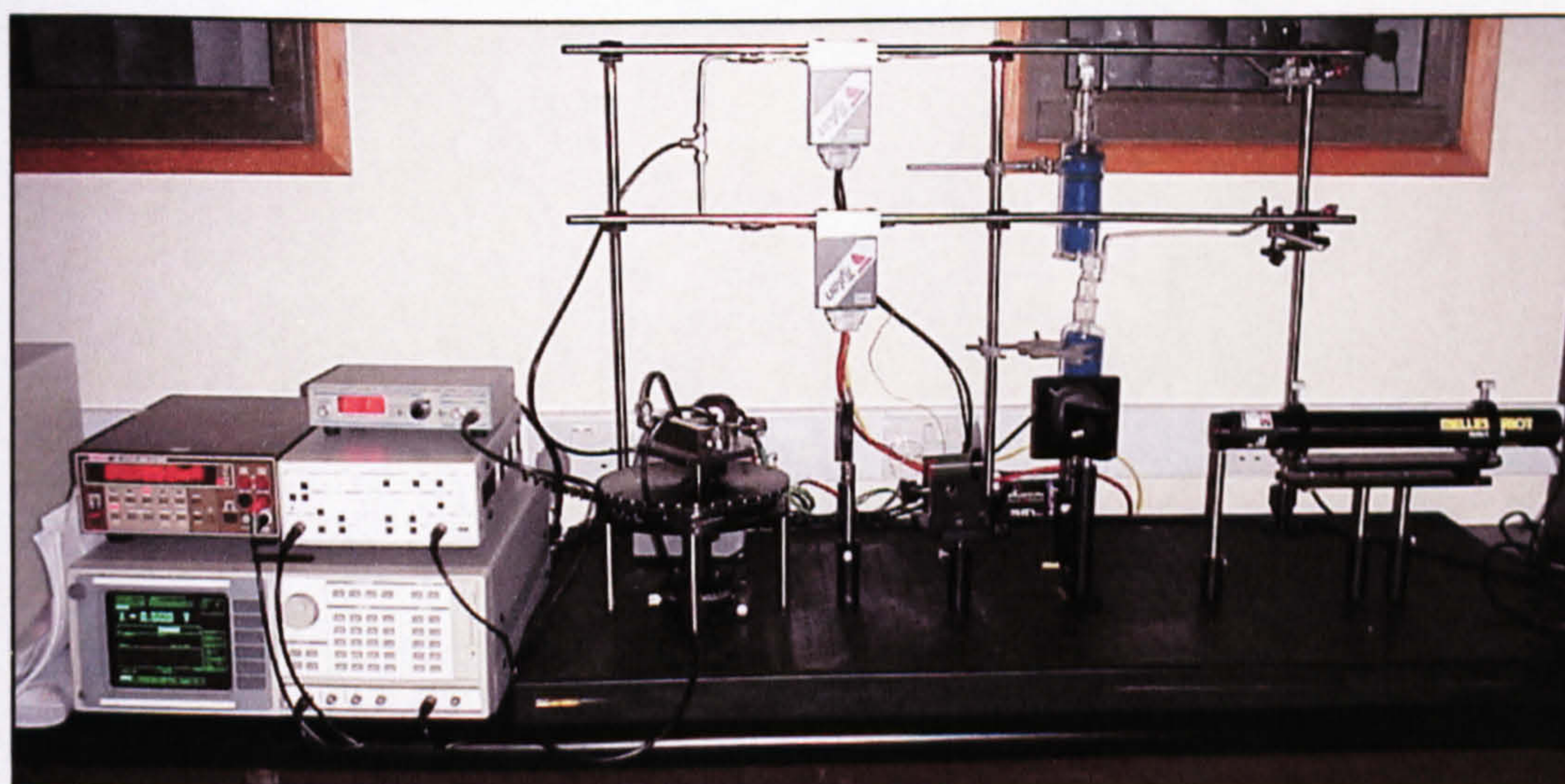


Figure 22 – SPR gas rig apparatus

Using Equation 8 the internal angle, θ_{int} (i.e. that displayed in the SPR graph) was converted into the position of the manual rotation stage required, θ_{rot} .

$$\theta_{\text{rot}} = \sin^{-1}\left(\frac{1.515 \sin \theta_{\text{int}}}{1.00}\right) \quad \text{Equation 8}$$

Where 1.515 and 1.00 are the refractive indices of BK7 and air respectively (at 632.8nm).

The stage was set to the corresponding angle and the sample detector centred on the beam. Nitrogen was then pumped through the system and the changes in the reflected intensities monitored with the lock-in amplifier (Stanford Research Systems, SR 850, from the sample detector) and Kiethley Scanner (199 DMM/Scanner, from the reference detector). When a flat baseline was achieved, the chlorine gas at the relevant concentration was introduced to the sample. After a period of time, the chlorine was switched off and the recovery under nitrogen monitored.

11.2 Ultraviolet-Visible Spectroscopy

With little sensitivity found with the surface plasmon resonance technique, the system was altered to allow for measurements with UV-VIS spectroscopy. A Charge Coupled Diode (CCD) array was exposed to light passing through the sample from a white light source via fibre optic bundles and a monochromator. This allowed spectra to be taken up to every 21 ms, although due to the low absorbance of the monolayers, the exposure time often accounted for results being taken at least every second. Also with some experiments lasting an hour, spectra were taken every 30 seconds to balance monitoring of reactions with number of spectra to analyse. The CCD array was cooled to 3 °C to minimize “dark noise signals” (any lower and ice crystals would have formed on the detector head possibly affecting the recorded spectrum). A cover was also designed to minimise any external light and reduce noise (though the windows were also blacked out and the lights turned off).

For clarity, spectra were also recorded using the Perkin Elmer Spectrophotometer (both before and after exposure to chlorine, with further scans taken to monitor the recovery in air). Initial studies showed that the time taken transferring the slide from the gas rig to the Spectrophotometer was negligible (comparing a transferred slide to one with the chlorine trapped in the sample cell).

Glass slides from the same cleaning batch were used for background scans with both spectra-capturing techniques and a freshly deposited slide then inserted into the sample cell. In all cases the film was first exposed to nitrogen before introducing the relevant concentration of chlorine.

CHAPTER THREE

Results and discussion

1. Phthalocyanines

A short series of phthalocyanine dyes (Figure 23) were characterised in the form of Langmuir-Blodgett films.

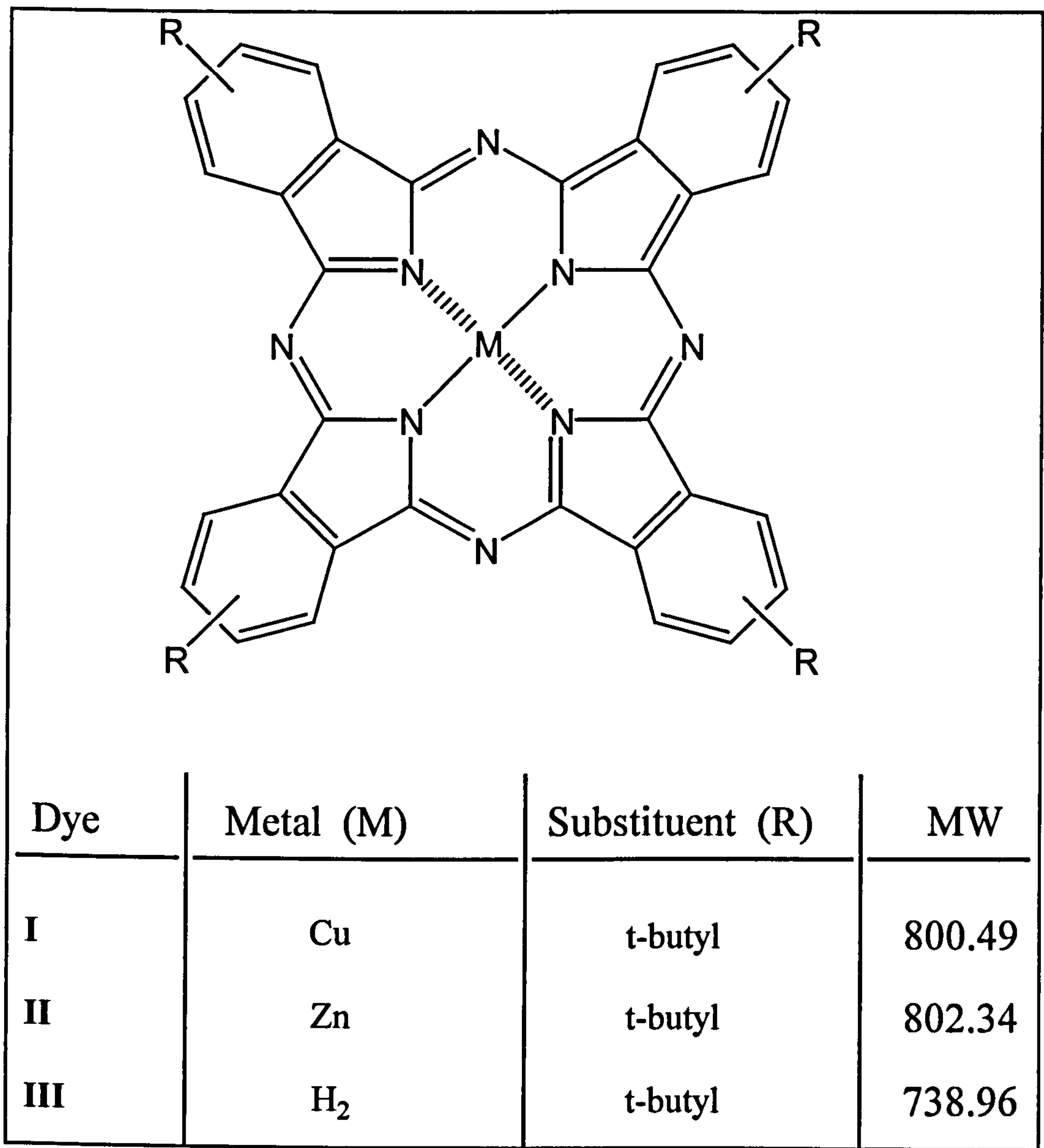


Figure 23 – Phthalocyanine dyes used (supplied by Prof. C. L. Honeybourne)

These materials have significant spectral features (after dissolving in trichloromethane) in two distinct regions – the so-called B-band between 300 and 400

nm and a more intense absorbance (Q-Band) between 600 and 700 nm (e.g. dye I, Figure 24). The higher wavelength features have been assigned to transitions between bonding and antibonding orbitals, e.g. $\pi\pi^*$ states ⁽¹²⁶⁾.

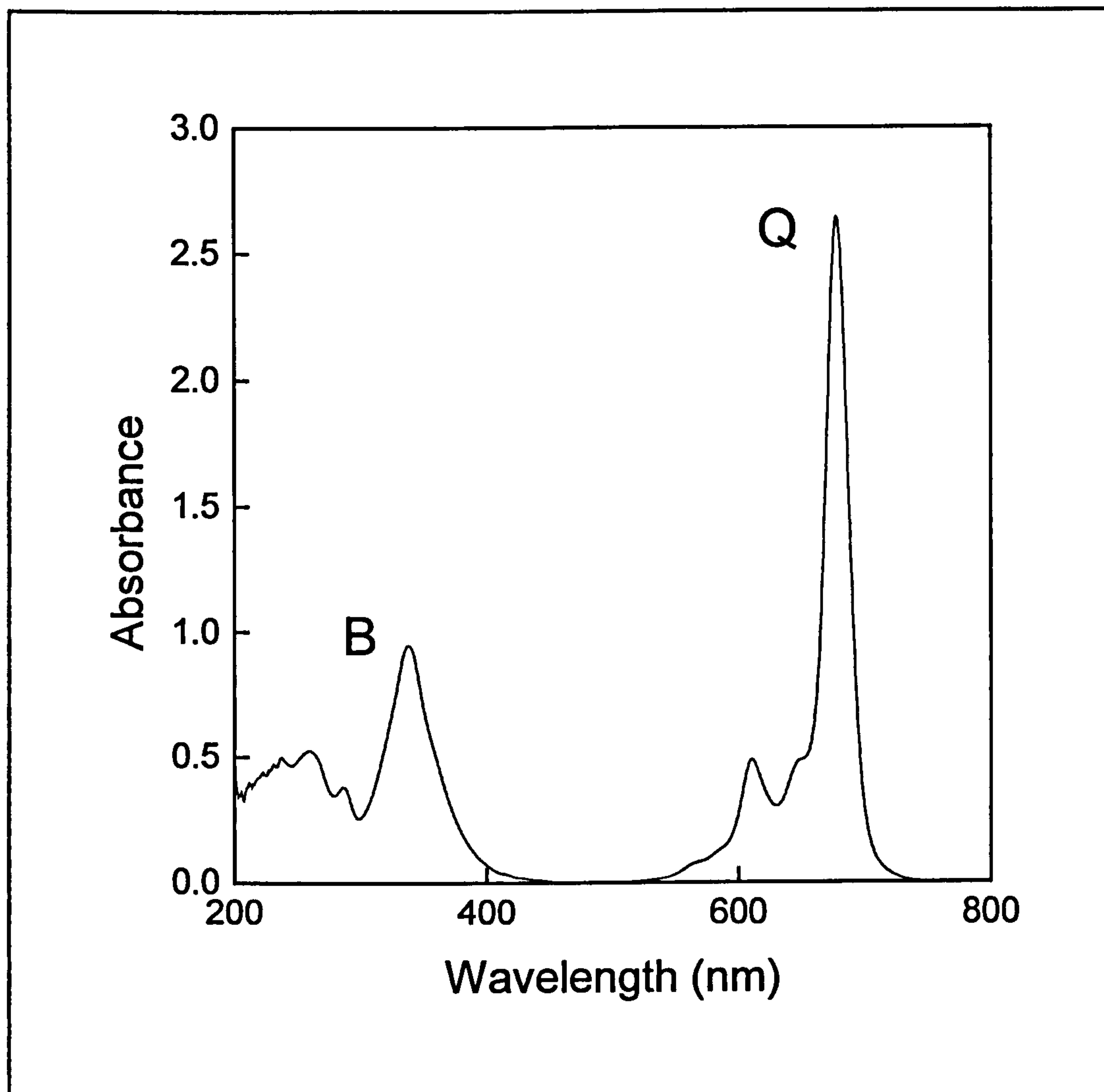


Figure 24 – UV-VIS absorption spectrum of dye I in trichloromethane

Compared with other macrocycles containing a high degree of unsaturation in the ligand, the Q-Band is broad consisting of a series of peaks. This increase in complexity has been associated with the electronic transitions from filled nonbonding orbitals, localized in the azomethine groups (which gives rise to $n\pi^*$ excited states) ⁽¹²⁷⁾.

When deposited as a Langmuir-Blodgett film, the spectra change in a number of ways. In dye **I**, the λ_{max} (i.e the most prominent spectral feature – in the case of phthalocyanines this occurs at around 650 nm) is blue-shifted by 62 nm probably due to solid-state packing effects (Figure 25).

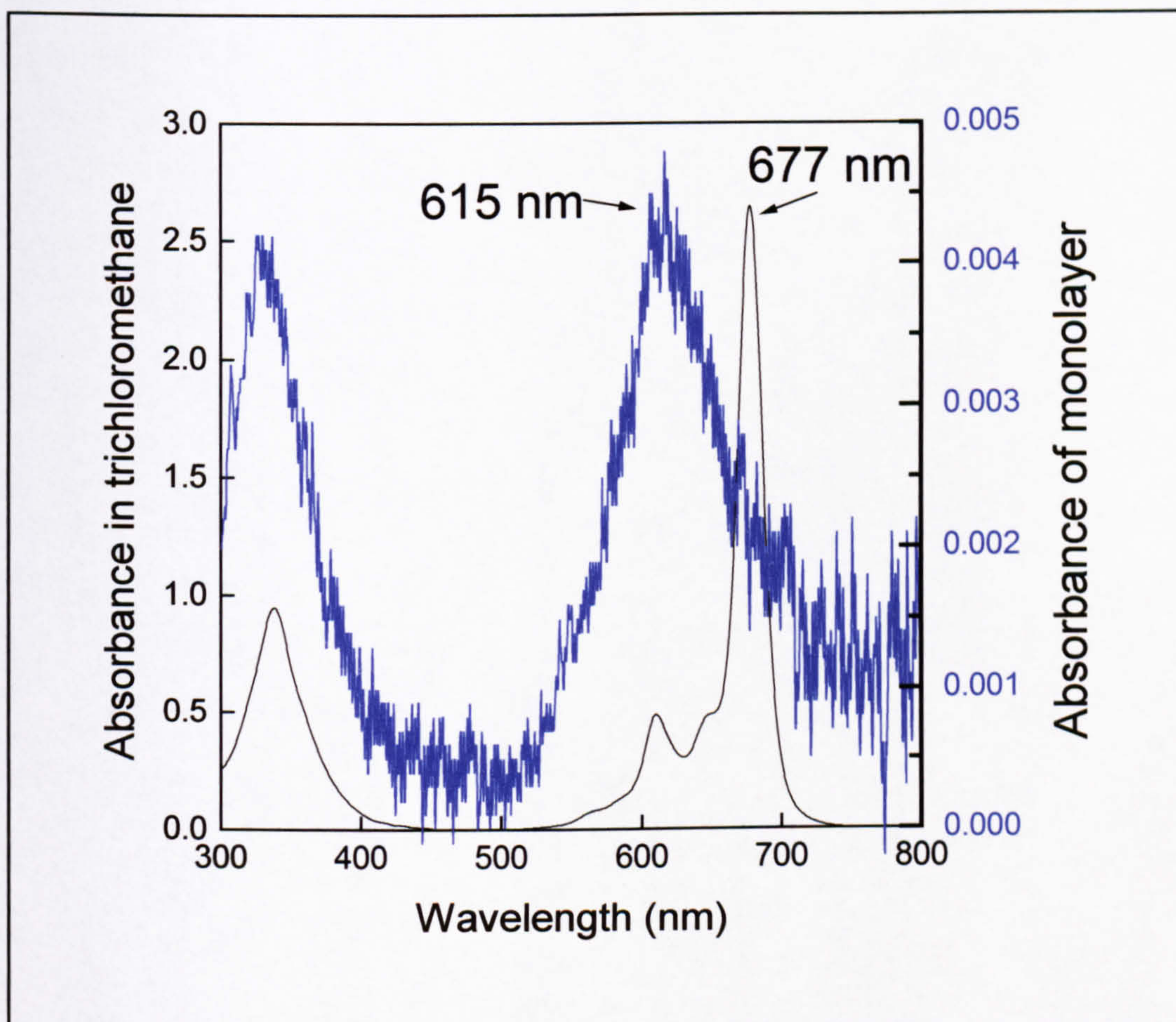


Figure 25 – Demonstration of solid-state packing effects in dye I; dye in trichloromethane (—) and monolayer (—) forms

The zinc phthalocyanine (dye **II**) does not demonstrate any of the blue-shifting seen in the copper moiety; in fact a small red-shift of around 6 nm is present (which is within experimental error) suggesting that the packing arrangement seen in dye **I** does not occur (Figure 26).

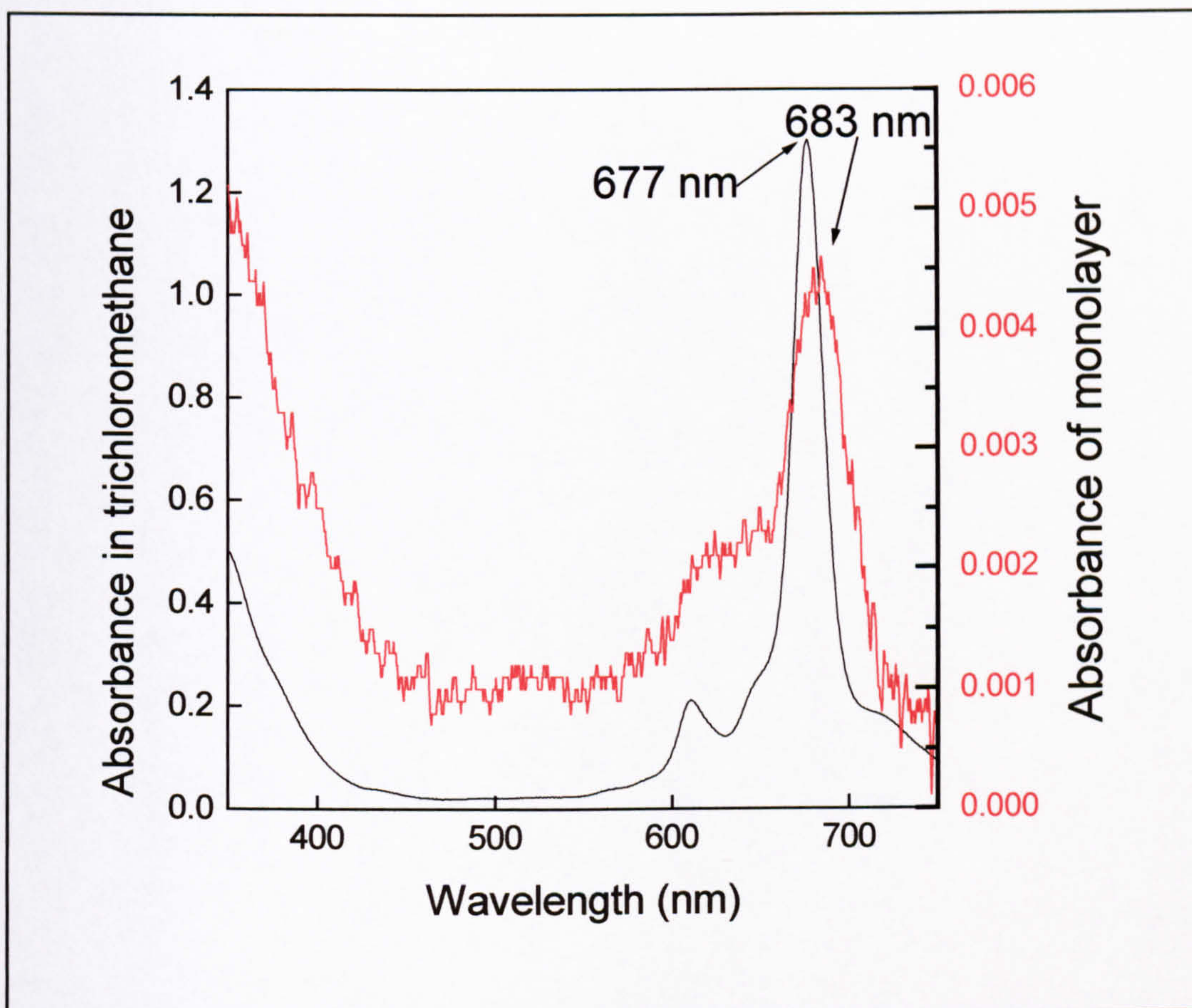


Figure 26 – Demonstration of the lack of solid-state packing effects in dye II; dye in trichloromethane (—) and monolayer (—) forms

For dye **III**, the analysis of the change in absorption spectra from solution to Langmuir-Blodgett film proves very difficult. The 2 main peaks seen in the trichloromethane spectrum (at 662 nm and 669 nm) have now been reduced to just one absorbance at 621 nm (Figure 27). It is also clear that (comparing monolayer absorbances for the three dyes) the intensity is significantly larger for the metal-free phthalocyanine (Table 6). This is a spectroscopic effect characteristic of a change in symmetry (the metal-free tetra-substituted moieties have, at best, a two-fold centre of symmetry, whilst the metallated have four-fold).

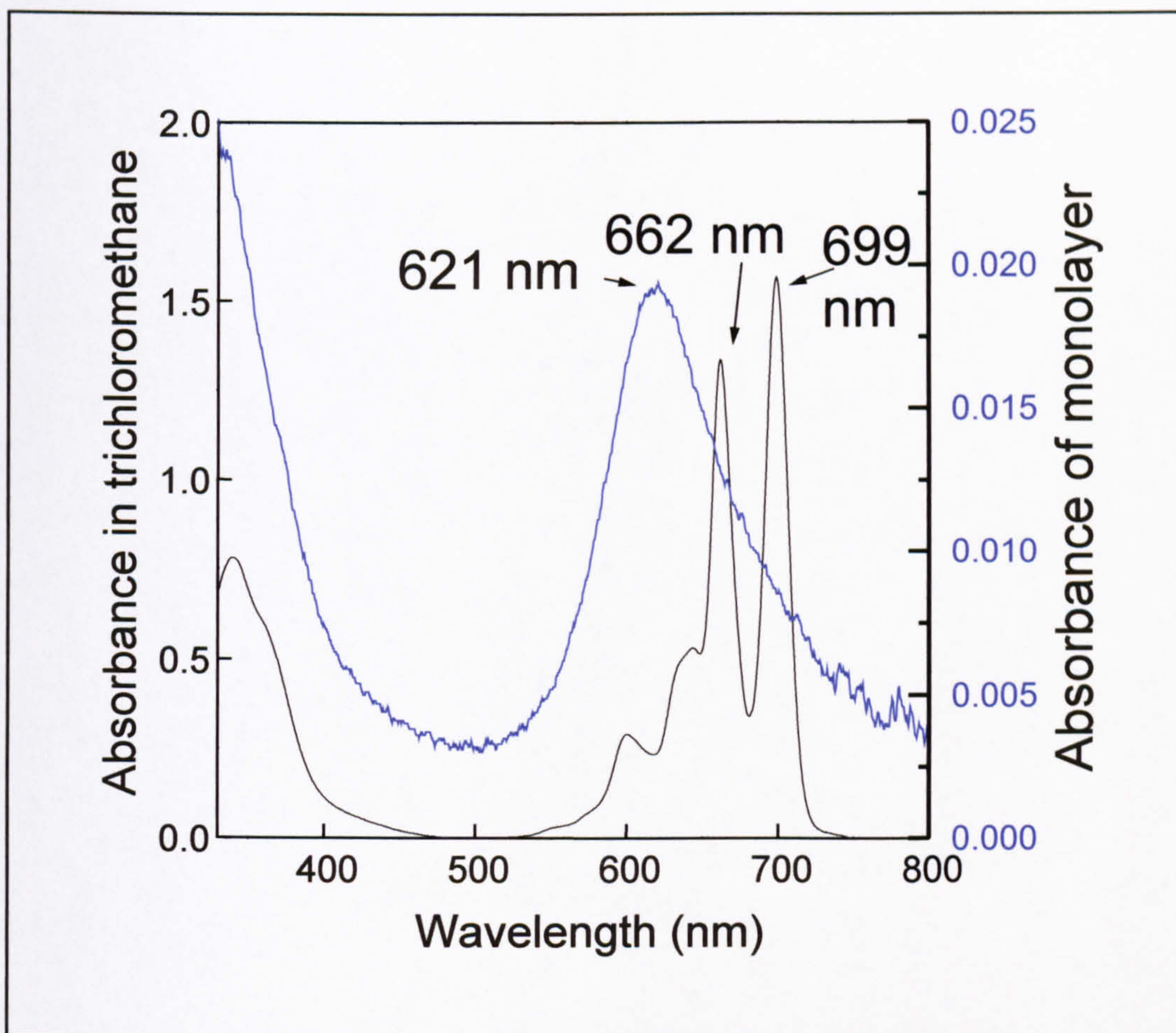


Figure 27 – Comparison of the UV-VIS absorbance of III in both trichloromethane (—) and monolayer (—) forms

Table 6 – Comparison of λ_{max} of monolayers of phthalocyanines

Dye	λ_{max} (Q-Band) / nm	Absorbance at λ_{max}
I	615	0.0045
II	683	0.0045
III	621	0.0195

Further clues to the nature of these molecules on the water surface (i.e. in floating film form) can be found in the analysis of their Langmuir films using pressure-area isotherm graphs. Initially, dye **III** appears to form the most stable and compact floating layer as it is a steep curve with no visible points of inflexion. The comparison

of the three macrocycles also indicates that the central atom contributes to the molecular area (Figure 28).

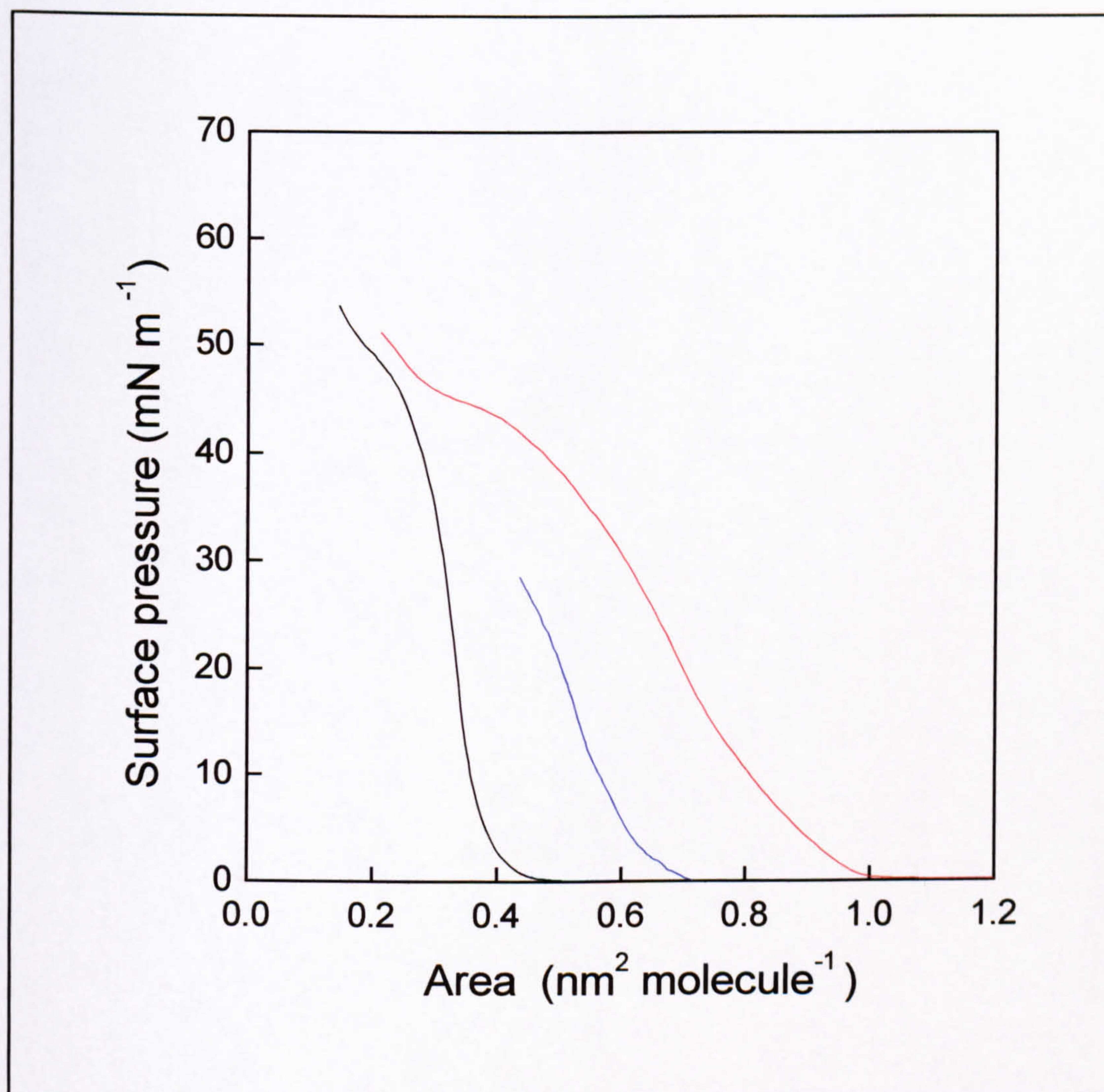


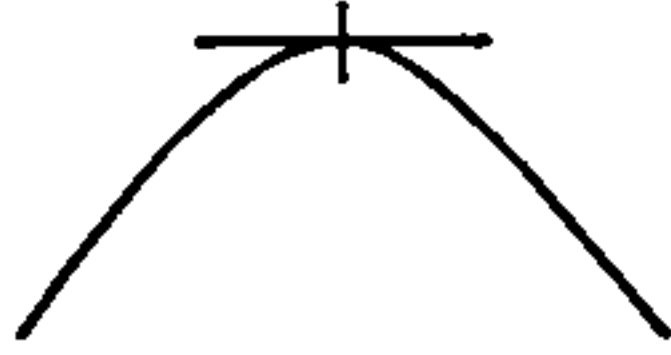
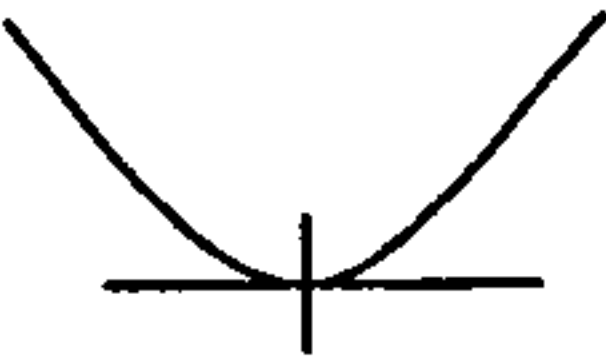
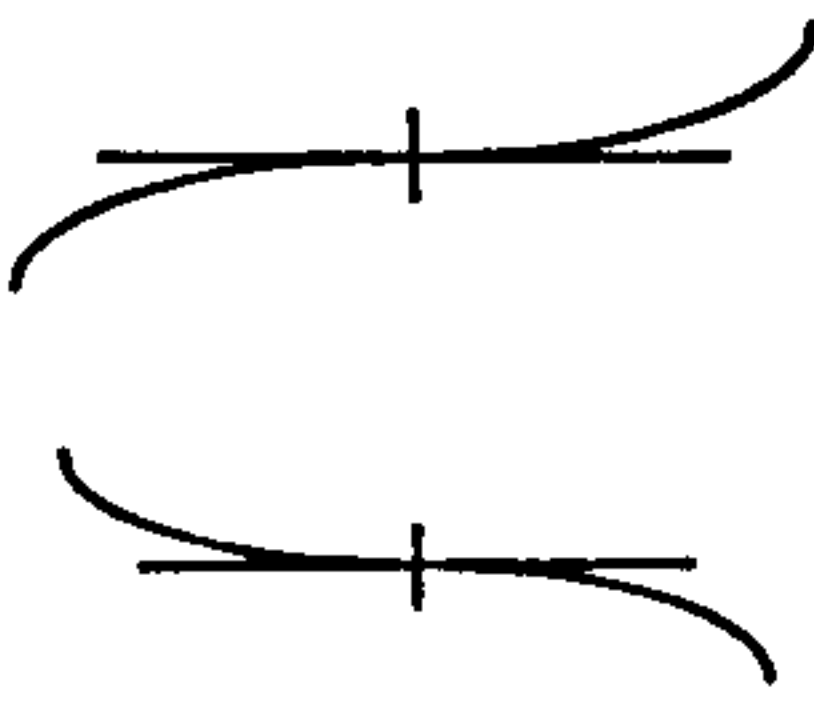

Figure 28 – Langmuir pressure-area isotherms of the three phthalocyanines

(— dye I, — dye II, — dye III)

The analysis of the isotherm often proves difficult as the changes in the Langmuir film often provide subtle variations in the pressure-area curve's gradient. One way of determining the location of these is to differentiate the data. When this differential is equal to zero, this is called a stationary point (Table 7). It is the general points of inflexion that are most difficult to determine with the naked eye and in an

isotherm curve, these may represent the breaking of a monolayer and formation of a multilayers in the Langmuir film.

Table 7 – Types of Special Point and the method of determination

Type of Point	Local maximum	Local minimum	Horizontal point of inflexion	General point of inflexion
Examples				
Differential used	1 st	1 st	1 st	2 nd
Sign to <i>left</i> of point where differential = 0	+	–	– +	– +
Sign to <i>right</i> of point where differential = 0	–	+	– +	+ –

The location of general points of inflexion (A_{inf}) can be found by equating the second-differential to zero (Equation 9), where Π is the surface pressure. If the sign changes when the area is $>A_{inf}$ and $<A_{inf}$ then it is likely to represent a breaking of the film. In other words, wherever the graph of the 2nd differential *crosses* the x-axis, there is a general point of inflexion.

$$\frac{d^2\Pi}{d(Area)^2} = 0$$

Equation 9

A further explanation of the 2nd differential graphs can be found later in this thesis (*H. Appendices*).

The second-differential of the isotherm of I shows that although the initial data may indicate that a poor Langmuir film is formed (demonstrated by the low breaking point), there is only one point of inflexion. This occurs at an area of 0.52 nm² molecule⁻¹, where the surface pressure is ~17 mN m⁻¹; it is likely that this is the start of multilayer

formation (Figure 29). Indeed, previous research has already highlighted the inflexion at this pressure and has shown that tetrakis-*tert*-butyl-phthalocyanato Cu (II) is found to have more than 1 preferred configuration on the water surface ⁽¹²⁸⁾. The initial orientation is determined by the concentration of the molecules on the subphase. At low initial concentrations the macrocycles prefer to lie flat on the water surface and as the number of molecules spread increases, the films become more vertically aligned.

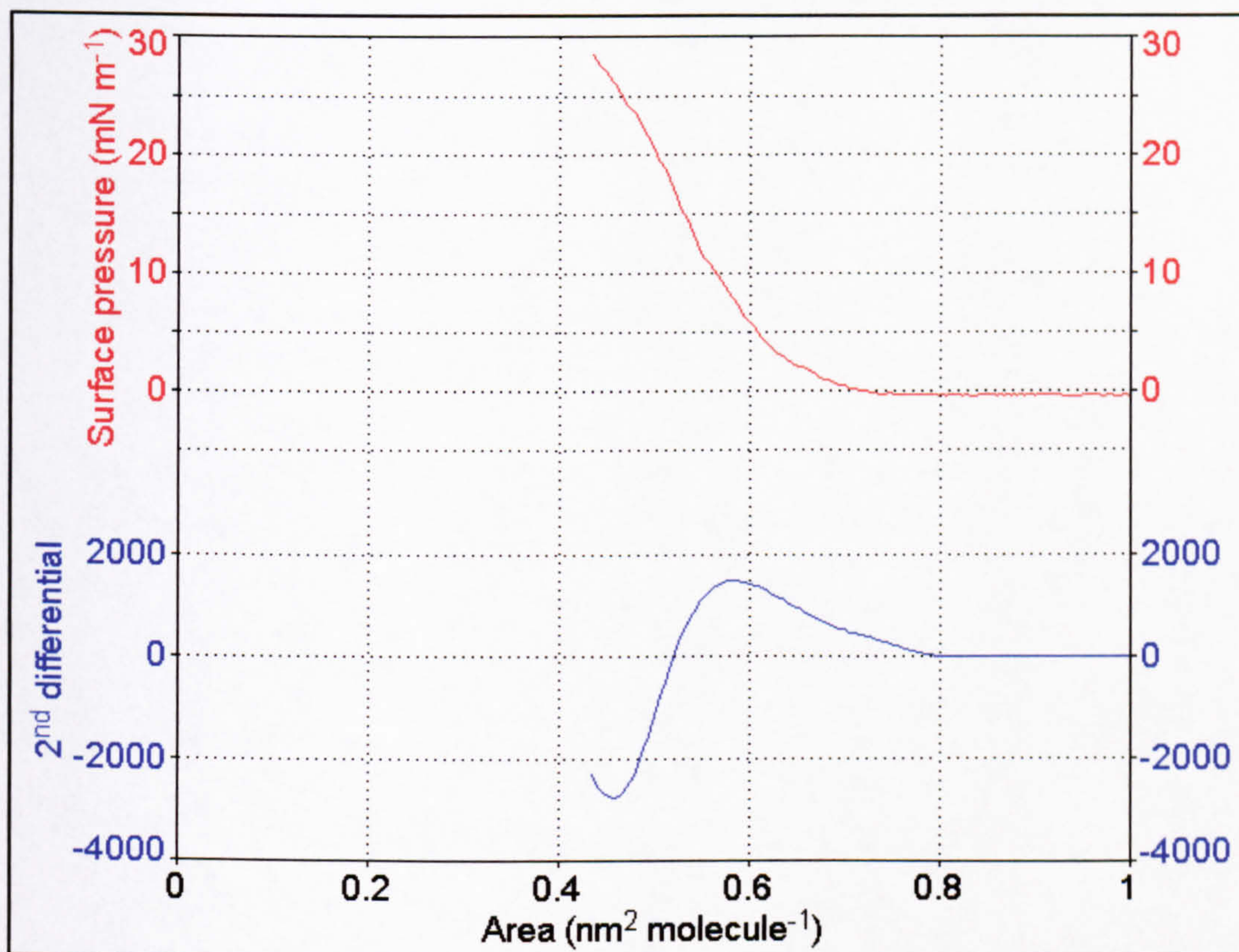


Figure 29 – Isotherm (—) and 2nd differential (—) of dye I

The formula for calculating the initial orientation on the surface is given in Equation 10, where N is the initial surface concentration (mol m^{-2}), v the volume of solution spread on the surface (l), c the concentration of the dye (g/l), MW the molecular weight of the dye (g mol^{-1}) and A_{trough} the initial area of the water surface (m^2).

$$N = \frac{v \cdot c}{A_{\text{trough}} \cdot MW}$$

Equation 10

If $N = 1 \times 10^{-7} - 3.8 \times 10^{-7} \text{ mol m}^{-2}$, then the molecules are facedown. If $N > 3.8 \times 10^{-7} \text{ mol m}^{-2}$, then they are tilted and densely packed.

The initial surface concentration during the experiments was $\sim 5 \times 10^{-7} \text{ mol m}^{-2}$, which suggests the tilted densely packed structure, is formed. Typically, after solvent evaporation, a single tetra-pyrrole macrocycle might be expected to adopt the facedown orientation on the subphase due to the hydrophilic interaction between the nitrogen-atom lone-pairs and the water. This does not occur in this case because the initial surface concentration is high enough to induce Pc-Pc interactions (an interaction between phthalocyanine molecules – mainly their delocalised π -systems), which partially overcome hydration of the N atoms^(129, 130). The molecules are effectively forming a columnar aggregate on the water surface (but with the length parallel not perpendicular to the subphase), which means the tilt angles of the molecules are only consistent within each stack.

The *t*-butyl groups attached to the periphery of the phthalocyanine macrocycle can be located in a number of places; many structural isomers are formed during synthesis. This produces some molecules with little or no symmetry and others with up to 4-fold symmetry. This may explain the low breaking point of the pressure-area isotherm of I; the random locations of the *t*-butyl groups on the macrocycle periphery induce greater steric hindrances in Pc-Pc interactions, meaning that a molecule is more easily squeezed out of the monolayer when compressed. For this reason, 8-substituted phthalocyanines are often found to form the most stable Langmuir films^(50, 131).

For the Zinc moiety, the first Langmuir film breakage occurs at around 20 mN m^{-1} , the pressure-area isotherm curve is broad and although it reaches 50 mN m^{-1} it is likely to be a multilayer structure at this point (Figure 30). This can be shown by the two further breakages present at *circa* 49 mN m^{-1} and 52 mN m^{-1} . The phthalocyanine metal atom may affect the self-assembly properties of the macrocycle seen in I; axial coordination of water by the zinc may inhibit the formation of rigid monolayers, bilayers or columnar aggregates⁽¹³²⁾.

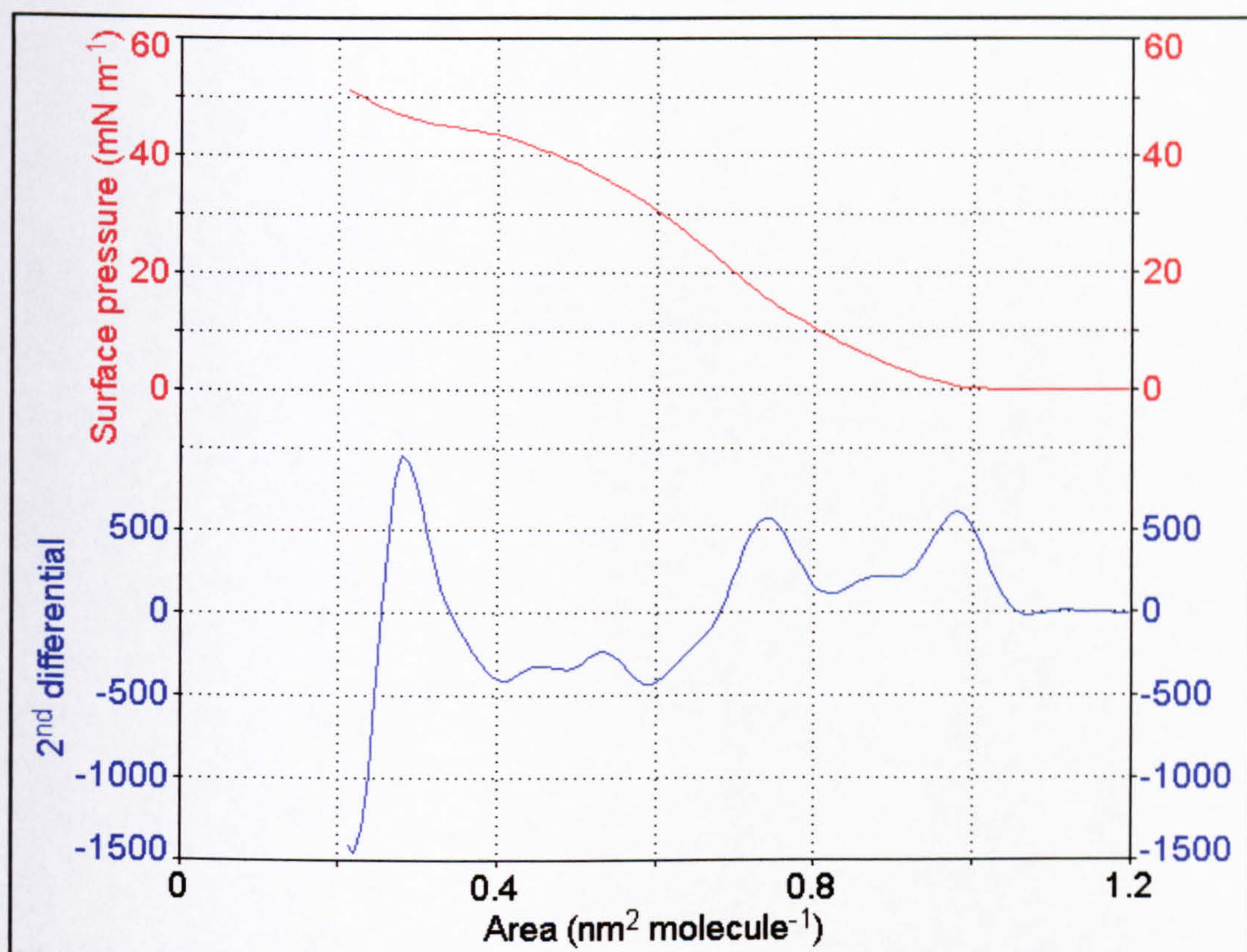


Figure 30 – Isotherm (—) and 2nd differential (—) of II

Similarly, the metal-free phthalocyanine has an early collapse (20 mN m⁻¹) and two collapses close together towards the end of compression (45 mN m⁻¹ and 48 mN m⁻¹). Again there are no signs of a horizontal point of inflexion, which may have indicated a re-orientation in the Langmuir film (Figure 31).

The comparison of the isotherms of the three phthalocyanines reveals more than the effect of the metal atom. The comparison leads to the conclusion that only **I** forms a stable densely packed structure (it has only one point of inflexion). This is confirmed by the UV-VIS spectra, where only **I** shows any signs of H-aggregation (also known as card stacking or a columnar aggregate parallel to the substrate's surface); there is a 62 nm blue shift. In all three dyes, the films break below 21 mN m⁻¹, which would confirm that the sterically hindered molecules with lower symmetry are easily squeezed out and multilayer formation takes place at low surface pressures.

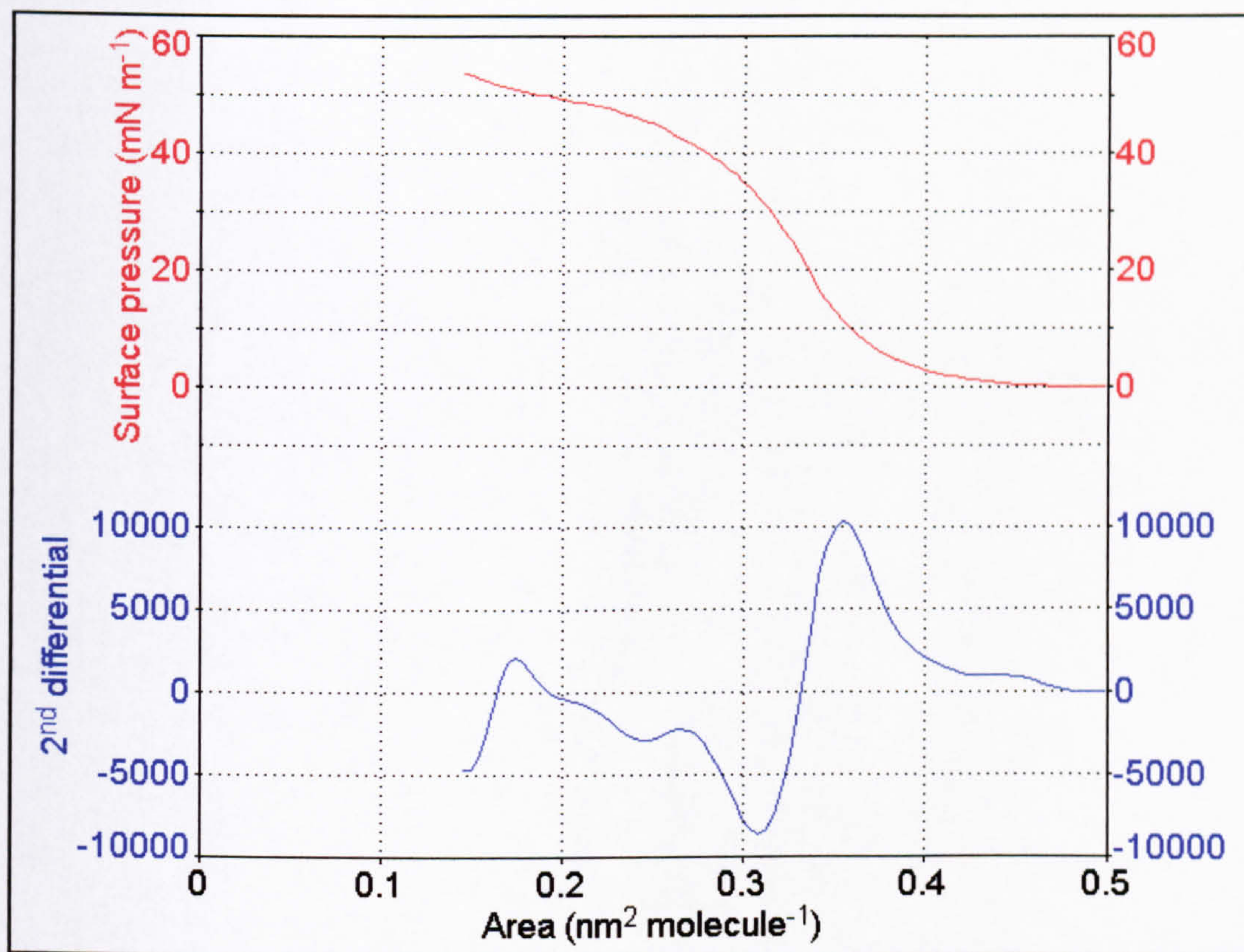


Figure 31 – Isotherm (—) and 2nd differential (—) of **III**

By monitoring the molecular area of the dye, it can be seen that at 10 mN m^{-1} the molecules are more easily squeezed out of the monolayer in **III** (Figure 32, arrows indicating the attainment of a pressure of 10 mN m^{-1}). This highlights the fact that the copper moiety forms a more stable monolayer than the metal-free phthalocyanine; a decrease in molecular area over 75 minutes of just 1.5% compared with 22.3% for **III**.

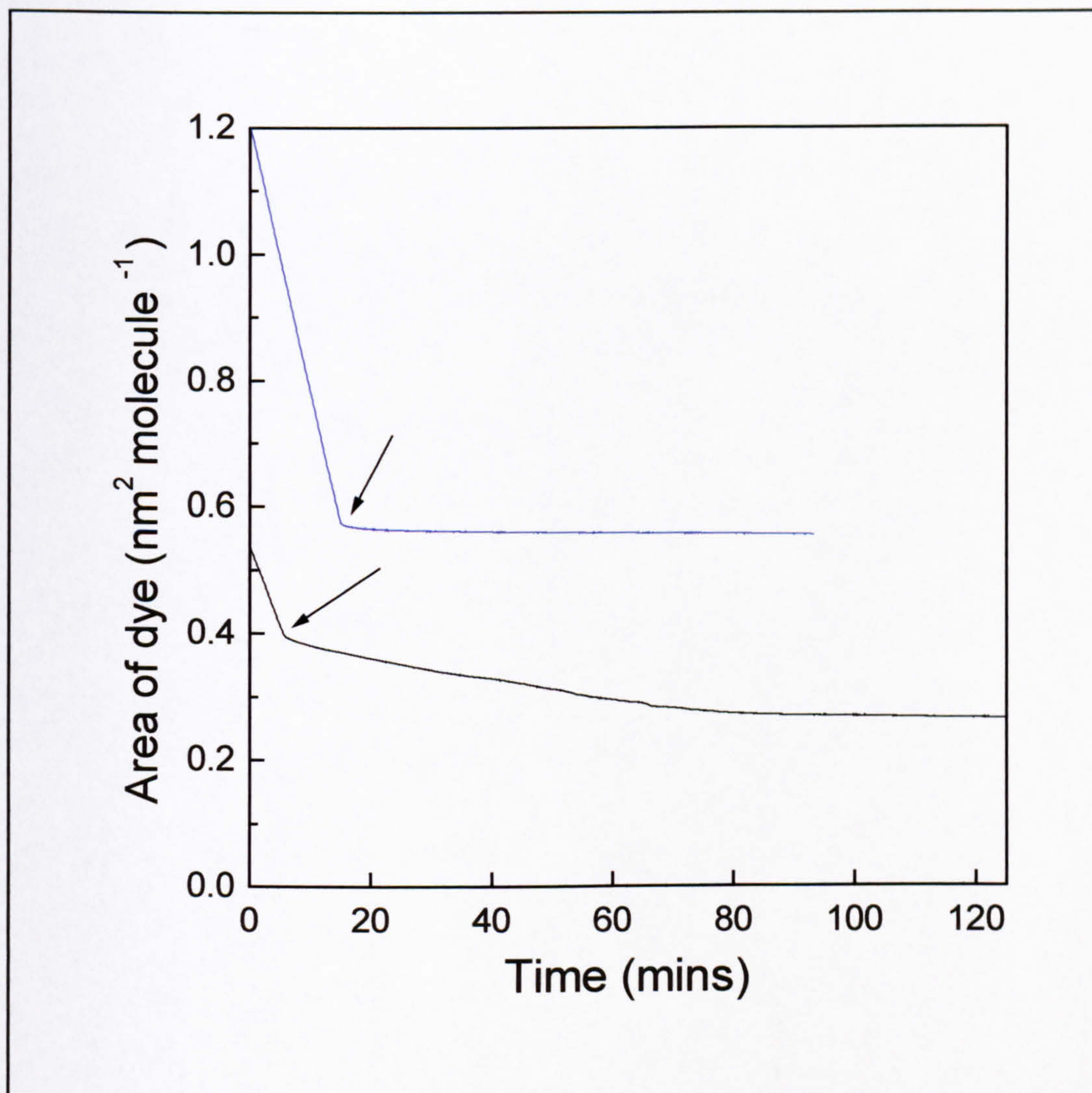


Figure 32 – Area-time graphs of dye I (—) and dye III (—) when held at 10 mN m^{-1} (arrows indicate where target pressure is attained)

There are two measurements commonly used to analyse the isotherm data: the extrapolated cross-sectional area (A_0) and the area at deposition (A_d)⁽⁶⁾. The former is found by extrapolating the tangent of the solid phase of the isotherm to the x-axis and the latter simply by reading off the value of the area where deposition occurs. The experimental value of A_0 for dye I of 0.62 nm^2 was found to be in agreement with previous research^(133, 134, 135). The extrapolated cross-sectional area found for III was slightly lower than previously reported⁽¹³⁰⁾.

Using a Quartz Crystal Microbalance (QCM) the nature of these molecules when deposited onto a substrate becomes much clearer. A minimum of 5 measurements

were taken per dye and then averaged and the variance of the results can be seen in the standard deviation (STD) of the data. Dyes **I** and **III** seem to form consistent Langmuir-Blodgett films which agree with the data collected from the isotherms, whereas the zinc moiety differs significantly from the Langmuir film data and the variance is much greater (Table 8 – molecular area at deposition, A_d , measurements are highlighted for both isotherm and QCM and were recorded at 10 mN m^{-1}).

Table 8 – Molecular area as measured by isotherm and QCM

Data Source		I	II	III
Isotherm	A_d / nm^2	0.57	0.81	0.36
	A_o / nm^2	0.62	0.90	0.38
QCM	A_d / nm^2	0.52	1.61	0.31
	STD / nm^2	0.01	0.8	0.03

The difference between A_d from the isotherm and the QCM from the zinc *t*-butyl phthalocyanine experiments may be the result of the poor Langmuir film formed. This would also account for the poor consistency in the data range as indicated by the STD.

To calculate the dimensions of the molecules (using Chem3D), measurements were taken for each length (Figure 33). Whilst the position of the *t*-butyl is unknown to a certain extent, this gives an approximation of the typical dimensions of the molecule (Table 9).

Table 9 – Measurements taken from Chem3D

Central atom	Macrocycle and t-butyls				Macrocycle only			
	1	2	3	4	1	2	3	4
Copper	1.5	1.5	1.9	2.0	1.1	1.1	1.3	1.5
Zinc	1.5	1.5	1.8	2.0	1.1	1.1	1.3	1.5
Metal free	1.5	1.4	1.9	1.9	1.1	1.1	1.4	1.4
All measurements are in nm and include VDWs average error in measurements is $\pm 0.05 \text{ nm}$								

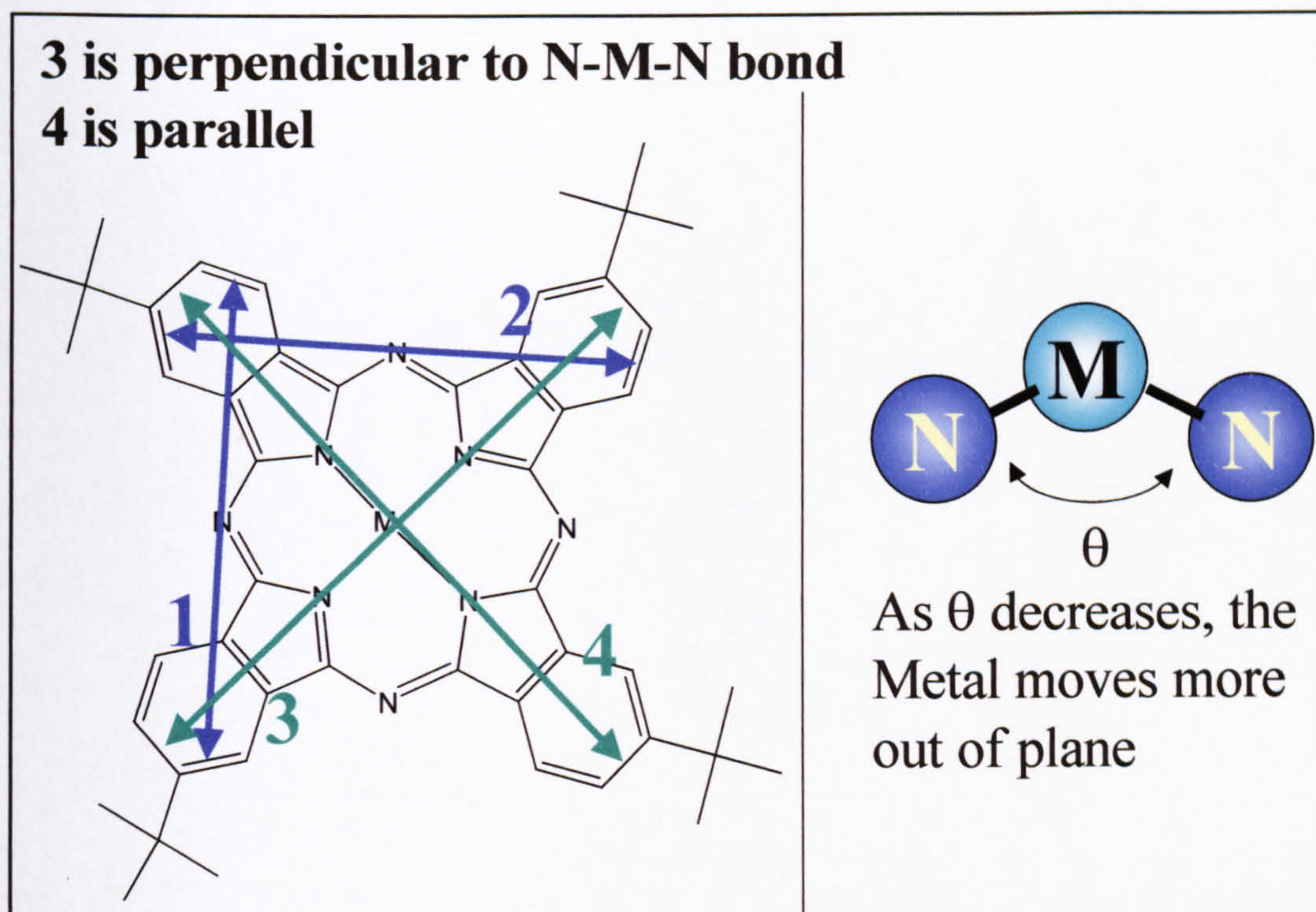


Figure 33 – Explanation of how phthalocyanine dimension measurements are taken using Chem3D (macrocycle only)

The insertion of a metal atom appears to only slightly contort the macrocycle, with the N-M-N bond slightly compressing the diagonal width of the molecule. This is demonstrated by the consistent values for 1 and 2 (which are effectively the perimeter measurements of the macrocycle) and the varying values of the diagonal lengths 3 and 4 (Figure 34). The reason why the macrocycle only appears to slightly contort lies in the N-M-N bond angle; the metal atoms do not sit in the same plane as the majority of the atoms in the heterocycle, requiring only a small contortion (Table 10). What the computer simulation does not take into account however is that there is so much resonance in the system, the metal atom actually complexes with all 4 pyrrole nitrogen atoms and the macrocycle is likely to form something like a square-based pyramid with the metal atom at its vertex.

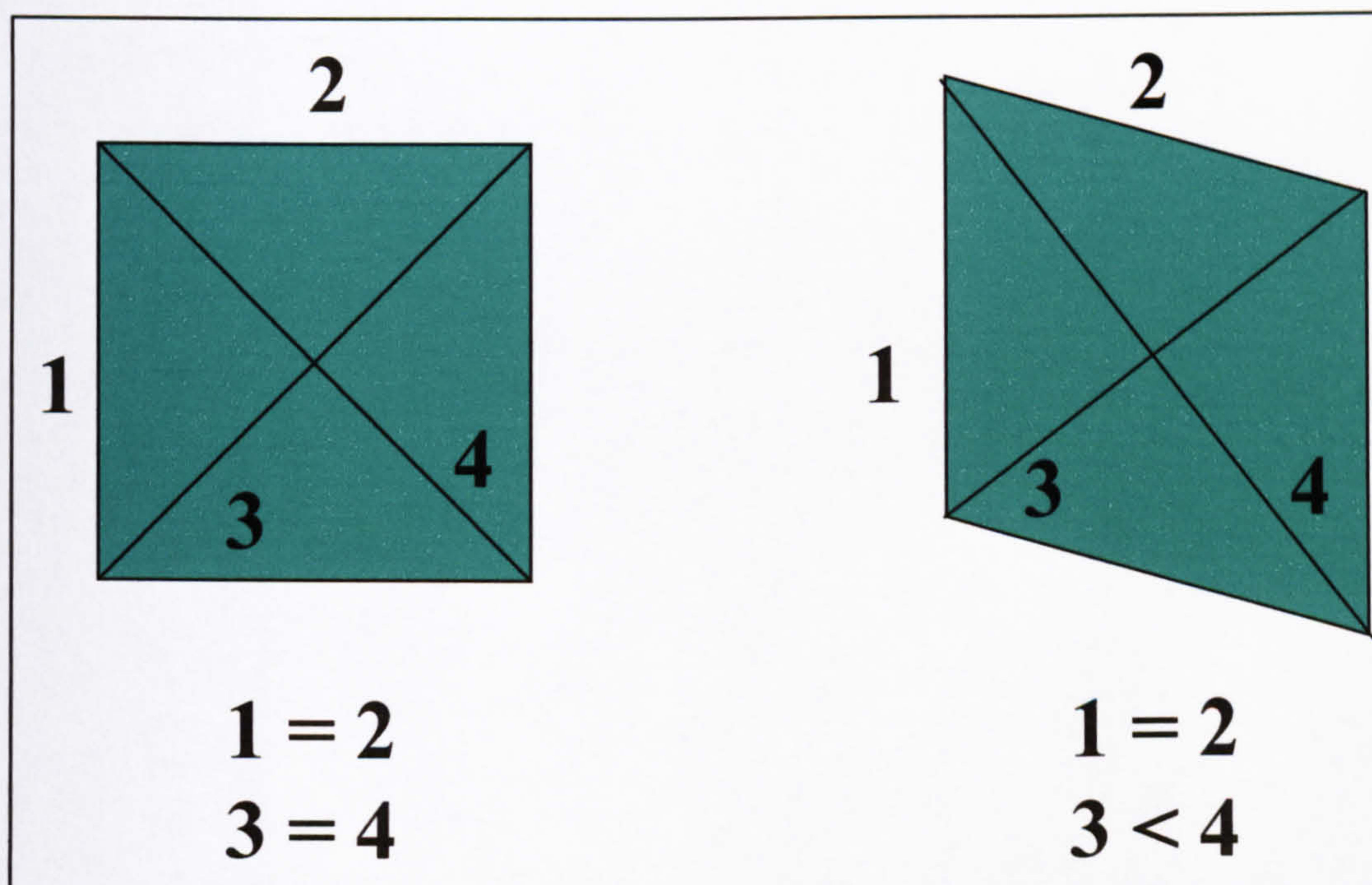


Figure 34 – Explanation of how Chem3D interprets the change in the shape of the macrocycle with the insertion of a metal atom (right) when compared with the metal free (left)

Table 10 – Angle of bonding of central atom in the phthalocyanine series

Dye	Central Metal Atom	N-M-N bond angle (°)
I	Cu	114.8
II	Zn	113.5
III	H ₂	n/a

Using surface plasmon resonance and comparing theoretical data with the experimental, it is possible to measure the thickness (d) of the monolayer. The values for the refractive index (n) and absorption coefficient (κ) can also be calculated from the real and imaginary parts of the dielectric permittivity (ϵ_r and ϵ_i respectively), which are also generated during fitting of the data (Table 11).

Table 11 – calculated thickness and optical properties of the phthalocyanine dyes

	I	II	III
ϵ_r	2.07	2.01	2.39
ϵ_i	0.98	0.95	0.89
d / nm	1.61	0.81	1.23
n	1.47	1.45	1.57
κ	0.32	0.33	0.28
Least Squares Error in fitting	4×10^{-4}	5×10^{-4}	6×10^{-3}

Using the SPR thickness and the results from the isotherm and QCM analysis, the average density of the molecule on the water surface and the quartz crystal can be calculated using Equation 11.

$$Density \text{ (g cm}^{-1}\text{)} = \frac{MW \cdot 10^{21}}{N_A \cdot A_{mol} \cdot d}$$

Equation 11

Where MW is the molecular weight of dye, A_{mol} is the molecular area ($\text{nm}^2 \text{ molecule}^{-1}$) from either the QCM or isotherm experiments, d is the thickness (nm) of the film as measured in the SPR experiments and N_A is Avogadro’s number.

The results show that only **II** varies significantly between isotherm and QCM (Table 12). This difference is likely to be the result of the QCM plate passing through the non-rigid Langmuir film and the molecules changing their orientation and/or the inter-molecular distance when transgressing from the high-pressure environment of the Langmuir film to the relatively low-pressure QCM plate. The results show that the metal-free phthalocyanine (**III**) has a multilayer structure present both pre- and post-deposition. This supports the data seen in the area-time graph and its LB UV-VIS spectrum (whilst the spectroscopic symmetry effects account for some of the difference between the peak absorbances it is unlikely that the difference would be so large).

For simple molecules such as fatty acids the Isotherm, QCM and SPR data can be used to calculate the average tilt angles in the Langmuir and Langmuir-Blodgett films. However, with such complex molecules and the degree of aggregation present (although H-aggregation is only indicated in **I**, it is likely that there will be some local

interactions in dyes II and III), it is not possible to give a true value for the average orientation of the molecules.

Table 12 – Density (g cm⁻³) calculations for the phthalocyanines

	I	II	III
Isotherm Density	1.4	2.0	2.8
QCM Density	1.6	1.0	3.2

2. Porphyrins

A series of porphyrin dyes were characterised as Langmuir-Blodgett films (Figure 35 and Table 13).

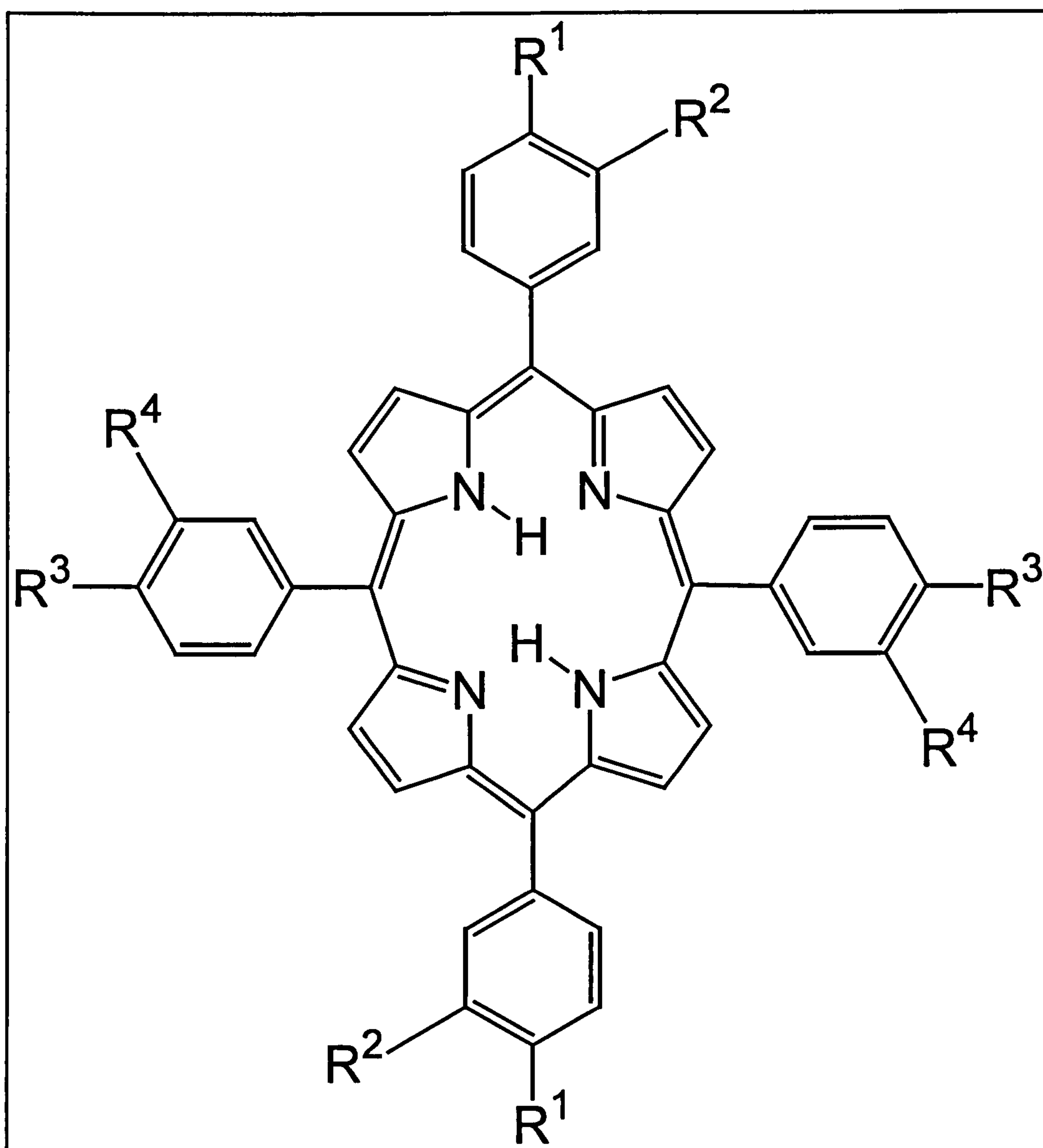

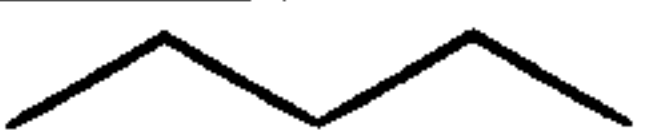
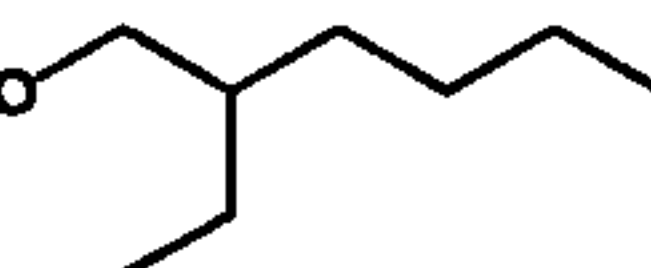
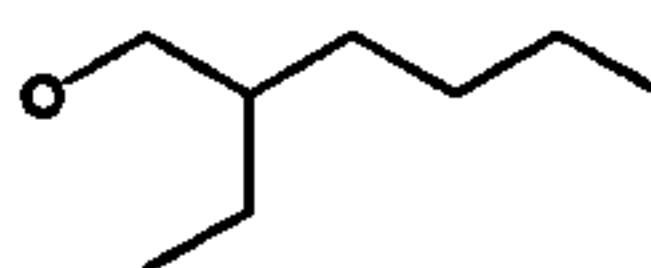
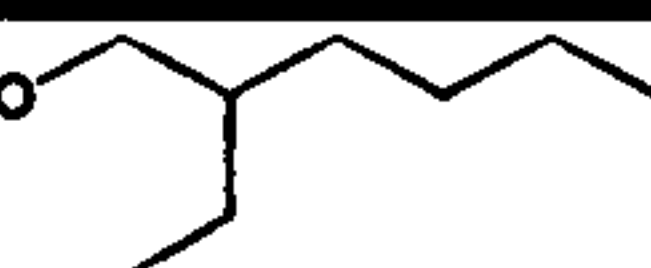
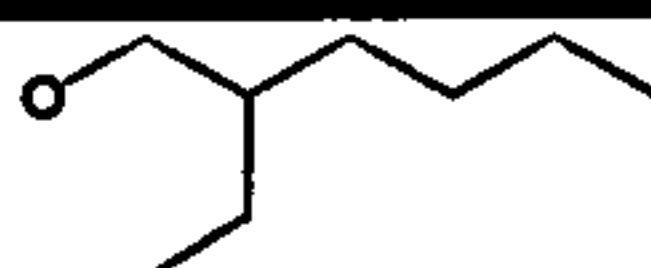
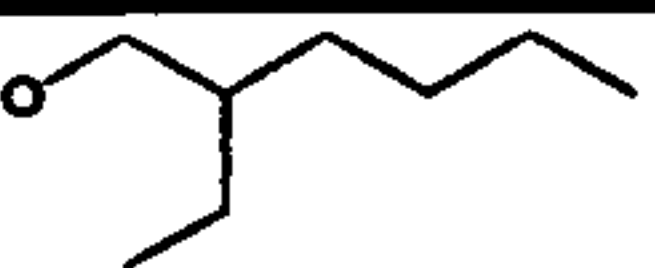
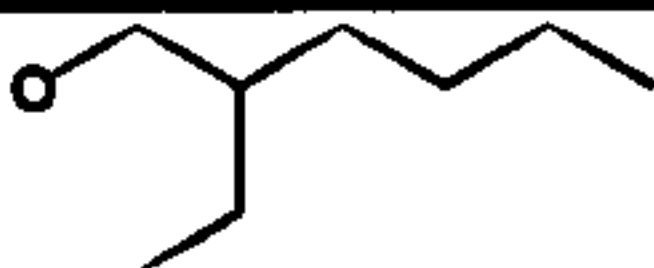
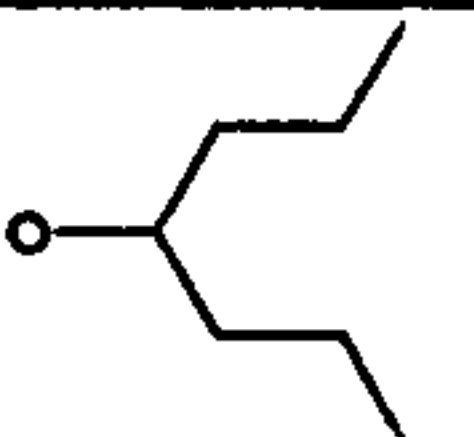
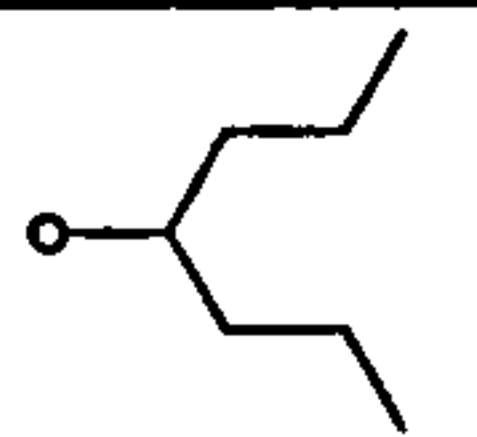
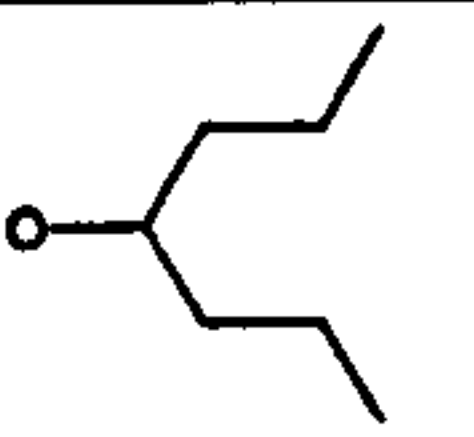
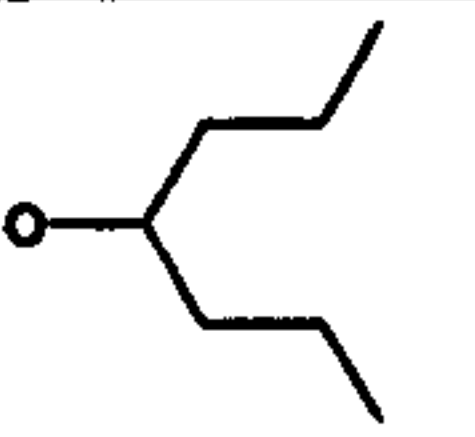


Figure 35 – Molecular structure of porphyrin dyes used (supplied by Dr. T. Richardson)

Table 13 – Substituents attached to porphyrinoid macrocycle

Dye	R ¹	R ²	R ³	R ⁴	MW
IV		H		H	895.27
V	NHCOC ₁₇ H ₃₅	H	NHCOC ₁₇ H ₃₅	H	1740.64
VI	OCOC ₁₇ H ₃₅	H	OCOC ₁₇ H ₃₅	H	1744.58
VII			NH ₂	H	1157.61
VIII					1654.46
IX					1528.22

The UV-VIS spectra of these porphyrins all have their peak absorbance at around 420 nm (the Soret or B band) and 4 less intense peaks between 500 and 700 nm, sometimes referred to as Q or satellite bands (Figure 36). These bands are interpreted as (π , π^*) in origin, where B implies a strongly allowed excited state and Q a quasi-allowed one. A comparison of the visible spectra of the metallated and metal free porphyrins shows a transition from a two-banded (D_{4h} -type) to a four-banded (D_{2h} -type) spectrum. This dramatic change can be attributed to the breaking of the D_{4h} symmetry of the porphyrin ring by the central proton axis. The addition of substituents to the phenyl groups of the tetraphenylporphyrin (TPP) ring exhibits Q bands which are red-shifted with respect to the TPP free base (although the Soret bands are at about the same wavelength) ⁽¹³⁶⁾. These Q bands are transitions normally numbered *I*, *II*, *III* and *IV* starting from the low-energy end, with *I* and *III* (which are forbidden transitions) increasing in intensity if the porphyrin molecule is made less symmetrical through substitution (*II* and *IV* are allowed vibrational bands). Generally, when the π -electron density around the periphery is increased (perhaps by the addition of electron-withdrawing groups), a bathochromic shift is observed ⁽¹³⁷⁾.

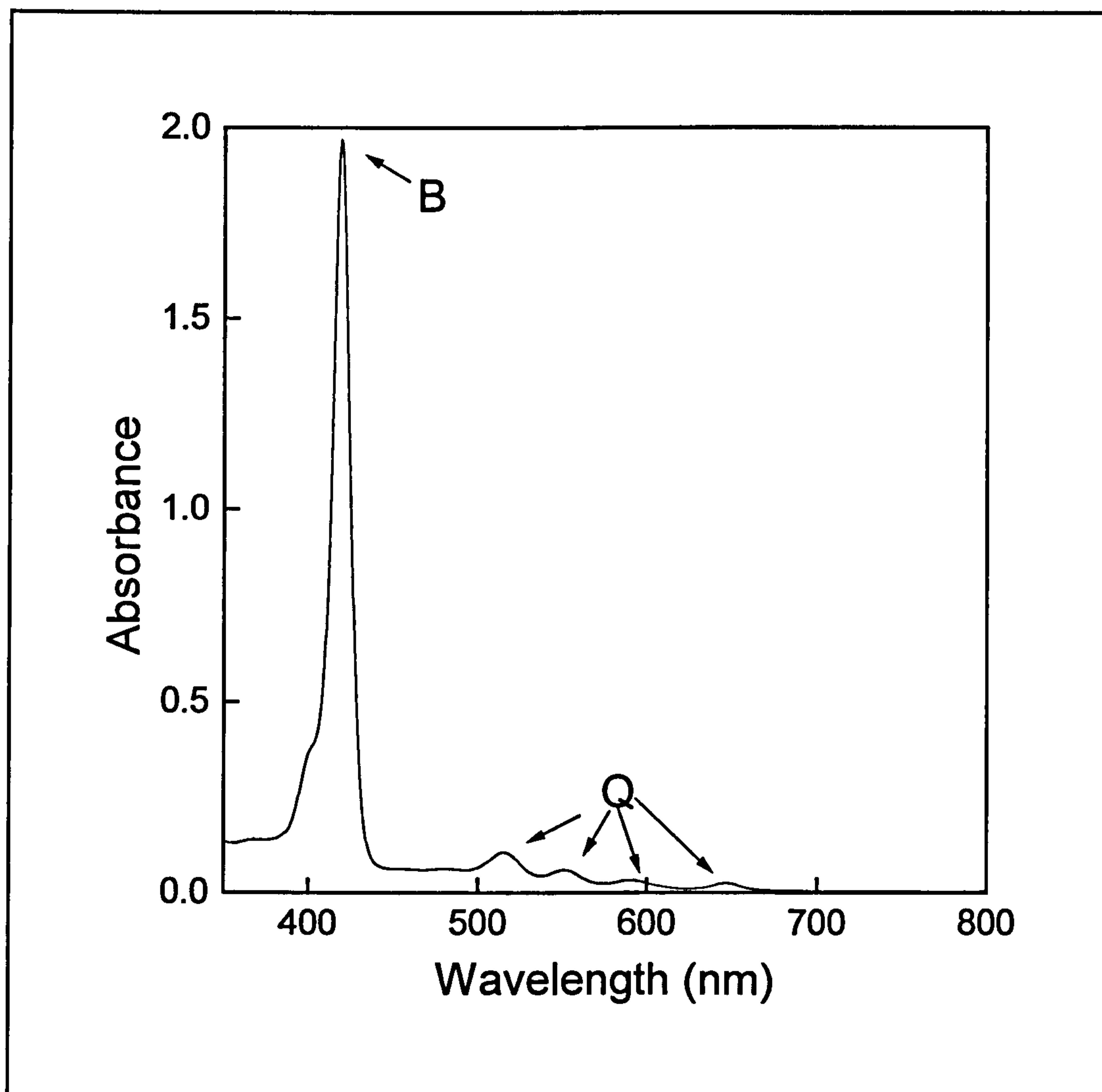


Figure 36 – UV-VIS absorption spectrum of dye IV in trichloromethane showing the main absorption and satellite bands characteristic to porphyrin dyes

2.1 Tetra-substituted porphyrins

Dyes IV, V and VI all fall into the tetra-substituted porphyrin category. Their UV-VIS spectra are very similar with the substituents having a small effect on the location of the Q bands (Table 14).

Table 14 – UV-VIS characteristics of the monolayers and solutions (trichloromethane) of the three dyes

Dye	B _{solution} (nm)	B _{monolayer} (nm)	Q _{solution} (nm)				Q _{monolayer} (nm)			
IV	419	449	515	551	590	646	523	553	594	647
V	422	427	516	552	589	646	516	554	593	652
VI	418	448	514	550	590	645	523	554	594	651

The comparison of the solution (trichloromethane) and the Langmuir-Blodgett spectra indicates that whilst dye V does not aggregate upon deposition, the red-shift of around 30 nm seen for both IV and VI in the B band suggests that an ordered structure may be present in the deposited layer.

The presence of the satellite bands (indeed a small shift is also present in one of the Q bands (*IV*) – from 514 / 515 to 523 nm) indicates that the peak at circa 440 nm present in both IV and VI dyes is the result of packing and not the formation of a dication species.

The oxidation and protonation of the porphyrin ring can be demonstrated through the addition of a few drops of acid to a trichloromethane solution of IV. This results in the destruction of the peaks at 419, 515, 590 and 646 nm and the formation of a dication with peaks at 447 and 670 nm (Figure 37).

Interestingly, when the porphyrin dication species is spread on a water surface and deposited as a Langmuir-Blodgett film the macrocycle appears to revert back to the unprotonated (original) form (from early observations of acid-contaminated solution).

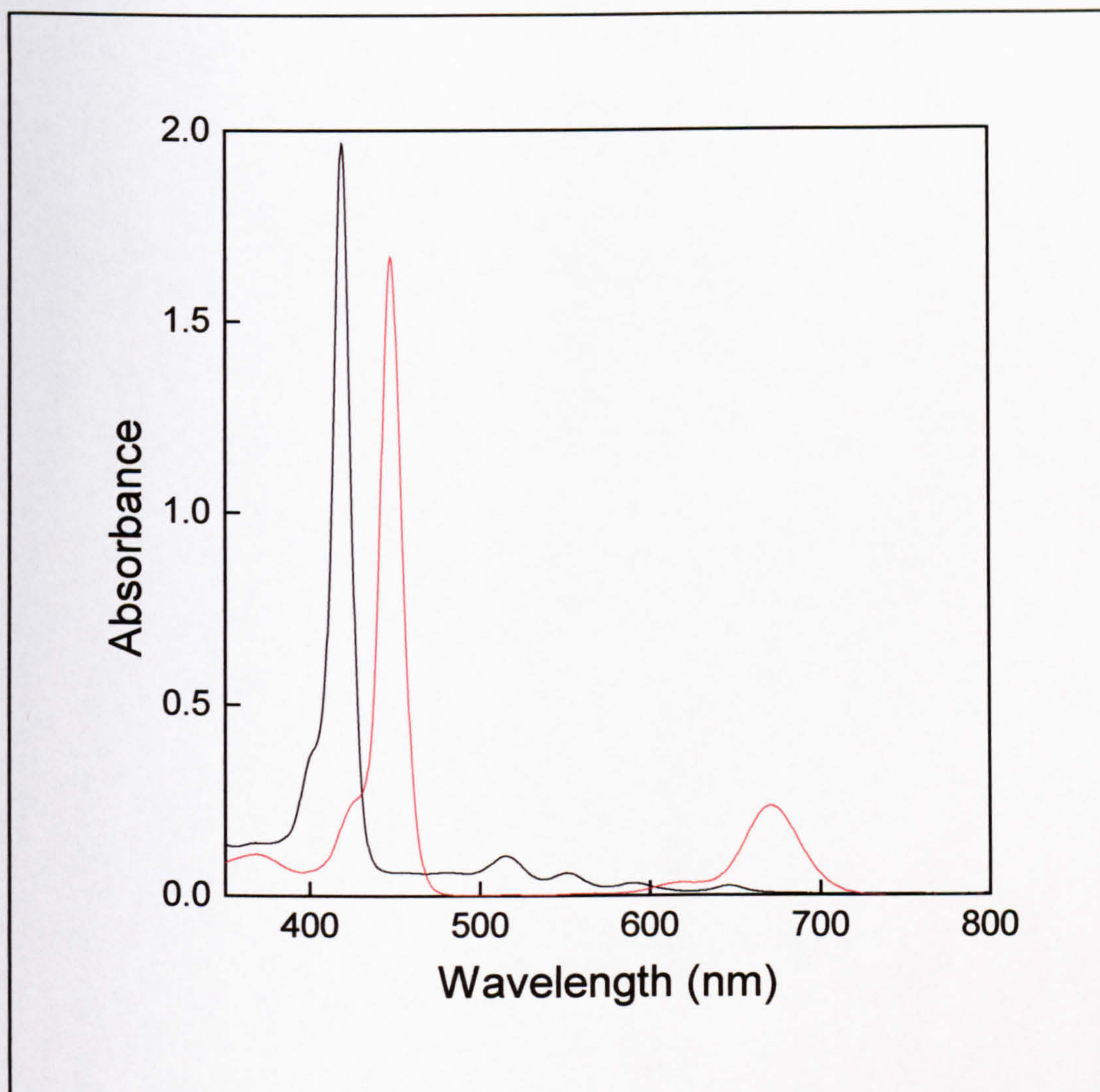


Figure 37 – Comparison of a trichloromethane solution of IV (—) and a trichloromethane solution of IV with a few drops of HCl added (—)

To determine the nature of any packing present in the Langmuir-Blodgett films, their pressure-area isotherms were examined.

The comparison of the three dyes suggests that **V** forms a good Langmuir film whilst the slow initial increase in surface pressure upon compression of **VI** and low breaking point of **IV** implies poorer films (Figure 38).

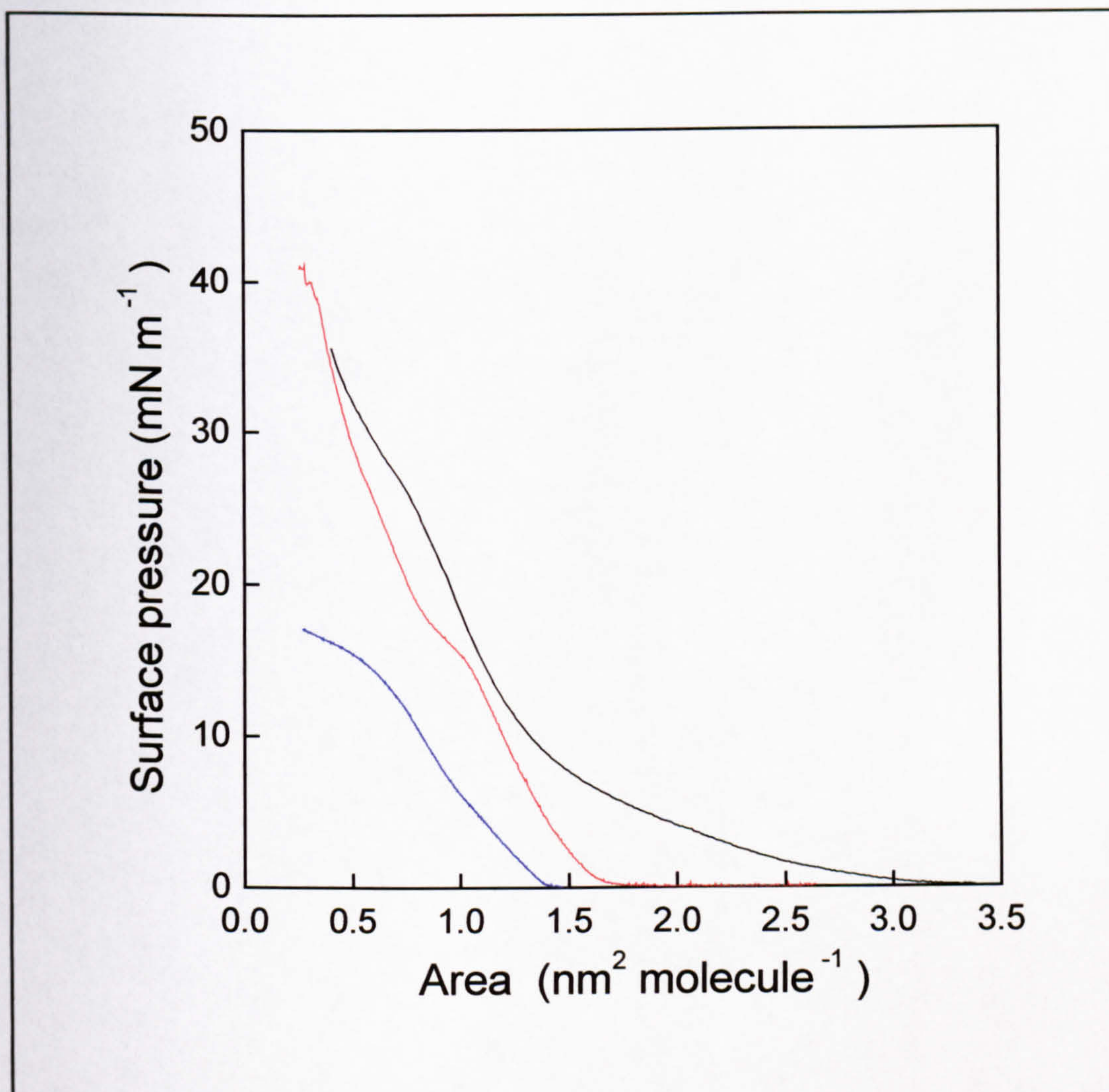


Figure 38 – Langmuir pressure-area isotherms of three porphyrins
 (— dye IV, — dye V, — dye VI)

The analysis of the isotherm of **IV** through double-differentiation of the data suggests that the molecules are randomly spaced out and clumping (i.e. multilayer island-like formation) is present at the air-water interface (Figure 39). This is in agreement with the suggestions of Bull *et. al.* ⁽¹³⁸⁾. The isotherm clearly has a number of points of inflexion that may be attributed to either the (further) formation of multilayer structures and/or the closure of any local gaps in the film. Whilst most Langmuir films have gaps present before compression, few retain them after the take-off (the point where the surface pressure increases with decreasing molecular area). The reason why these gaps occur in porphyrin Langmuir films may be due to the formation of multilayer structures facilitated by the π -electron interactions between adjacent molecules. These island-like

structures when located around the Wilhelmy plate induce a local decrease in the surface tension and as more islands are pushed together by the decreasing surface area, the density increases and with it the surface pressure. The gaps in the solid dye at the air water interface ensure that there is a slow increase in pressure when compared with materials that have uniform floating film. This can be seen in the UV-VIS absorption spectra, where the intensities can vary between depositions of the same material under the same conditions.

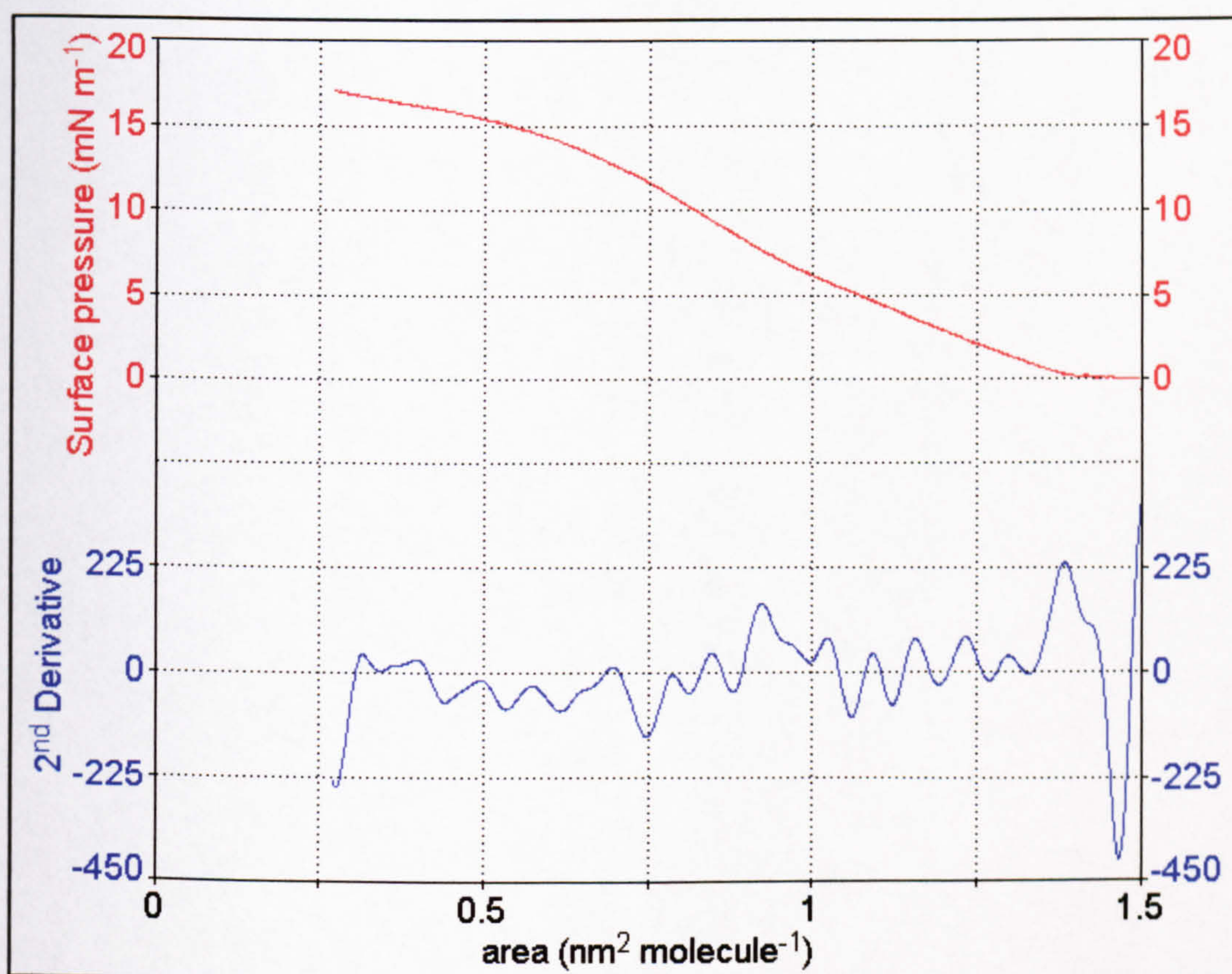


Figure 39 – Isotherm (—) and 2nd differential (—) of IV

The pressure-area isotherm of V has a visible point of inflexion at around 15 mN m⁻¹ and 4 others at various pressures (10, 21, 28, 35 mN m⁻¹). This indicates that the monolayer film starts to break at around 14 mN m⁻¹ followed by formation of multilayers (signified by the points of inflexion between 15 and 40 mN m⁻¹) (Figure 40). The isotherm is similar to previously reported work, but the take-off is 1.7 nm² molecule⁻¹ (cf. 2.8 nm² molecule⁻¹)⁽⁸³⁾. The reason for this difference could be

the compression speed during the isotherm experiments. The barrier speed used in all isotherm experiments was $30 \text{ cm}^2 \text{ min}^{-1}$ which is considered the best compromise between allowing for molecular rearrangement and preventing any loss of dye molecules to the edge of the trough, barriers or into the subphase itself. This value was not reported in the aforementioned previous research and any increase in the compression speed would particularly have an effect on molecules that form patchy films containing multilayer structures.

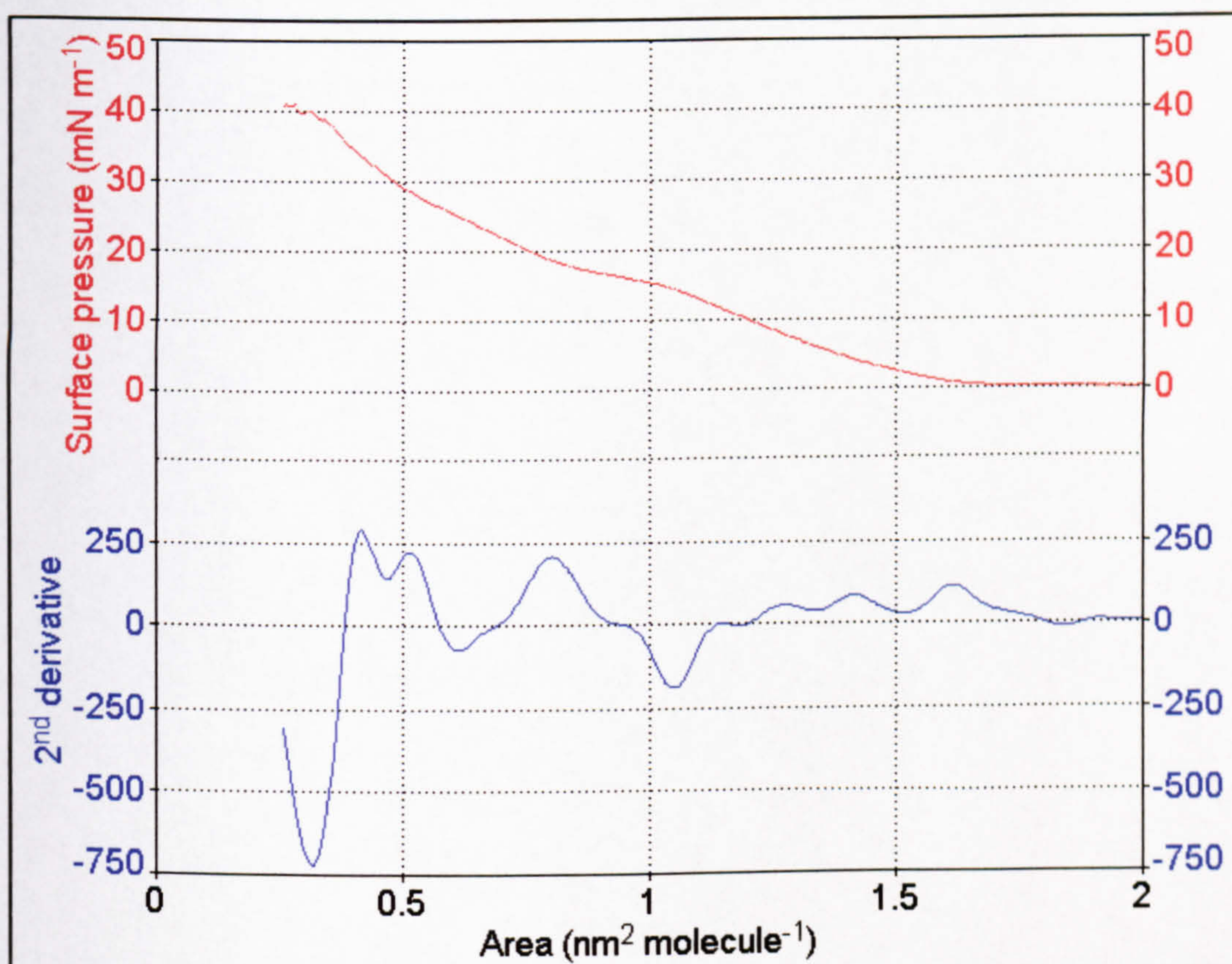


Figure 40 – Isotherm (—) and 2nd differential (—) of V

In comparison the broad isotherm of **VI** is similar to **IV**, whilst it has an obvious significant change in gradient, the dye clearly forms a patchy, poor Langmuir film particularly at low pressures (Figure 41). There are many points of inflexion after take-off and it is likely that there are molecules aggregating together in multilayer structures at the air-water interface.

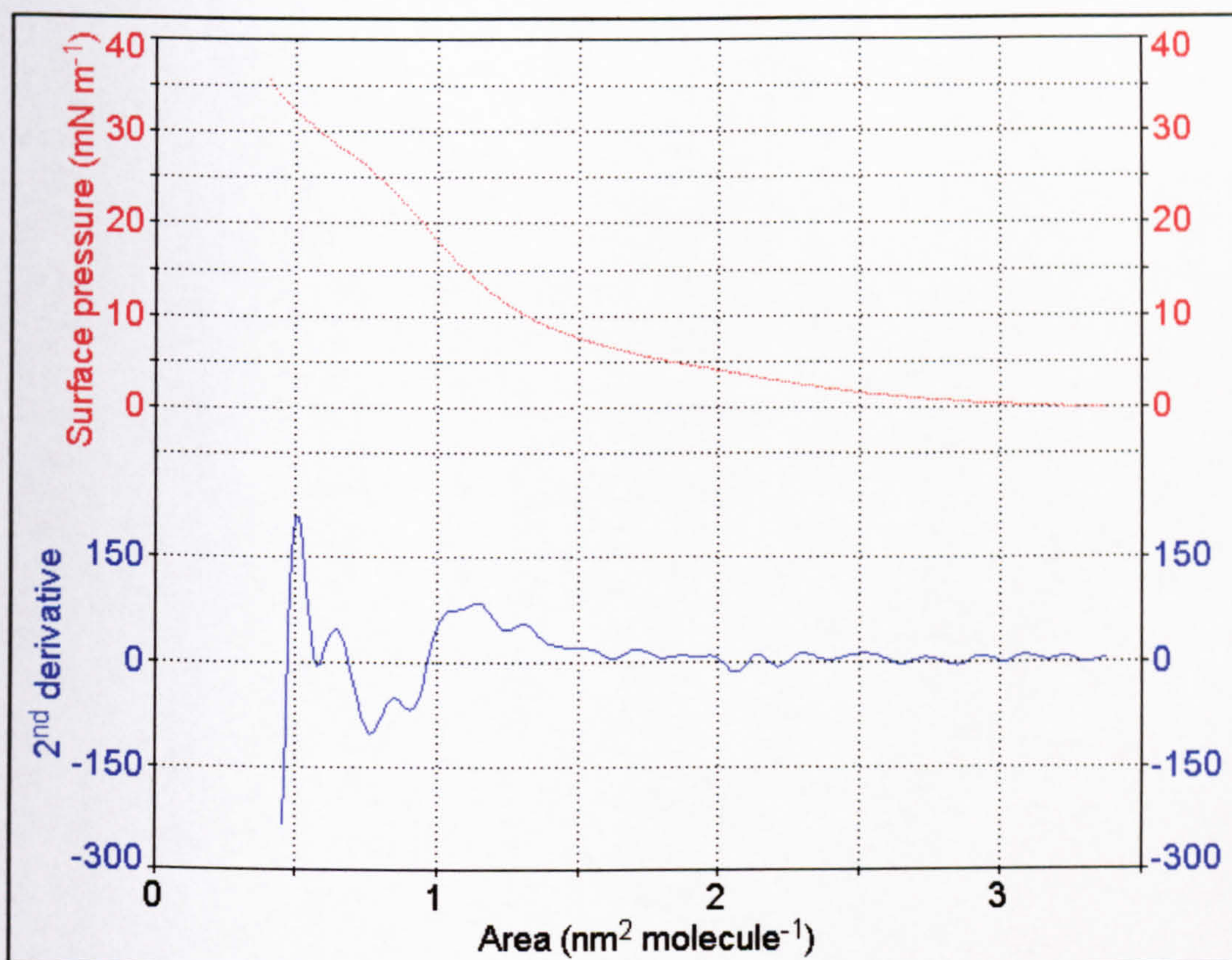


Figure 41 – Isotherm (—) and 2nd differential (—) of VI

One further point to consider is the peripheral substituent attached to the tetraphenylporphyrin macrocycle in dye V, it contains -NHCO- . In nature, two molecules containing this structure are bound together through hydrogen bonding. The classic example of this type of bonding is between the base pairs in DNA. Therefore aggregation is likely to be more prevalent between adjacent molecules of this dye than some other long chain substituents where steric hindrances might encourage monomers.

The presence of island-like structures on the water surface means that QCM analysis is very difficult (Table 15). The results do not correlate with those obtained from the pressure-area isotherms.

Indeed even with the combination of the calculated SPR results (Table 16) to estimate the average density of the films the true nature of the materials on the surface of substrate or subphase is not clear (Table 17). The densities are not similar when calculated from isotherm and QCM data, indicating some clumping on the water surface (and further aggregation when the quartz substrate is passed through the air-water interface, demonstrated by the increase in density from isotherm calculations to QCM).

The only conclusions that can be drawn is that their nature is to form poor Langmuir (and subsequently Langmuir-Blodgett) films which are difficult to characterise.

Table 15 - Comparison of isotherm and QCM data for dyes IV to VI

Data Source		IV	V	VI
Isotherm	A_d / nm^2	0.82	1.20	1.33
	A_o / nm^2	1.33	1.55	2.65
QCM	A_d / nm^2	0.23	0.54	0.69
	STD / nm^2	0.02	0.03	0.13

Table 16 – Calculated SPR data for IV, V and VI

	IV	V	VI
ϵ_r	2.30	2.32	2.17
ϵ_i	0.29	0.30	0.83
d / nm	1.45	4.51	2.24
N	1.55	1.53	1.50
κ	0.10	0.10	0.28
Least Squares Error in fitting	8×10^{-4}	3×10^{-4}	7×10^{-4}

Table 17 – Density (g cm^{-3}) of IV, V and VI in both Langmuir and LB form

	IV	V	VI
Isotherm Density	1.3	0.5	1.0
QCM Density	4.5	1.2	1.9

2.2 Porphyrins with more than 4 substituents

Dye **VII** differs from all the other porphyrins studied because there is more than 1 type of substituent attached; it has 2 amino and 4 ethylhexyloxy components.

The addition of up to 4 more substituents to the tetraphenylporphyrin ring provides little change in the UV-VIS spectra (Table 18). In each case these macrocycles have their main absorption band (when deposited as LB films) red-shifted from that in trichloromethane, which is due to π - π interactions between molecules on the substrate. The comparison with a tetra-substituted porphyrin (e.g. **VI** – highlighted) shows that the main absorption band is slightly blue shifted in solution and red-shifted in monolayer form, but the satellite bands are relatively unchanged.

Table 18 – Comparison of UV-VIS spectra of porphyrin dyes IV-IX (N_{subs} = number of substituents)

Dye	N_{subs}	$B_{solution}$ (nm)	$B_{monolayer}$ (nm)	$Q_{solution}$ (nm)				$Q_{monolayer}$ (nm)			
VI	4	418	448	514	550	590	645	523	554	594	651
VII	2 + 4	426	432	520	558	591	652	522	561	603	656
VIII	8	424	438	519	557	594	650	520	558	597	656
IX	8	425	446	520	558	596	649	522	562	601	660

The pressure-area isotherms of these more sterically hindered porphyrins demonstrate that **IX** appears to form the best Langmuir film of these three dyes; it has a higher breaking point and a steeper curve (Figure 42).

Dye **VII** is similar in structure to **VIII** (NH_2 and H replacing half of the substituents). It is noticeable that **VIII** might appear to form poorer Langmuir films than **VII** and this may be due to the hydrophilic NH_2 groups helping to orientate the molecules on the water surface, reducing the interaction between the subphase and the hydrophobic ethylhexyloxy groups.

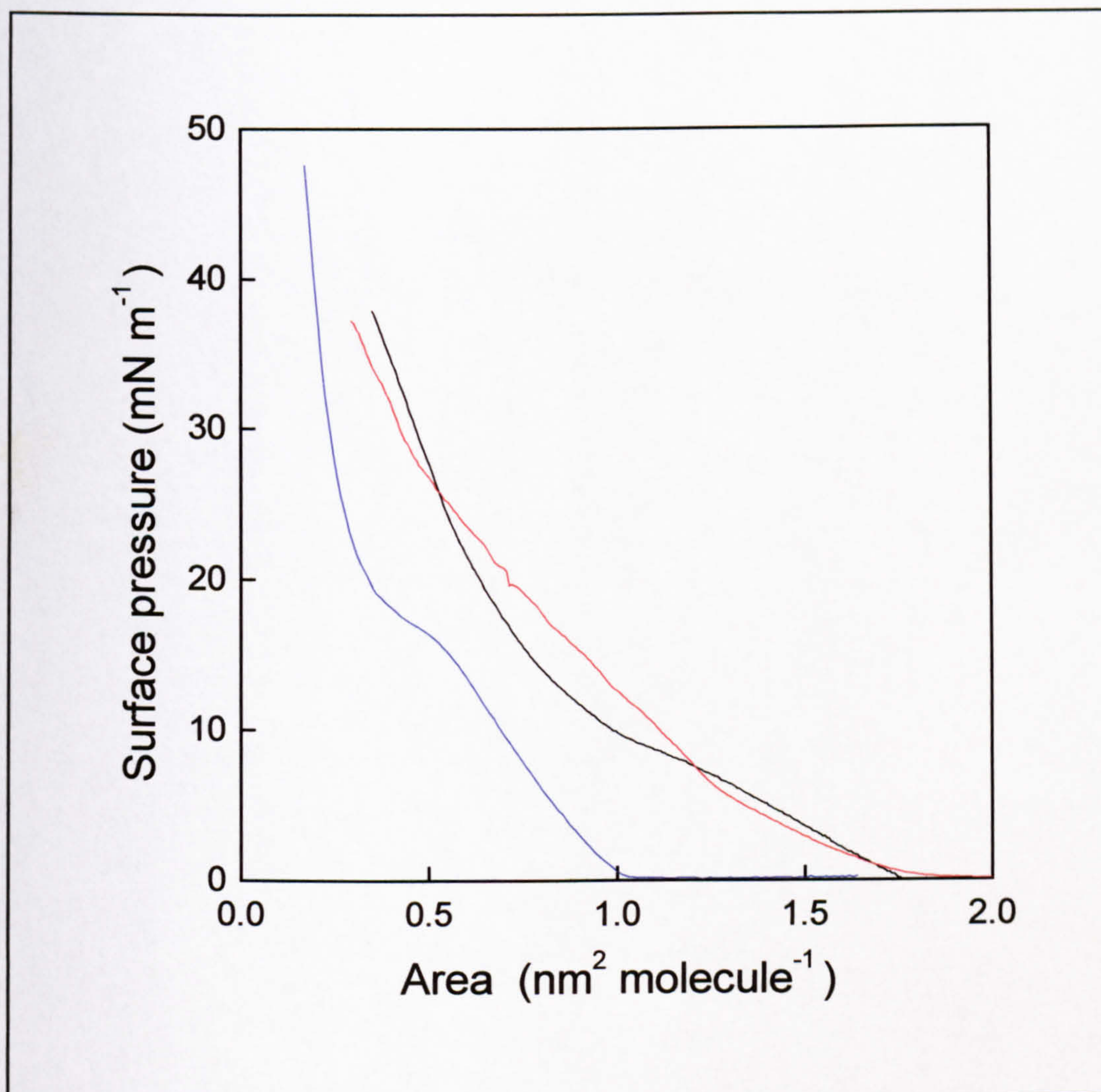


Figure 42 – Comparison of pressure-area isotherms of dyes VII (—), VIII (—) and IX (—)

The analysis of the 2nd differential of the pressure-area isotherm of **VII** shows that the Langmuir film formed is actually quite poor; the curve has stationary points just after take-off, indicating patchiness and surface-aggregation (Figure 43). The presence of both ether and amino groups indicates that hydrogen-bonding will occur between macrocycles which, coupled with the π - π interactions of the central rings, is more favourable than the hydrophilic nature of the central ring system and NH_2 groups.

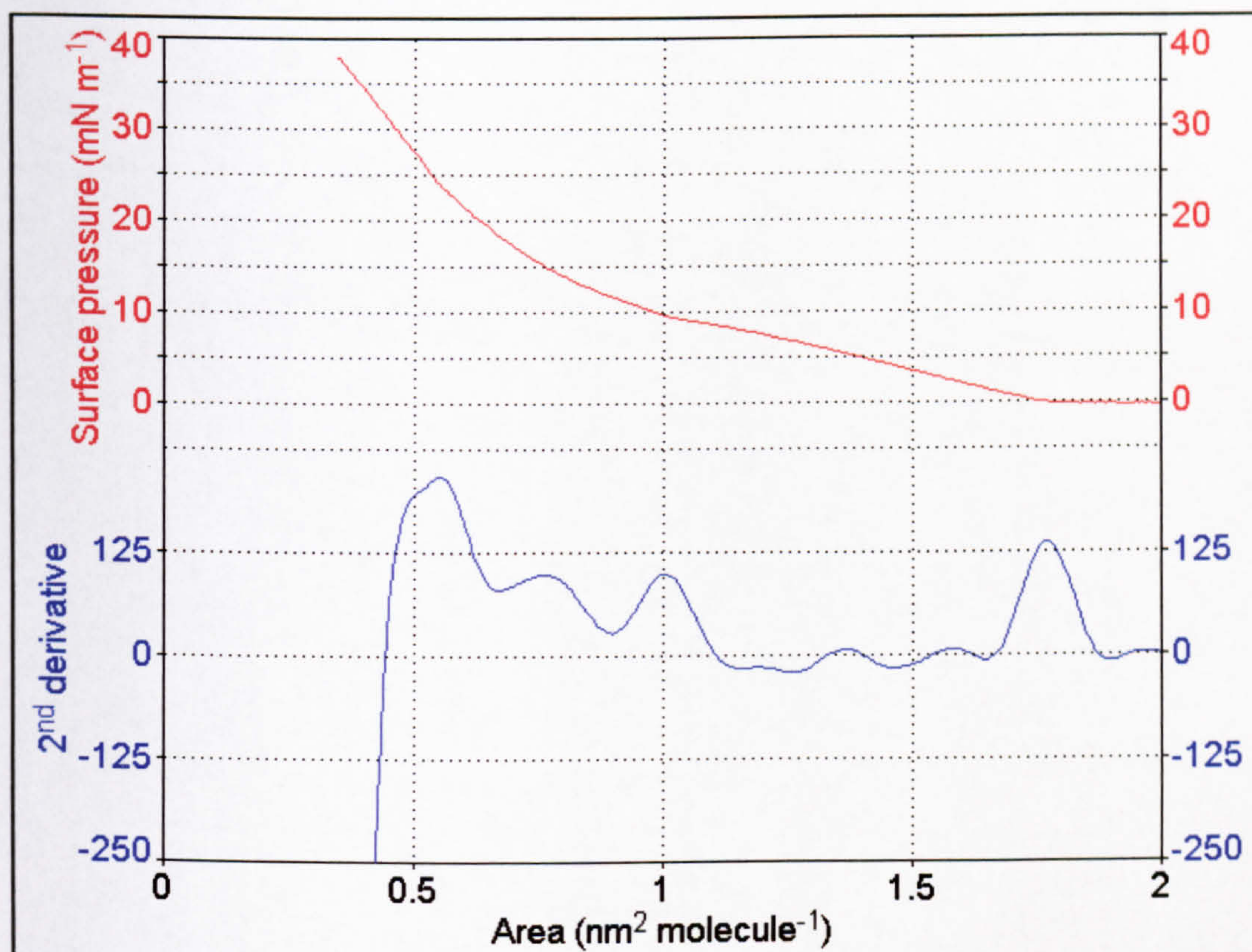


Figure 43 – Isotherm (—) and 2nd differential (—) of VII

The 2nd differential of the isotherm of **VIII** shows that the removal of the hydrophilic NH₂ groups and addition of more hydrophobic propylbutyloxy groups creates a poorer Langmuir film, with a greater number of points of inflexion after take-off; the formation of multilayer structures is likely to be prolific at the air-water interface.

Whilst both dyes form poor floating layers with the formation of island like structures, what is interesting is the difference in their 2nd differential curves. Dye **VII** has points of inflexion almost directly after take-off indicating that the formation of the multilayers is relatively simple, whereas with **VIII** the formation is slightly hindered and the points of inflexion are further from the take-off. The steric hindrances of the propylbutyloxy groups are likely to be the reason for this difference, whilst in **VII** the hydrogen-bonded -NH₂ and -OCH(C₃H₇)C₃H₇ groups counteract this effect.

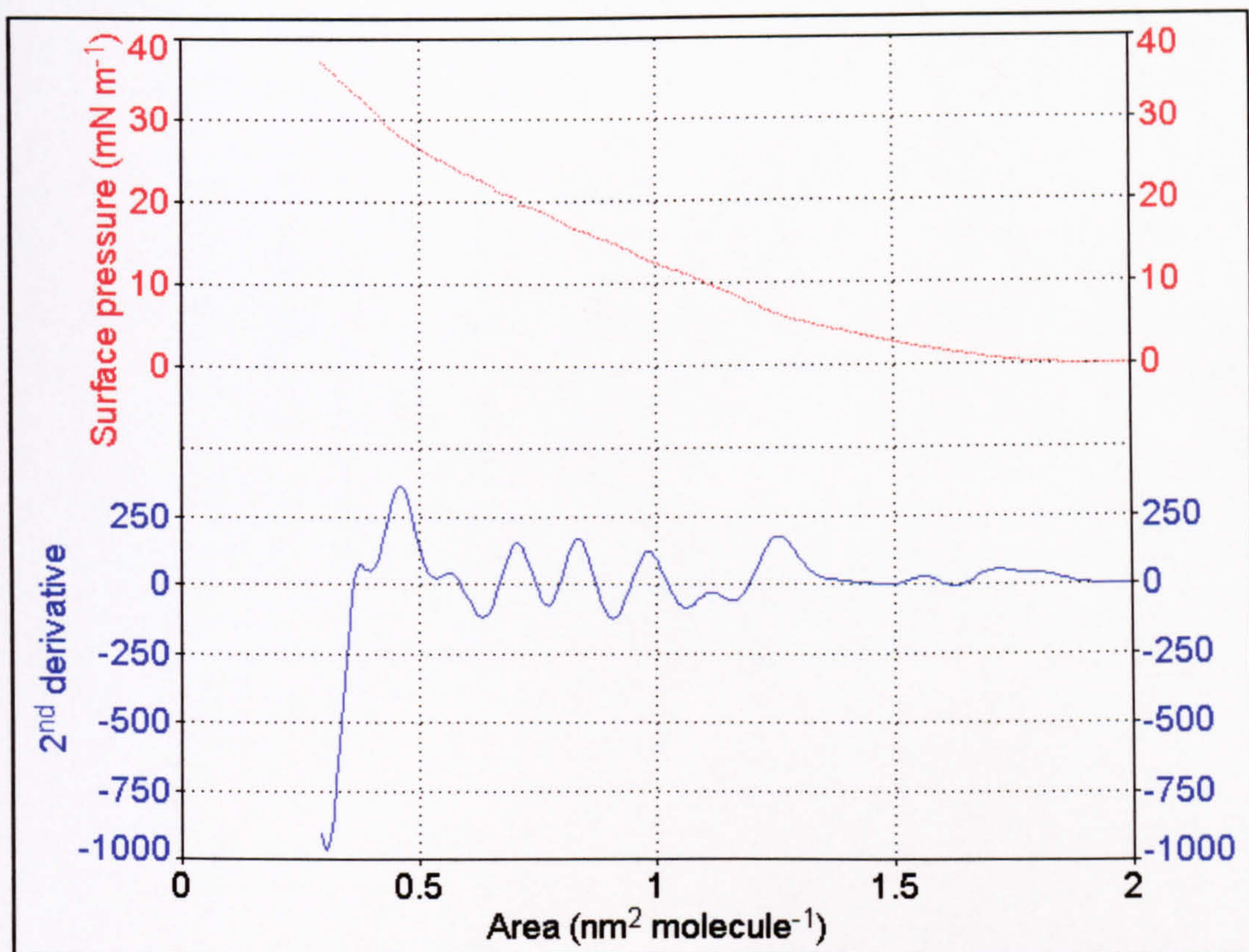


Figure 44 – Isotherm (—) and 2nd differential (—) of VIII

As indicated previously, the pressure-area isotherm of **IX** suggests a more compact (and hence ordered) film compared with the other two dyes. The 2nd differential of this curve shows that although there is some variation around zero after take-off, there is no clear point of inflexion until $0.6 \text{ nm}^2 \text{ molecule}^{-1}$ which is the start of the clearly visible plateaux in the isotherm (Figure 45). The reasons for the improved Langmuir film are not easily explained from the structure of the porphyrin. The propylbutyloxy substituents are hydrophobic, which coupled with the hydrophilic centre ring system, might suggest a “dead spider” orientation (Figure 46).

Using Chem3D it is possible to estimate the dimensions of the dye (Table 19). The results show (when compared to the isotherm data) that the orientation is likely to be a tilted edge-on configuration which maximises the π - π interactions (confirmed by the 20 nm red-shift in the B band of the monolayer from the solution spectrum) and minimises the interaction between the hydrophobic propylbutyloxy groups and the water subphase.

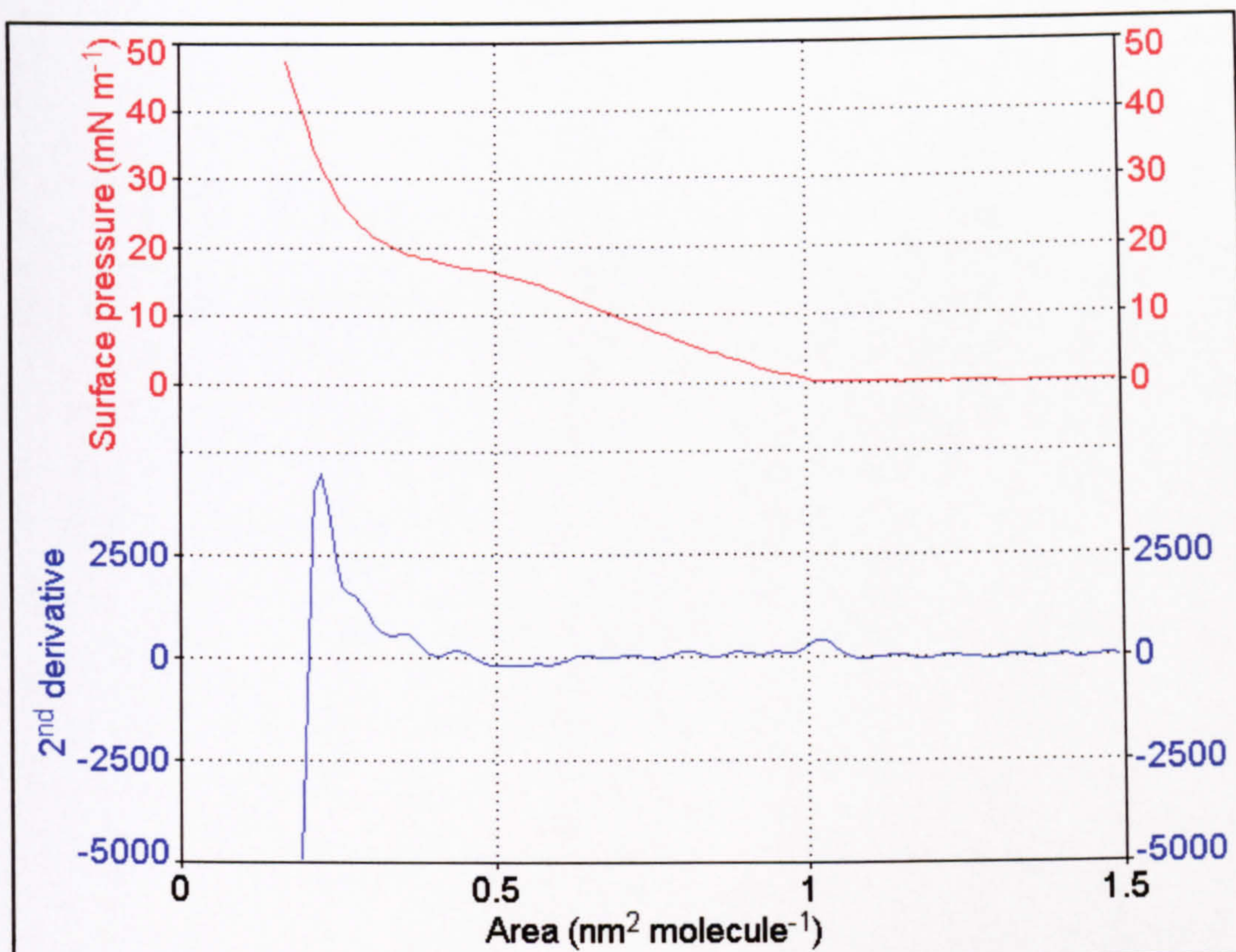


Figure 45 – Isotherm (—) and 2nd differential (—) of IX

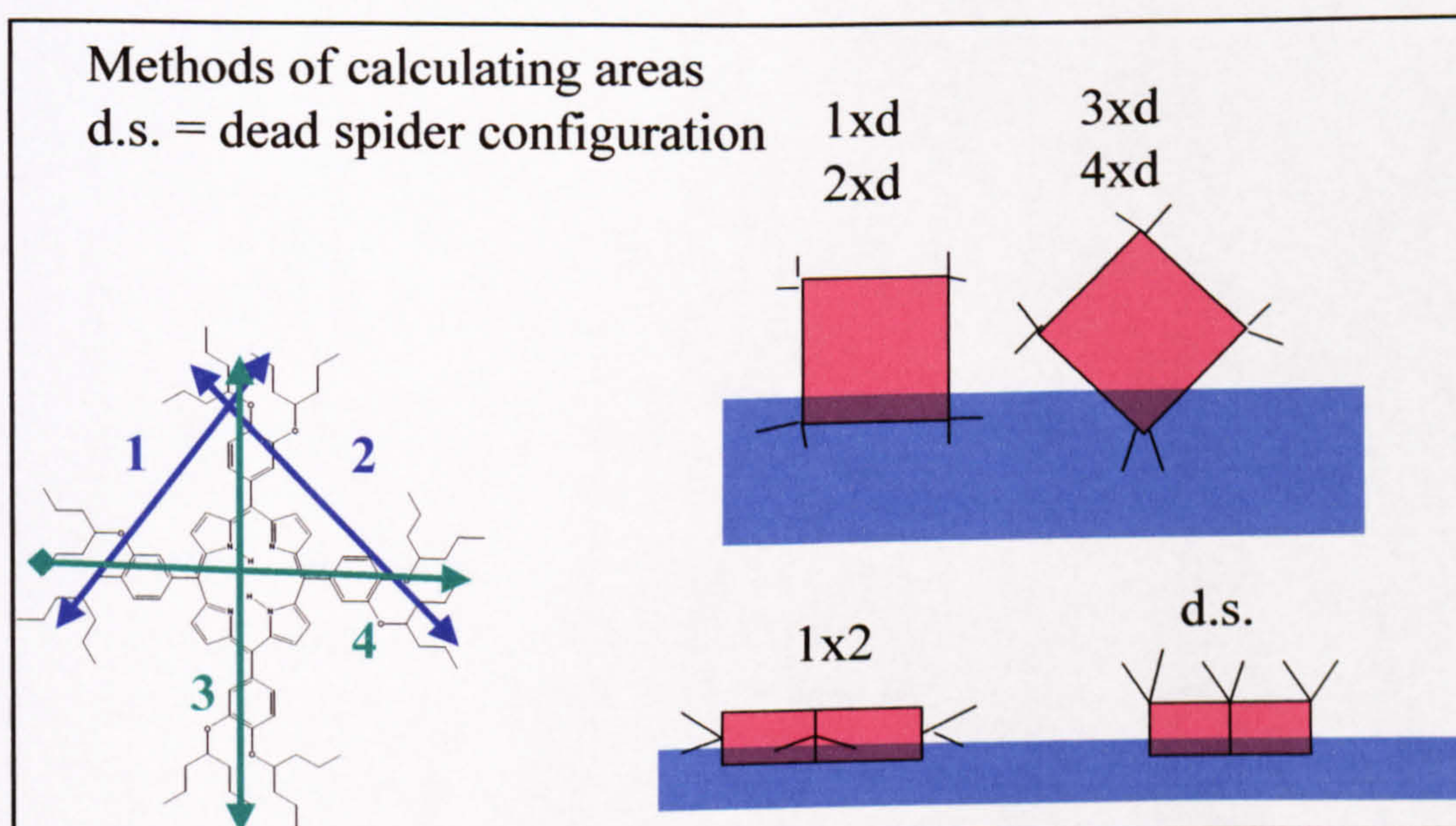


Figure 46 – diagram illustrating different representations of areas

Table 19 – Theoretical measurements and calculated areas of IX

Thickness (d)		measurements				Calculated area			
		1	2	3	4	1 x 2	d.s.	1 x d	3 x d
IX	0.3	2.0	2.0	2.3	2.3	4.0	1.7	0.4	0.5
All measurements are in nm and include VDWs average error in measurements is ± 0.1 nm									

From the QCM studies of these three dyes, it can be seen that the formation of multilayer structures can be facilitated through the interruption of floating layer (Table 20). Even the “good” Langmuir film of **IX** forms multilayers when the quartz crystal passes through the air-water interface, demonstrated by the reduction in molecular area. The comparison A_d from the isotherm and QCM should yield similar results for a stable monolayer. There may be a slight expansion due to the transition from high pressure environment of the Langmuir film to the relatively low pressure quartz crystal.

Table 20 - Comparison of isotherm and QCM data for dyes VII to IX

Data Source		VII	VIII	IX
Isotherm	A_d / nm^2	0.98	1.11	0.69
	A_o / nm^2	1.73	1.48	0.99
QCM	A_d / nm^2	0.54	0.65	0.28
	STD / nm^2	0.04	0.43	0.01

The results of the SPR experiments give a much clearer indication of the orientation of the molecules on the substrate surface (Table 21).

Clearly, **IX** does form multilayers upon deposition; 11.74 nm is far too great to be a monolayer (the thickness clearly cannot exceed the maximum length of the molecule – measured as 2.3 nm, *see* Table 19) and the degree of angular shift and decrease in surface plasmon resonance (from gold scan to gold and LB film scan) means that it is not an error in theoretical fitting routine.

Whilst **VII** does not form a monolayer (which would be 2.0 nm if an edge-on orientation was adopted), the initial interpretation of the SPR scan of **VIII** might indicate monolayer formation. In fact, if the molecules were face-down on the water

(and hence substrate) surface, the thickness would be no more than 1 nm (which assumes 0.3 for the thickness of the central ring and 0.6 nm for the upright propylbutyloxy substituents and 0.1 nm for VDW forces).

Table 21 – Calculated SPR data for VII, VIII and IX

	VII	VIII	IX
ϵ_r	2.50	2.26	2.37
ϵ_i	0.54	0.61	0.38
d / nm	5.31	1.84	11.74
n	1.49	1.52	1.50
κ	0.10	0.20	0.11
Least Squares Error in fitting	1×10^{-3}	3×10^{-3}	9×10^{-4}

The calculation of the density of the dyes in both Langmuir and Langmuir-Blodgett form shows an increase from the air-water interface to the substrate – indicating the presence of island-like structures (Table 22). It is not possible to calculate the Langmuir density for **IX** by this method as there may be a significant change between the floating film and that deposited onto a substrate.

Table 22 – Density (g cm⁻³) of VII, VIII, and IX in both Langmuir and LB form

	VII	VIII	IX
Isotherm Density	1.3	0.5	N/A
QCM Density	4.5	1.2	1.9

3. Bis-phthalocyanine / porphyrin triple-decker sandwich

The use of hybrid porphyrin-phthalocyanine sandwiches has been investigated in the past to determine whether the advantages of each macrocycle can be incorporated into one material. In this case a phthalocyanine free base was linked to two tetraphenylporphyrin free bases with Gadolinium atoms (Figure 47 and Figure 48).

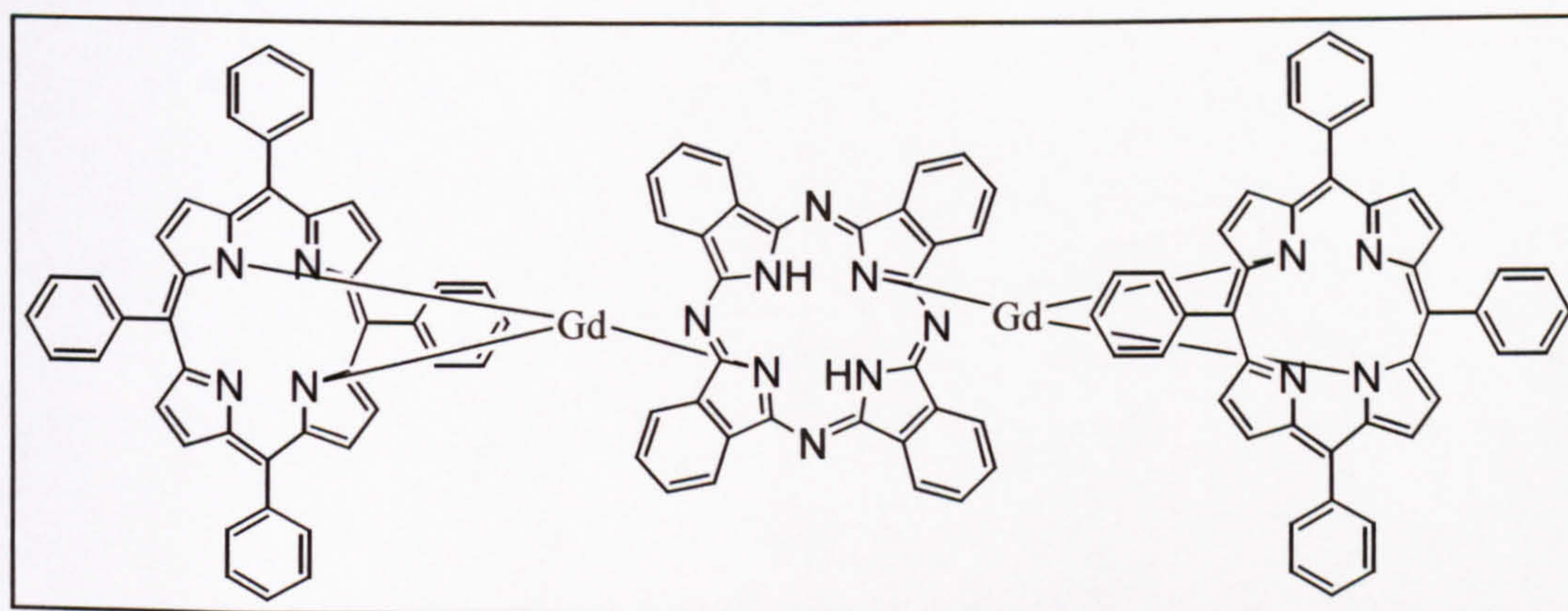


Figure 47 – Molecular structure of X (supplied by Dr. T. Richardson)

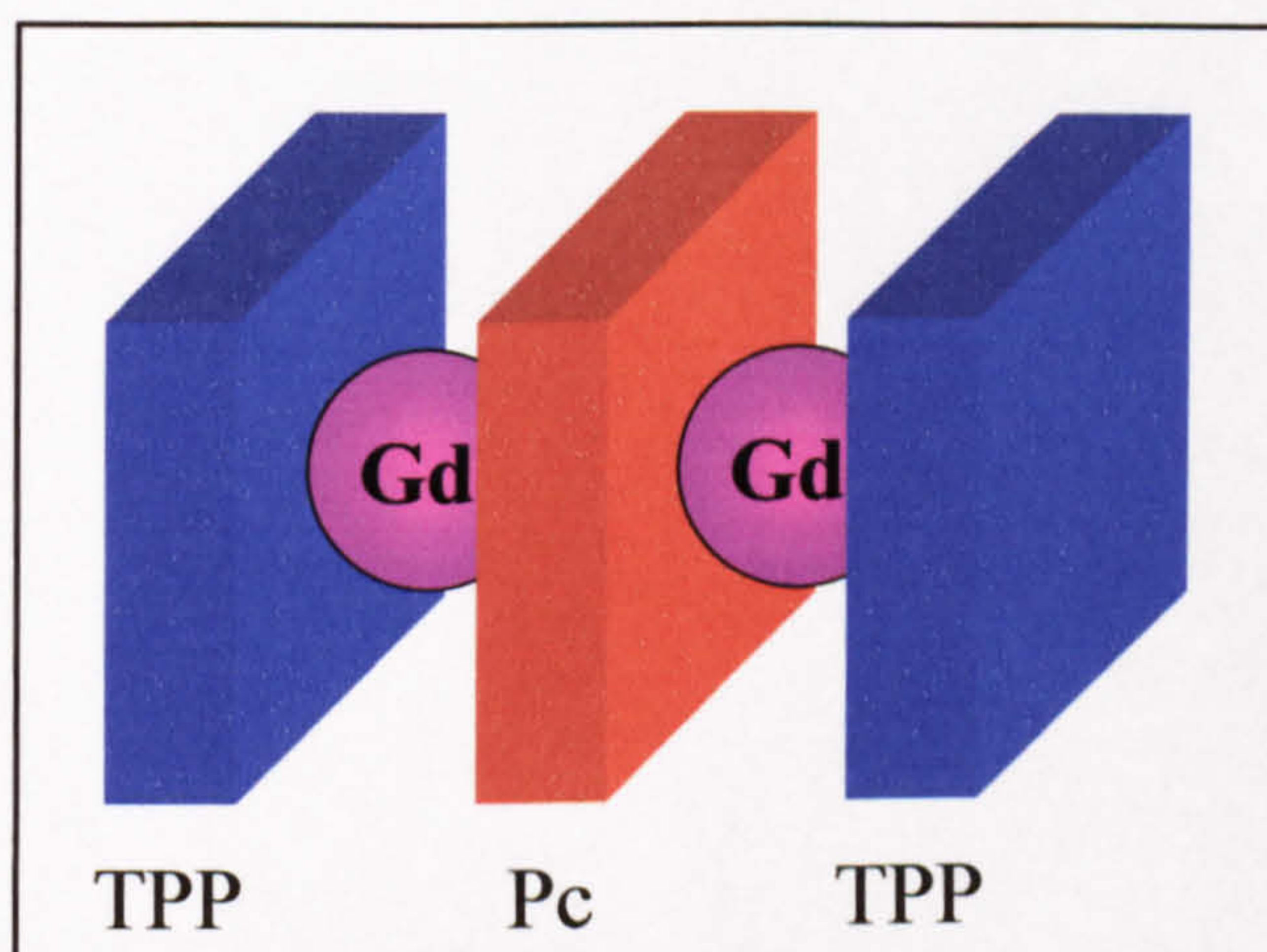


Figure 48 – Physical representation of layout of molecules in X

The UV-VIS spectrum of the dye has a main absorption peak in trichloromethane at 770 nm (which is red-shifted to 814 nm in monolayer form) (Figure 49). Additionally, there are small peaks either side of the main absorbance at 690 and 840 nm.

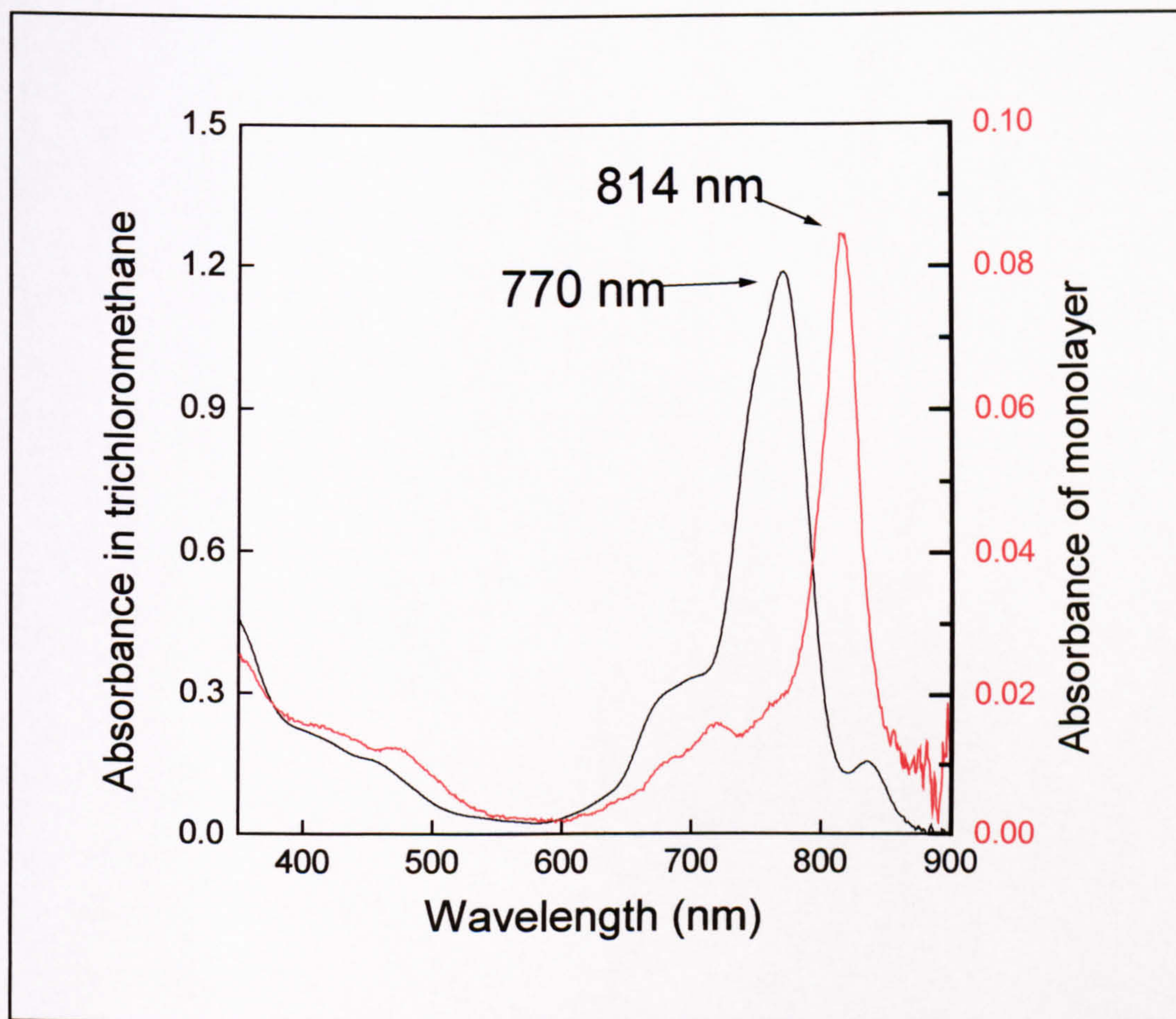


Figure 49 – Comparison of UV-VIS spectra of X in trichloromethane (—) and monolayer (—) forms

The pressure-area isotherm of X (and its 2nd differential) shows that the floating layer is full of patches and aggregation (Figure 50). There are points of inflexion for almost the entire length of the isotherm curve and the rate of increase of the pressure with decrease in molecular area is particularly slow. This shows that this dye does not favour forming Langmuir films at all.

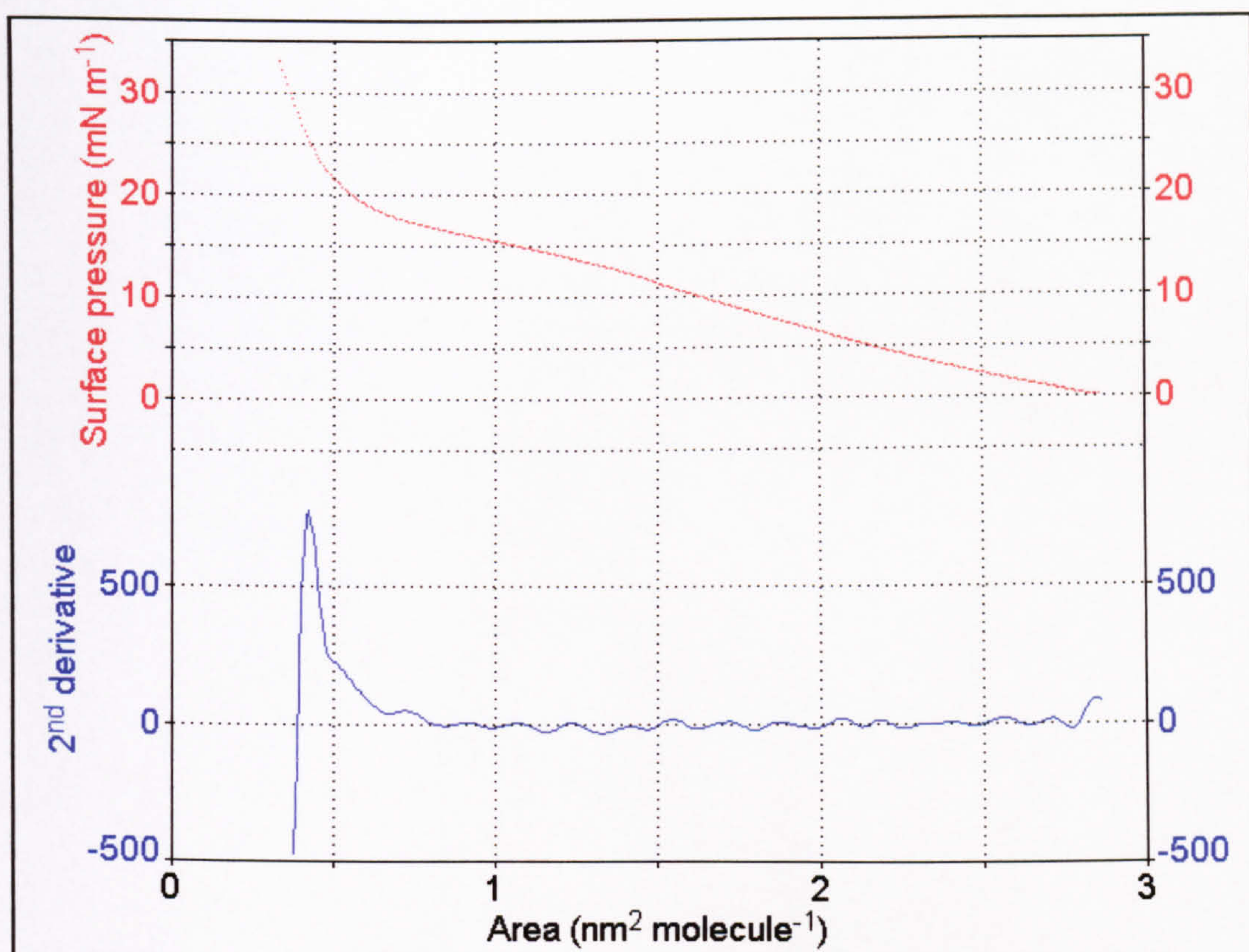


Figure 50 – Isotherm (—) and 2nd differential (—) of X

The comparison of the data from isotherm and QCM experiments also indicates the presence of gaps on the water surface (Table 23). The large increase in molecular area calculated from the deposited layer is indicative of a film where gaps are not closed but accentuated with the passing of a quartz crystal through the air-water interface.

Table 23 – Comparison of isotherm and QCM data

Data Source		X
Isotherm	A_d / nm^2	1.63
	A_o / nm^2	2.58
QCM	A_d / nm^2	2.22
	STD / nm^2	0.32

The calculation of the optical properties and layer thickness through SPR characterisation reveals a layer thickness of 2.46 nm (Table 24). It is not clear as to the nature of the molecule on the surface as the edge on orientation has a thickness of circa 2 nm and the face-on orientation is likely to be similar (0.3 nm for each macrocycle = 1.5 nm inc VDW, Gd radius ~ 0.2 nm = 0.4 gives a total of 1.9 nm).

Table 24 – Calculated SPR data for X

	X
ϵ_r	2.37
ϵ_i	0.26
d / nm	2.46
n	1.54
κ	0.08
Least Squares Error in fitting	3×10^{-4}

The calculation of the molecular densities of the dyes on the water subphase and quartz substrate show that indeed the gaps in the film expand during the deposition process (Table 25).

Table 25 – Density (g cm⁻³) of VII, VIII, and IX in both Langmuir and LB form

	X
Isotherm Density	0.84
QCM Density	0.62

4. Chlorine sensitivity

Initially, materials were tested for their chlorine sensitivity using the SPR apparatus. The poor results and difficult chlorine concentration controls led to a simpler UV-VIS spectroscopy approach using 50 ppm chlorine.

4.1 SPR gas sensing

The dyes studied using this technique were I, IV, V and VII. This use of such a wide variety of dyes was an attempt to obtain an insight into the mechanisms involved in chlorine sensing using the SPR (fixed angle) technique.

Only dye I showed a detectable response to the chlorine with the SPR apparatus; the resonance moved to a slightly lower angle (from 44.875° to 44.625°) (Figure 51 and Figure 52).

It has been suggested by Honeybourne *et al* ⁽⁸⁵⁾ that the data in the range of 1 – 10 ppm appears to follow (Equation 12).

$$R = R_{\max} - Be^{\left(\frac{-t}{\tau}\right)} \quad \text{Equation 12}$$

Where R is the SPR response to chlorine, R_{\max} is the maximum response, B is a constant and τ , the time constant, is a quadratic function of the ratio of the film thickness and the Fick diffusion constant ⁽⁸⁵⁾.

The change in the SPR curve is due to the oxidising gas molecules reacting with the central π -electron system and reducing the absorbance of the dye.

Dyes IV, V and VII did not give a detectable response when exposed to the chlorine gas in the range 1 – 10 ppm; the response at 10 ppm was less than 1%. Perhaps only the outer layer is exposed to the analyte gas and the island-like formations of these porphyrins on the substrate surface may actually help to protect the majority of the dye

molecules from the oxidising gas. A much larger dose of chlorine may be required to allow any changes in the LB film to be detected.

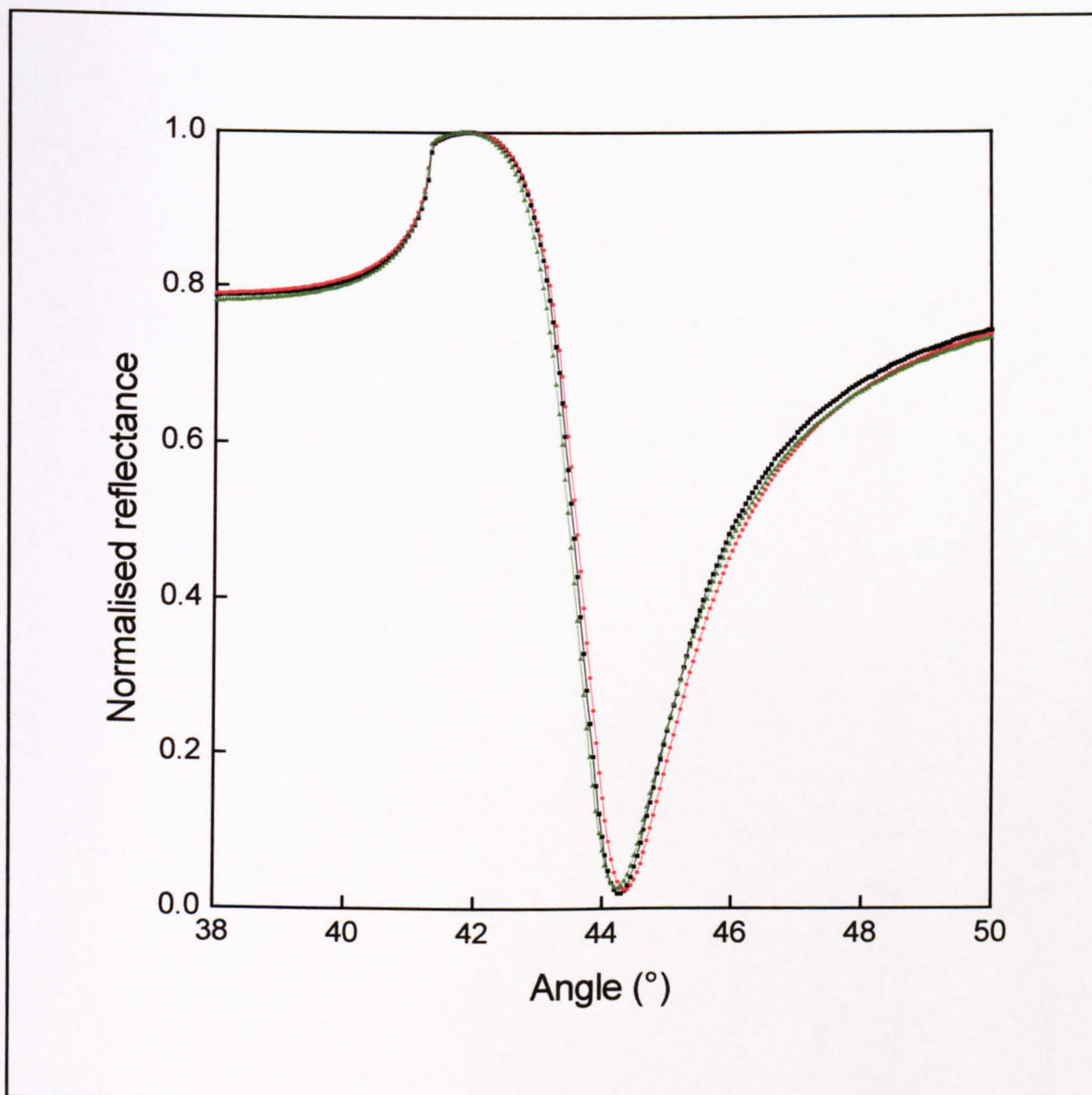


Figure 51 – SPR scan of a gold layer (—), dye (I) (—) and dye exposed to 10 ppm chlorine (—) symbols = data, lines = theoretical plot

The good gas-sensing results obtained in other work with similar porphyrins were performed using films deposited under non-standard conditions; the rate of deposition was nearly 150 times faster than used in this thesis^(81, 87). This allowed large gaps to form in the LB film, giving it a higher permeability to the gas and therefore a greater response. The results obtained in this thesis with poor gas-sensitivity are akin to those obtained elsewhere with a higher deposition pressure⁽⁸³⁾. This demonstrates that

for these non-uniform LB films, where the concentration of the dye molecules varies across the surface, other deposition techniques need to be considered.

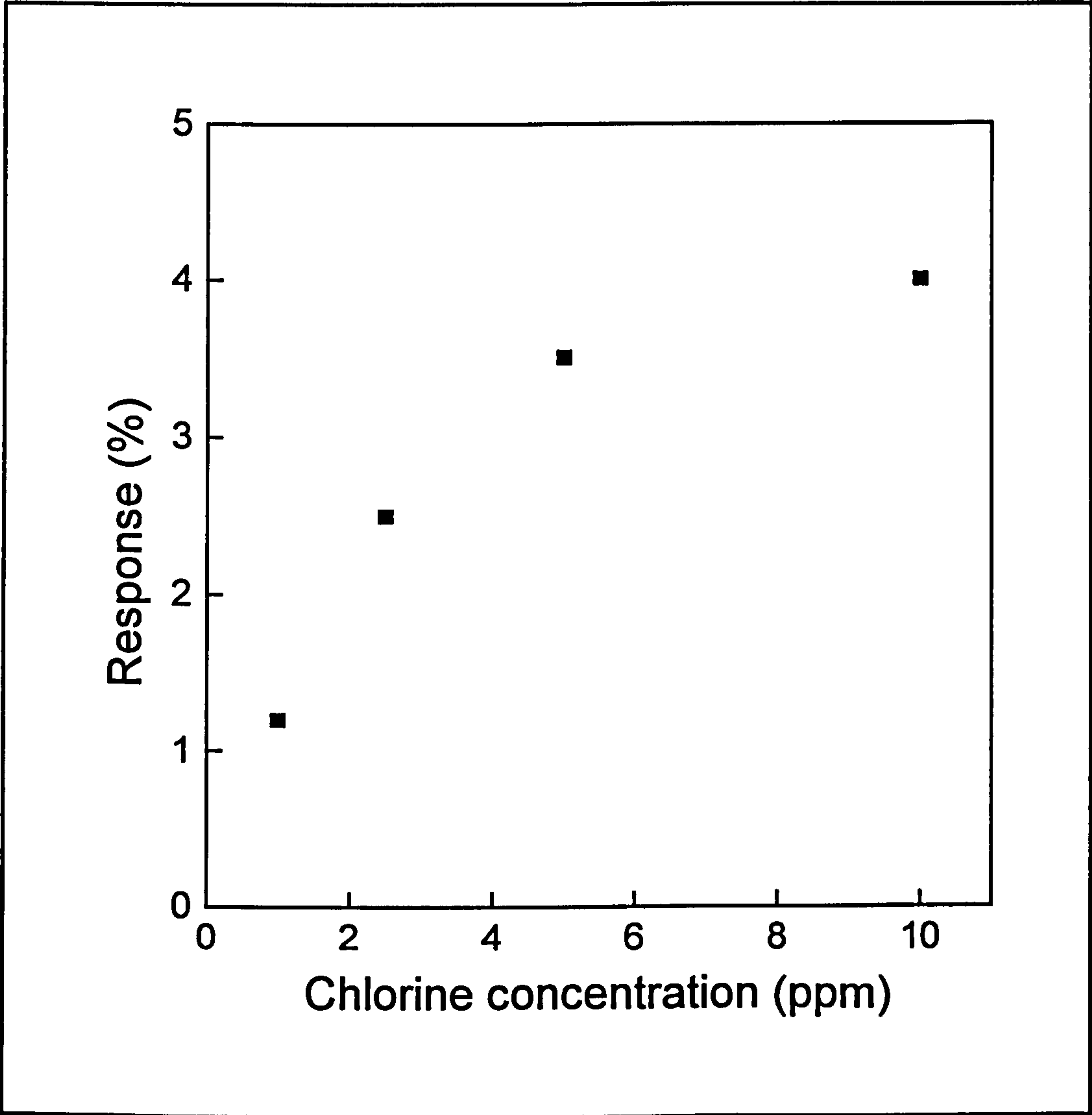


Figure 52 – SPR dose-response curve for I

4.2 UV-VIS gas sensing

4.2.1 Phthalocyanines

The results from the SPR experiments on **I** (*see* SPR sensing section) indicate that there should be a change in the UV-VIS spectrum around the wavelength of the laser and this is indeed the case (Figure 53).

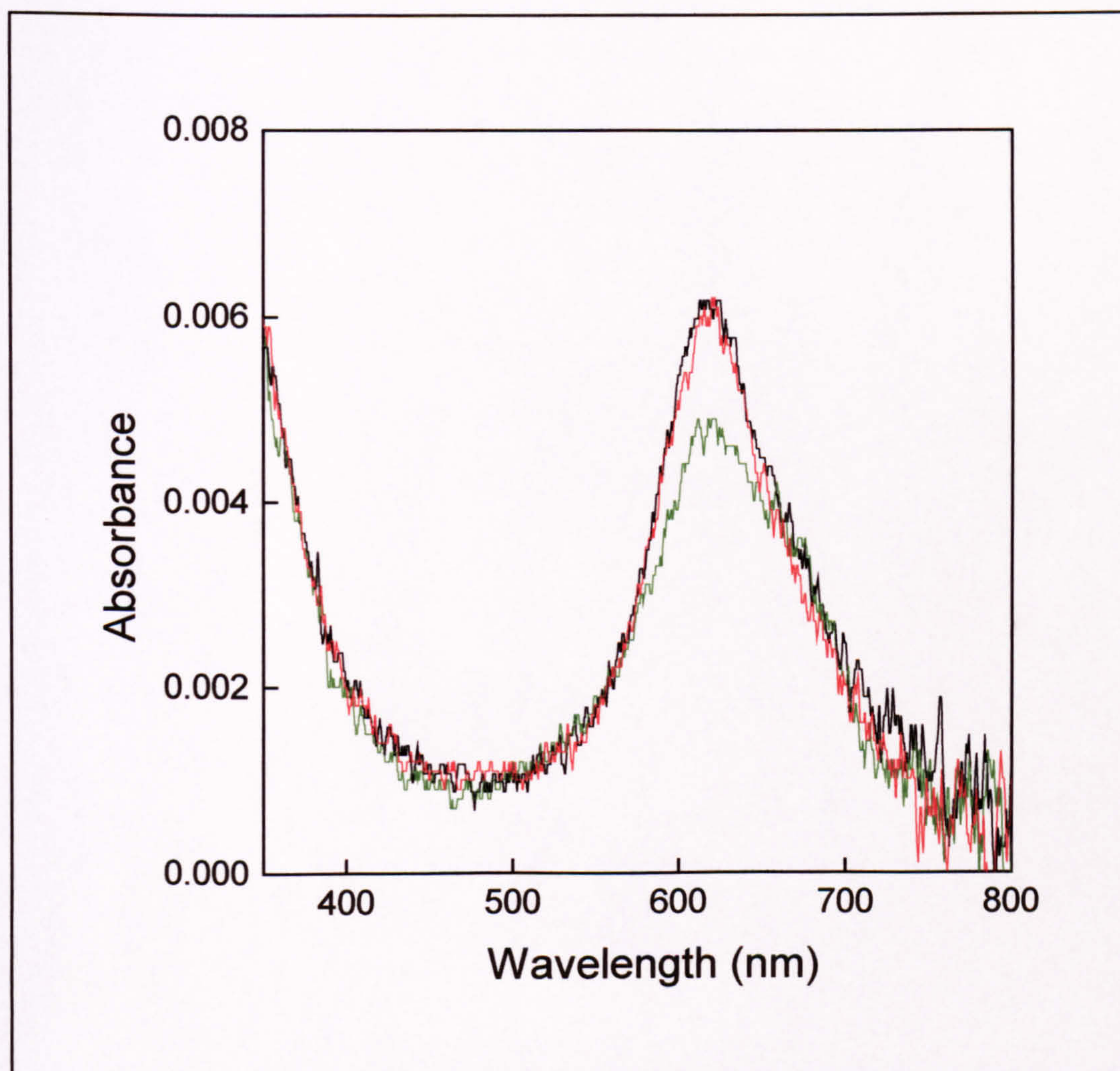


Figure 53 – UV-VIS spectra of a monolayer of **I** (—) after exposure to 50 ppm chlorine for 30 mins (—) and its subsequent recovery after 24 hours in air (—)

The absorbance at the laser wavelength (632.8 nm) is reduced when the LB film is exposed to the oxidising gas, which results (in the SPR experiment) in a reduction in ϵ_i (represented in the SPR graph by the shift of the resonance to lower angles) (Equation 13).

$$\epsilon_i = \frac{-2n\lambda}{4\pi d} \ln(10^{-4})$$

Equation 13

The recovery of the dye after exposure to air for 24 hours indicates that the chlorine is not chemically reacting with the phthalocyanine molecules. The gas is acting as an electron-acceptor, forming a charge-transfer complex with the phthalocyanine (the positive charge delocalised over the central π -electron ring). It is this reduction in available free electrons in the π -electron system that lowers the absorbance.

The exposure of a multilayer (10 passes through the air-water interface) to the chlorine shows that the film is relatively porous; the reduction in absorbance is accompanied by the recovery after 24 hours in air (Figure 54).

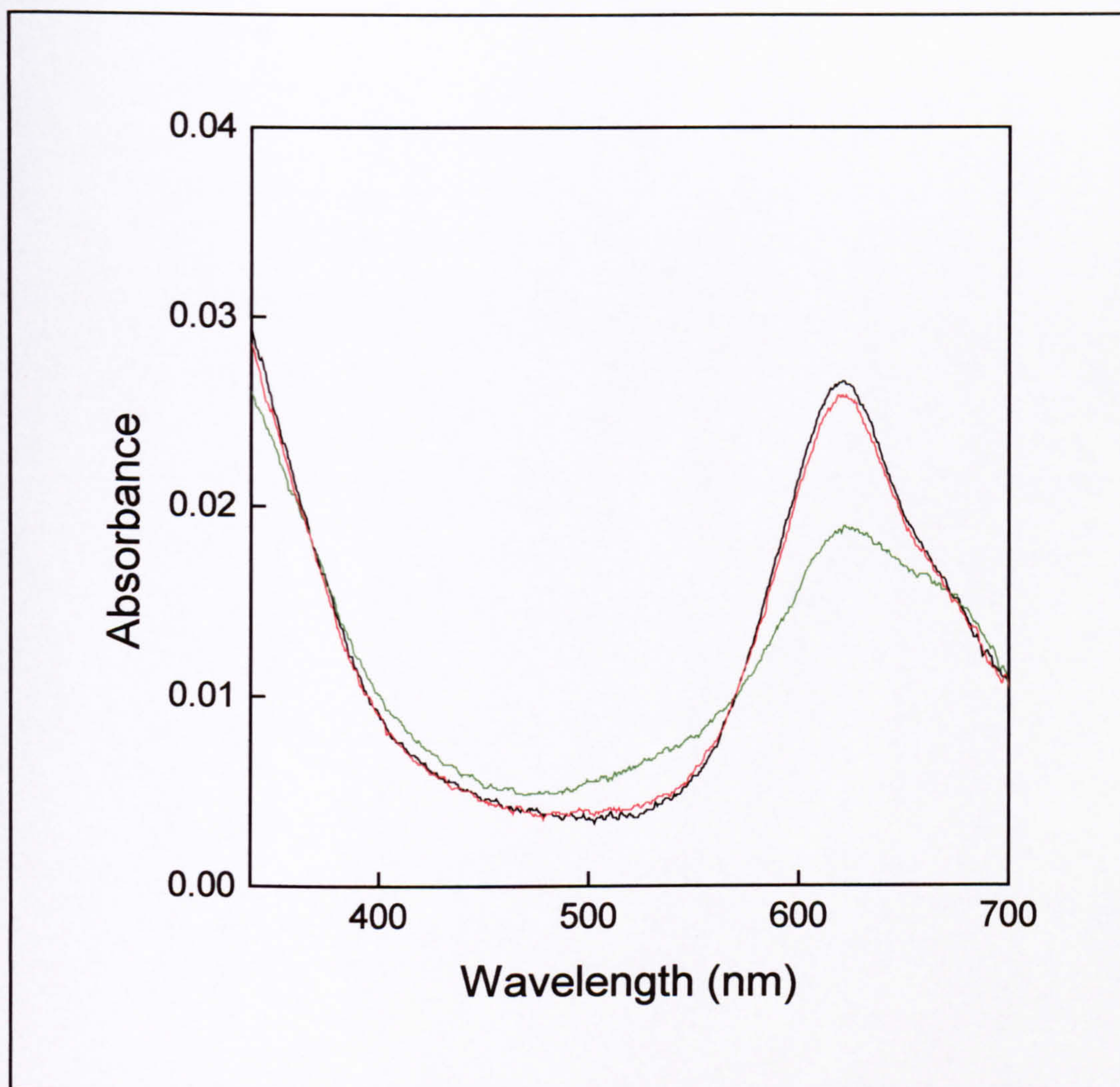


Figure 54 – UV-VIS spectra of a multilayer of I (—) after exposure to 50 ppm chlorine for 30 mins (—) and its subsequent recovery after 24 hours in air (—)

The formation of a new peak at 670 nm can be seen through the increase in the Full-Width Half-Max (FWHM) measurements of the spectral features before and after exposure to the chlorine gas. The fresh film has a FWHM value of 116 nm whereas after attack from the oxidising gas, this changes to 138 nm. The changes in the spectra of the film may be caused by a reduction in symmetry. The charge-transfer complex reduces the resonance of the π -electron system and therefore the copper atom remains bound to the same pyrrole nitrogens (thereby reducing the symmetry from D_{4h} to D_{2h}).

In trichloromethane, the chlorine absorbance peak (which is located circa 200 nm) dominates the spectrum (Figure 55). The reduction in absorption bands is extensive due to the gas diffusing easily through the solution of dye molecules and there

is no recovery (even after bubbling air through the solution) as the chlorine molecules become trapped in the solvent.

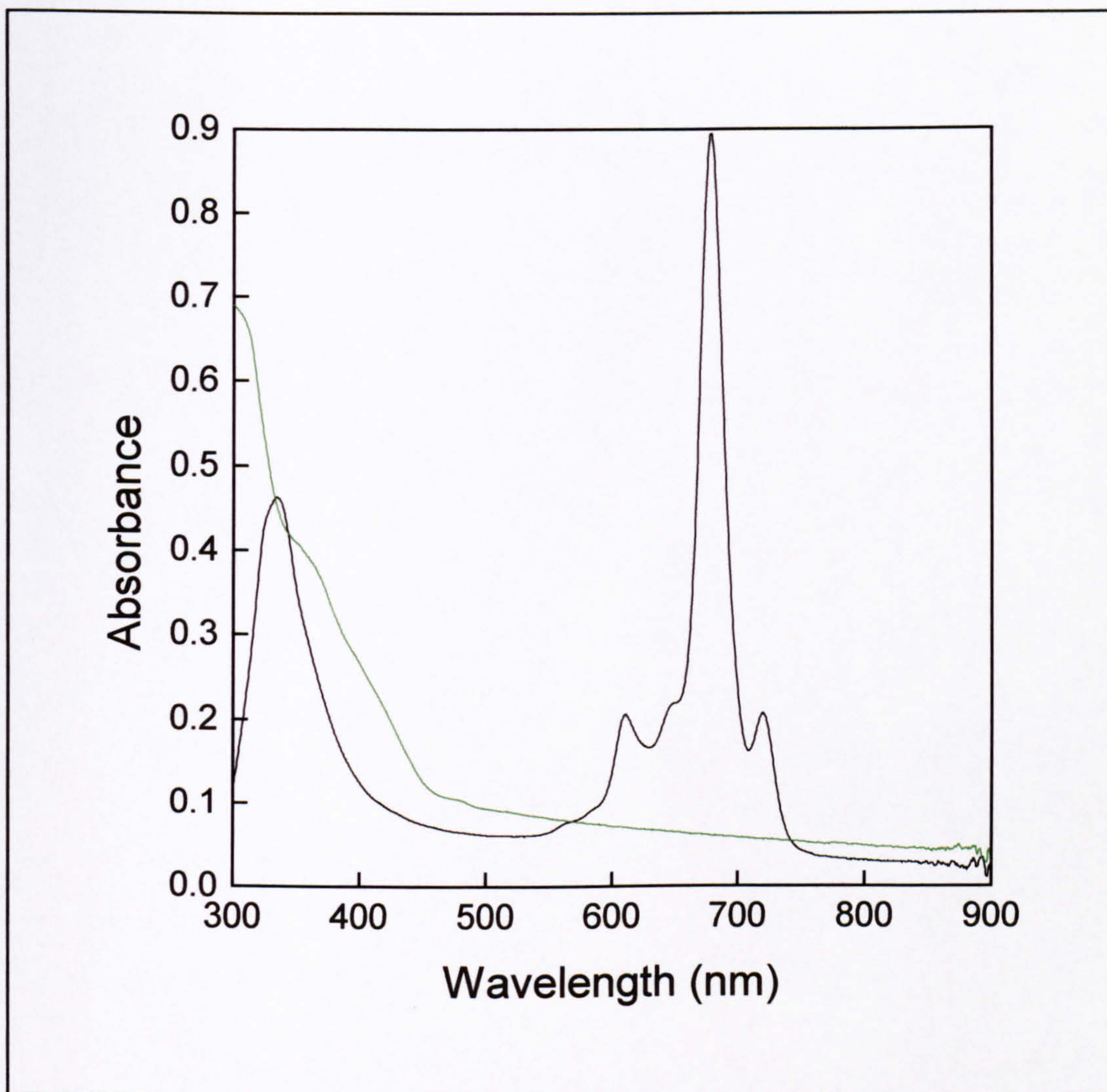


Figure 55 – UV-VIS spectra of I in trichloromethane (—) and after bubbling through 50 ppm for 30 minutes (—)

Dye **II** does not form the ordered floating (and hence deposited) films of **I**. The density calculation indicates that a monolayer is deposited onto the substrate and (from the isotherm and QCM data) the molecules may adopt a more face-down orientation. This is confirmed with the UV-VIS gas sensitivity experiments. The reduction in the absorption band around 700 nm after exposure to 50 ppm chlorine (30 mins) is far greater than that shown for **I** (Figure 56).

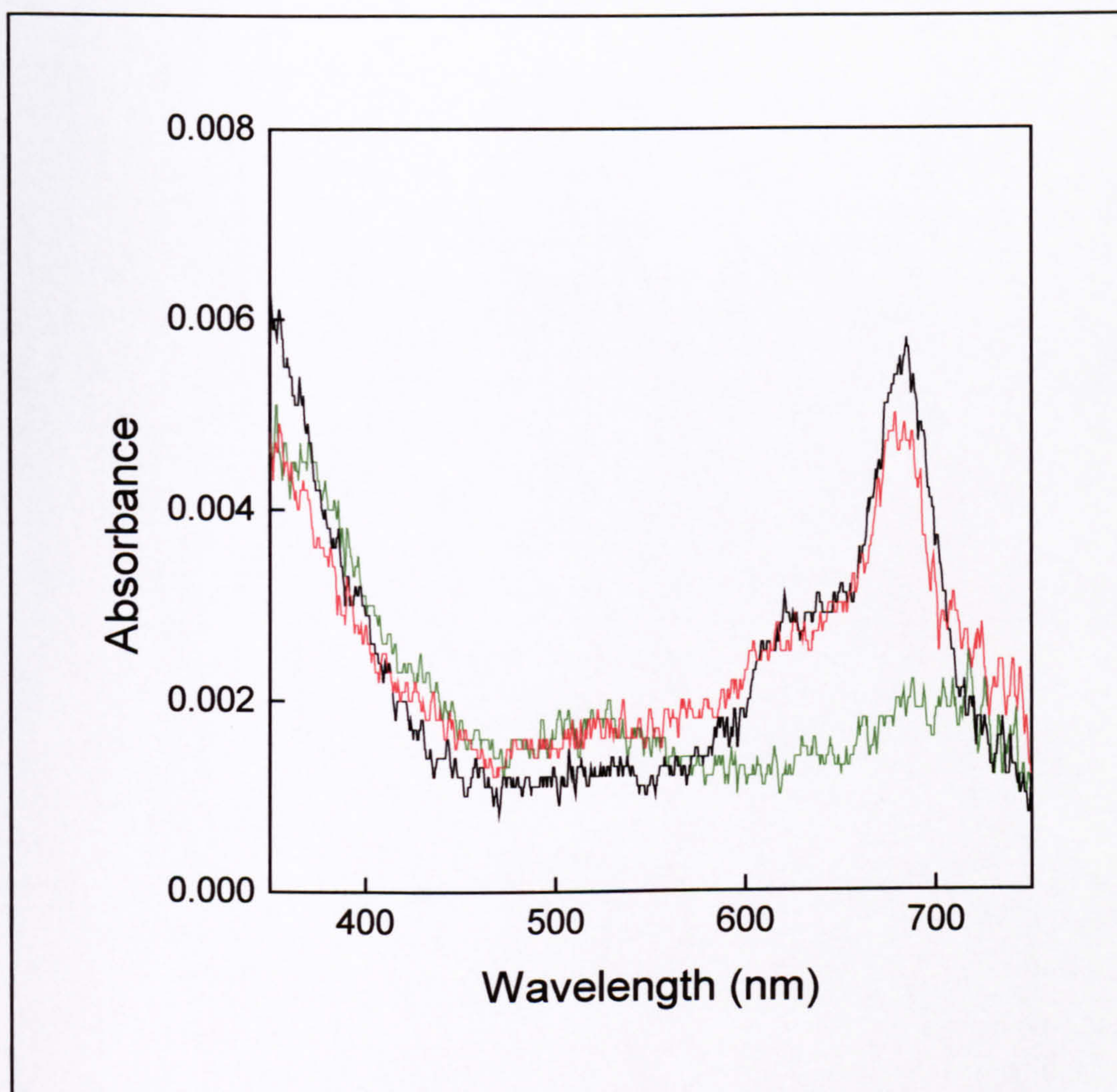


Figure 56 – UV-VIS Spectra of monolayer of II (—) after exposure to 50 ppm chlorine for 30 mins (—) and its subsequent recovery after 24 hours in air (—)

It has been previously suggested that the axial coordination of the zinc atoms promote the face down orientation (and hinder multilayer formation)⁽¹³²⁾. This means that the central π system will be exposed to the oxidising gas; whereas with **I** the densely packed tilted orientation will require the gas molecules to diffuse through the film (reducing the initial response and increasing the response time).

The multilayer (10 passes through the air-water interface) also shows a large response to the chlorine gas, though a poorer recovery (compared with the monolayer or copper moiety) (Figure 57).

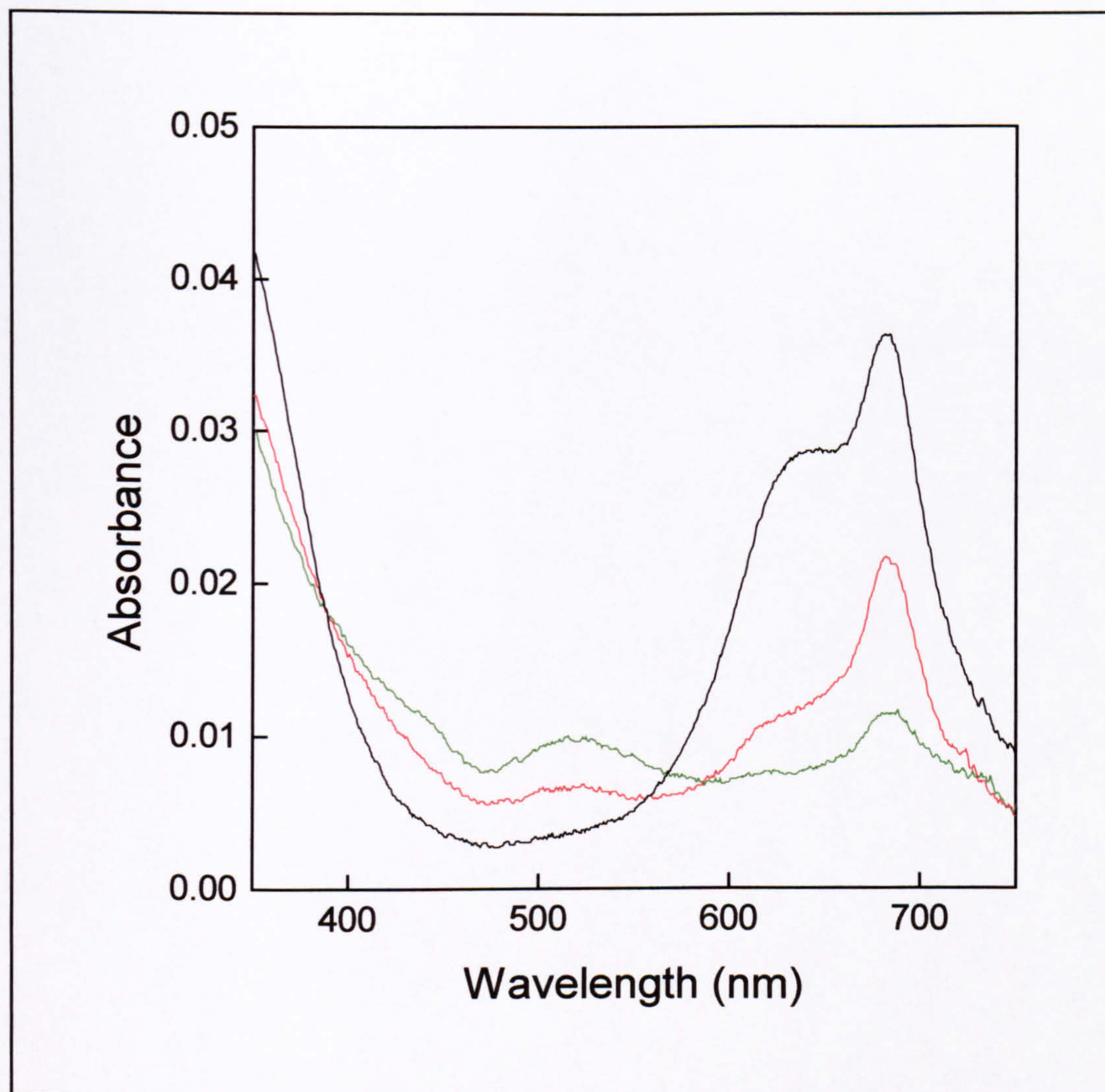


Figure 57 - UV-VIS spectra of a multilayer of II (—) after exposure to 50 ppm chlorine for 30 mins (—) and its subsequent recovery after 24 hours in air (—)

The trichloromethane solution of **II** shows the same near-total reduction in the main absorption band as **I** but with the growth of a small peak at 836 nm.

Films created from single and multiple passes through the air-water interface with dye **III** spread on the subphase, show UV-VIS spectra which change only slightly upon exposure to 50 ppm chlorine for 30 mins. There is a small reduction in absorbance of the Q band and a slight red-shift (in the film created from 5 passes the peak absorbance moves from 621 nm to 630 nm).

The weak sensitivity may be the result of the poor LB film formed by the dye; multilayers are present at the air-water interface and therefore transferred onto the substrate on each pass which creates pockets of densely packed dye molecules. These

islands may reduce the gas response (and increase the response time), particularly if the regions are highly compact.

The metal-free moiety will also be less sensitive to the chlorine gas because the metal atom helps to delocalise the positive charge created by oxidising gas and the central π -electron ring forming a charge-transfer complex.

The comparison of the three dyes and their response to chlorine shows that the response is best for the zinc moiety with nearly 3 times the response of I (Table 26).

Table 26 – Comparison of the response (%) of three dyes in monolayer and multilayer form

Dye	<i>Response (%)</i>	
	<i>Monolayer</i>	<i>Multilayer</i>
I	21.0	28.2
II	63.2	67.9
III	5.6	6.7

4.2.2 Porphyrins

The majority of the porphyrin dyes studied showed a poor sensitivity to chlorine gas with less than 15 % response after 50 ppm for 30 minutes (Figure 58 and Table 27).

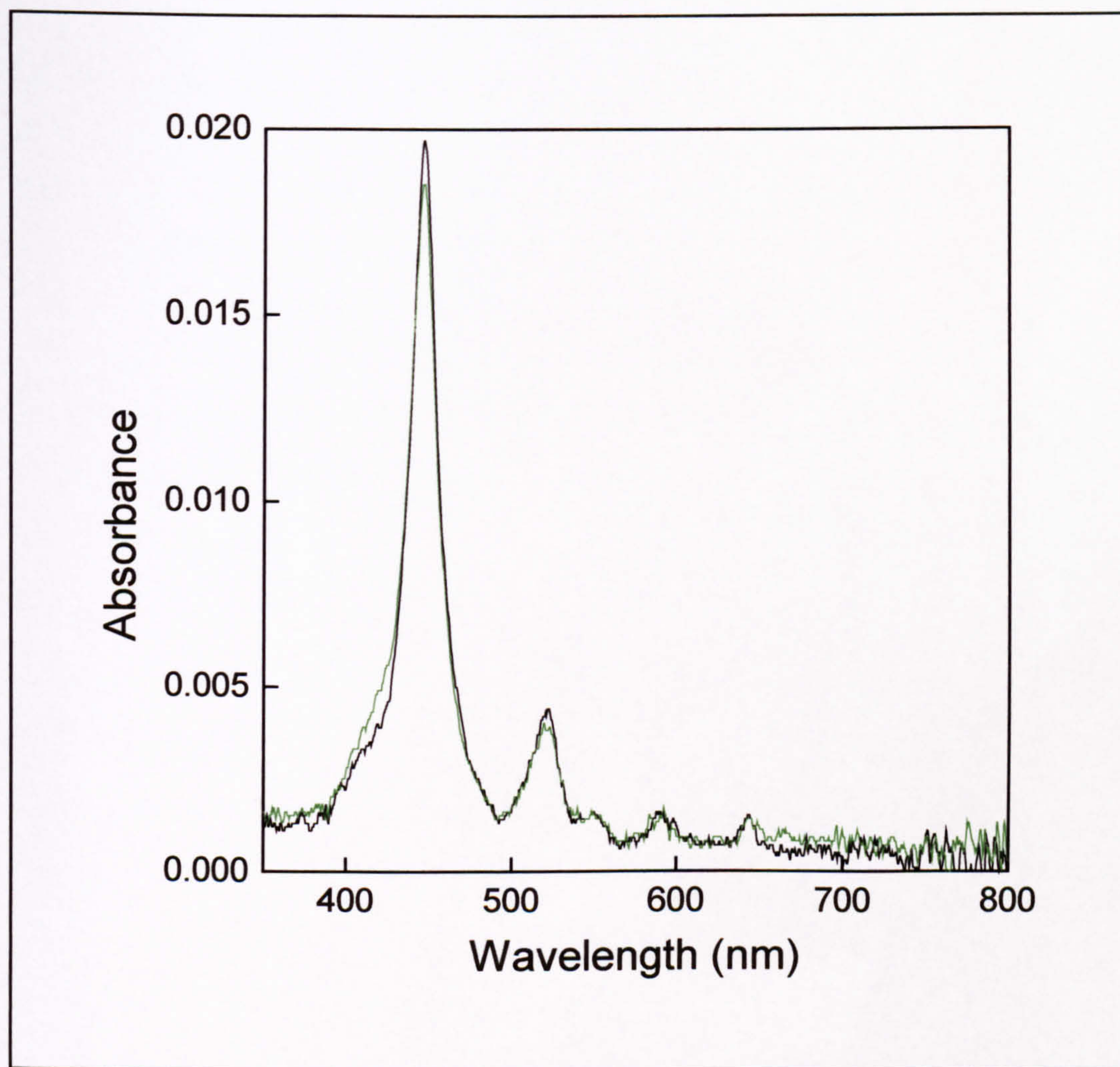


Figure 58 – An example of poor sensitivity to 50 ppm chlorine; LB film of IV (—) and after 30 mins exposure to the gas (---)

Table 27 – Comparison of poor response of dyes to chlorine

Dye	Monolayer Response (%)
IV	6
VI	< 1
VIII	< 1
IX	12

The response of these 4 dyes to the chlorine is very different. Perhaps the most interesting comparison is that of dyes **VIII** and **IX**. They have similar substituents (ethers) but very different responses. The Langmuir films of these materials are also quite different, with **IX** clearly forming a better floating layer than **VIII**. This suggests that the “dead spider” orientation adopted by **IX** allows the chlorine atoms to easily interact with the π -electron rings, whilst the island-like formations of **VIII** may indeed restrict the chlorine from reaching some of the reaction sites. This is in contrast to the previously published work on this dye, where good sensitivity is reliant on non-standard film-transfer conditions (i.e. a very high deposition speed) ^(80, 81, 82, 87, 99).

The other two dyes both form poor Langmuir and LB films (similar to **VIII**) and their response to chlorine is poor.

The effect of different deposition conditions on the sensitivity of **VII** to the chlorine was determined through a series of experiments. Firstly, the dye was deposited as a monolayer and exposed to a small amount of chlorine (<10 ppm) (Figure 59).

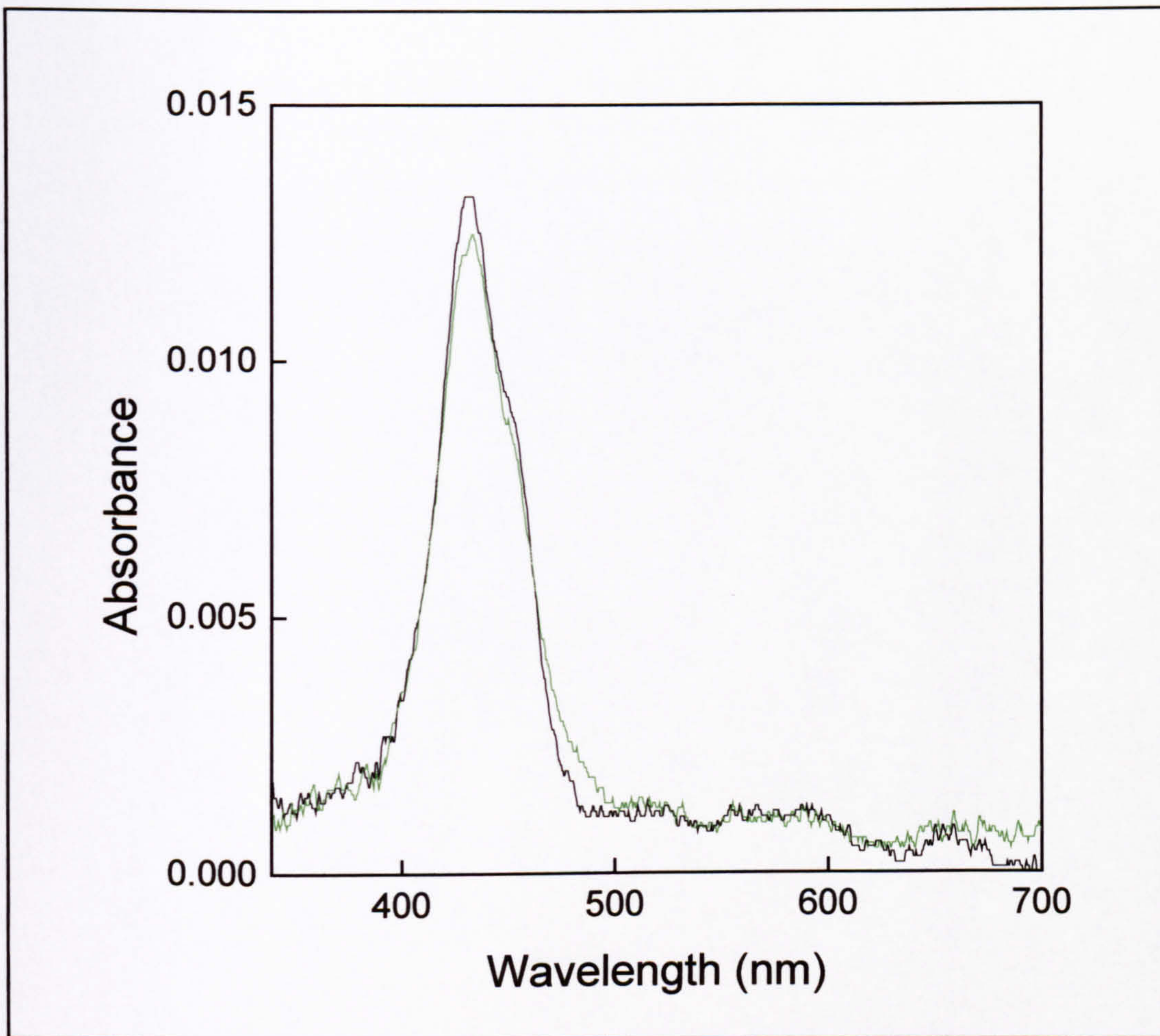


Figure 59 – Monolayer of VII (—) after exposure to <10 ppm chlorine for 30 mins (---)

A 12% reduction in the intensity of the main absorption peak (due to oxidation) and the growth of the dication peak (circa 490 nm) shows that this dye is responsive to chlorine gas. The increase in the chlorine concentration naturally results in an increase in the response of the dye (Figure 60).

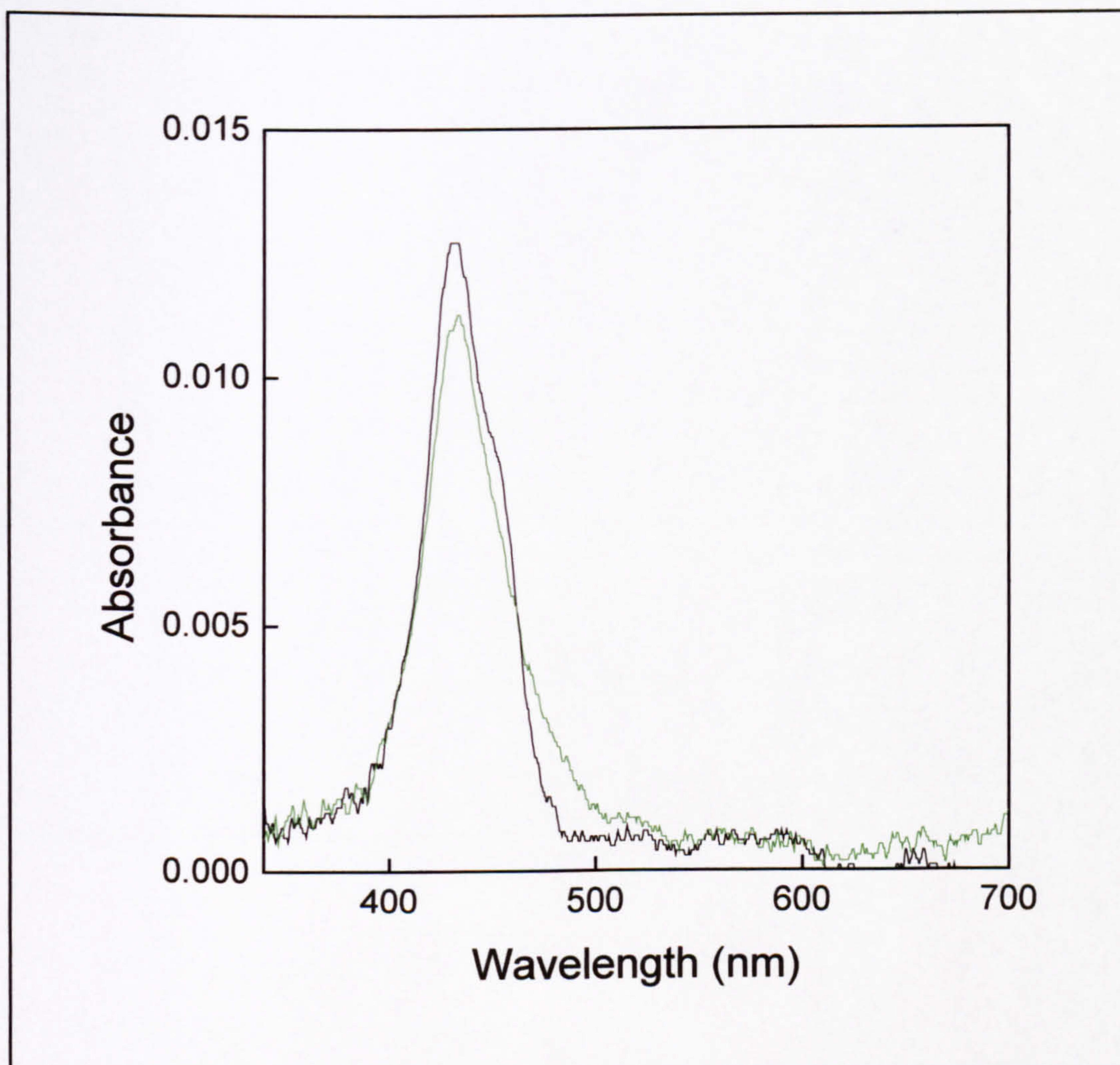


Figure 60 – Monolayer of VII (—) after exposure to 10 ppm chlorine for 30 mins (—)

An increase in the deposition pressure may result in a greater number of sites for the gas to attack. This results in an increased response of the dye to the chlorine (particularly the evident in the growth of the peaks at circa 480 and 750 nm) (Figure 61).

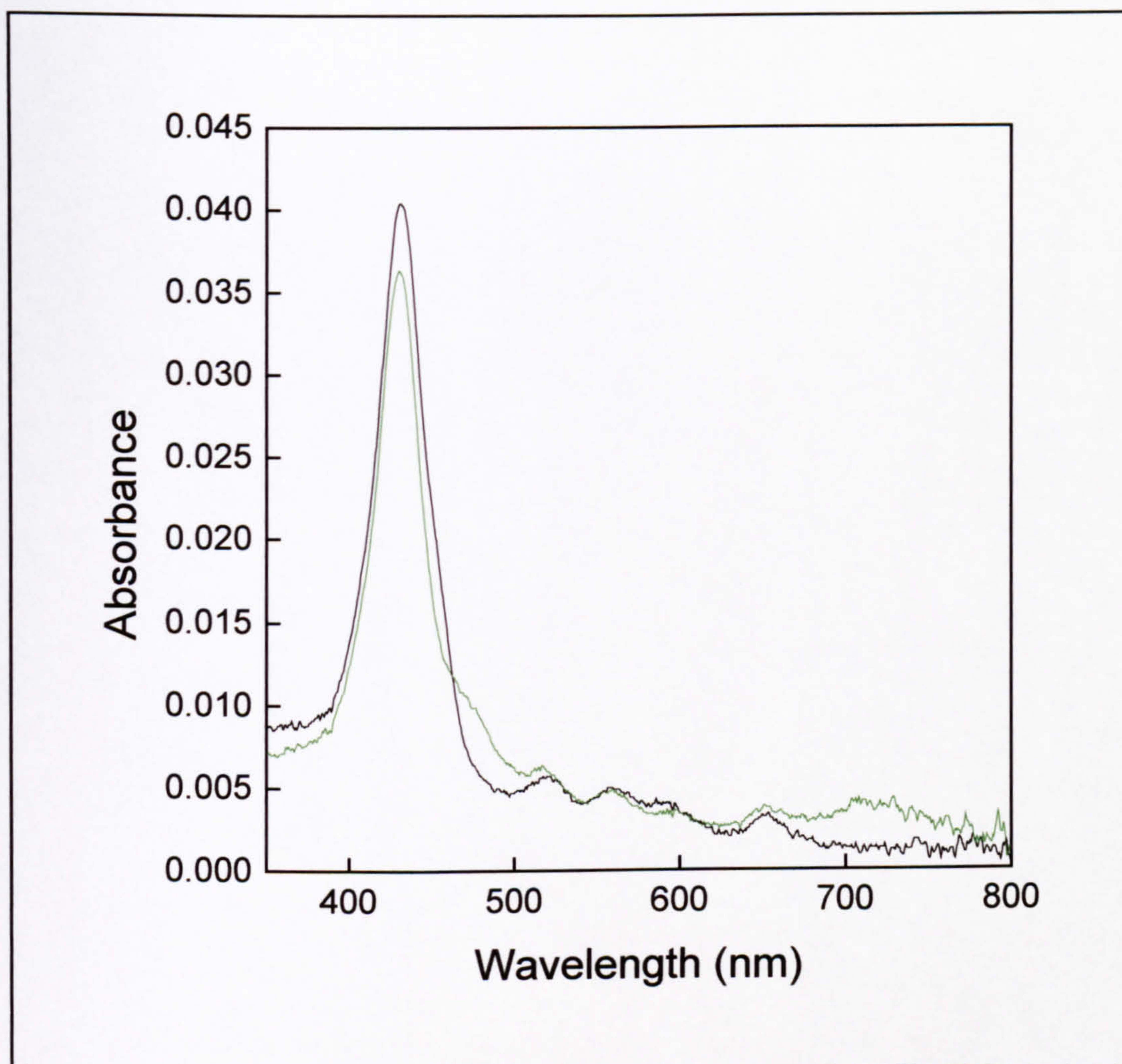


Figure 61 – Monolayer of VII deposited at a higher surface pressure (—) after exposure to 10 ppm for 30 mins (---)

A further increase in the chlorine concentration of the analyte gas exposed to this high-pressure monolayer shows the response of the film increases dramatically (Figure 62). The reduction in the main absorbance as a result of oxidation of the macrocycle is clearly evident, although the degree of protonation of the dye has hardly changed with the increased gas concentration (if anything the dication production is lower for the increased Cl_2 ppm). This indicates that in these experiments the water required for the protonation of the macrocycle may come from the gas. There are two possible sources of water that can be used to protonate the porphyrin free base – the gas mixture or the LB film itself. Other workers have suggested that the water trapped in the LB film is used by the chlorine atoms to form an acid and hence protonate the

macrocycle ^(80, 87). In those cases, there was a dessicator present on the gas lines to remove any water vapour.

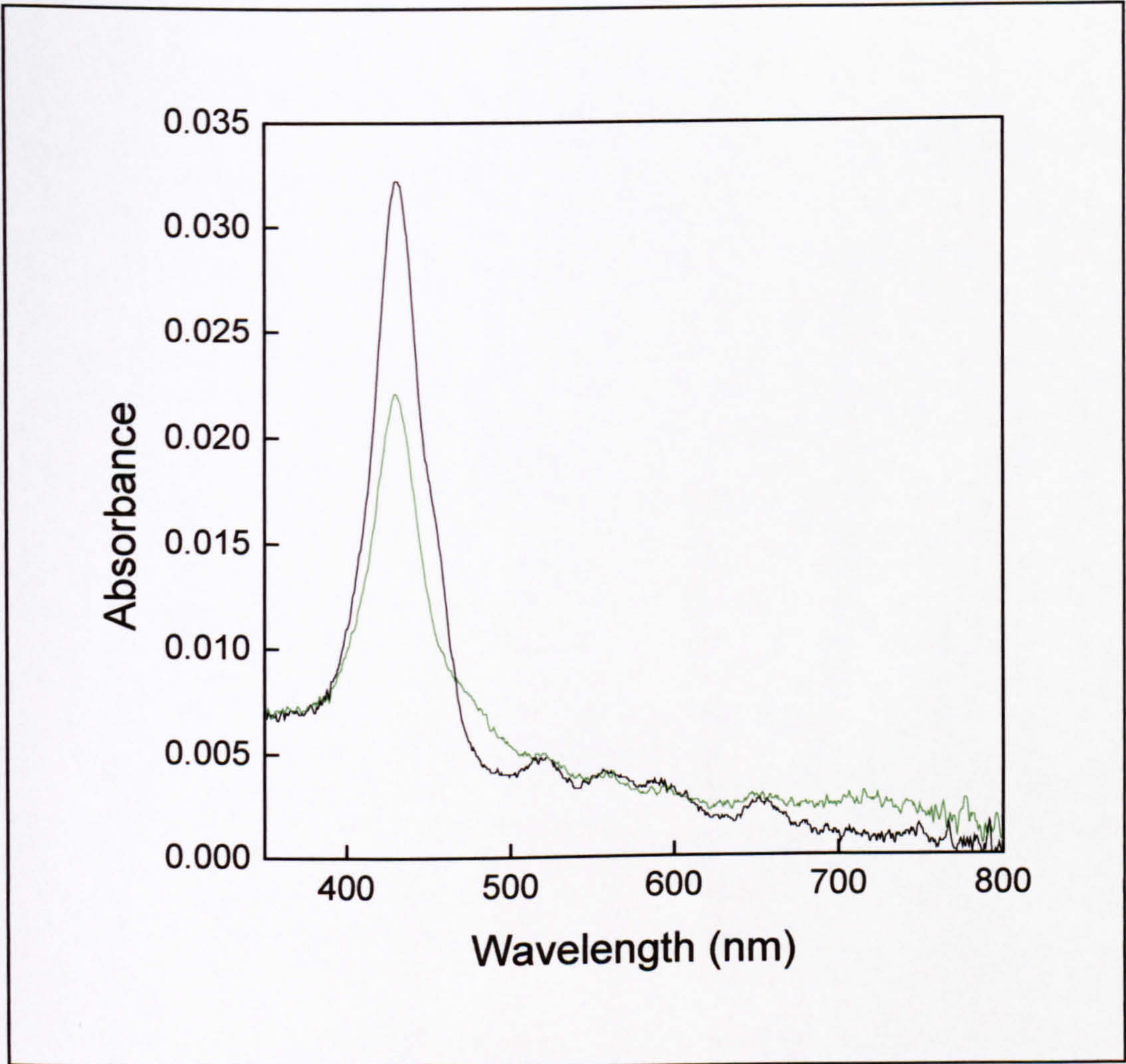


Figure 62 – Monolayer of VII deposited at a higher pressure (—) after exposure to 50 ppm chlorine for 30 mins (—)

For these experiments there was no such filter. The result is indicative of the gas lines supplying the water for a number of reasons. The source can be determined through analysis of the results and step-by-step elimination of the various possible contaminants (Table 28). Another point to consider is that the Cl₂ was purchased from BOC Special Gases is balanced (100 ppm in N₂) with nitrogen, which is guaranteed to have a low water concentration. The N₂ cylinder is the standard industrial gas used throughout the world and can contain up to 5% water.

Table 28 – Possible sources of water vapour and the effect of increasing Cl₂ concentration

Possible source of water vapour	Result of increased chlorine concentration	Reasons
LB film	Increase in protonation	More chlorine atoms to combine with the water to form the acid and therefore the dication
Cl ₂ line	Increase in protonation	A combination of more chlorine atoms and more water molecules will result in more acid molecules – therefore more protonation
N ₂ line	Decrease in protonation	As the Cl ₂ concentration is increased the amount of nitrogen required to balance it is reduced, therefore the water vapour is also reduced

Of course, there may be water in the N₂ line **and** trapped in the LB film. This provides the explanation for the slight decrease in the observed dication formations for only the high-pressure monolayers when chlorine is increased. There will be more water trapped in the low-pressure film as there are a larger number of holes and defects in which the water molecules can reside. This compensates for the loss of water due to the decrease in N₂ associated with the higher Cl₂ concentration.

The comparison of multilayers (5 passes through the air-water interface) exposed to 10 ppm and 50 ppm (Figure 63) demonstrates little change in the dication formation and only a slight decrease in the oxidation of the macrocycle for the increased concentration. This indicates that there is little water trapped in the film.

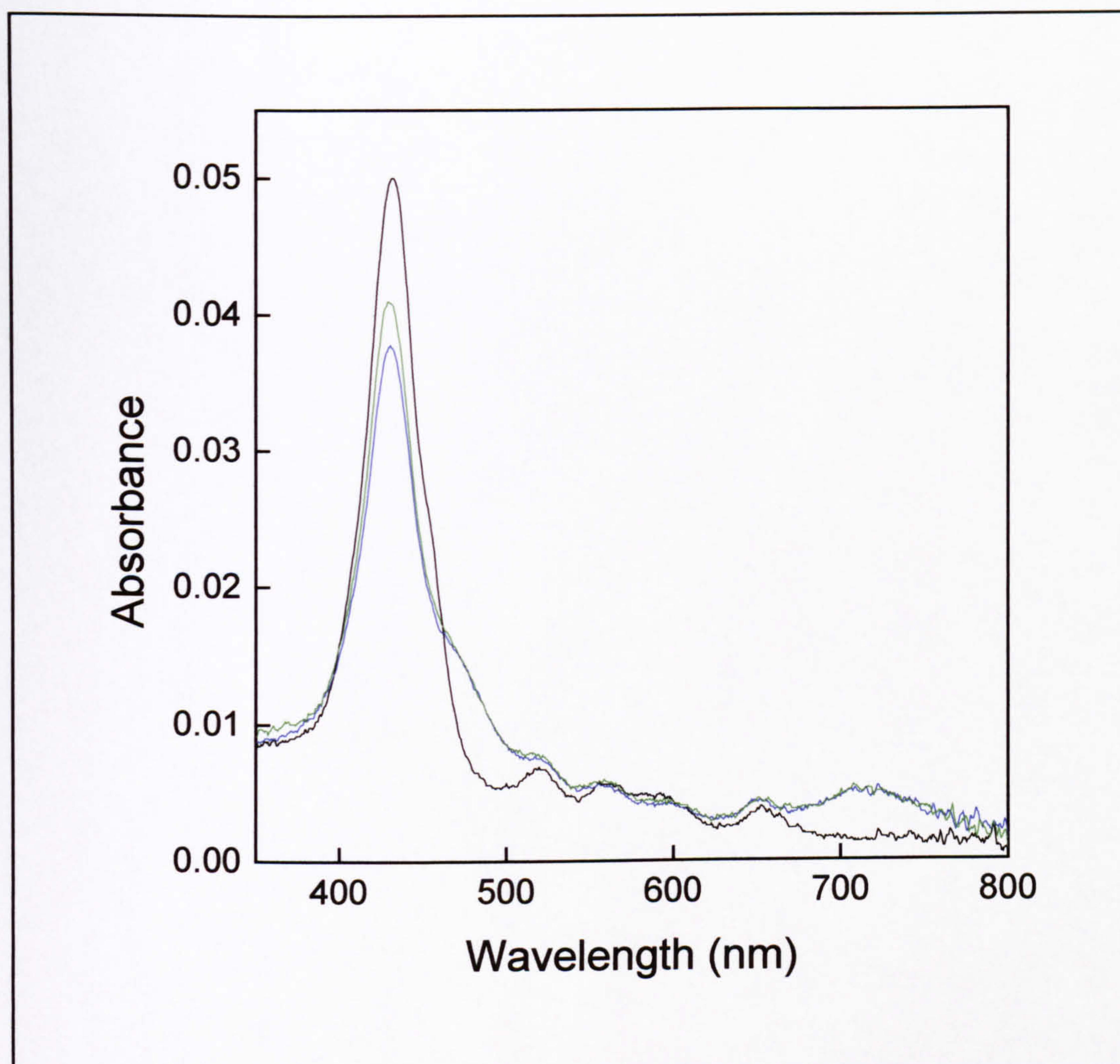


Figure 63 – Multilayer of VII (—), after exposure to 10 ppm chlorine for 60 mins (—), after exposure to 50 ppm for 30 mins (—)

It can be seen that the multilayer films show both oxidation and protonation processes quite clearly. The reduction of the main absorption band and the growth of the dication peak (circa 480 nm) can be monitored during the exposure to the chlorine (Figure 64).

In the diagrams, spectra were recorded every 30 seconds and the absorbances at 428 nm and 468 nm recorded. The intensities were then plotted against the time and the data fitted to the classic 2nd order decay curve. It is a 2nd order decay because there are two processes involved: the initial response of the surface and a bulk diffusion response. The two time constants calculated from the theoretical curve which is fitted to the experimental data shows that indeed this is a 2 stage response.

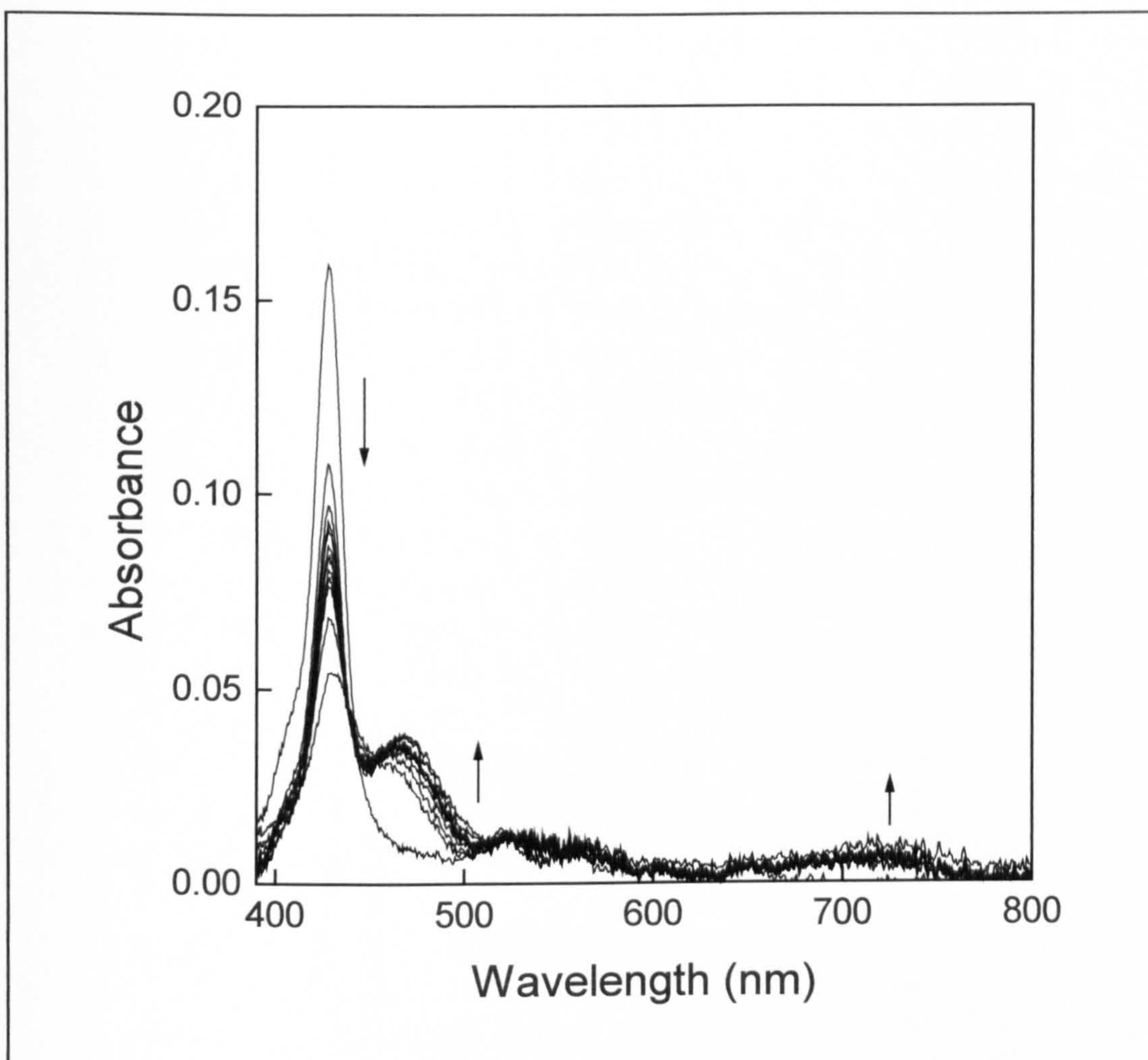


Figure 64 – UV-VIS spectra of V during exposure to 50 ppm chlorine (arrows indicate direction of peak growth/decay as time progresses)

The 1st time constant is 31 seconds, whilst the 2nd constant is 425 seconds. This shows that the surface response is much faster than that of the bulk diffusion, as expected. These values are slightly different from the previously reported values of 33 and 329 seconds ⁽⁸³⁾. The reason for the discrepancies may lie in the deposition conditions; in the reported work the films were deposited rapidly, which resulted in highly porous films. This means that there is less surface coverage (which results in a slightly higher 1st time constant), whilst the holes in the film allow the gas to diffuse through the film quickly (giving a much lower 2nd time constant).

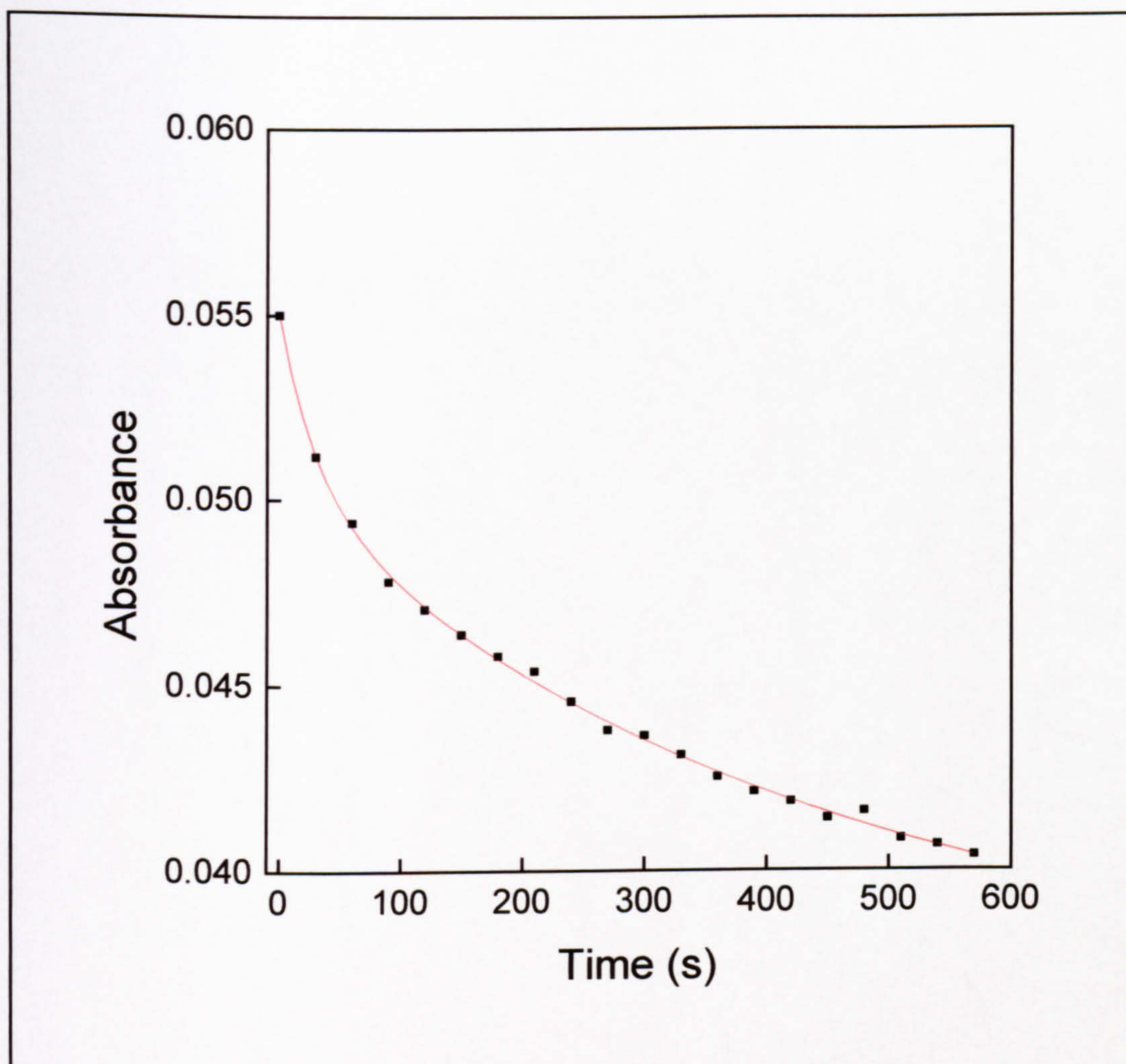


Figure 65 – Absorbance decrease at 428 nm (■) during exposure to 50 ppm chlorine and the fitted theoretical 2nd order decay curve (—)

The response of V to the chlorine gas can also be compared to previous work through the normalised absorbance decay (Figure 66). The lines marked on the graph represent the final normalised absorbance of the same dye in previous work for low (—) and high (—) deposition pressures. The reason why the decay isn't as extensive as that of the previous work again lies in the deposition conditions. The porous multilayers deposited by other workers appear to facilitate bulk diffusion, which would have a higher number of reaction sites and therefore a greater response (Richardson refs).

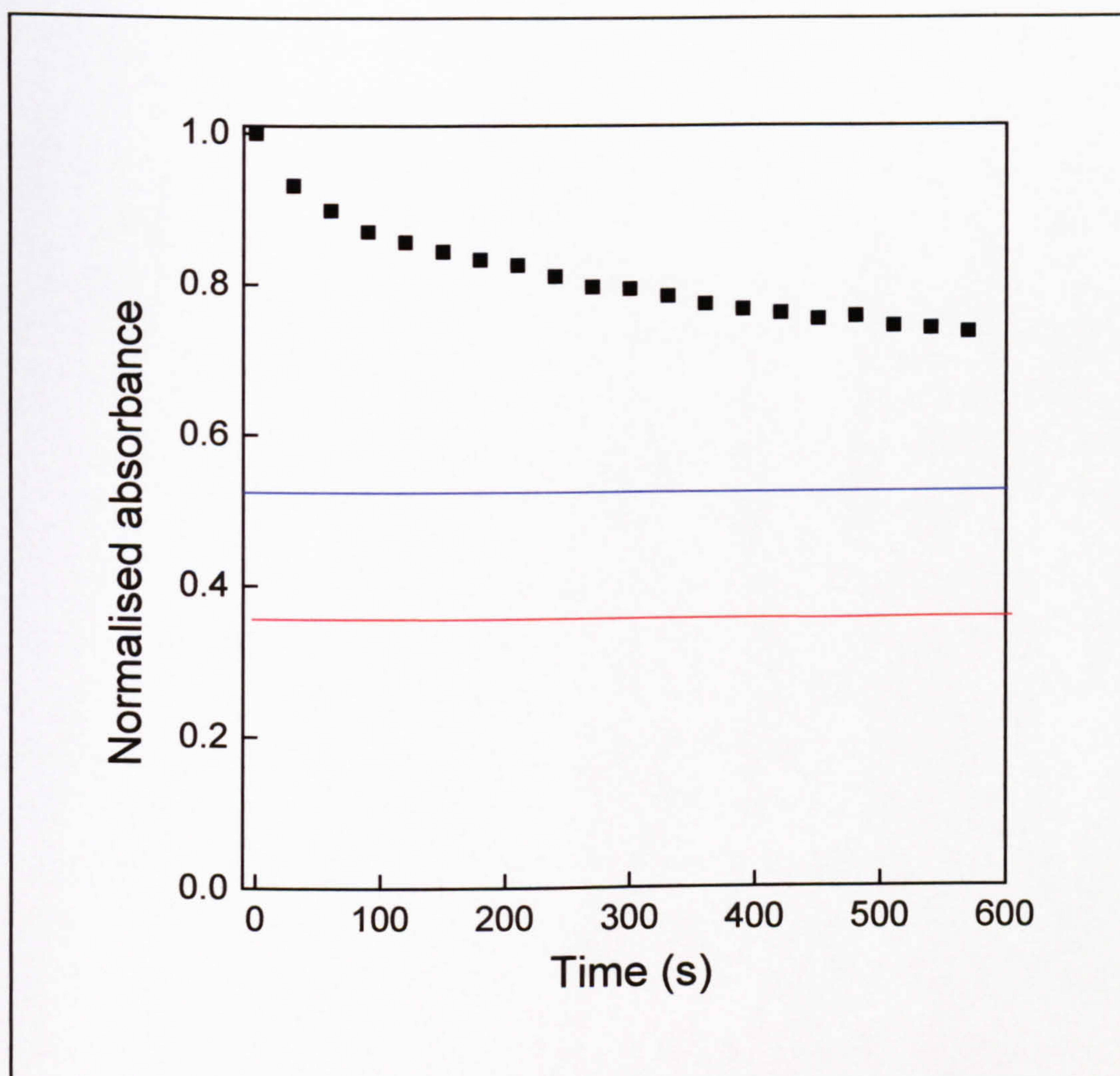


Figure 66 – The decay of the normalised absorbance whilst exposed to 50 ppm chlorine (■) and the corresponding results for previous work at low (—) and high (—) deposition pressures

The effect of the substituent on the sensitivity of the material is difficult to determine. There are a number of factors which may result in a decreased response to the oxidising gas when comparing similar materials. For example, the orientation of the porphyrin on the substrate may prevent the gas from binding with some dye molecules. The electron-withdrawing strength of the substituents may also alter the ability of the central π -electron system to react with the chlorine atoms to form the dication (resulting in a diminished sensitivity to the gas).

Quality is described in the Collins English Dictionary as a “degree or standard of excellence” ⁽¹³⁹⁾. The 2nd differential graphs provide a method of estimating the quality of the Langmuir-Blodgett films; through the measurement of the number of points of

inflexion. The greater the number of these points, the poorer the film is likely to be. The dyes can be then ranked 1 to 6 for their quality and also their response to chlorine (based on the percentage response of the monolayer) (Table 29).

Table 29 – Comparison of the quality of the Langmuir-Blodgett film with Chlorine sensitivity

Dye	IV	V	VI	VII	VIII	IX
“Quality” of LB film	6	2	5	3	4	1
Response to Cl ₂	4	2	5=	1	5=	3

The results indicate that the film quality may indeed play a part in the sensitivity of these materials to the gas. The dyes are split into two groups – ones that form comparatively good films (yellow) and those that don’t (white). The most responsive sensors fall into the group with the fewest points of inflexion whilst the poorer deposited films result in a lower (if any) sensitivity to chlorine.

The gas reacts with the porphyrin by initially oxidising the macrocycle, followed by protonation and formation of the dication. If the gas cannot interact with the π -electron system (due to the orientation of the molecules in the LB film), this reaction will have a higher activation energy and hence the dye will be less sensitive.

4.2.3 Bis-phthalocyanine / porphyrin triple-decker sandwich

The triple-decker sandwich dye **X** is not suitable for UV-VIS gas-sensing as it degrades in light (Figure 67). The spectrum gradually decreases significantly in less than 24 hours making it useless as an optical sensor.

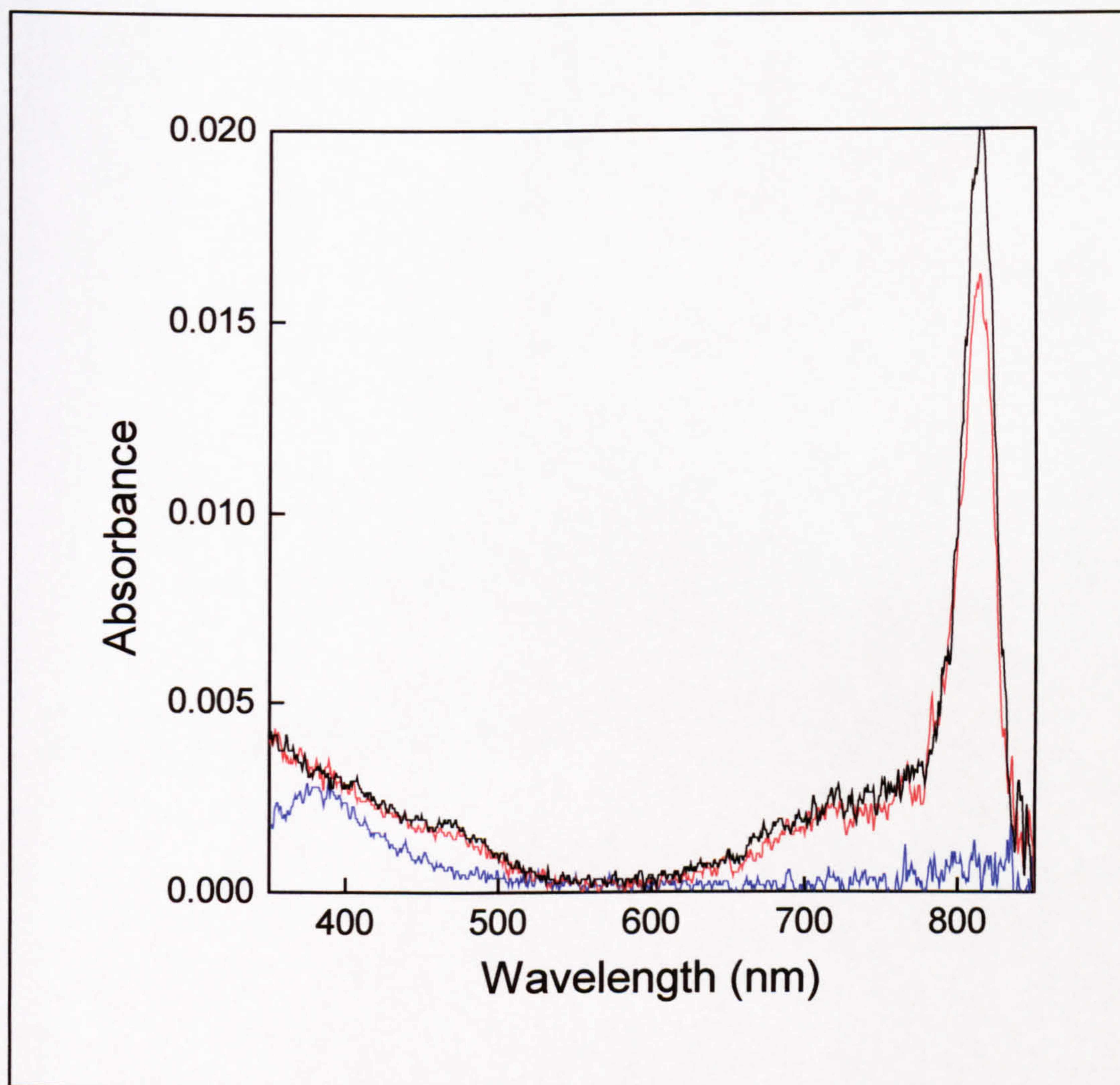


Figure 67 – Dye X (—), after 24 hours in the dark (—) or 24 hours under normal laboratory lighting (—)

CHAPTER FOUR

Conclusions and suggestions for further work

1. Conclusions

The use of differentiation to aid the analysis of the Pressure-Area isotherms provides an accurate and reliable method of determining the quality of deposited Langmuir-Blodgett films. Further work on this new concept may eventually provide a method of grading all LB films for direct comparisons of differing deposition conditions.

The effect of the metal atom on the quality of the Langmuir (and Langmuir-Blodgett) film formed can be seen in the comparison of copper, zinc and metal-free *t*-butyl phthalocyanines. The results of the copper phthalocyanine are comparable to work performed by other research groups and suggest that it adopts an edge-on orientation due to the strong interactions between the π -electron rings, whilst the axial-coordination of water molecules to the zinc atom means the metallated phthalocyanine molecules assume a more face-down position.

The porphyrin molecules can be split into two groups – those forming poor LB films and not-so poor LB films. Surprisingly, the two octa-substituted “ether” dyes do not form similar floating layers. The ethylhexyloxy porphyrin is a poor dye for use with Langmuir-Blodgett work, whilst the not-so-different propylbutyloxy porphyrin forms possibly the best film of all the porphyrins. The results of the characterisation are similar to the work of Richardson’s research group but due to differing experimental conditions, not the same. The work in this thesis, performed at much slower compression and deposition speeds, appear to produce more uniform films.

The SPR Cl_2 -sensing studies produced a good result for I, but were discontinued because the control over the chlorine concentration and background noise was notoriously difficult.

The UV-VIS Cl_2 -sensing studies produced a fascinating series of results for the phthalocyanines where the face-down zinc phthalocyanine are far more sensitive than the edge-on copper and random metal-free moieties.

The gas-sensing properties of the porphyrins generally match the results of the quality of the film. This showed that the orientation of the dye molecules might play a vital role in the chlorine-sensitivity of the films. Indeed, the results from Richardson on

the same porphyrins (but deposited in non-standard conditions) show that not only the orientation but the porosity of the film play an important role in the chlorine sensitivity. The fast deposition of Richardson's porphyrin films produce thicker, more porous films that have a higher sensitivity than the more uniform thinner films produced in this thesis. If this is indeed the case a simple spacer molecule could be used to decrease the density of the film and increase its chlorine sensitivity (*see* 2. Suggestions for further work).

One of the porphyrins (V) demonstrated a two-stage response to the chlorine for the oxidation of the macrocycle. The time constants obtained were comparable to results obtained from the same dye by Richardson. The lower density of the other research group's films explains the differences; a lower surface coverage produces a slower surface response and the higher porosity provides faster bulk diffusion.

The porphyrin/phthalocyanine triple-decker sandwich dye not only formed a poor Langmuir film, but also was also highly sensitive to light, making it unsuitable for chlorine gas sensors of this type.

2. Suggestions for further work

2.1 Alterations to deposition conditions

We have already seen that the orientation of the molecules plays an important role in the sensitivity of the films to the chlorine gas. One possible solution to poor sensing films, without the need to deposit in non-standard conditions, is to use another floating molecule to dilute (and hence separate) the dye molecules on the water surface. It is important that this spacer molecule is both inert to the analyte gas and the dye molecules to prevent any changes from the exposure to chlorine.

Some of these experiments have already been carried out and have shown some initial promise.

Firstly, stearic acid (S. A.) was deposited onto a glass slide and then checked for any changes in the absorption spectrum after exposure to chlorine gas. Then it was mixed with the dye in trichloromethane to determine if acid was weak enough for the dye to remain its pure form (cf. the dication upon the addition of a few drops of HCl) (Figure 68).

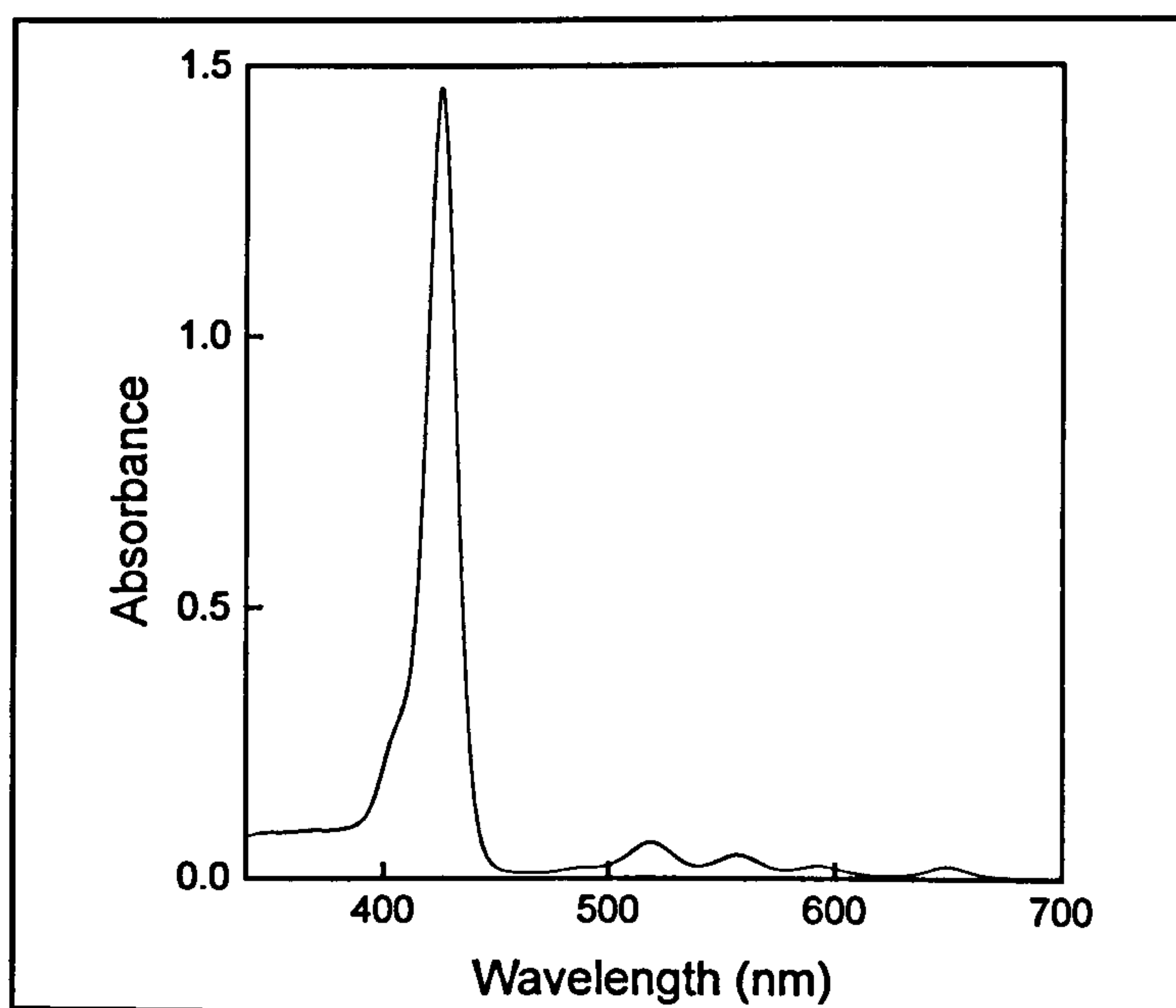


Figure 68 – Mixture of VIII and stearic acid (1:10) in trichloromethane

The 4 satellite bands and location of the Soret band shows that the acid has not protonated the LB film.

Secondly, the mixed film was deposited as a monolayer and exposed to chlorine gas. The comparison to the pure dye deposited under the same conditions shows that it may be worth exploring this further (Figure 69 and Figure 70).

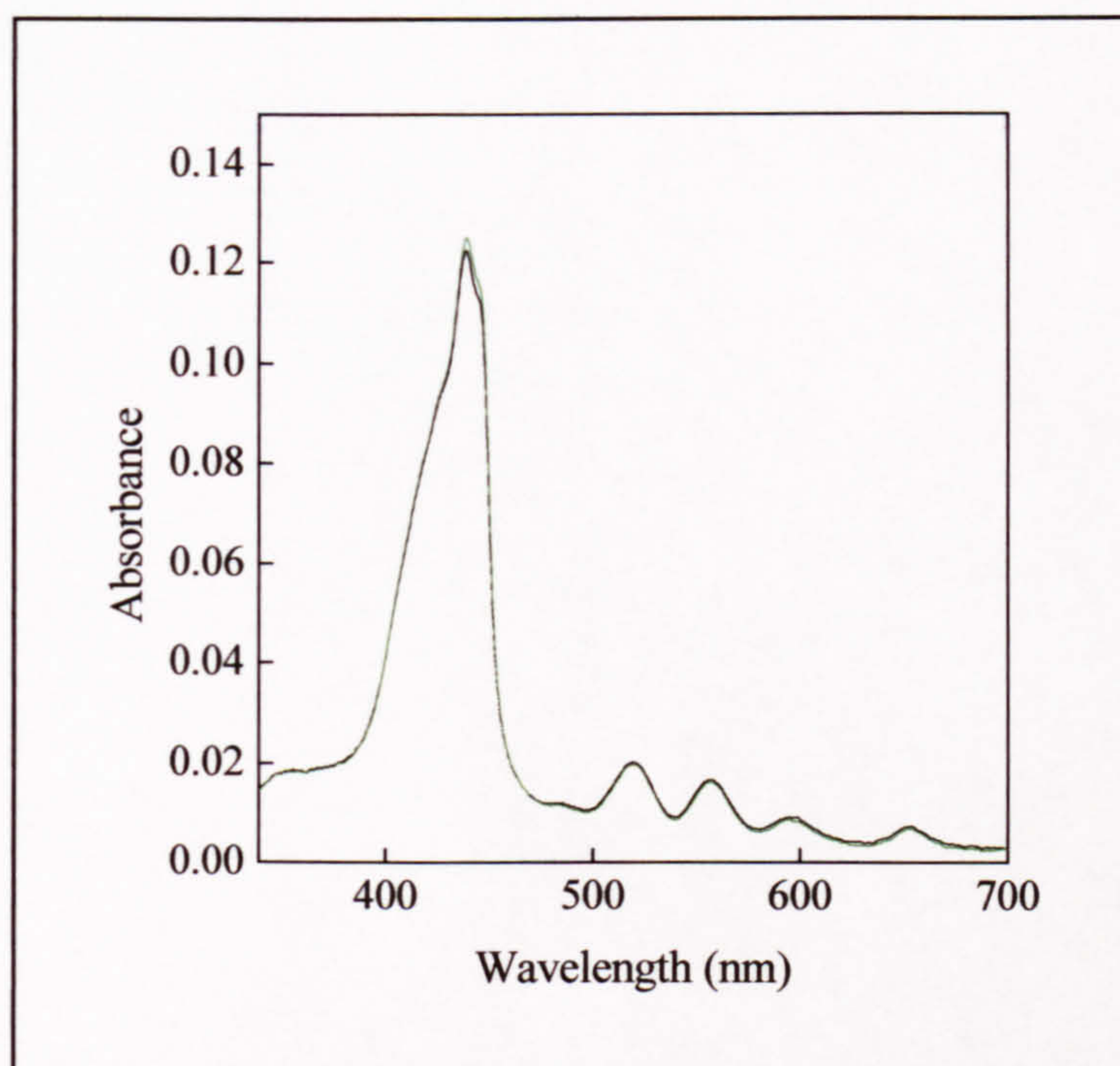


Figure 69 – Monolayer of VIII (—) after exposure to 50 ppm chlorine for 30 mins (---)

The sensitivity of multilayers can also be increased using this method. The simple deposition of mixed layers, however, does not alter the response of the film to the chlorine (Figure 71). There must be stearic acid layers deposited between each mixed film layer (Figure 72).

Another method of improving the sensitivity was the increased deposition pressure (Figure 73). This yielded a surprising improvement in the response to chlorine and should be investigated further (possibly with the use of S. A. spacer layers for multilayers).

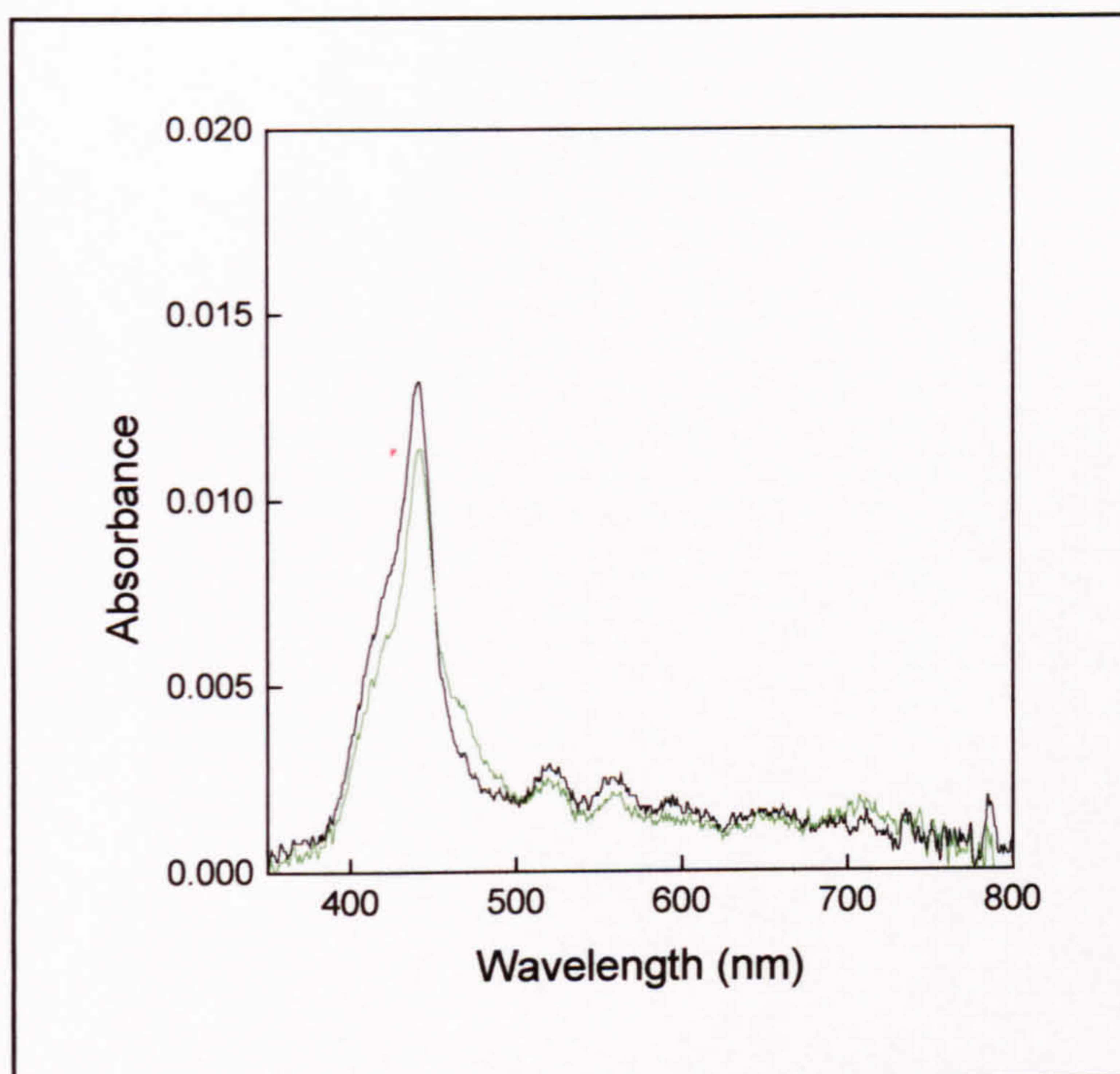


Figure 70 – Monolayer of VIII and S. A.(1:10) (—) after exposure to 50 ppm for 30 mins (---)

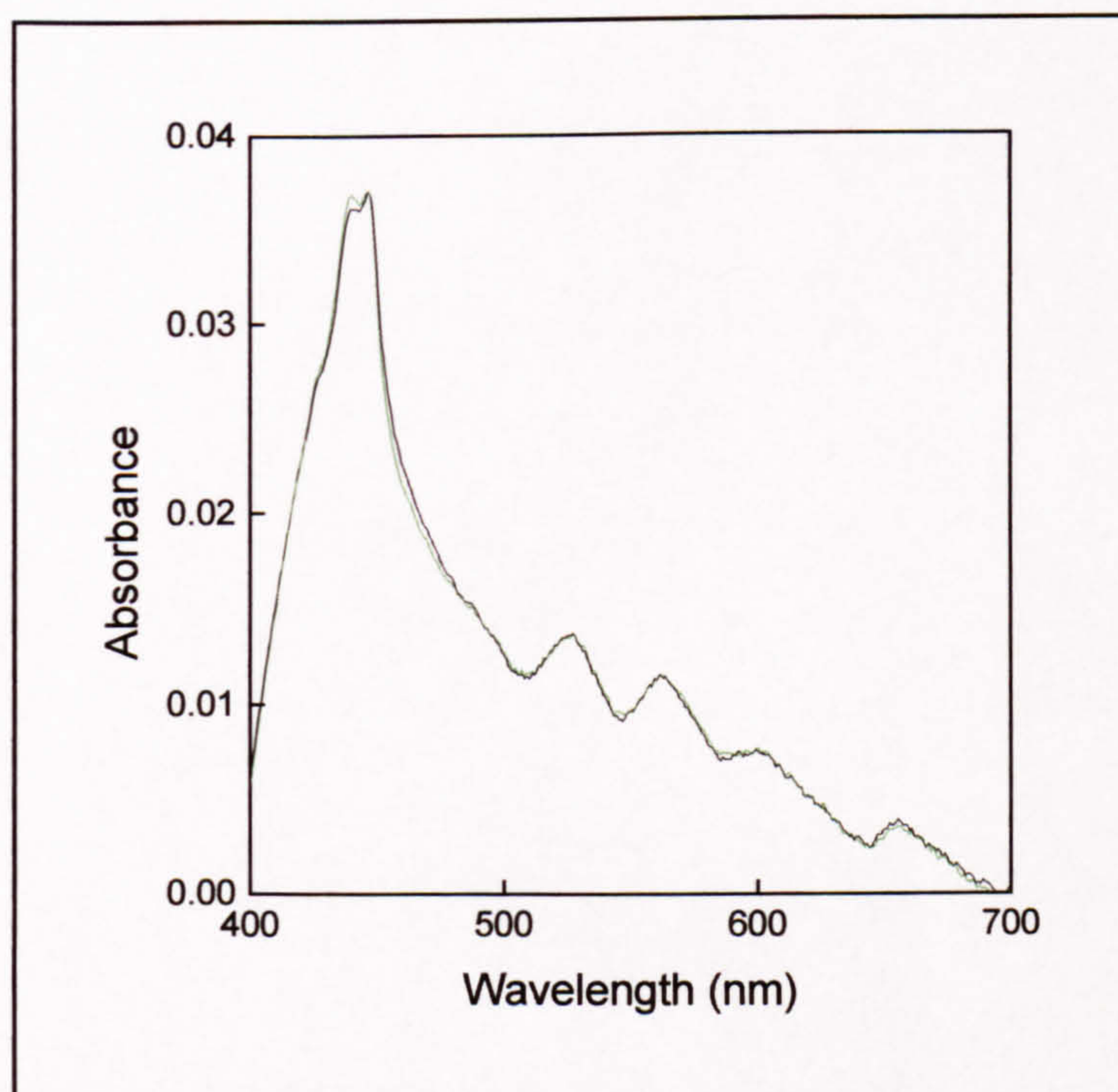


Figure 71 – Multilayer (5 passes) of mixed floating film of VIII and S. A. (1:10) (—) after exposure to 50 ppm chlorine for 30 mins (---)

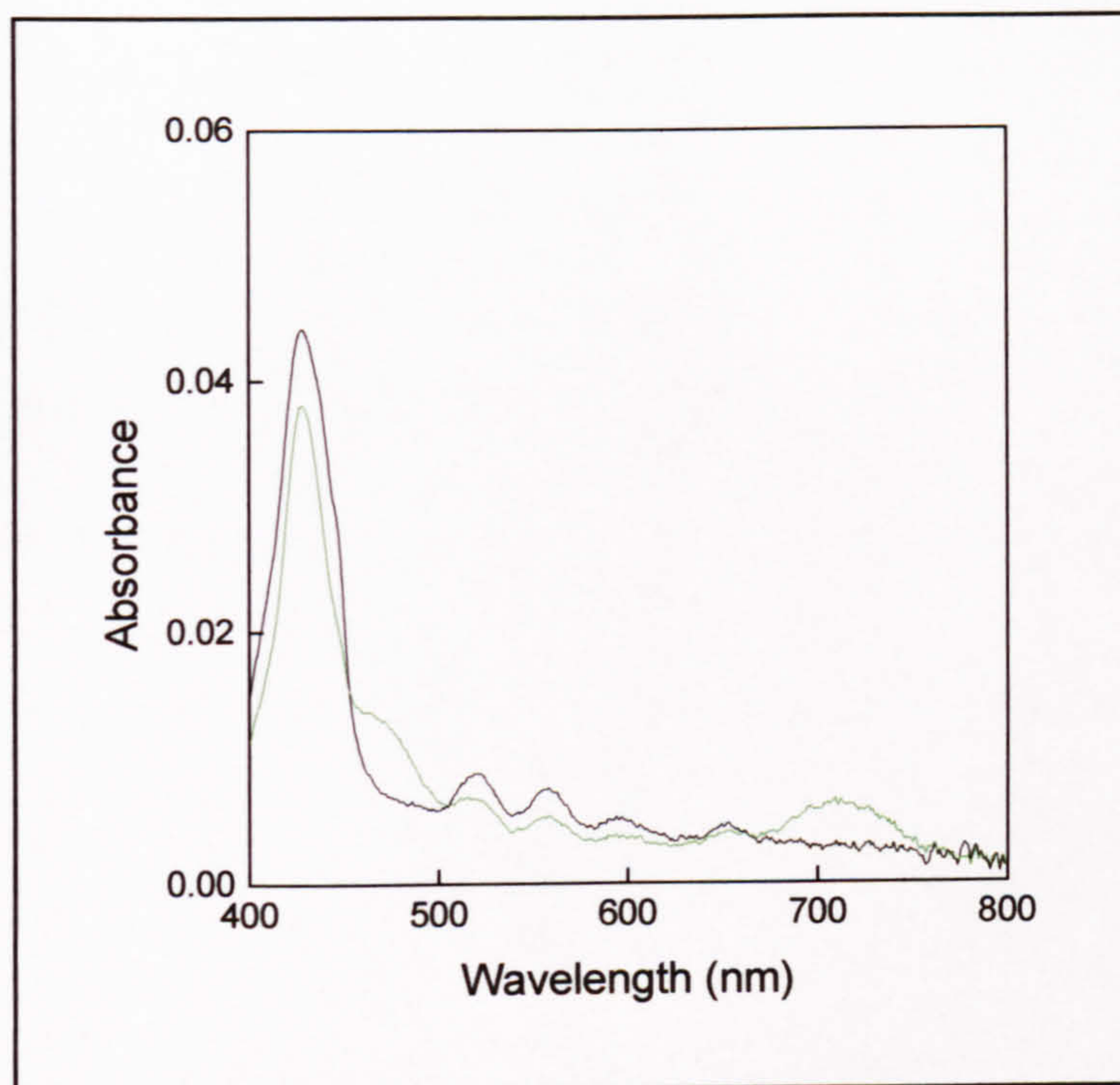


Figure 72 – Multilayer of VIII and S. A. mixed film (1:10, 5 passes) with 4 x S. A. spacer layers (—) after exposure to 50 ppm chlorine for 30 mins (---)

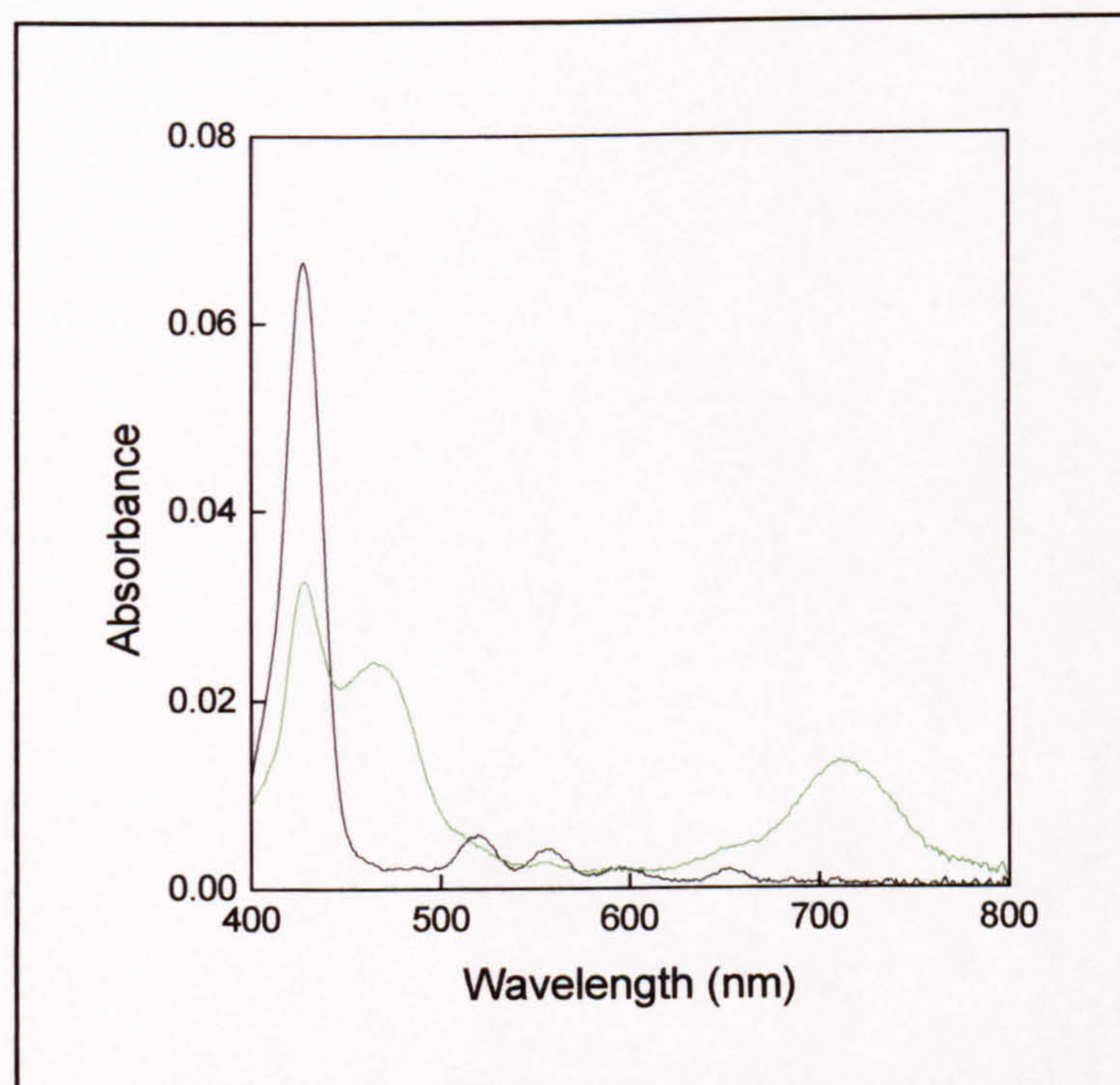


Figure 73 – Monolayer of VIII deposited at high pressure (—) and exposed to 50 ppm chlorine for 30 mins (---)

2.2 Investigation of chain lengths in ether substituents

Dyes VII, VIII and IX are similar in chemical structure, but very different in Langmuir film and Gas-sensing properties. The effect of altering the chain lengths of the ether substituents should be investigated to determine which provides the best floating monolayer and is most responsive to chlorine.

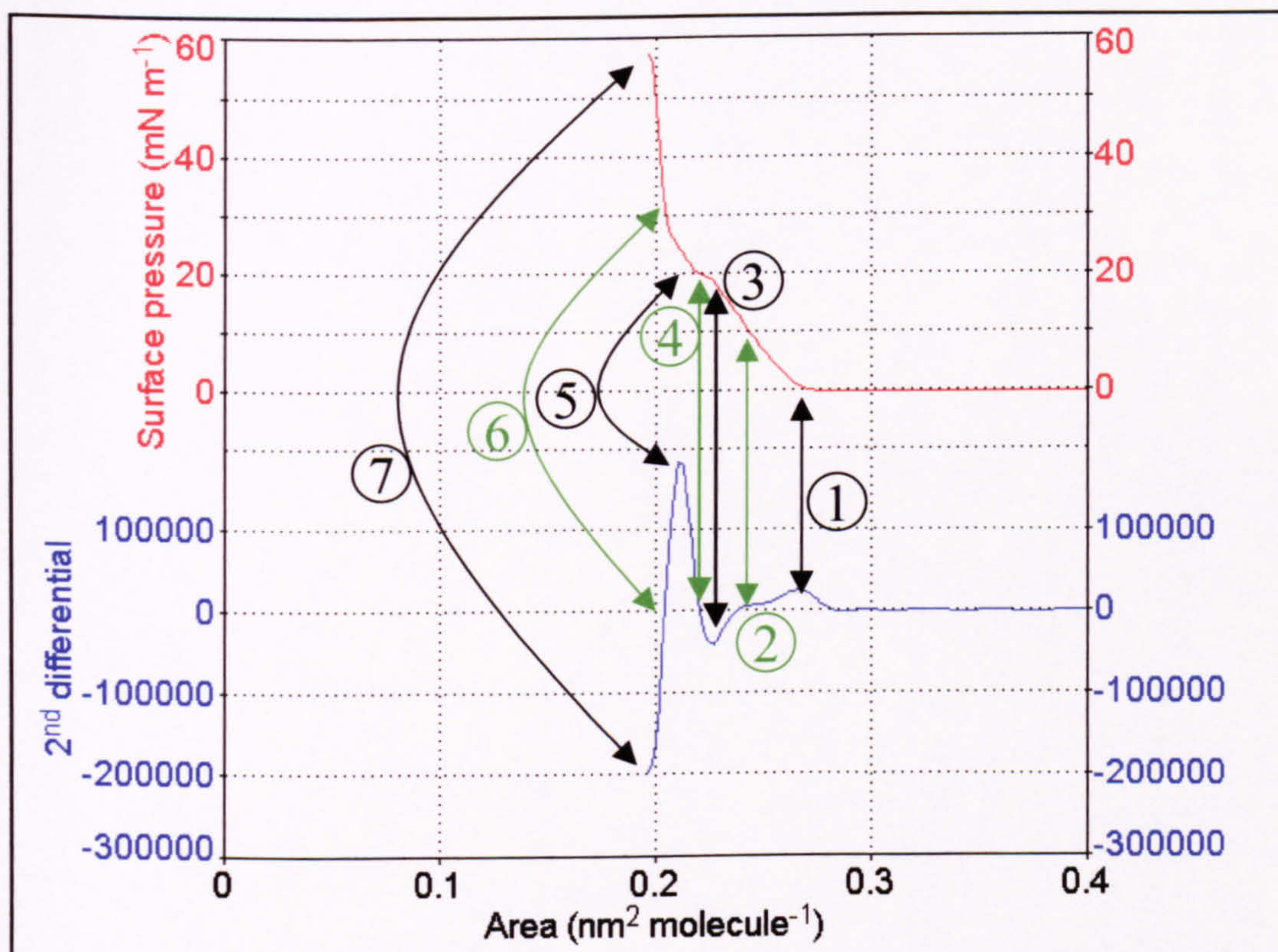
2.3 Potential commercial investigations

If a commercial sensor is to be built, dyes must be chosen which have absorbances that decay or grow within the range of the light source (for example circa 680 nm for a cheap red LED) when the film is exposed to the analyte gas. Other issues such as the requirements for background scans should also be investigated.

Appendix

Explanation of 2nd differential graphs

The example below is an isotherm of stearic acid – a standard calibration material used with Langmuir troughs. Using the 2nd differential several features become evident.



- ① and ⑤ are maxima in the 2nd differential. They correspond to the large changes in the gradient of the isotherm where the former marks the take-off point and the latter indicates the end of the plateaux associated with the orientation change of the molecules on the water surface.

② , ④ and ⑥ are points of inflexion in the isotherm. In the 2nd differential, they mark a change in the gradient directly between minima and maxima. In the case of the latter point, it marks the *start* of the collapse of the floating film. For stearic acid, the gradient of the curve is steep at this point, indicating that whilst the dye molecules are stable at the air-water interface, only a slight reduction in the area will result in the collapse of the monolayer.

⑦ is the point of collapse of the film. In most stearic acid isotherms this would be denoted by a global minima. However, in this case the experiment was terminated before the surface pressure reached the point where the collapse is clearly evident (a decrease can be seen in the pressure with decreasing area).

Acknowledgements

There are many people I wish to thank for their help and support during this thesis. Firstly my family for their support throughout. Secondly, my supervisor Professor Geoff Ashwell, who always knew how best to encourage me. Thirdly, Professor Colin Honeybourne, whose advice during the final stages of the PhD was invaluable. Fourthly, Dr. Andrew Green, Dr. Karl Skjonnemand, Dr. Nick Rees and Rick Hamilton whose expertise guided me through the many questions I badgered them about over the years. And finally Dr. Tim Richardson (Sheffield University) who provided the majority of the dyes that I worked on during my PhD.

References

- ¹ Petty MC, in *Introduction to Molecular Electronics*, Edward Arnold, London (1995)
- ² Ashwell GJ, Gandolfo DS, Hamilton R, *Journal of Materials Chemistry*, 2002, **12** (3), 416, Molecular rectification: characterisation of a dye sandwiched between gold electrodes
- ³ Palacin S, *Advances in Colloid and Interface Science*, 2000, **87**, 165, Phthalocyanines in Langmuir-Blodgett films: from molecular design to supramolecular architecture
- ⁴ Bourgoin JP, Barraud A, Vandevyver M, in *Molecular Electronics and Molecular Electronic Devices*, vol. 3, ed. Sienicki K, CRC Press Inc., Florida (1994)
- ⁵ Ruaudel-Teixier A, Vandevyver M, Barraud A, *Molecular Crystals and Liquid Crystals*, 1985, **120**, 319, Novel Conducting LB films
- ⁶ Martin P, Szablewski M, in *Tensiometers and Langmuir-Blodgett Troughs*, 4th edn., ed. Grunfeld F, Nima Technology Ltd., Coventry (1995)
- ⁷ Küster W, *Z. Physiol. Chem.*, 1912, **82**, 463
- ⁸ Fischer H, Seile K, *Ann. Chem.*, 1929, **468**, 98
- ⁹ Moss GP, *Pure Appl. Chem.*, 1987, **59**, 779
- ¹⁰ *Molecule Of The Month - Phthalocyanine*
(<http://www.chm.bris.ac.uk/motm/phthalocyanine/pbpc.html>) visited on 15/2/02

¹¹ Linstead RP, *J. Chem. Soc.*, 1934, **1016**

¹² IUPAC Goldbook

(<http://www.iupac.org/goldbook/H02867.pdf>) visited on 01/03/03

¹³ What Does Aromatic Really Mean?

(<http://www.geocities.com/Athens/Thebes/5118/obc/arom.htm>) visited on 15/02/02

¹⁴ Samways E, *Bank of England - Ink R&D Department*, Personal Communication, 24/3/03

¹⁵ *The Orange Forum*

(<http://www.orangeforum.or.jp/e/index.html>) visited on 15/5/02

¹⁶ *Removable Optical Media – How They Work*

(<http://g3.mssm.org/mca/jasper3/ROM.html>) visited on 15/5/02

¹⁷ *CD Media World*

(http://www.cdmediaworld.com/hardware/cdrom/cd_dye.shtml) visited on 15/5/02

¹⁸ Cook M.J, in *Spectroscopy of New Materials*, ed. by Clark R. J. H. and Hester R. E., John Wiley and Sons Ltd. (1993)

¹⁹ Kaliya OL, Lukyanets EA, Vorozhtsov GN, *Journal of Porphyrins and Phthalocyanines*, 1999, **3**, 592, Catalysis by phthalocyanines for technology, ecology and medicine

²⁰ Kuznetsova NA, Pykhtina EV, Ulanova LA, Derkacheva VM, Negrinovski VM, Kaliya OL, Lukyanets EA, *Zhurnal Obshchei Khimii*, 1995, **65** (9), 1541, Phthalocyanine-sensitized photogeneration of hydroxy radicals in aqueous suspensions

- ²¹ Law KY, *Chemical Reviews*, 1993, **93** (1), 449, Organic photoconductive materials – recent trends and developments
- ²² Morenzin J, Schlebusch C, Kessler B, Eberhardt W, *Physical Chemistry Chemical Physics (PCCP)*, 1999, **1**, 1765, Phthalocyanine/C₆₀ composites as improved photosensitive materials
- ²³ Tanaka D, Rikukawa M, Sanui K, Ogata N, *Synthetic Metals*, 1999, **102**, 1492, Fullerene/phthalocyaninatometal complex and their LB films
- ²⁴ Zhao Y, Gan L, Zhou D, Huang C-H, Jiang J, Liu W, *Solid State Communications*, 1998, **106** (1), 43, Photocurrent generation from a self-assembling guest-host LB film of C₆₀ (HOOCCHNHCHCOOH) and octopentyloxy phthalocyanine
- ²⁵ Guldi DM, *Chemical Society Reviews*, 2002, **31**, 22, Fullerene-porphyrin architectures; photosynthetic antenna and reaction centre models
- ²⁶ Imahori H, Yamada K, Hasegawa M, Taniguchi S, Okada T, Sakata Y, *Angewandte Chemie: International Edition in English*, 1997, **36** (23), 2626, A sequential photoinduced electron relay accelerated by fullerene in a porphyrin-pyromellitimide-C₆₀ triad
- ²⁷ Guldi DM, Luo C, Swartz A, Scheloske M, Hirsch A, *Chemical Communications*, 2001, 1066, Self-organisation in photoactive fullerene porphyrin based donor-acceptor ensembles
- ²⁸ Fukuzumi S, Ohkubo K, Imahori H, Shao J, Ou Z, Zheng G, Chen Y, Pandey RK, Fujitsuka M, Ito O, Kadish KM, *Journal of the American Chemical Society*, 2001, **123**, 10676, Photochemical and electrochemical properties of zinc chlorin-C₆₀ dyad as compared to corresponding free-base chlorin-C₆₀, free-base porphyrin-C₆₀ and zinc porphyrin-C₆₀ dyads

- ²⁹ Boyd PDW, Hodgson MC, Rickard CEF, Oliver AG, Chaker L, Brothers PJ, Bolskar RD, Tham FS, Reed CA, *Journal of the American Chemical Society*, 1999, **121**, 10487, Selective supramolecular porphyrin/fullerene interactions
- ³⁰ George A, *New Scientist*, 2002, **2348**, 54, Nanotechnology – Starting small, thinking big
- ³¹ D’Souza F, Deviprasad GR, El-Khouly ME, Fujitsuka M, Ito O, *Journal of the American Chemical Society*, 2001, **123**, 5277, Probing the donor-acceptor proximity on the physicochemical properties of porphyrin-fullerene dyads: “Tail-on” and “Tail-off” binding approach
- ³² Claessens CG, Blau WJ, Cook MJ, Hanack M, *Monatshefte für Chemie*, 2001, **132**, 3, Phthalocyanines and phthalocyanine analogues: the quest for applicable optical properties
- ³³ Nalwa HS, Miyata S, in *Nonlinear optics of organic molecules and polymers*, Chemical Rubber Corp (1997), Boca Raton, FL
- ³⁴ de la Torre G, Torres T, Agulló-López F, *Adv Mater* 1997, **9**, 265
- ³⁵ de la Torre G, Vazquez P, Agulló-López F, Torres T, *Journal of Materials Chemistry*, 1998, **8**, 1671
- ³⁶ Luther-Davies B, Samoc M, *Curr Opin Solid ST M*, 1997, **2**, 213, Third-order nonlinear optical organic materials for photonic switching
- ³⁷ Shirk JS, Lindle JR, Bartoli FJ, Hoffman CA, *Appl. Phys. Lett*, 1989, **55**, 1287, Off-resonant third-order optical nonlinearities of metal-substituted phthalocyanines

- ³⁸ Ho ZZ, Ju CY, Hetherington WM, *Journal of Applied Physics*, 1987, **62**, 716, 3rd Harmonic generation in phthalocyanines
- ³⁹ Prasad PN, Casstevens MK, Samoc M, *SPIE Proceedings*, 1989, **1056**, 117, Nonlinear optical effects in Langmuir-Blodgett films
- ⁴⁰ *Food Product Design: The Electronic Nose*
(<http://www.foodproductdesign.com/archive/1995/0695QA.html>) - visited on 3/7/02
- ⁴¹ Chromophores – Dyes and Colours
(<http://instruct.uwo.ca/chemistry/223/Chromophores%20partial%20per.pdf>) - visited on 10/7/02
- ⁴² Brook RA, Dooling CM, Jones LT, Richardson TH, *Materials Science and Engineering C – Biomimetic and Supramolecular systems*, 2002, **22**, 427, Mixed monolayer LB films of EHO and calix[8]arene
- ⁴³ Fietzek C, Seiler M, Gorlach B, Schutz P, Weimar U, Hanack M, Ziegler C, Bertagnolli H, *Journal of Materials Chemistry*, 2002, **12**, 2305, Reversible intercalation of volatile amines into stacks of soluble phthalocyanines
- ⁴⁴ Ariga K, Endo K, Aoyama Y, Okahata Y, *Colloids and Surfaces A – Physicochemical and Engineering Aspects*, 2000, **169**, 177, QCM analyses on adsorption of gaseous guests to cast films of porphyrin-resorcinol derivatives
- ⁴⁵ Zhou R, Josse F, Gopel W, Ozturk ZZ, Bekaroglu O, *Applied Organometallic Chemistry*, 1996, **10**, 557, Phthalocyanines as sensitive materials for chemical sensors
- ⁴⁶ Gas Detectors
(<http://www.gasdetect.com/gasmain.html>) - visited on 20/11/01

⁴⁷ Lexis-Nexis TM Executive

(<http://web.lexis-nexis.com/executive/>) – visited on 21/12/00

⁴⁸ *Chlorine Kills (GP) A Dossier of Chlorine Accidents*, Compiled by Sabra Lees, Greenpeace International (1991)

⁴⁹ Ding HM, Erokhin V, Ram MK, Paddeu S, Valkova L, Nicolini C, *Thin Solid Films*, 2000, **379**, 279, A physical insight into the gas-sensing properties of copper(II) tetra-(tert-butyl)-5,10,15,20-tetraazaporphyrin Langmuir-Blodgett films

⁵⁰ Cook MJ, *Pure and Applied Chemistry*, 1999, **71**, 2145, Phthalocyanine thin films

⁵¹ Levin PP, Costa SMB, Lopes JM, Serralha FN, *Spectrochimica Acta Part A – Molecular and Biomolecular Spectroscopy*, 2000, **56**, 1745, Effect of zeolite properties on ground-state and triplet-triplet absorption, prompt and oxygen induced delayed fluorescence of tetraphenylporphyrin at gas/solid interface

⁵² *Quartz Crystal Microbalances*

(http://www.inapg.inra.fr/ens_rech/siab/asteq/elba/qcm.htm) - visited on 3/7/02

⁵³ A Thick-Film Acoustic Wave Sensor

(<http://www.ecs.soton.ac.uk/publications/rj/1994/transduc/white/white.html>) - visited on 24/3/01

⁵⁴ Skjonnemand K, *Optical and structural characterisation of ultra-thin films (PhD Thesis)*, Cranfield University (2000), Cranfield

⁵⁵ Spreeta technology at TI

(<http://www.ti.com/sc/docs/products/msp/control/spreeta/>) - visited on 30/5/01

⁵⁶ An introduction to Biacore's SPR technology

(http://www.biacore.se/proteomics/pdf/technology_brochure.pdf) - visited on 30/5/01

⁵⁷ Hamilton R, Nanomaterials Group – Cranfield University, *Personal Communication*, 12/09/00

⁵⁸ Wilde JN, Petty MC, Saffell J, Tempore A, Valli L, *Measurement and Control*, 1997, **30**, 269, Surface plasmon resonance imaging for gas sensing

⁵⁹ Zhang L-M, Uttamchandani D, *Electronics Letters*, 1988, **24** (23), 1469, Optical chemical sensing employing surface plasmon resonance

⁶⁰ DiNatale C, Paolesse R, Macagnano A, Mantini A, Mari P, D'Amico A, *Sensors and Actuators B – Chemical*, 2000, **68**, 319, Qualitative structure-sensitivity relationship in porphyrin based QMB chemical sensors.

⁶¹ D'Amico A, Di Natale C, Paolesse R, Macagnano A, Mantini A, *Sensors and Actuators B – Chemical*, 2000, **65**, 209, Metalloporphyrins as basic material for volatile sensitive sensors

⁶² Paolesse R, Di Natale C, Dall'Orto VC, Macagnano A, Angelaccio A, Motta N, Sgarlata A, Hurst J, Rezzano I, Mascini M, D'Amico A, *Thin Solid Films*, 1999, **354**, 245, Porphyrin thin films coated quartz crystal microbalances prepared by electropolymerization technique

⁶³ Paolesse R, Di Natale C, Macagnano A, Davide F, Boschi T, D'Amico A, *Sensors and Actuators B – Chemical*, 1998, **47**, 70, Self-Assembled monolayers of mercaptoporphyrins as sensing material for quartz crystal microbalance chemical sensors

⁶⁴ Valkova L, Borovkov N, Maccioni E, Pisani M, Rustichelli F, Erokhin V, Patternolli C, Nicolini C, *Colloids and Surfaces A – Physicochemical and Engineering Aspects*, 2002, **198**, 891, Influence of molecular and supramolecular factors on sensor properties

of Langmuir-Blodgett films of *tert*-butyl-substituted copper azaporphyrines towards hydrocarbons

⁶⁵ Urbanczyk M, Jakubik W, Kochowski S, *Sensors and Actuators B - Chemical*, 1994, **22** (2), 133, Investigation of sensor properties of copper phthalocyanine with the use of surface acoustic-waves

⁶⁶ Granito C, Wilde JN, Petty MC, Houghton S, Iredale PJ, *Thin Solid Films*, 1996, **284-285**, 98, Methylbenzene vapour sensing using copper and nickel phthalocyanine Langmuir-Blodgett films

⁶⁷ Mukhopadhyay S, Hogarth CA, Thorpe SC, Cook MJ, *Journal of Materials Chemistry*, 1994, **5**, 321, Room temperature methylbenzene sensing using phthalocyanine Langmuir-Blodgett films

⁶⁸ Jiang DP, Zhang LG, Fan Y, Ren XG, Guan ZS, Li YJ, Lu AD, *Thin Solid Films*, 1997, **293**, 277, The effects of detected gases on spectroscopic properties of phthalocyanine Langmuir-Blodgett films

⁶⁹ Nakagawa K, Sadaoka Y, Supriyatno H, Kubo Akiko, Tsutsumi C, Tabuchi K, *Sensors and Actuators B*, 2001, **76**, 42, Optochemical HCl gas detection using alkoxy substituted tetraphenylporphyrin-polymer composite films – effects of alkoxy chain length on sensing characteristics

⁷⁰ Supriyatno H, Nakagawa K, Sadaoka Y, *Sensors and Actuators B*, 2001, **76**, 36, Optochemical HCl gas detection using mono-substituted tetraphenylporphyrin-polymer composite films

⁷¹ Supriyatno H, Nakagawa K, Sadaoka Y, *Sensors and Materials*, 2001, **13**, 6, 359, Optochemical sensor for HCl gas based on tetraoxyphenylporphyrin dispersed in an acrylate polymer matrix

- ⁷² Roisin P, Wright JD, Nolte RJM, Sielcken OE, Thorpe SC, *Journal of Materials Chemistry*, 1992, 2 (1), 131, Gas-sensing properties of semiconducting films of crown-ether-substituted phthalocyanines
- ⁷³ Fedorov MI, Nemirovskii AE, Ivanov AV, Vasil'eva NA, *Instruments and Experimental Techniques*, 1998, 41 (6), 850, A semiconductor ammonia gas analyser
- ⁷⁴ Gu C, Sun L, Zhang T, Li T, Hirata M, *Thin Solid Films*, 1994, 244, 909, A gas-humidity sensor fabricated with phthalocyanine Langmuir-Blodgett film
- ⁷⁵ Li X, Xu H, Zhou Q, Jiang D, Zhang L, Lu A, *Thin Solid Films*, 1998, 324, 277, Gas sensing properties of asymmetrically substituted phthalocyanines bearing once crown ether ring
- ⁷⁶ Lu A, Zhang L, Jiang D, Li Y, Fan Y, *Thin Solid Films*, 1994, 244, 955, Study on the stability of a copper phthalocyanine Langmuir-Blodgett film gas-sensitive element
- ⁷⁷ Hart JP, Abass AK, Cowell D, *Biosensors and Bioelectronics*, 2002, 17, 389, Development of disposable amperometric sulfur dioxide biosensors based on screen print electrodes
- ⁷⁸ Smith VC, Batty SV, Richardson T, Foster KA, Johnstone RAW, Sobral AJFN, Rocha Gonsalves AM d'A, *Thin Solid Films*, 1996, 284-285, 911, Chlorine sensing properties of porphyrin thin films
- ⁷⁹ Richardson T, Smith VC, Johnstone RAW, Sobral AJFN, Rocha-Gonsalves AM d'A, *Thin Solid Films*, 1998, 327-329, 315, Optical response of monolayer films of metal-free sulfonamido-porphyrin

⁸⁰ Richardson T, Dooling CM, Worsfold O, Jones LT, Kato K, Shinbo K, Kaneko F, Treggoning R, Vysotsky MO, Hunter CA, *Thin Solid Films*, 2001, **393**, 259, Taking advantage of optical and electrical properties of organic molecules for gas-sensing applications

⁸¹ Dooling CM, Worsfold O, Richardson T, Treggoning R, Vysotsky MO, Hunter CA, Kato K, Shinbo K, Kaneko F, *Journal of Materials Chemistry*, 2001, **11**, 392, Fast, reversible optical sensing of NO₂ using 5,10,15,20-tetrakis [3,4-bis (2-ethylhexyloxy) phenyl]-21*H*, 23-*H*-porphine assemblies

⁸² Worsfold O, Dooling CM, Richardson T, Vysotsky MO, Treggoning R, Hunter CA, Malins C, *Journal of Materials Chemistry*, 2001, **11**, 399, Nitrogen dioxide sensing characteristics of sol-gel glass thin films containing substituted porphyrin dyes

⁸³ George CD, Richardson T, Hofton ME, Vale CM, Neves MGM, Cavaleiro JAS, *Materials Science and Engineering C*, 1999, **8-9**, 559, Chlorine gas sensing using thin films of *meso*-tetra (*p*-stearamidophenyl) porphyrin

⁸⁴ Hassan AK, Ray AK, Travis JR, Ghassemlooy Z, Cook MJ, Abass A, Collins RA, *Sensors and Actuators B - Chemical*, 1998, **49**, 235, The effect of NO₂ on optical absorption in Langmuir-Blodgett films of octa-substituted amphiphilic copper phthalocyanine molecules

⁸⁵ Honeybourne CL, Portus D, Ratcliffe NM, Richardson T, Ashwell GJ, *Polish Journal of Chemistry*, 2002, **76**, 367, Deposition and characterisation by surface plasmon resonance of Langmuir-Blodgett monolayers of three macrocyclic conjugated tetrapyrrole compounds exposed to chlorine gas

⁸⁶ Lloyd JP, Pearson C, Petty MC, *Thin Solid Films*, 1988, **160**, 431, Surface plasmon resonance studies of gas effects in phthalocyanine Langmuir-Blodgett films

- ⁸⁷ Richardson TH, Dooling CM, Worsfold O, Jones LT, Kato K, Shinbo K, Kaneko F, Treggonning R, Vysotsky MO, Hunter CA, *Colloids and Surfaces A – Physicochemical and Engineering Aspects*, 2002, **198-200**, 843, Gas sensing properties of porphyrin assemblies prepared using ultra-fast LB deposition
- ⁸⁸ Baron MG, Narayanaswamy R, Thorpe SC, *Sensors and Actuators B – Chemical*, 1995, **29**, 358, A kineto-optical method for the determination of chlorine gas
- ⁸⁹ Rocha-Santos TAP, Gomes MTSR, Duarte AC, Oliveira JABP, *Talanta*, 2000, **51** (6), 1149, A quartz crystal microbalance sensor for the determination of nitroaromatics in landfill gas
- ⁹⁰ Kim SR, Kim JD, Choi KH, Chang YH, *Sensors and Actuators B - Chemical*, 1997, **40** (1), 39, NO₂ sensing properties of octa (2-ethylhexyloxy) metallophthalocyanine LB films using quartz-crystal microbalance
- ⁹¹ Kim SR, Choi SA, Kim JD, Choi KH, Park SK, Chang YH, *Synthetic Metals*, 1995, **71** (1-3), 2293, The characteristics of metallophthalocyanine monolayer, multilayer and application to the gas sensor for NO₂
- ⁹² Holcroft B, Roberts GG, *Thin Solid Films*, 1987, **160** (1-2), 445, Surface acoustic wave sensors incorporating Langmuir-Blodgett films
- ⁹³ Yunquan C, Wuming Z, Guang L, *Sensors and Actuators B - Chemical*, 1994, **20**, 247, SAW gas sensor with copper tetrasulphonated phthalocyanine film
- ⁹⁴ O'Donnell J, Honeybourne CL, *Journal of Physics: Condensed Matter*, 1991, **3**, S337, Acousto-electrical and surface plasmon resonant responses from NOX-doped Langmuir-Blodgett films of macrocycles

- ⁹⁵ Jakubik W, Urbanczyk M, Opilski A, *Ultrasonics*, 2001, **39** (3), 227, Sensor properties of lead phthalocyanine in a surface acoustic wave system
- ⁹⁶ Nieuwenhuizen MS, Nederlof AJ, Coomans A, *Fresenius Zeitschrift für Analytische Chemie*, 1988, **330** (2), 123, A SAW gas sensor for NO₂ - chemically immobilized phthalocyanines as chemical interfaces
- ⁹⁷ Nieuwenhuizen MS, Nederlof AJ, *Analytical Chemistry*, 1988, **60** (3), 236, Surface acoustic wave gas sensor for nitrogen dioxide using phthalocyanines as chemical interfaces – effects of nitric oxide, halogen gases and prolonged heat treatment
- ⁹⁸ Rapp M, Binz D, Kabbe I, Von Schickfus M, Huklinger S, Fuchs H, Schrepp W, Fleischmann B, *Sensors and Actuators B – Chemical*, 1991, **4**, 103, A new high-frequency high-sensitivity SAW device for NO₂ gas detection in the sub-ppm range
- ⁹⁹ Kato K, Dooling CA, Shinbo K, Richardson TH, Kaneka F, Treggoning R, Vysotsky MO, Hunter CA, *Colloids and Surfaces A – Physicochemical and Engineering Aspects*, 2002, **198**, 811, Surface plasmon resonance properties and gas response in porphyrin Langmuir-Blodgett films
- ¹⁰⁰ Simpson TRE, Cook MJ, Petty MC, Thorpe SC, Russell DA, *Analyst*, 1996, **121** (10), 1501, Surface plasmon resonance of self-assembled phthalocyanine monolayers – possibilities for optical gas sensing
- ¹⁰¹ Wright JD, Cado A, Peacock SJ, Rivalle V, Smith AM, *Sensors and Actuators B – Chemical*, 1995, **29** (1-3), 108, Effects of nitrogen dioxide on surface plasmon resonance of substituted phthalocyanine films
- ¹⁰² Jory MJ, Cann PS, Sambles JR, *Journal of Physics D – Applied Physics*, 1994, **27** (1), 169, Surface-plasmon polariton studies of 18-crown-6 metal-free phthalocyanine

¹⁰³ Nikitin PI, Beloglazov AA, Valeiko MV, Creighton JA, Smith AM, Sommerdijk NAJM, Wright JD, *Sensors and Actuators B - Chemical*, 1997, 38-39, 53, Silicon-based surface plasmon resonance chemical sensors

¹⁰⁴ Wenfeng Q, Wenping H, Yunqi L, Shuqin Z, Yu X, Daoben Z, *Sensors and Actuators B - Chemical*, 2001, 75, 62, The gas sensitivity of a substituted metallophthalocyanine, tetra-iso-propoxyphthalocyaninato copper (II)

¹⁰⁵ Wenping H, Yunqi L, Shenggao L, Shuqin Z, Daoben Z, Bo X, Chunlin B, Cheng W, *Thin Solid Films*, 2000, 360, 256, The gas sensitivity of a metal-insulator-semiconductor field-effect transistor based on Langmuir-Blodgett films of a new asymmetrically substituted phthalocyanine

¹⁰⁶ Rella R, Serra A, Siciliano P, Tepore A, Valli L, Zocco A, *Thin Solid Films*, 1996, 286, 256, Effects of NO₂ oxidizing gas on a novel phthalocyanine Langmuir-Blodgett thin film

¹⁰⁷ Tepore A, Serra A, Arnold DP, Manno D, Micocci G, Genga A, Valli L, *Langmuir*, 2001, 17, 8139, Study of gas sensing performances of Langmuir-Blodgett films containing an alkyne-linked conjugated-porphyrin dimer

¹⁰⁸ Yunqi L, Wenping H, Yu X, Shenggao L, Daoben Z, *Journal of Physical Chemistry B*, 2000, 104, 11859, Characterisation, second-harmonic generation and gas-sensitive properties of Langmuir-Blodgett films of 1,8-naphthalimide-tri-*tert*-butylphthalocyanine

¹⁰⁹ Altindal A, Öztürk ZZ, Dabak S, Bekaroğlu Ö, *Sensors and Actuators B - Chemical*, 2001, 77, 389, Halogen sensing using thin films of crosswise-substituted phthalocyanines

- ¹¹⁰ Capone S, Rella R, Siciliano P, Vasanelli L, Valli L, Troisi L, *Thin Solid Films*, 1998, **327-329**, 465, On the characterisation and gas sensing properties of Cu (II) tetra (alkylamino carbonyl) phthalocyanine LB films
- ¹¹¹ Rella R, Serra A, Siciliano A, Tepore A, Valli L, Zocco A, *Sensors and Actuators B – Chemical*, 1997, **42**, 53, Applications in gas-sensing devices of a new macrocyclic copper complex
- ¹¹² Rella R, Serra A, Siciliano P, Tepore A, Troisi L, Valli L, *Thin Solid Films*, 1996, **284-285**, 870, Characterization of novel copper phthalocyanine Langmuir-Blodgett films for NO₂ detection
- ¹¹³ Rella R, Serra A, Siciliano P, Tepore A, Valli L, Zocco A, *Langmuir*, 1997, **13**, 6567, Langmuir-Blodgett multilayers based on copper phthalocyanine as gas sensor materials: active layer-gas interaction model and conductivity modulation
- ¹¹⁴ Wilson A, Rigby GP, Wright JD, Thorpe SC, Terui T, Maruyama Y, *Journal of Materials Chemistry*, 1992, **2** (3), 303, Effects of heat treatment on chemical, morphological and NO₂ –sensing properties of lead phthalocyanine films
- ¹¹⁵ Parr ATJ, Vinton SJ, Krier A, Collins RA, *Czechoslovak Journal of Physics*, 1993, **9** (10), 969, Morphology and gas sensitivity of erbium di-phthalocyanine thin films
- ¹¹⁶ Abass AK, Krier A, Collins RA, *Journal of Physics D*, 1993, **26**, 1120, The influence of chlorine on the electrical properties of lead phthalocyanine thin film gas sensors
- ¹¹⁷ Baker S, Roberts GG, Petty MC, *IEE Proceedings*, 1983, **130**, 1(5), 260, Phthalocyanine Langmuir-Blodgett-film gas sensor

- ¹¹⁸ Ding X, Xu H, *Sensors and Actuators B – Chemical*, 2000, **65**, 108, Gas-sensing properties of asymmetrically substituted amphiphilic phthalocyanines
- ¹¹⁹ Newton MI, Starke TKH, Willis MR, McHale G, *Sensors and Actuators B – Chemical*, 2000, **67**, 307, NO₂ detection at room temperature with copper phthalocyanine thin film devices
- ¹²⁰ Rella R, Siciliano P, Manno D, Serra A, Taurino A, Tepore A, Valli L, Zocco A, *Sensors and Actuators B – Chemical*, 1997, **44**, 585, Gas-sensing properties of multilayers of two new macrocyclic copper complexes
- ¹²¹ Ding X, Shen S, Zhou Q, Xu H, *Dyes and Pigments*, 1999, **40**, 187, The synthesis of asymmetrically substituted amphiphilic phthalocyanines and their gas-sensing properties
- ¹²² Dogo S, Germain J-P, Maleysson C, Pauly A, *Thin Solid Films*, 1992, **219**, 251, Interaction of NO₂ with copper phthalocyanine thin films II: Application to gas sensing
- ¹²³ Dogo S, Germain J-P, Maleysson C, Pauly A, *Sensors and Actuators B – Chemical*, 1992, **8**, 257, Gas-sensing properties of metallo-phthalocyanine thin films as a function of their crystalline structure
- ¹²⁴ Gu C, Sun L, Zhang T, Li T, Zhang X, *Thin Solid Films*, 1998, **327-329**, 383, High-sensitivity phthalocyanine LB film gas sensor based on field effect transistors
- ¹²⁵ Sauerbrey, G.Z, *Physics* (1959) **155**, 206-, from Dyer, A.N., PhD thesis, Cranfield University (2000)
- ¹²⁶ Optical properties of copper phthalocyanine (CuPc) thin films
(www.geocities.com/egyptiansssa/ESSSA/issue241/11.pdf) - visited on 20/2/01

- ¹²⁷ Ferraudi G, in *Phthalocyanines: properties and applications*, ed. Leznoff CC, VCH Publishers Inc., Canada (1989)
- ¹²⁸ Valkova LA, Shabyshev LS, Borovkov NY, Feigin LA, Rustichelli F, *Journal of inclusion phenomena and macrocyclic chemistry*, 1999, **35**, 243, Supramolecular assembly formation in monolayers of *tert*-butyl substituted copper phthalocyanine and tetrabenzotriazaporphin
- ¹²⁹ Liu Y, Xu Y, Zhu D, Zhao X, *Thin Solid Films*, 1996, **289**, 282, Second harmonic generation in Langmuir-Blodgett films of an asymmetrically substituted metallophthalocyanine
- ¹³⁰ Lee Y-L, Chen Y-C, Chang C-H, Yang Y-M, Maa J-R, *Thin Solid Films*, 2000, **370**, 278, Surface characterization of the monolayer and Langmuir-Blodgett films of tetra-*tert*-butyl-copper phthalocyanine
- ¹³¹ Cook MJ, McMurdo J, Miles DA, Poynter RH, Simmons JM, Haslam SD, Richardson RM, Welford K, *Journal of Materials Chemistry*, 1994, **4** (8), 1205, Monolayer behaviour and Langmuir-Blodgett film properties of some amphiphilic phthalocyanines: factors influencing molecular organisation within film assembly
- ¹³² Smolenyak P, Peterson R, Nebesny K, Törker M, O'Brien DF, Armstrong NR, *Journal of the American Chemical Society*, 1999, **121**, 8628, Highly ordered thin films of octasubstituted phthalocyanines
- ¹³³ Chyla A, Sworakowski J, Szczurek A, Brynda E, Nešpůrek S, *Molecular Crystals and Liquid Crystals*, 1993, **230**, 1,
- ¹³⁴ Emelyanov YL, Khatko VV, Tomchenko AA, *Synthetic Metals*, 1996, **79**, 173, Preparation and thermostable properties of Langmuir-Blodgett films of copper tetra-*tert*-butyl phthalocyanine complex

¹³⁵ Brynda E, Koropecný I, Kalvoda L, Nešpůrek S, *Thin Solid Films*, 1991, **199**, 375,
Electrical and photoelectrical properties of copper tetra [4-*t*-butylphthalocyanine]
Langmuir-Blodgett films

¹³⁶ Gouterman M in *The Porphyrins: Physical Chemistry, Part A, Vol. III*,
ed. Dolphin D, Academic Press, New York (1978).

¹³⁷ Stern ES, Timmons CJ in *Gillam and Stern's Introduction to electronic absorption
spectroscopy in organic chemistry 3rd edition*, Edward Arnold, London (1971).

¹³⁸ Bull RA, Bulkowski JE, *Colloid Interface Sci*, 1983, **92**, 1

¹³⁹ *English Dictionary 21st Century edition*, Harper Collins, Glasgow (2000)